Chemistry of Airborne Particles
from Metallurgical Processing

by

Neil Travis Jenkins

S. B. Materials Science and Engineering
Massachusetts Institute of Technology, 1997

Submitted to the Department of Materials Science and Engineering
in partial fulfillment of the requirements for the degree of

Doctor of Philosophy

at the

MASSACHUSETTS INSTITUTE OF TECHNOLOGY

September, 2003

Author ....
Department of Materials Science and Engineering
August 22, 2003

Certified by ....
Thomas W. Eagar
Thomas Lord Professor of Materials Engineering and Materials Systems
Department of Materials Science and Engineering
Thesis Supervisor

Accepted by ....
Harry L. Tuller
Professor of Ceramics and Electronic Materials
Chair, Graduate Committee
Department of Materials Science and Engineering

Chemistry of Airborne Particles from Metallurgical Processing

by

Neil Travis Jenkins

Submitted to the Department of Materials Science and Engineering on
August 22, 2003, in partial fulfillment of the requirements for the degree of
Doctor of Philosophy in Metallurgy

Abstract

Airborne particles fall into one of three size ranges.

The nucleation range consists of nanoparticles created from vapor atom collisions. The decisive parameter for particle size and composition is the supercooling of the vapor.

The accumulation range, which comprises particles less than 2 micrometers, consists of particles formed from the collision of smaller primary particles from the nucleation range. The composition of agglomerates and coalesced particles is the same as the bulk vapor composition.

Coarse particles, the composition of which is determined by a liquid precursor, are greater than 1 micrometer and solidify from droplets whose sizes are controlled by surface, viscous, and inertial forces.

The relationship between size and composition of airborne particles could be seen in welding fume, a typical metallurgical aerosol.

This analysis was performed with a cascade impactor and energy dispersive spectrometry with both scanning electron microscopy (SEM-EDS) and scanning transmission electron microscopy (STEM-EDS). Other methods for properly characterizing particles were discussed.

In the analysis, less than 10% of the mass of fume particles for various types of gas metal arc welding (GMAW) were coarse, while one-third of flux cored arc welding (FCAW) fume particles were coarse. Coarse particles had a composition closer to that of the welding electrode than did fine particles.

Primary particles were not homogeneous. Particles larger than the mean free path of the carrier gas had the same composition as that of the vapor, but for particles 20 to 60 nanometers, smaller particles were more enriched in volatile metals than larger particles were. This was explained by the cooling path along the bubble point line of a binary phase diagram.

Particles were not necessarily homogenous internally. Because nanoparticles homogenize quickly, they may form in a metastable state, but will not remain in that state. In this analysis, the presence of multiple stable immiscible phases explains this internal heterogeneity.

The knowledge contained herein is important for industries that depend on the properties of nanoparticles, and for manufacturing, where industrial hygiene is important because of respirable particle by-products, such as high-energy-density metallurgical processing.

Thesis Supervisor: Dr. Thomas W. Eagar, ScD. P.E.
Title: Thomas Lord Professor of Materials Engineering & Materials Systems

Table of Contents

List of Figures

List of Tables

List of Symbols

A	area
Bi	Biot number
C	elemental composition
C_{+j}	elemental composition of core at point $+j$ from center of particle
C_p	heat capacity
d	diameter of particle or feature
d^*	critical nucleus diameter
d_0	initial particle diameter
D	diffusion coefficient
I	current
k_{air}	thermal conductivity of air
k_B	Boltzman constant
L	heat of phase change
M_A	atomic weight of species A
O	Ohnesorge number
P	pressure
P_A	vapor pressure of species A,
$P_{A,\infty}$	vapor pressure over a flat surface of species A
q	electrical charge on surface
Q	heat
r	radius
R	gas constant
t	time
T	temperature
T_b	boiling temperature
v	velocity
V	volume
W	Weber number
α	# neighbor particles that combine with any given primary particle
γ	surface energy or surface tension
ΔG	free energy of phase change or reaction
$\Delta G^{\circ}_{reaction}$	equilibrium free energy of reaction
ε	emissivity
ε_o	permeability of vacuum
η	viscosity of the carrier gas
κ	molar concentration of particles in volume of carrier gas
Ξ	fissility
ρ	density
σ	electrical conductivity or Stefan-Boltzman number
σ_g	geometric standard deviation
X_{+j}	point composition at point $+j$ from center of particle
Ω	molar volume

(equations formulated with SI units)

acronyms:

ACGIH	American Conference of Governmental Industrial Hygienists
CMD	count median diameter
CrVI	hexavalent chromium
CTWD	contact tip to work distance
DCEP	direct current electrode positive
FCAW	flux-cored arc welding
GMAW	gas metal arc welding
GTAW	gas tungsten arc welding
ipm	inches per minute
MMD	mass median diameter
OSHA	Occupational Safety and Health Administration
PEL	Permissible Exposure Limit
SMAW	shielded metal arc welding
TLV	Threshold Limit Value
TWA	time-weighted-average
wfs	wire feed speed

(see Chapter 4 for acronyms of chemical and particle size analysis methods)

Acknowledgements

Textbooks and Heaven only are Ideal;
Solidity is an imperfect state.
Within the cracked and dislocated Real
Nonstoichiometric crystals dominate.
Stray Atoms sully and precipitate;
Strange holes, excitons, wander loose; because
Of Dangling Bonds, a chemical Substrate
Corrodes and catalyzes …

from "The Dance of Solids" by John Updike
in <u>Midpoint and Other Poems</u>, Alfred A. Knopf, 1969

Chapter 1

Introduction

High-temperature metallurgical processing, like welding, can cause significant evaporation. In gas metal arc welding (GMAW), this can be about 10% of the consumable electrode. Vaporization is also significant in other processes like thermal spraying, combustion, casting and any laser or electron-beam manufacturing. When the vapor condenses, submicron airborne particles are formed. The composition of such particles can vary with size (Cox, et al., 1985; Dams & Zhang, 1987; Linak & Wendt, 1993; Narayana, et al., 1995).

Chemical heterogeneity with size is important for manufacturing and is critical in industrial hygiene because the respirability of airborne particles is dependent on particle size, which can affect exposure to a possible toxin. Particles smaller than 100
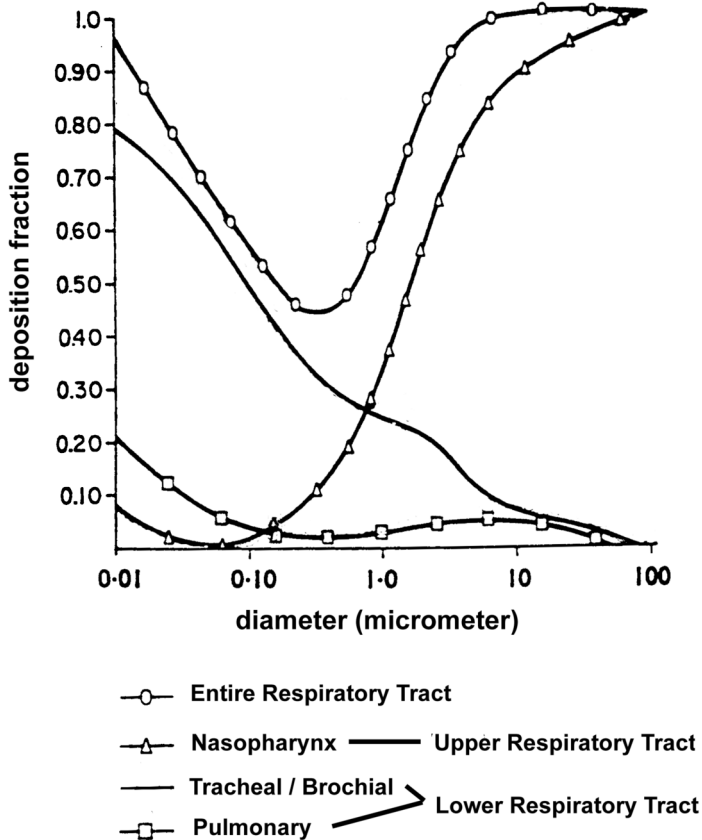
Figure 1.1 Deposition of particles in human respiratory tract (2150 ml tidal volume) (International Commission on Radiological Protection, 1966).
 Reprinted by permission of Lippincott, Williams & Wilkins.

micrometers can be airborne, but not all airborne particles are deposited in the lungs (see Figure 1.1). Objects greater than 10 micrometers in size are trapped on the
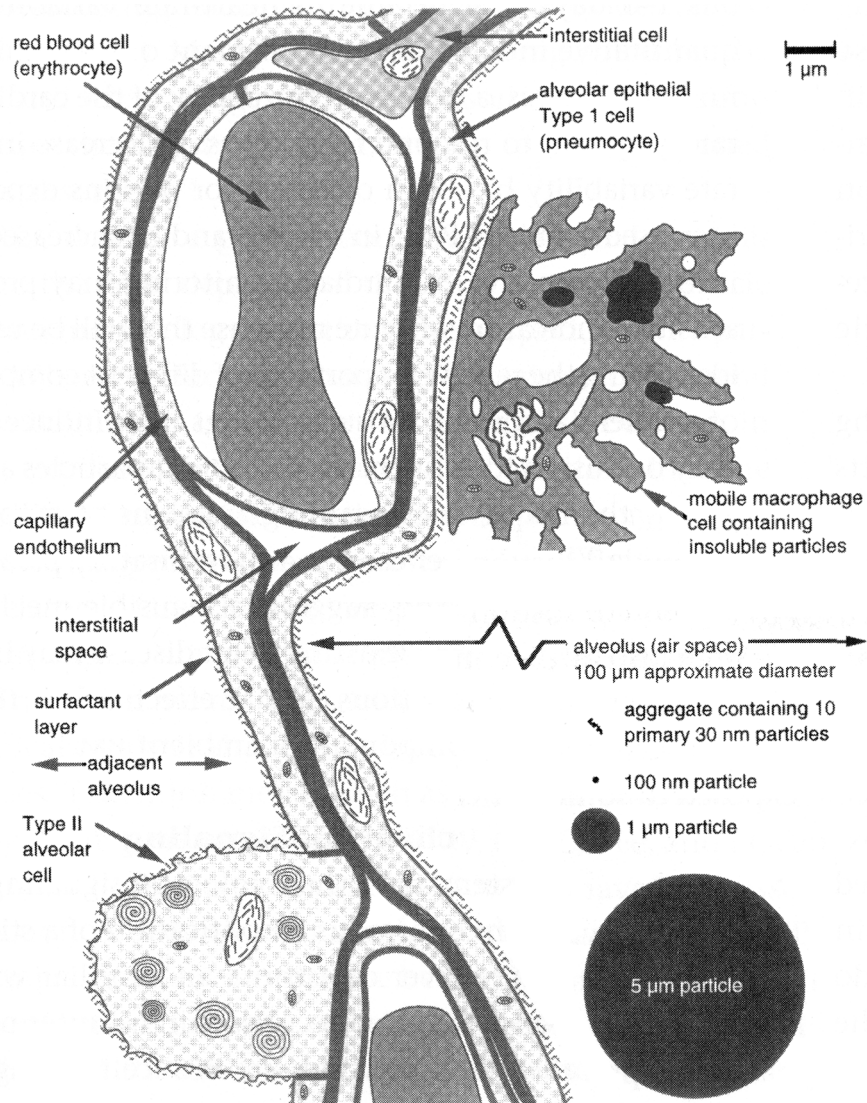
Figure 1.2 Size scale of particles in human lung (Lighty, et al., 2000).
Reprinted by permission of Air & Waste Management Association.

walls of the human airway before they reach the lungs and are carried away in the mucus, which is then transported to the digestive tract. Particles smaller than 0.1 micrometer are inhaled and deposit in the lungs (Figure 1.2). Particles or agglomerates between 0.1 and 1 micrometer can be exhaled, meaning that only about 30% of particles of this size eventually deposit in the lungs where they eventually dissolve into the blood (Hewett, 1995).

Increasing numbers of industrial applications, such as powder metallurgy, electromagnetic coatings, optical fibers, catalysts and sunscreens, incorporate submicron particles. The nanopowder market, which comprises these and other products, is projected to double between 2000 and 2005 to almost $1 billion (Rittner, 2002).

Quite generally, particles are formed one of three ways: 1. from solids and liquids by mechanical means (e.g., grinding or liquid atomization), 2. chemically in solutions and colloids or 3. from a vapor by condensation. Particles formed mechanically under natural conditions are at least 1 micrometer in diameter (unless fabricated means with certain materials are employed, such as special mechanical attrition or electrostatic capillaries). Particles chemically formed from an aqueous solution can be of almost any reasonable size, but such solutions are not commonly used in high-temperature processes and thus this path is not considered here. Particles created by condensation are 0.001 to 1 micrometer in diameter (Kodas & Hampden-Smith, 1999). Because condensation methods are the easiest to scale up for manufacturing, they are the main source of such powders.

Condensed ultrafine powders used in manufacturing are created with heat sources like: resistive heating (Gleiter, 1989), exploding wires (Kotov & Samatov, 1999), ion sputtering (Gurav, et al. 1993), laser evaporation or ablation (Rieheman, 1998), thermal plasmas (Dong, et al. 1999; Balabanova, 2000), and flames (Axelbaum, et al., 1997). For a good review, see Gurva, et al., 1993.

Control of particle size has been extensively studied. For example, researchers have found that small particle size is best achieved with high cooling rates, low evaporation temperatures, low pressures and low molecular weight of the inert carrier gas and low metal vapor concentration (Panda & Pratsinis, 1995). However, controlling the chemistry of condensed material can be difficult; more so than controlling that of particles formed mechanically or chemically (Kodas & Hampden-Smith, 1999).

The change in chemistry with particle size can be explained by principles of aerosol science and physical chemistry, as illustrated by a study of fume (particulate material that condenses from metal vapor) formed during welding. Welding fume is also of particular concern for health reasons.

There are nearly 0.5 million workers who perform welding and cutting operations full-time in the United States (Bureau of Labor Statistics, 2001) and as many as 1 million to 2 million additional workers weld intermittently. Welding is essential to the construction of modern naval vessels, among other fabrication.

Arc welding can be dangerous. Physical hazards include heat, noise and vibration, and electrical power. Radiation from the arc can cause eye and skin damage. Chemicals in the welding environment are found in gases and respirable particles and each of these chemicals can create adverse side effects after ingestion, when delivered in the appropriate dose and chemical state.

Carbon and low alloy steels represent 90% of all metal used in the world. Welders are primarily exposed to the elements in steel: iron, manganese and silicon. Iron and its oxides are metabolized in the human body, but silicon dioxide can be a lung irritant and manganese and its oxides can be neurotoxins. Approximately 5% of all metal fabrication requires stainless steel, which also contains chromium and nickel.

Hexavalent chromium and nickel are of concern because they can be carcinogenic in certain circumstances (Antonini, et al., 1998).

Epidemiological studies have demonstrated that welders are more likely than the general populace to develop acute metal fume fever, acute chemical pneumonitis and chronic bronchitis. They also may have a higher risk of lung cancer, but the causes of this risk are uncertain because confounding variables such as tobacco use and asbestos exposure, have not been adequately taken into account (Sferlazza & Beckett, 1991).

The solid chemical compounds released into the environment by welding enter the human body chiefly through the inhalation of fume. Arc welding causes about 10% of the consumable welding electrode to vaporize. Most of the vapor recondenses in the weld pool, but approximately one-tenth of it (about 1% of the electrode) travels out of the high-temperature arc region and condenses into metal oxide nanoparticles that aggregate into submicron clusters (Haidar, 1999).

Primary particles of welding fume range in size from a few nanometers to a few hundred nanometers. They exist in aggregates ranging from 0.01 to 2 micrometers (Voitkevich, 1995). A small fraction of unagglomerated particles may be in the range of 1 to 100 micrometers (Deam, et al., 1997), meaning that welding fume particles have a high probability of deposition in the lung alveoli.

Welding fume is composed of complex particles, most of which consist of metal oxides and of materials from electrode coatings. Major elements found include iron, manganese, chromium, nickel, silicon, potassium, sodium, calcium, titanium, aluminum, magnesium, fluorine, and oxygen. Chromium, nickel and manganese in their pure states are the most toxic, but they are not pure in welding fume. It is not possible to analyze overall toxicity based on the individual toxicities of the respective components. While two chemicals may be nontoxic when ingested alone, they may prove fatal when ingested together, or vice versa. For example, pure manganese oxide has been shown to cause neurological damage, but it has been hypothesized that iron ingested along with manganese will block the transport of manganese across the blood-brain-barrier, thus preventing neurological harm (Aschner & Aschner, 1990). The chemical state of the element in question is important also. Manganese is the most toxic element found in carbon steel welding fume. Its toxicity varies with valence state: +4 is the most toxic (Voitkevich, 1995). Hexavalent chromium is carcinogenic, but trivalent chromium is not. In addition, insoluble hexavalent chromium compounds are more toxic than soluble hexavalent chromium compounds (Cohen, 1997). The total volume deposited in the lung cells and the aerosol surface are also important factors for the induced pathological reactions. Insoluble particles deposited in the lung are scavenged by alveolar macrophage cells. The ability of these cells to clear the lung is affected by the total deposited volume of the aerosols. The chemistry and conformation of the particle surface influence the interactions with the alveolar macrophages. Toxic aerosols can change cell function (mutagenity, cell damage) or encourage growth of nearby epithelium cells (Haferkamp, 1998).

In 1995, the American Conference of Governmental Industrial Hygienists (ACGIH) reduced the Threshold Limit Value (TLV) for manganese airborne particulate from 1000 μ g/m^3 to 200 μ g/m^3. It has also announced plans to reduce the TLV for insoluble nickel compounds from 1000 μ g/m^3 to 100 μ g/m^3 and to 50 μ g/m^3 for soluble compounds. More importantly, the Occupational Safety and Health Administration (OSHA) has indicated that it will reduce the Permissible Exposure Limit (PEL) for hexavalent chromium (as chromates) from the present ceiling value of 100 μ g/m^3 to an eight-hour time-weighted-average (TWA) between 0.5 μ g/m^3 and 5.0 μ g/m^3 (National Shipbuilding Research Program, 1996).

A Navy / Industry Task Group estimated that it would cost the U.S. Navy initially \$3 to \$22 million and afterwards \$5 to \$46 million annually to comply with the proposed OSHA hexavalent chromium PEL. The magnitude of the cost will naturally depend on how much the PEL is lowered (National Shipbuilding Research Program, 1996).

The OSHA and ACGIH standards are based on studies of chromium in electroplating shops (Beckett, 1996) and manganese from paint pigments and in mines. While it is known that manganese and chromium are present in welding fume, their exact chemical forms are not completely understood. They may or may not be similar to the chemistry of chromium and manganese introduced into the environment by other industrial processes. The chemical reactivity of the components of welding fume must be analyzed in order to determine whether data from other industries are applicable to welding fume. Without such information, OSHA will assume that the chemistry is the same and will produce standards that will severely restrict welding activity. By comparing an informed study of welding fume chemistry to known toxic effects of manganese and chromium, the U.S. Navy, OSHA and others will be able to more accurately assess whether the restrictions on welding fume are required to protect worker's health.

The initial interest in the relationship between particle size and fume composition was caused by the failure of researchers (listed in Chapter 2) to adequately explain the dependence of bulk fume chemistry on welding parameters. For example, the decrease in the amount of volatile elements in welding fume created under globular conditions when compared to fume created from spray, has been blamed on non-vapor fume formation, oxygen-aided evaporation, spatter combustion, volatile oxides, or electrode droplet surface temperature variations.

These explanations are too simplistic because the particles found in welding fume are not strictly uniform and homogeneous. However, it will be shown in Chapter 3 that welding fume is composed of typical airborne particles and therefore can be described with general aerosol science. In Chapter 4, ways to correctly analyze the chemistry of particles will be described and in Chapter 5, they will be applied to welding fume. This knowledge can then be correctly coupled with thermochemical data in order to understand the relationships between particle composition and particle size. The insight gained from studying welding fume can be applied to airborne particles formed in other metallurgical processes.

In summary, the question to be answered in this thesis is:

What is the relationship between the size and composition of airborne particles formed from metallurgical processing?

References

Antonini, J. M., Krishna Murthy, G. G., Rogers, R. A., Albert, R., Eagar, T. W., Ulrich, G. D., & Brain, J. D. (1998). How welding fumes affect the welder. *Welding Journal*, 77(10), 55–59.

Aschner, M., & Aschner, J. L. (1990). Manganese transport across the blood-brain barrier: Relationship to iron homeostasis. *Brain Research Bulletin*, 24, 857–860.

Axelbaum, R. L., Dufaux, D. P., Frey, C. A., & Sastry, S. M. L. (1997). A flame process for synthesis of unagglomerated, low-oxygen nanoparticles: Application to Ti and TiB2. *Metallurgical and Materials Transactions B*, 28B, 1199.

Balabanova, E. (2000). Mechanism of nanoparticle generation by high-temperature methods. *Vacuum*, 58(2–3), 174–182.

Beckett, W. S. (1996). Chapter 42: Welding. In P. Harbor, M. B. Schenker & J. R. Balmes (Eds.), *Occupational and Environmental Respiratory Disease*. St. Louis: Mosby-Year Book, Inc.

Bureau of Labor Statistics. (2001). Welders, cutters, and welding machine operators. *Occupational Outlook Handbook*, 2000–2001.

Cohen, M. D., Kargacin, B., Klein, C. B., & Costa, M. (1993). Mechanisms of chromium carcinogenicity and toxicity. *CRC Critical Review of Toxicology*, 23, 255–281.

Cox, X. B., Linton, R. W., & Butler, F. E. (1985). Determination of chromium speciation in environmental particles - multitechnique study of ferrochrome smelter dust. *Environmental Science & Technology*, 19(4), 345-352.

Dams, R., & Zhang, Y. (1987). Elemental composition of dust in an iron foundry as determined by instrumental neutron activation analysis. *Journal of Radioactive and Nuclear Chemistry*, 110(2), 305–320.

Deam, R., Bosworth, M., Chen, Z., French, I., Haidar, J., Lowke, J., Norrish, J., Tyagi, V., & Workman, A. (1997). Investigation of fume formation mechanisms in GMAW. *Proceedings of the Technological Developments and Advances for Australian Industry, 1997 International Welding and Joining Research Conference*, Silverwater, Australia: Welding Technology Institute of Australia.

Dong, X. L., Zhang, Z. D., Zhao, X. G., Chuang, Y. C., Jin, S. R., & Sun, W. M. (1999). The preparation and characterization of ultrafine Fe-Ni particles. *Journal of Materials Research*, 14(2), 398–406.

Gleiter, H. (1989). Nanocrystalline materials. *Progress in Materials Science*, 33, 223–228.

Gurav, A., Kodas, T., Pluym, T., & Xiong, Y. (1993). Aerosol processing of materials. *Aerosol Science and Technology*, 19(4), 411–452.

Haferkamp, H., Bach, F. W. Goede, M. Puester, T., & Seebaum, D. (1998). Emissions generated during laser cutting and safety precautions. *Welding in the World*, 41, 169–176.

Haidar, J. (1999). An analysis of heat transfer and fume production in gas metal arc welding. III. Journal of Applied Physics, 85(7), 3448-3459.

Hewett, P. (1995). Estimation of regional pulmonary deposition and exposure for fumes from SMAW and GMAW mild-steel and stainless-steel consumables. *American Industrial Hygiene Association Journal*, 56(2), 136–142.

International Commission on Radiological Protection. (1996). Task group on lung dynamics, depositions and retention models for internal dosimetry of the human respiratory tract. *Health Physics*, 21, 173–207.

Kodas, T. T., & Hampden-Smith, M. J. (1999). *Aerosol Processing of Materials*. New York: Wiley-VCH.

Kotov, Y. A., & Samatov, O. M. (1999). Production of nanometer-sized AlN powders by the exploding wire method. *Nanostructured Materials*, 12, 119–122.

Lighty, J., Veranth, J., & Sarofim, A. (2000). Combustion aerosols: Factors governing their size and composition and implications to human health. J*ournal of The Air & Waste Management Association*, 50(9), 1565–1618.

Linak, W. P., & Wendt, J. O. L. (1993). Toxic metal emissions from incineration—mechanisms and control. *Progress In Energy and Combustion Science*, 19(2), 145–185.

Narayana, D. S. S., Sundararajan, A. R., Manjula, B., Kumari, S. C. V., & Subramanian, V. (1995). Chemical characteristics of stainless steel welding fumes. *Journal of Aerosol Science*, 26, S531–S532.

National Shipbuilding Research Program (1996). *Impact of Recent and Anticipated Changes in Airborne Emission Exposure Limits on Shipyard Workers* NSRP 0463, March, University of Michigan.

Panda, S., & Pratsinis, S. E. (1995). Modeling the synthesis of aluminum particles by evaporation-condensation in an aerosol flow reactor. *Nanostructured Materials*, 5(7–8), 755–767.

Rittner, M.N. (2002) Market analysis of nanostructured materials, *American Ceramic Society Bulletin*, 81, 11–4.

Riehemann, W. (1998). Synthesis of nanoscaled powders by laser-evaporation of materials. *Proceedings of the Materials Research Society Symposium*, 501, 3–14.

Sferlazza, S. J., & Beckett, W. S. (1991). The respiratory health of welders. *American Review of Respiratory Diseases*, 143, 1134–1148.

Voitkevich, V. (1995). *Welding Fumes: Formation, Properties and Biological Effects*. Cambridge, England: Abington Publishing.

Chapter 2

Previous Research on Welding Fume

Extensive welding fume research started in the late seventies; since then there have been about 300 publications on the subject (see reference list), including at least 7 doctoral dissertations, 5 masters theses, 7 reports published by various welding societies and an international conference. Many, including but not limited to those listed, report toxicological data such as epidemiologies and animal studies.

About 30 publications are concerned with just measuring welding fume formation rates. Approximately 50 reports are solely about the characterization of the bulk chemistry of welding fume. Of those, 17 measure hexavalent chromium content, 10 investigate the crystallographic structure and phase composition, and 8 analyze the surface of welding fume.

Another 50 papers develop theories and models to explain the dependence of fume formation on welding parameters. Of those, approximately 20 attempt to predict the bulk fume chemistry, but do not take account of the size or origin of fume particles.

About 25 papers and reports analyze the size distribution of welding fume through various methods. Of these, 5 are concerned with how particle size affects deposition during inhalation. Eight publications study the chemical composition of individual particles. Information about the previous research into welding fume particle size will be presented later.

2.1 General Welding Fume Information

Bullough, J. (1996). Fume control in arc welding. *Plant Engineer,* 40(6), 20–21.

Cary, H. B. (1994). The importance of being a welder. *Welding Journal,* 73(10), 59–68.

Dare, P. R. M., & Hewitt, P. J. (1984). Welding fume: the problems of comparing electrodes. *Welding and Metal Fabrication,* 52(2), 56–57.

Gorbach, V. D., Koryukaev, Y. S., Safiulin, N. S., & Stegantsev, V. P. (1998). Safety of labour and environment protection as factors taken into account when planning and applying welding and cutting processes in Russian shipbuilding. *Commission XII of the International Institute of Welding – Welding in the World*.

Hewitt, P. J. (1996). Health and safety in metal arc welding. *Proceedings of the IIW Asian Pacific Welding Congress*, Auckland, New Zealand, W. Scholz (Ed.). Cambridge, England: Abington.

Hobbs, P. J. (1992). The source and control of welding fume. *Welding and Metal Fabrication,* 60(7), 316, 318.

Howden, D. G. (1992). Emission of fumes and gases during welding (Emissao de fumos e gases na soldagem). *Proceedings of the Latin American Regional Welding Congress, Rio de Janiero, 4–10 April 1992*, Sao Paulo, Brazil: Associacao Brasileira de Soldagem.

Howden, D. G. (1996). Origin and magnitude of fumes and harmful gases in welding (Origen y magnitud de los humos y gases nocivos en el soldeo). *Soldadura y Tecnologias de Union,* 7(39), 31–44.

Long, N. J. T. (1987). Welding fume control. *Welding & Metal Fabrication,* 55(7), 217–219.

Louloudes, D. T. (1996). Welding fume and its answers (Humos de soldadura y sus soluciones). *Soldadura y Tecnologias de Union,* 7(37), 34–40.

Krause, H.-J., & Press, H. (1986). Measurement of the welding fume quantities and analysis of the fume composition during resistance welding. *Proceedings of the International Conference on Health hazards and Biological Effects of Welding Fumes and Gases*, R. M. Stern, A. Berlin, A. Fletcher, K. Hemminki, J. Jarvisalo & J. Peto (Eds.). Amsterdam: Excerpta Medica.

National Shipbuilding Research Program (1996). *Impact of Recent and Anticipated Changes in Airborne Emission Exposure Limits on Shipyard Workers NSRP 0463,* March, University of Michigan.

Oakley, P. J. (1976). The problems of fumes in the welders environment. *Welding Journal,* June, 465–472.

Oakley, P. J. (1979). Ways to measure rates of fume emission. *Welding Design and Fabrication,* 52(11), 74–76.

Ohmi, T., Miyoshi, S., Shirai, Y., & Kojima, T. (1995). Metal fume-free welding technology for advanced semiconductor grade gas delivery system. *Journal of the Electrochemical Society,* 142(7), 2362–2372.

Olander, L. (1985). Welding fume buoyant plume. *Aerosol Science and Technology,* 4(3), 351–358.

Pumphrey, T. (1999). Arc-welding fume control. *Welding Design and Fabrication,* Februrary (48, 50, 52).

Reding, L. (1992). Controlling welding fume: a design approach. *Welding Journal,* September, 61.

Smith, D. C. (1970). Flux-cored electrodes - their composition and use. *Welding Journal,* 49(7), 535–547.

2.2 Effect of Welding Fume Exposure on Health

Antonini, J. M., Krishna Murthy, G. G., Rogers, R. A., Albert, R., Eagar, T. W., Ulrich, G. D., & Brain, J. D. (1998). How welding fumes affect the welder. *Welding Journal,* 77(10), 55–59.

Antonini, J. M., Clarke, R. W., Krishna Murthy, G. G., Sreekanthan, P., Jenkins, N. T., Eagar, T. W., & Brain, J. D. (1998). Freshly generated stainless steel welding fume induces greater lung inflammation in rats as compared to aged fume. *Toxicology Letters,* 98, 77–86.

Becker, N. (1999). Cancer mortality among arc welders exposed to fumes containing chromium and nickel. *Journal of Occupational and Environmental Medicine,* 41(4), 294–303.

Brown, K. (2000). Fume composition related to welding process and consumables. *Welding in the World,* 44(1), 39.

Cecchetti, G. (1986). Environmental monitoring of welding fumes and gases. *Proceedings of the International Conference on Health Hazards and Biological Effects of Welding Fumes and Gases*, R. M. Stern, A. Berlin, A. Fletcher, K. Hemminki, J. Jarvisalo & J. Peto (Eds.). Amsterdam: Excerpta Medica.

Clapp, D. E., & Owen, R. J. (1977). An investigation of potential health hazards of arc welding fume growth with time. *Welding Journal,* 56(12), 380s–385s.

Coate, W. B. (1985). *Toxicity of Welding Fume in Rats*. Miami, FL: American Welding Society.

Coenen, W., Grothe, I., Kuhnen, G., Pfeiffer, W., & Schenk, H. (1985). Welding Fume Exposure At Workplaces - Nickel and Chromate In Welding Fume. *Staub Reinhaltung der Luft,* 45(11), 512–515.

Danielsen, E., Langård, S., & Andersen, A. (2000). Incidence of cancer among welders and other shipyard workers with information on previous work history. *Journal of Occupational and Environmental Medicine,* 42(1), 101–109.

Duarte, S. (1994). Welding fume filters: are they all the same? *Welding Design & Fabrication,* 67(9), 28–30.

Gray, C. N., Hewitt, P. J., & Dare, P. R. M. (1982). New approach would help control welding fumes at source (MIG and MMA) Part one: Biomedical background. *Welding and Metal Fabrication,* September, 318–324.

Hewitt, P. (1996). Occupational health in metal arc welding. *Indoor Built Environment,* 43(5), 253–262.

Koch, D. (2000). The basics of respiratory protection. *The American Welder,* March/April, 11–14.

Matczak, W., & Chmielnicka, J. (1993). Relation between various chromium compounds and some other elements in fumes from manual metal arc stainless steel welding. *British Journal of Industrial Medicine,* 50(3), 244–251.

Nielsen, R., Gwosdow, A. R., Berglund, A. G., & Dubois, A. B. (1987). The effect of temperature and humidity levels in as protective mask on user acceptability during exercise. *American Industrial Hygiene Association,* 48, 639–645.

Sferlazza, S. J., & Beckett, W. S. (1991). The respiratory health of welders. *American Review of Respiratory Diseases,* 143, 1134–1148.

Spiegel–Ciobanu, V.-E. (1995). *Hazardous Substances in Welding and Allied Processes ZH 1/223 Edition 1995,* Translation of "Schadstoffe in der Schweisstechnik": Norddeutsche Metall-Berufsgenossenschaft.

Stettler, L. E., Groth, D. H., & Mckay, G. R. (1977). Identification of stainless steel welding fume particles in human lung and environmental samples using electron probe microanalysis. *American Industrial Hygiene Association Journal,* 38(2), 76–82.

Titus, A. C., & et al. (1935). Electric welding I. the respiratory hazard. *Journal of Industrial Hygiene,* 17(4), 121–128.

2.3 Methods for Formation Rate Measurement

American Welding Society. (1992). *Method for Sampling Airborne Particulates Generated by Welding and Allied Processes ANSI/AWS F1.1-92*. Miami, FL: American Welding Society.

Brown, K. L. (1996). Development of environmental release estimates for welding operations. *Proceedings of the IIW Asian Pacific Welding Congress 4–9 February 1996, Auckland, New Zealand*, New Zealand Welding Committee, W. Scholz (Ed.). Cambridge, England: Abington.

Miller, T. M., & C., J. R. (1979). An assessment of the fume characteristics of Australian electrodes for manual metal arc welding. *Australian Welding Research,* January, 1–9.

Moreton, J. (1982). Assessment of welding fume hazards. *Annals of Occupational Hygiene,* 25(4), 421–430.

Moreton, J. (1986). The case for standardization of tests for welding fume emission rate and chemical composition determination. *Annals of Occupational Hygiene,* 30, 435–444.

Rihar, G., & Suban, M. (1996). Fume emission in arc welding*. Proceedings of the International Conference for Filler Materials and Other Consumables for Welding and Allied Techniques,* Porec, Croatia, Hrvatsko Drustvo Za Tehniku Zavarivanja (Croatian Welding Society), S.Kralj (Ed.). Zagreb, Croatia.

2.4 Formation Rate Measurements

BOC Gases. (1994). Shielding gas, wire type have drastic effect on fume emissions. *Welding Design and Fabrication,* 67(7), 14.

Castner, H. R. (1995). Gas metal arc welding fume generation using pulsed current. *Welding Journal,* 74(2), S59–S68.

Castner, H. R. (1996). Fume generation rates for stainless steel, nickel and aluminum alloys. *Welding Journal,* 75, 393s–401s.

Eichhorn, R., & Oldenburg, T. H. (1986). Welding fumes emitted during welding of high-alloyed materials - evaluation of amount, chemical composition and morphology, including the influence of welding parameters*. Proceedings of the Conference of Health Hazards and Biological Effects of Welding Fumes and Gases*, R. M. Stern, et al. (Ed.). Amsterdam: Excerpta Medica.

Floreani, A., & Ascanio, C. (2000). *Influence of Welding Wire Copper Coating in the GMA Welding Process and Fumes IIW/CVIII N 1897* Report of the International Institute of Welding.

French, I. E., Tyagi, V. K., & Brooks, G. (1996). The influence of power source characteristics on particulate fume generation and composition. *Proceedings of the IIW Asian Pacific Welding Congress 4–9 February 1996*, Auckland, New Zealand, W. Scholz (Ed.). Cambridge, England: Abington.

Golovatyuk, A., & Levchenko, O. (1985). Parameters of mass generation and [arc] welding aerosols and their use in practice. *Welding Production,* 32(10), 42–44.

Harris, I. D. (2000). Fume generation in GMAW and FCAW*. Proceedings of Conference for Gas Metal Arc Welding for the 21st Century,* American Welding Society & Edison Welding Institute, Orlando Florida: American Welding Society.

Henderson, I. D., Lowe, W. H., Powell, G. L. F., & Herfurth, G. (1988). Fume rates of gas-shielded and open-arc wires for hardfacing and surfacing; AWRA research contract 105. *Australian Welding Research,* 16, 44–46.

Henderson, I. D., Senff, U. E., & Wilson, A. J. (1986). Fume generation and chemical analysis of fume for a selected range of flux-cored structural steel wires. *Australian Welding Research,* 15, 4–11.

Hilton, D. E., & Plumridge, P. N. (1991). Particulate fume generation during GMAW and GTAW. *Welding and Metal Fabrication,* December, 555–560.

Jakubcik, L. (1999). Effect of shielding atmosphere composition on aerosol production in MAG welding of unalloyed steels (Vliv slozeni ochranne atmosfery na produkci …). *Zvaranie/Svarovani,* 48(3), 65–66.

Lyttle, K. A. (1999). Decrease fume, increase productivity: optimized consumables selection for an improved working environment and reduced welding costs. *Proceedings of 1999 International Conference of the International Institute of Welding International Institute of Welding*, International Institute of Welding.

Moreton, J. (1985). Fume emission rates for open-arc welding processes. *Metal Construction,* 17(5), 308–310.

Moreton, J., Smars, E. A., & Spiller, K. R. (1985). Fume emission when welding stainless steel. *Metal Construction,* 17, 794–798.

Press, H., & Florian, W. (1985). Formation of toxic substances in gas shielded arc welding. *Welding in the World,* 23, 1–23.

Quimby, J. B., & Ulrich, G. D. (1999). Fume formation rates in gas-shielded metal arc welding. *Welding Journal,* April, 142–149.

Tandon, R. K., Crisp, P. T., Ellis, J., & Baker, R. S. (1983). Variation in the chemical composition and generation rates of fumes from stainless steel electrodes under different AC welding conditions; AWRA Contract 90. *Australian Welding Journal,* Autumn, 27–30.

Willingham, D. C., & Hilton, D. E. (1986). FFR effects of argon and helium based gases. *Welding and Metal Fabrication,* 54, 228–229.

Willingham, D. C., & Hilton, D. E. (1986). Some aspects of fume emissions from MIG welding stainless steel. *Welding and Metal Fabrication,* July, 226–229.

Wisniewski, G. (1991). The effect of MAG arc welding parameters on environmental pollution. *Welding International,* 5(12), 949–953.

Xin, H., Geng, Z., & North, T. H. (2001). Fume generation during solid- and metal-cored wire welding. *Welding Journal,* 7, 173s–183s.

2.5 Formation Theories and Models

Bosworth, M., & Farmer, A. (1999). Metal vapour transfer in GMAW [MIG/MAG welding] and its contribution to fume formation. *Australasian Welding Journal,* 44, 42–47.

Bosworth, M., & Gordon, T. (1999). The influence of power source characteristics on Cr(VI) in fume generated during GMAW [MAG welding] of stainless steel. *Australasian Welding Journal,* 44, 48–51.

Bosworth, M. R., & Deam, R. T. (2000). Influence of GMAW droplet size on fume formation rate. *Journal of Physics D - Applied Physics,* 33(20), 2605–2610.

Caram, H. S., & Turkmen, N. (2002). Pulsing parameters to control metal transfer and fume formation rates in GMAW. *Presentation at Edison Welding Institute,* Columbus, Ohio.

Corderoy, D. J. H., Wills, B., & Wallwork, G. R. (1980). Gas/weld metal reactions in MIG arc plasm*a. Proceedings of the International Conference of Weld Pool Chemistry and Metallurgy,15–17 April 1980 London,* N. Bailey (Ed.). Cambridge, England: The Welding Institute, Abington Hall.

Deam, R. T., Simpson, S. W., & Haidar, S. W. (2000). A semi-empirical model of the fume formation from gas metal arc welding. *Journal of Physics D - Applied Physics,* 33(11), 1393–1402.

Dennis, J. H., Hewitt, P. J., Redding, C. A. J., & Workman, A. D. (2001). A model for prediction of fume formation rate in gas metal arc welding (GMAW), globular and spray modes, dc electrode positive. *Annals of Occupational Hygiene,* 45(2), 105–113.

Ferree, S. E. (1995). New generation of cored wires creates less fume and spatter. *Welding Journal,* December, 45.

Grong, O., & Christensen, N. (1983). Factors controlling MIG weld metal chemistry. *Scandinavian Journal of Metallurgy,* 4, 155–165.

Haidar, J. (1999). An analysis of heat transfer and fume production in gas metal arc welding. III. *Journal of Applied Physics,* 85(7), 3448–3459.

Heile, R. F., & Hill, D. C. (1975). Particulate fume generation in arc welding processes. *Welding Journal,* 54(7), 201s–210s.

Hewitt, P. J., & Madden, M. G. (1988). The influence of gas composition and flow rate on fume formation in the micro and macro environments of welding arcs. *Proceedings of the 2nd International Symposium of Ventilation for Contaminant Control 20–23 September 1988, London,* The British Occupational Hygiene Society, Oxford: Pergamon Press.

Ioffe, I., Maclean, D., Perelman, N., Stares, I., & Thornton, M. (1995). Fume formation rate at globular to spray mode transition during welding. *Journal of Physics - D Applied Physics,* 28(12), 2473–2477.

Irving, B. (1992). Inverter power sources check fume emissions in GMAW. *Welding Journal,* February, 53–57.

Kobayashi, M., Maki, S., Hashimoto, Y., & Suga, T. (1978). Some considerations about formation mechanism of welding fumes. *Welding in the World, Le Soudage Dans Le Monde,* 16((11/12)), 238–249.

Kobayashi, M., & Suga, T. (1985). Fume generation in CO_2 arc welding. *R&D, Research and Development (Kobe Steel, Ltd),* 35, 12–16.

Levchenko, O. (1992). Effect of CO_2 welding conditions of structural steels on fume formation. *Paton Welding Journal,* 4(9–10), 525–527.

Levchenko, O. (1996). Processes of welding fume formation (review). *Paton Welding Journal,* 8, no.4, April, 210–215.

Levchenko, O. (1998). Methods of reducing the generation of welding fumes (review). *Welding International,* 12, no.9, 747–752.

Ma, J., & Apps, R. L. (1982). MIG transfer discovery of importance to industry. *Welding and Metal Fabrication,* September, 307–316.

Ma, J., & Apps, R. L. (1983). Analysing metal transfer during MIG welding. *Welding and Metal Fabrication,* 51(3), 119–122.

Ma, J., & Apps, R. L. (1983). New MIG process results from metal transfer mode control. *Welding and Metal Fabrication,* 51(4), 168–170.

Malmquist, K. G., Johansson, G., Bohgard, M., & Akelsson, K. (1986). Process dependent characteristics of welding fume particles. *Proceedings of the International Conference of Health Hazards and Biological Effects of Welding Fumes and Gases*, R. M. Stern, et al. (Eds.). Amsterdam: Elsevier Science.

Malyshev, N. I. (1984). Limiting stage of evaporation of manganese from electrode droplets in arcing in argon. *Welding Production (Svarochnoe Proizvodstvo),* 31(10), 17–19.

Medack, J., & Heinze, B. (1990). The emission and composition of welding fumes generated during the mag welding of metal coated sheet. *Welding International,* 4(11), 908–910.

Mendez, P., Jenkins, N. T., & Eagar, T. W. (2000). Effect of electrode droplet size on evaporation and fume generation in gmaw*. Proceedings of the Conference of Gas Metal Arc Welding for the 21st Century, Dec. 6–8, 2000 Orlando, Florida*, Miami, Florida: American Welding Society.

Norin, P. A., & Malyshev, N. I. (1982). Losses of manganese from electrode droplets in arc-welding in air. *Welding Production (Svarochnoe Proizvodstvo),* 29(2), 22–24.

Pokhodnya, I. K., Shvachko, V. I., Yavdoshchin, I. R., & Ponomarev, S. S. (1982). The vaporization of manganese when welding steel. *Avt. Svarka. (Automatic Welding),* 36(11), 24–26.

Somsky, P. (1991). *Fume Generation Control in Inconel 625 Welding with the Pulsed GMAW Process RC349/2/91*: Welding Institute of Canada.

Suga, T., & Kobayashi, M. (1984). Fume generation in CO_2 arc welding by flux-cored wire. *Yosetsu Gakkai Ronbunshu / Quarterly Journal of the Japan Welding Society,* 2(4), 68–75.

Takano, Y., Udagawa, T., & Tam, K. L. (2000). Analysis of generated amount of fume depending on various welding conditions - research on decreasing the welding fumes. *Proceedings of the IIW Asian Pacific Welding Congress 4–9 February 1996, Auckland, New Zealand,* New Zealand Welding Committee, W. Scholz (Ed.). Cambridge, England: Abington

Tandon, R. K., Ellis, J., Crisp, P. T., & Baker, R. S. (1984). Fume generation and melting rates of shielded metal arc welding electrodes. *Welding Journal,* 63(8), 262s–266s.

Thornton, M., & Stares, I. (1994). Analysis of particulate fume generation rates from gas metal arc [GMA] welding. *Welding Review International,* November, 353–365.

Ushio, M., & Suga, T. (1999). Fume generation in CO_2 welding. *Transactions of JWRI,* 28(2), 1–8.

Zhou, S., Norrish, J., & Chen, Z. (1998). Influence of different metal transfer modes on welding fume generation during gas metal arc [GMA (MIG/MAG)] welding. *Proceedings of the 1998 Materials Processing, Biennial Materials. Conference,* Wollongong, Australia: Institute of Materials Engineering Australasia.

2.6 Fume Chemistry Theories and Models

Bosworth, M., & McAllister, T. (1998). Thermal mechanisms for the production of Cr(VI) in welding fume, predictions of welding fume, arc sheath voltages and demixing in arcs, 212-935-98, *CSIRO Telecommunications and Industrial Physics,* Lindfield, Australia: CSIRO.

Buki, A. A., & Feldman, A. M. (1980). Prediction of composition of aerosol formed in welding in shielding gases. *Welding Production (English translation),* 27(2), 8–12.

Dennis, J. H., French, M. J., Hewitt, P. J., Mortazavi, S. B., & Redding, C. A. J. (1996). Reduction of hexavalent chromium concentration in fumes from metal cored arc welding by addition of reactive metals. *Annals of Occupational Hygiene,* 40(3), 339–344.

Dennis, J. H., French, M. J., Hewitt, P. J., Mortazavi, S. B., & Redding, C. J. (2002). Control of exposure to hexavalent chromium and ozone in gas metal arc welding of stainless steels by use of a secondary shield gas. *Annals of Occupational Hygiene,* 46(1), 43–48.

Dennis, J. H., French, M. J., Hewitt, P. J., Mortazavi, S. B., & Redding, C. J. (2002). Control of occupational exposure to hexavalent chromium and ozone in tubular wire arc-welding processes by replacement of potassium by lithium or by addition of zinc. *Annals of Occupational Hygiene,* 46(1), 33–42.

Eagar, T.W. Sreekanthan, P., Jenkins, N. T., Krishna Murthy, G.G., Antonini, J.M. & Brain, J.D. (1998). Study of chromium in gas metal arc welding fume. *Proceedings of the Trends in Welding Conference*, American Welding Society.

Gray, C. N., Hewitt, P. J., & Dare, P. R. M. (1982). New approach would help control welding fumes at source (MIG and MMA) Part two: MIG fumes. *Welding and Metal Fabrication, October,* 393–397.

Gray, C. N., Hewitt, P. J., & Hicks, R. (1980). The prediction of fume compositions in stainless steel metal inert gas welding. *Proceedings of the International Conference of Weld Pool Chemistry and Metallurgy, 15–17 April 1980, London,* N. Bailey (Ed.). Cambridge, England: The Welding Institute, Abington Hall.

Hewitt, P. J., & Hirst, A. A. (1991). Development and validation of a model to predict the metallic composition of flux–cored arc–welding fumes. *Annals of Occupational Hygiene,* 35(2), 223–232.

Hewitt, P. J., & Madden, M. G. (1986). Welding process parameters and hexavalent chromium in MIG fume. *Annals of Occupational Hygiene,* 30, 427–434.

Kobayashi, M., Maki, S., Hashimoto, Y., & Suga, T. (1983). Investigations on chemical composition of welding fumes. *Welding Journal,* 62(7), 190s–196s.

Levchenko, O. (1996). Processes of welding fume formation (review). *Paton Welding Journal,* 8(4), April, 210–215.

Mcallister, T., & Bosworth, M. (1999). Thermal mechanisms for the production of Cr(VI) [hexavalent chromium] in welding fume [in arc welding of stainless steels]. *Australasian Welding Journal,* 44, 42-46.

Podgaetskii, V., Golovatyuk, A., & Levchenko, O. (1989). Mechanism of formation of welding aerosol and prediction of its composition in CO2 welding. *Paton Welding Journal,* 1(8), 561–564.

Tandon, R. K., Ellis, J., Crisp, P. T., Baker, R. S., & Chenhall, B. E. (1986). Chemical investigation of welding fumes from hardfacing and HSLA–steel electrodes. *Welding Journal,* 65(9), S231–S236.

Van Bemst, A., Willi, A., & Delporte, R. (1973). Contribution a l'etude des fumees de soudage et a la determination de saines conditions de travail. Contribution to the Study of Welding Fumes and to the Determination of Healthy Working Conditions. *Revue de la Soudure/Lastijdschrift,* 29(3), 167–182.

Workman, A. D., Hewitt, P. J., & Dennis, J. H. (1997). Predictions of the contribution to fume formation rates from evaporation of metal from droplets formed in gas metal arc welding of steel. *Australasian Welding Journal,* 42(2), 33–37.

2.7 Welding Society Reports & Multiple Technique Characterization

American Welding Society (1990). *Effects of Welding on Health* (Vol. I–IX). Miami, Florida.

R. M. Stern, A. Berlin, A. Fletcher, K. Hemminki, J. Jarvisalo & J. Peto (Eds.). (1986) *Proceedings of the International Conference on Health hazards and biological effects of welding fumes and gases, Copenhagen, 18–21 February 1985*, organized jointly by the Commission of the European Communities (CEC, Luxembourg). Amsterdam: Excerpta Medica.

Eichhorn, F., & Oldenburg, T. (1986). *Untersuchung der Scheissrauchentstehung beim Schweissen mit mittel– und hochlegierten Zusatzwerkstoffen*. Duesseldorf, BRD: DVS.

Evans, R. M., Flanigan, L. J., Howden, D. G., Lee, K. W., Luce, R. G., Martin, D. C., Pattee, H. E., & Robinson, R. E. (1979). *Fumes and Gases in the Welding Environment*, Batelle–Columbus Laboratories. Miami, FL: AWS Research Committee on Safety and Health.

Fasiska, E. J., Wagenblast, H. W., & Nasta, M. (1983). *Characterization of Arc Welding Fume*. Miami, FL: American Welding Society.

Hewitt, P. J., & Gray, C. N. (1983). Some difficulties in the assessment of electric–arc welding fume. *American Industrial Hygiene Association Journal,* 44(10), 727–732.

Iwamoto, N., Umesaki, N., Kamai, M., Kobayashi, M., Tsutsumi, S., Taga, M., & Kume, A. (1984). Behavior of manganese in welding fume (i). *Transactions of JWRI (Japanese Welding Research Institute),* 13, 21–26.

Jenkins, N., Moreton, J., Oakley, P. J., & Stevens, S. M. (1981). *Welding Fume - Sources, Characteristics, Control* (Vol. 1–2). Cambridge, England: The Welding Institute, Abington Hall, Abington.

Tandon, R. K., Crisp, P. T., Ellis, J., Baker, R. S., & Chenhall, B. E. (1984). Chemical investigation of some electric arc welding fumes and their potential health effects. *Australian Welding Research,* 13, 55–60.

Voitkevich, V. (1995). *Welding Fumes: Formation, Properties and Biological Effects*. Cambridge, England: Abington Publishing.

2.8 Hexavalent Chromium Measurements

Castner, H. R., & Null, C. L. (1998). Chromium, nickel and manganese in shipyard welding fumes. *Welding Journal,* 77(6), 223S–231S.

Dyg, S., Anglov, T., & Christensen, J. M. (1994). Preparation of filters loaded with welding dust – a homogeneity and stability study of hexavalent chromium. *Analytica Chimica Acta,* 286(3), 273–282.

Farwer, A., & Schwarzbach, E. (1986). New knowledge on the actual pollution caused by active–gas metal–arc welding of high–alloy and mild steels. *Schweissen und Schneiden,* 38, e54–e56.

Gray, C. N. (1987). Letters to the Editor: Hexavalent chromium in welding fume and the role of ozone. *Annals of Occupational Hygiene,* 31, 269–270.

Gray, C. N., Goldstone, A. M., Dare, P. R. M., & Hewitt, P. J. (1983). The evolution of hexavalent chromium in metallic aerosols. *American Industrial Hygiene Association Journal,* 44, 384–388.

Griffiths, T., & Stevenson, A. C. (1989). Binder developments for stainless electrodes. *Welding Review,* 8, 192–196.

Karlsen, J. T., Torgrimsen, T., & Langard, S. (1994). Exposure to solid aerosols during regular MMA welding and grinding operations on stainless–steel. *American Industrial Hygiene Association Journal,* 55(12), 1149–1153.

Kimura, M., Kobayashi, M., Godai, T., & Minato, S. (1979). Investigations on chromium in stainless steel welding fumes. *Welding Journal,* July, 195s–204s.

Moreton, J., Bettelley, J., Mathers, H., Nicholls, A., Perry, R. W., Ratcliffe, D. B., & Svensson, L. (1983). Investigation of techniques for the analysis of hexavalent chromium, total chromium and total nickel in welding fume: a cooperative study. *Annals of Occupational Hygiene,* 27(2), 137–156.

Moreton, J., Day, S. E., & Jenkins, N. (1986). Fume emission rate measurements and fume analysis on four stainless steel welding consumables. *Proceedings of the International Conference on Health Hazards And Biological Effects Of Welding Fumes And Gases, Copenhagen, 18–21 February 1985* Danish Welding Institute, R. M. Stern, A. Berlin, A. Fletcher, K. Hemminki, J. Jarvisalo & J. Peto (Eds.). Amsterdam: Excerpta Medica.

Mori, T., Matsuda, A., Akashi, S. O., M., Takeoka, K., & Yoshinaka, M. (1991). The 3–dimensional distribution of chromium and nickel–alloy welding fumes. *Acta Medica Okayama,* 45(4), 233–240.

Olah, L., & Pivoluska, J. (1985). Determination of chromium[vi] in welding fumes by radionuclide x–ray fluorescent analysis. *Journal of Radioanalytical And Nuclear Chemistry–Letter,* 96(6), 575–584.

Pedersen, B., Thomsen, E., & Stern, R. M. (1987). Some problems in sampling analysis and evaluation of welding fumes containing Cr(VI). *Annals of Occupational Hygiene,* 31, 325–338.

Spini, G., Profumo, A., Riolo, C., Beone, G. M., & Zecca, E. (1994). Determination of hexavalent, trivalent and metallic chromium in welding fumes. *Toxicological and Environmental Chemistry,* 41(3–4), 209–219.

Thomsen, E., & Stern, R. M. (1979). A simple analytical technique for the determination of hexavalent chromium in welding fumes and other complex matrices. *Scandinavian Journal of Work and Environmental Health,* 5, 386–403.

Thomsen, E., Stern, R. M., & Pedersen, B. (1986). Exposure monitoring and chemical analysis of welding fume*. Proceedings of the International Conference on Health Hazards And Biological Effects Of Welding Fumes And Gases, Copenhagen, 18–21*

February 1985 Danish Welding Institute, R. M. Stern, A. Berlin, A. Fletcher, K. Hemminki, J. Jarvisalo & J. Peto (Eds.). Amsterdam: Excerpta Medica.

Zatka, V. J. (1985). Speciation of hexavalent chromium in welding fumes interference by air oxidation of chromium. *American Industrial Hygiene Association Journal,* 46(6), 327–331.

2.9 Surface Characterization

Grekula, A., Ristolainen, E., Tanninen, V. P., Hyvarinen, H. K., & Kalliomaki, P. L. (1986). Surface and bulk chemical analysis on metal aerosols generated by manual metal arc welding of stainless steel. *Journal of Aerosol Science,* 17, 1–9.

Minni, E. (1986). Assessment of the use of electron spectroscopy and sputtering for studies of solid fume particles. *Proceedings of the International Conference on Health Hazards And Biological Effects Of Welding Fumes And Gases, Copenhagen, 18–21 February 1985* Danish Welding Institute, R. M. Stern, A. Berlin, A. Fletcher, K. Hemminki, J. Jarvisalo & J. Peto (Eds.). Amsterdam: Excerpta Medica.

Minni, E., Gustafsson, T. E., Koponen, M., & Kalliomaki, P.– L. (1984). A study of the chemical structure of particles in the welding fumes of mild and stainless steel. *Journal of Aerosol Science,* 15(1), 57–68.

Minni, E., Hofmann, S., & Sivonen, S. J. (1990). An AES study of particles in the welding fumes of mild and stainless steel. *Surface and Interface Analysis,* 16(1–12), 563–564.

Tandon, R. K., Payling, R., Chenhall, B. E., Crisp, P. T., Ellis, J., & Baker, R. S. (1985). Application of X-ray photoelectron spectroscopy to the analysis of stainless–steel welding aerosols. *Applications of Surface Science,* 20(4), 527–537.

Tanninen, V. P., Hyvarinen, H.–K., Grekula, A., & Kalliomaki, P.–L. (1986). X–ray diffraction and x–ray emission spectroscopy in chemical compound analysis of welding fumes*. Proceedings of the International Conference on Health Hazards and Biological Effects Of Welding Fumes And Gases, Copenhagen, 18–21 February 1985* Danish Welding Institute, R. M. Stern, A. Berlin, A. Fletcher, K. Hemminki, J. Jarvisalo & J. Peto (Eds.). Amsterdam: Excerpta Medica.

Tanninen, V. P., Hyvarinen, H. K., Grekula, A., & Ristolainen, E. (1985). Surface enrichment of the elements in welding fume particles analyzed by auger–electron spectroscopy. *Ultramicroscopy,* 17(2), 182–182.

Voitkevich, V. G. (1988). Etude, par spectroscopie photoelectronique a rayons X, de l'heterogeneite de la composition des particules de fumees de soudage [Investigation of heterogeneity of welding fume particle composition by the method of X-ray photoelectron spectroscopy]. *Welding in the World, Le Soudage Dans Le Monde,* 26, 108–111.

2.10 Phase Composition and Crystallographic Structure

Farrants, G., Reith, A., Schuler, B., & Feren, K. (1988). A simple, direct method for the collection of particles from air samples for transmission electron-microscopy and digital image-analysis. *Journal Of Microscopy–Oxford,* 149, 159–164.

Golovatyuk, A., Levchenko, O., Veblaya, T., Zykov, G., Kharchenko, N., & Levchenko, L. (1984). Application of physical methods for examining the composition of the solid component of welding fumes. *Welding Production (Svarochnoe Proizvodstvo),* 31(3), 43–45.

Hyvarinen, H.–K., Tanninen, V.-P., Grekula, A., & Kalliomaki, P.–L. (1985). Profile fitting analysis of the X-ray powder diffraction pattern of a complicated metal aerosol. *Physica Status Solidi A – Applied Research,* 90(1), K15–K18.

Karlsen, J. T., Farrants, G., Torgrimsen, T., & Reith, A. (1992). Chemical–composition and morphology of welding fume particles and grinding dusts. *American Industrial Hygiene Association Journal,* 53(5), 290–297.

Kobayashi, M., & Tsutsumi, S. (1986). Investigation on crystalline materials in welding fumes of covered electrodes. *Proceedings of the International Conference on Health Hazards and Biological Effects of Welding Fumes and Gases,* R. M. Stern, A. Berlin, A. Fletcher, K. Hemminki, J. Jarvisalo & J. Peto (Eds.). Amsterdam: Excerpta Medica.

Pilyankevich, A. N., & Im, N. (1984). Electron microscopic examination of the solid phase of the fumes formed in electric arc welding. *Welding Production,* 31(3), 46–47.

Rodelsperger, K., Bruckel, B., Barbisan, P., Walter, D., & Woitowitz, H. (2000). The amount of ultrafine particles in welding fume aerosols. *Staub, Reinhaltung Der Luft,* 60(3), 79–82.

Tanninen, V. P., Hyvarinen, H.–K., Grekula, A., & Kalliomaki, P.–L. (1986). X-ray diffraction and X-ray emission spectroscopy in chemical compound analysis of welding fumes*. Proceedings of the International Conference on Health Hazards and Biological Effects of Welding Fumes and Gases*, R. M. Stern, A. Berlin, A. Fletcher, K. Hemminki, J. Jarvisalo & J. Peto (Eds.). Amsterdam: Excerpta Medica.

Tanninen, V. P., Hyvarinen, H. K., Grekula, A., & Kalliomaki, P. L. (1985). Experimental improvements in analysis of aerosol samples by X-ray-powder diffraction. *Journal of Aerosol Science,* 16(5), 373–378.

Tanninen, V. P., Mikkola, E., Hyvarinen, H. K., Grekula, A., & Kalliomaki, P. L. (1985). Determination of the valence of the iron in welding fumes with the k–beta emission–spectrum. *X-Ray Spectrometry,* 14(4), 188–191.

2.11 Other Characterization

Kalliomaki, K., Kalliomaki, P.–L., Kelha, V., & Vaaranen, V. (1980). Instrumentation for measuring the magnetic lung contamination of steel welders. *Annals of Occupational Hygiene,* 23, 175–184.

Iwamoto, N., Makino, Y., Kobayashi, M., Tsutsumi, S., Taga, M., & Kume, A. (1984). ESR study on welding fume. *Transactions of JWRI (Japanese Welding Research Institute,* 13, 35–38.

North, M. R., & Haswell, S. J. (1988). Elemental analysis of welding fumes by x–ray–fluorescence spectrometry. *Journal Of Analytical Atomic Spectrometry,* 3(5), 687–694.

2.12 Particle Size Distribution

Berner, V., & Berner, A. (1982). Mass size distributions and elemental frequency distributions of arc welding smokes. *Journal of Aerosol Science*, 13, 191–193.

Deam, R., Bosworth, M., Chen, Z., French, I., Haidar, J., Lowke, J., Norrish, J., Tyagi, V., & Workman, A. (1997). Investigation of fume formation mechanisms in GMAW*. Proceedings of the Technological Developments and Advances for Australian Industry, 1997 International Welding and Joining Research Conference, 10–12 Nov.1997* Silverwater, Australia: Welding Technology Institute of Australia.

Eichhorn, F., & Oldenburg, T. (1986). *Untersuchung der Scheissrauchentstehung beim Schweissen mit mittel– und hochlegierten Zusatzwerkstoffen*. Duesseldorf, BRD: DVS.

Farrants, G., Schuler, B., Karlsen, J., Reith, A., & Langard, S. (1989). Characterization of the morphological properties of welding fume particles by transmission electron-microscopy and digital image-analysis. *American Industrial Hygiene Association Journal,* 50(9), 473–479.

Gustafsson, T. E., Tossavainen, A., & Aitio, A. (1986). Scanning electron microscopic studies on flame cutting and welding fumes in a steel foundry. *Proceedings of the International Conference on Health Hazards and Biological Effects of Welding Fumes and Gases*, R. M. Stern, A. Berlin, A. Fletcher, K. Hemminki, J. Jarvisalo & J. Peto (Eds.). Amsterdam: Excerpta Medica.

Heile, R. F., & Hill, D. C. (1975). Particulate fume generation in arc welding processes. *Welding Journal,* 54(7), 201s–210s.

Hewett, P. (1991). *Particle Size Analysis of Welding Fumes and Prediction of Regional Pulmonary Deposition.* Ph.D. Thesis: University of Pittsburgh; 0178.

Jin, Y. (1994). Fume generation from gas metal arc–welding processes. *Staub Reinhaltung Der Luft,* 54(2), 67–70.

Ren, J. (1997). *Distribution Of Particles In Welding Fume.* M.S. Thesis: Chemical Engineering University of New Hampshire.

Zimmer, A. T. (2001). Characterization of the aerosols resulting from arc welding processes. *Journal of Aerosol Science,* 32, 933–1008.

Zimmer, A. T., Baron, P. A., & Biswas, P. (2002). The influence of operating parameters on number–weighted aerosol size distribution generated from a gas metal arc welding process. *Journal of Aerosol Science,* 33(3), 519–531.

2.13 Particle Size Distribution and Inhalation Toxicology

Ahlberg, M. S., Hansson, H.–C., & Fangmark, I. (1990). Growth of a welding fume aerosol as a function of relative humidity*. Proceedings of the Third International Aerosol Conference, Aerosols: Science, Industry, Health, and Environment, September 24–27, Kyoto, Japan*, Oxford, England: Pergamon Press.

Hewett, P. (1995). Estimation of regional pulmonary deposition and exposure for fumes from SMAW and GMAW mild–steel and stainless–steel consumables. *American Industrial Hygiene Association Journal,* 56(2), 136–142.

Rudell, B., Akselsson, K. R., & Berlin, M. H. (1988). Growth of welding aerosol particles in high relative humidity and particle deposition in the human respiratory airways. *Journal of Aerosol Science,* 19, 1153–1156.

Spiegel–Ciobanu, V. E. (1999). Assessment of particle–shaped substances [particulate fume] in welding technology (Beurteilung partikelformiger Stoffe in der Schweisstechnik). *Schweissen und Schneiden,* 51(4), 212–215.

Yu, I., Kim, K., Chang, H., Song, K., Han, K., Han, J., Maeng, S., Chung, Y., Park, S., Chung, K., Han, J., & Chung, H. (2000). Pattern of deposition of stainless steel welding fume particles inhaled into the respiratory systems of Sprague–Dawley rats exposed to a novel welding fume generating system. *Toxicology Letters,* 116(1–2), 103–111.

2.14 Relationship between Chemistry and Particle Size

Berner, V., & Berner, A. (1982). Mass size distributions and elemental frequency distributions of arc welding smokes. *Journal of Aerosol Science*, 13, 191–193.

Fasiska, E. J., Wagenblast, H. W., & Nasta, M. (1983). *Characterization of Arc Welding Fume*. Miami, FL: American Welding Society.

Grekula, A., Peura, R., & Sivonen, S. (1986). Quantitative energy dispersive x–ray microanalysis of welding fumes. *Proceedings of the International Conference on Health Hazards and Biological Effects of Welding Fumes and Gases*, R. M. Stern, A. Berlin, A. Fletcher, K. Hemminki, J. Jarvisalo & J. Peto (Eds.). Amsterdam: Excerpta Medica.

Hewett, P. (1995). The particle size distribution, density and specific surface are of welding fumes from SMAW and GMAW mild and stainless steel consumables. *American Industrial Hygiene Association Journal,* 56(2), 128–135.

Kalliomaki, P. L., Grekula, J. A., Hagberg, & Sivonen, S. (1987). Analytical electron microscopy of welding fumes. *Journal of Aerosol Science,* 18(6), 781–784.

Kura, B. (1998). *Evaluation of Cr(VI) Exposure Levels in the Shipbuilding Industry GCRMTC Project No. 32 ONR Cooperative Agreement No. N00014–94–2–0011,* Gulf Coast Region Maritime Technology Center, University of New Orleans. New Orleans.

Narayana, D. S. S., Sundararajan, A. R., Manjula, B., Kumari, S. C. V., & Subramanian, V. (1995). Chemical characteristics of stainless steel welding fumes. *Journal of Aerosol Science,* 26, S531–S532.

Tandon, R. K., Crisp, P. T., Ellis, J., & Baker, R. S. (1984). Generation rate, particle size and chemical measurements of fume from some hardfacing and HSLA steel electrodes, AWRA document no. P9–68–84. *Australian Welding Research,* 13(Dec), 45–49.

2.15 Masters Theses

Balmforth, M. (2001). *Manganese and Health in the Welding Environment.* M.S. Thesis: Materials Science and Engineering, Massachusetts Institute of Technology, Cambridge, Massachusetts.

Quimby, J. (1997). *Fume Formation Rates in Gas Metal Arc Welding.* M.S. Thesis: Chemical Engineering University of New Hampshire.

Ren, J. (1997). *Distribution of Particles in Welding Fume.* M.S. Thesis: Chemical Engineering University of New Hampshire.

Sreekanthan, P. (1997). *Study of Chromium in Welding Fume.* M.S. Thesis: Materials Science and Engineering, Massachusetts Institute of Technology, Cambridge, Massachusetts.

Wallace, M. E. (2000). *Control Technology Assessment of Arc Welding Operations.* MS Thesis: University of Cincinnati, Cincinnati, OH.

2.16 Doctoral Dissertations

Albert, R. (1996). *Fume Generation in Gas Metal Arc Welding.* Ph.D. Dissertation: Chemical Engineering, University of New Hampshire, Durham, NH.

Gray, C. N. (1980). *Fume Formation in Electric Arc Welding.* Ph.D. Dissertation: University of Bradford, Bradford BD7 1DP, UK.

Hewett, P. (1991). *Particle Size Analysis of Welding Fumes and Prediction of Regional Pulmonary Deposition.* Ph.D. Dissertation: University of Pittsburgh; 0178.

Hirst, A. (1990). *Fume Formation in Flux Cored Metal Inert Gas Welding.* Ph.D. Dissertation: University of Bradford, Bradford BD7 1DP, UK.

Jin, Y. (1993). *Particle Transport in Turbulent Buoyant Plumes Rising in a Stably Stratified Environment.* Tekn.Dr. Thesis: Kungliga Tekniska Hogskolan, Sweden.

Tandon, R. (1985). *A Study of the Chemistry and Mutagenicity of Welding Fume.* Ph.D. Dissertation: University of Wollongong, Australia.

Zimmer, A. T. (2000). *Aerosol Formation Mechanisms, Metallurgical Aspects and Engineering Control of Fumes Generated From Arc Welding Operations.* PhD Dissertation: University of Cincinnati, Cincinnati, Ohio.

Chapter 3

Airborne Particle Size

To understand the relationship between the size and composition of airborne particles or aerosols, one must understand how the particles form. Aerosol researchers categorize particle formation by size, which determines the forces that dominate in the formation process (see Figure 3.1).

Particle volume distribution of atmospheric aerosol measured with electrical and optical counters (Whitby, 1978) Reprinted with permission from Pergamon Press.
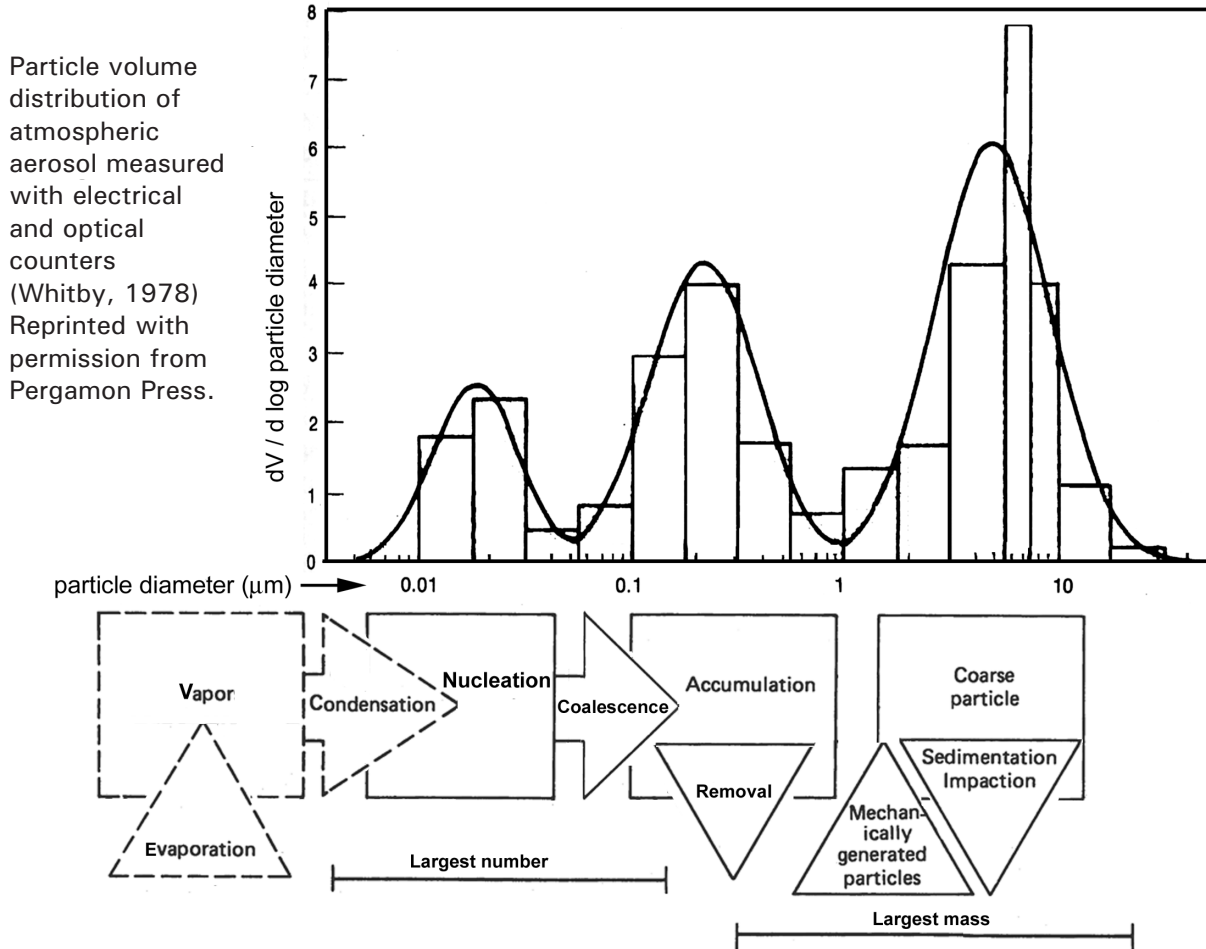
Figure 3.1 Size distribution common to airborne particles

It has been found that for most airborne particles, regardless of their parent material, three major size ranges exist, often called the (transient or aitken) nucleation range, accumulation range, and coarse (particle) range. In contrast to the coarse particles, those in the nucleation and accumulation ranges are often grouped together as "fine" particles.

The nucleation range includes any group of atoms large enough to be considered a stable liquid or solid. The accumulation range is made up of particles that were created from the collision of smaller condensed particles. The size of coarse particles is

determined by the balance between surface and inertial forces. This will be illustrated below.

3.1 Nucleation Range

Adjacent to vaporization or combustion sources, individual discrete particles can be found with diameters a few nanometers to less than 100 nanometers. These particles in the nucleation range have a mode of about 0.02 micrometers. They condense as solids or liquids[1] from a supersaturated vapor or as a result of a chemical reaction (Willeke & Baron, 1993). The size range of the nuclei can be understood with classical nucleation theory as illustrated in Equation 3.1,

$$d^* = \frac{4\gamma\Omega}{\Delta G} \quad \text{where} \quad \Delta G = RT \ln \frac{P_A}{P_{A,\infty}} \quad \text{or} \quad \Delta G = \Delta G^{\circ}_{reaction} + RT \ln \frac{\Pi P_{reactants}}{\Pi P_{products}} \quad 3.1$$

where
d^* is the critical diameter of the nucleus,
γ is the surface energy of the new phase,
Ω is the molar volume,
ΔG is the free energy of phase change or reaction
R is the gas constant,
T is the ambient temperature,
P_A is the actual vapor pressure of the relevant species,
$P_{A,\infty}$ is the equilibrium vapor pressure over a flat surface at ambient temperature,
$\Delta G^{\circ}_{reaction}$ is the equilibrium free energy of reaction,
$P_{reactants}$ are the vapor pressures of the various gaseous reactants
$P_{products}$ are the vapor pressures of the various gaseous products.

For condensing vapors, a simplification of Equation 3.1 using the Clapeyron equation for gases can be made where the actual vapor pressure is one atmosphere. See Equation 3.2 where L is the heat of phase change and T_b is the boiling temperature. This shows how the critical size of a stable nucleus is dependent on the vapor supercooling (T_b - T).

$$d^* = \frac{-4\gamma\Omega T_b}{L(T_b - T)} \quad\quad\quad 3.2$$

---

1. Here and throughout this thesis, a distinction between solid and liquid particles is often not made. When compared with the properties of a material's vapor, the respective properties of the material's liquid and solid states are not substantially different; the only real difference is in the mechanical properties. When those are important, the differences between the liquid and the solid will be noted. Otherwise, it will not be addressed whether particles condense as solids directly from the gas or whether they become liquids before solidifying.

It is interesting to note that surface tension scales with the heat of vaporization, because both are determined by atomic bond strength, meaning that the ratio of surface tension to heat of vaporization does not vary markedly from material to material. For liquid metals from sodium to copper, it varies only by a factor of 4. This knowledge suggests some reason for the similar range of condensation nuclei for all materials, despite the seeming diversity in properties.

Table 3.1 Properties of liquid metals extrapolated to boiling temperature (Brandes, 1983)

Metal	Atomic weight (g/mol)	Density (kg/m^3)	$T_{boiling}$ (K)	Heat of evaporation (kJ/mol)	Surface energy (J/m^2)	Ratio of surface energy to volumetric heat of evaporation (m)
Al	26.98	1864	2792	286	0.26	$1.3*10^{-11}$
Ba	137.33	2809	1973	177	0.28	$7.6*10^{-11}$
Ca	40.08	1228	1757	151	0.30	$6.5*10^{-11}$
Cr	52.00	6041	2944	342	1.45	$3.6*10^{-11}$
Cu	63.55	6817	2833	305	1.09	$3.3*10^{-11}$
Fe	55.85	5845	3134	340	1.22	$3.4*10^{-11}$
K	39.10	664	1052	80	0.07	$4.9*10^{-11}$
Mg	24.31	1473	1363	128	0.41	$5.2*10^{-11}$
Mn	54.94	5156	2334	231	0.93	$4.3*10^{-11}$
Mo	95.94	9340	4610	590	1.73	$3.0*10^{-11}$
Na	22.99	741	1156	98	0.12	$3.9*10^{-11}$
Ni	58.69	6212	3186	374	1.22	$3.1*10^{-11}$
Si	28.09	1915	3543	385	0.62	$2.4*10^{-11}$
Ti	41.87	5235	3560	426	1.22	$2.3*10^{-11}$

One can see that the decisive parameter is the supercooling. The ratio of surface tension to heat of evaporation for liquid metals is about $4x10^{-11}$ (see Table 3.1) One can easily determine that the critical diameter for liquid metals cooled to a temperature less than 80% of the boiling point will be equivalent to an atomic radius; in other words, there is no barrier to nucleation. As soon as the vapor is chilled beyond that and becomes supersaturated, nucleation and growth occurs as fast as vapor molecules collide with the nuclei until the nuclei grow too large for most collisions. Such is one extreme.

The other extreme, when supercooling is less than ~0.2 T_b, is treated by classical nucleation theory, with the typical equations for the nucleation and growth rates.

For most metals it is unlikely that this other extreme will occur (see Figure 3.2). First, when the supercooling is small enough that classical nucleation theory applies, the nucleation and growth rates will be slow. Second, and more pragmatically, it is
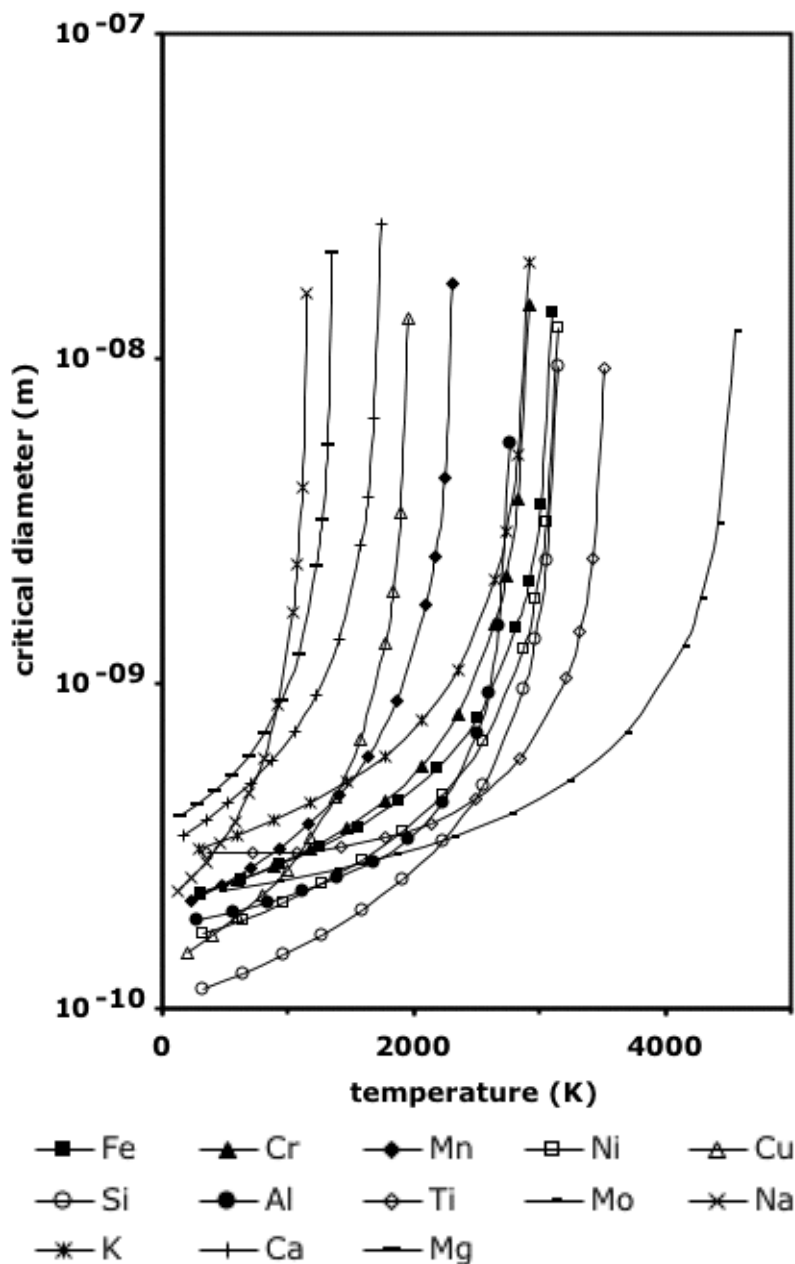
Figure 3.2 Critical diameter predicted by classical nucleation theory for common metals. Data from Brandes, 1983. Last point for each metal is at 99% of boiling temperature.

hard to hold a metallic vapor at a point greater than 0.8 T_b. There are few reactors that can withstand temperatures of greater than 2500K. Generally, metallic vapors evolve from an high-energy-density point source from which they are quickly transported into a cool region. Alkali and alkaline earth metals have low boiling points, so they nucleate and grow in a classical fashion in typical metallurgical reactors. But with those metals, it is difficult to control possible chemical reactions.

After nucleation, particles can grow by vapor condensation, chemical reaction and colliding with other particles. Chemical reaction growth rates depend on the particu-

lar reaction. The rate of growth from vapor condensation can be modeled generally with Equation 3.3:

$$\frac{d\mathbf{d}}{d\mathbf{t}} \propto \frac{\Omega(P_A - P_{A,\infty})}{\sqrt{2\pi M_A RT}} \qquad 3.3$$

where M_A is the atomic weight of the condensate and t is time. This is valid for particles smaller than the mean free path of the carrier gas. For larger particles, a correction factor (Fuchs) based on the Knudsen number (the ratio between mean free path and particle size) can be applied (Kodas & Hampden-Smith, 1999).

Colliding molecules and particles coalesce, if liquid, or sinter, if solid, to form larger particles, or they simply adhere to one another as agglomerates through van der Waals and electrostatic attraction (see Figure 3.3 for example). If particles are
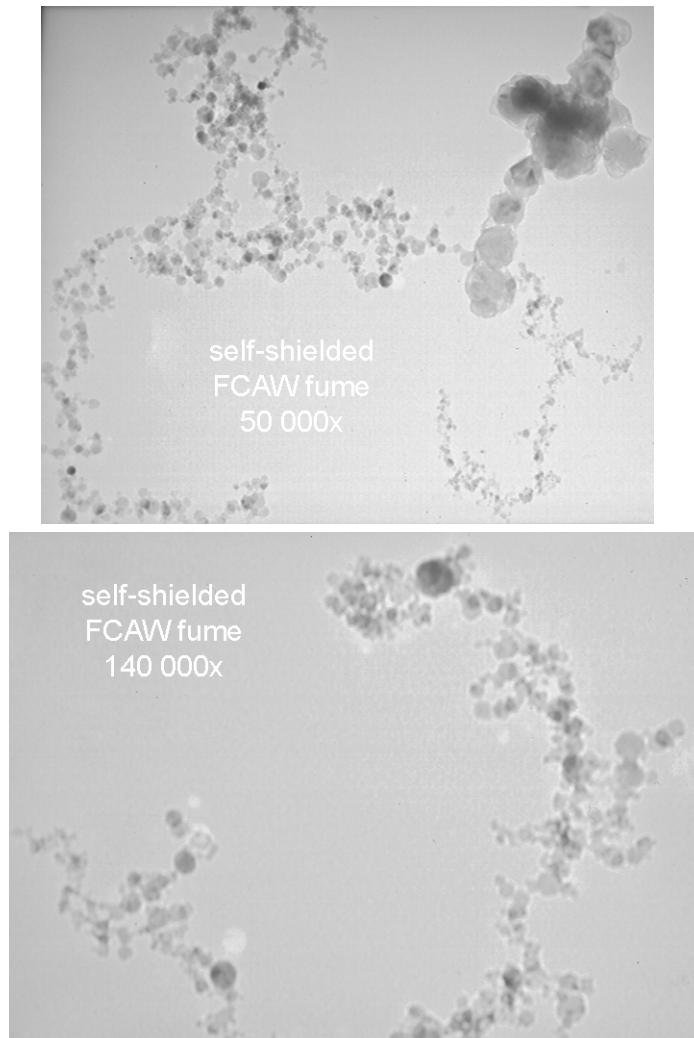
Figure 3.3 Transmission electron micrograph of aerosol particles from mild steel FCAW fume

smaller than the mean free path of the carrier gas, they behave like gas molecules: vapor easily condenses on them and other small particles readily collide with them. As particles or agglomerates grow, it becomes increasingly difficult for vapor molecules and/or smaller particles to reach them, but particles larger than the mean free path still readily collide. The mean free path is about 70 nanometers for air and for argon at standard conditions (Poirier & Geiger, 1994). This is the upper limit to the nucleation range.

One can see that the distinction between the nucleation and accumulation ranges is not well defined, because as the nucleated particles collide and coalesce, they move from one range to the other. Some researchers (Hinds, 1993) claim that nuclei will not agglomerate with other nuclei; instead such researchers argue that nuclei will be scavenged by pre-existing agglomerates. This forms the distinct mode seen in Figure 3.1. This is probably common in atmospheric aerosols, where agglomerates exist already and where there may not be a large concentration of nuclei particles. However, near evaporation sources, the high concentration of nuclei aids agglomeration between nuclei, so the nucleation range blurs into the accumulation range. In any case, over time, all particles in the nucleation range will eventually end up in the accumulation range.

3.2 Accumulation Range

Small particles move in Brownian motion, similar to gas molecules but more slowly if they are substantially bigger. When particles collide, they tend to stick, either because they are liquid or because of electrostatic and van der Waals forces. The rate at which nucleated particles agglomerate to possibly later coalesce or sinter, has been modeled, notably by Friedlander (1977). For monodisperse aerosols of particles larger than the mean free path, with a constant volumetric concentration of particles, the change in particle size with time can be predicted by Equation 3.4:

$$d \ = \ d_0\left(1 \ + \ \frac{4RT}{3\eta_g}\kappa t\right)^{\frac{1}{3}} \hspace{3cm} 3.4$$

where d_0 is the initial particle diameter, η_g is the viscosity of the carrier gas and κ is the molar concentration of particles in the volume of carrier gas. This is not entirely realistic, since particles are rarely monodisperse. Polydisperse particles agglomerate more quickly because the smaller-than-average particles diffuse more quickly and the larger-than-average particles have greater surface areas to be hit. Friedlander (1977) developed a model for polydisperse aerosols that is essentially the same as Equation 3.4 but shows time raised to the 2/5 power instead of 1/3. Therefore, the monodisperse model suffices to show the trends. It has also been noted that accumulation may be increased by the presence of charged species from an arc plasma (Buckle, et al.,1986). Figure 3.4 shows how the diameter of agglomerates increases with time for various initial number concentrations. The largest particles generally found in the accumulation range are about 2 micrometers. This is not reflected in Equation 3.4, but one can see in Figure 3.4 that particle growth quickly slows. Thus for low number concentrations it takes hours or days to grow past 2 micrometers, which may be enough time for particles to impact with a surface and be removed

from the air. This model also assumes a constant volume fraction of aerosol to carrier gas, as indicated by the initial number concentration. This is unrealistic for non-laboratory conditions - mixing from nearby air will quickly reduce the volume fraction and halt agglomeration growth. For example, the particle concentration near a welding arc could be determined by dividing the measured fume formation rate (for example, 0.5 g/min) by the shielding gas flow rate (20 L/min is typical); these values would yield a concentration of about 10^{24} atoms/m^3, or 10^{21} m^{-3} for 1 nm particles or 10^{16} m^{-3} for 10 nm particles. This is approximately what Ren measured in welding fume with an electrical aerosol analyser (Ren, 1997). The designer of the chamber, in which Ren created the fume, simulated shop-like air conditions with a flow of ~200 L/min (Quimby, 1997). Here is another factor of 10 for dilution. Dilution of the aerosol is likely the main reason why researchers have observed that agglomerates are less than 2 micrometers.
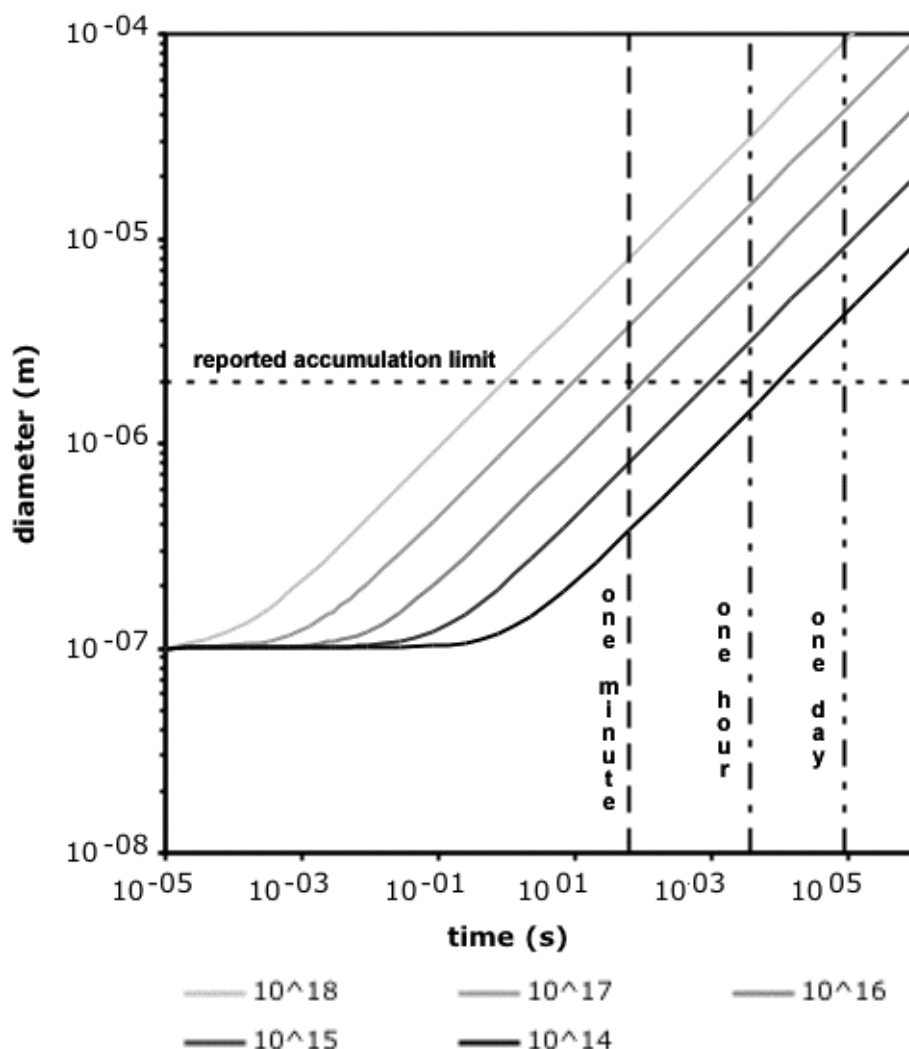
Figure 3.4 Particle size change due to agglomeration with respect to time for a monodisperse aerosol of constant aerosol-to-carrier-gas fraction and initial number concentration of particles. Air viscosity is from standard conditions, the initial particle diameter is 0.1 micrometer and particle density is 5 g/cm^3

Similar equations exist for particles smaller than the mean free path, which would be appropriate for any agglomeration in the nucleation range. Because the particles are smaller than the mean free path, they behave like gas molecules and diffuse much more quickly; hence agglomerates grow at about 4 times the rate described in Equation 3.4 (Hinds, 1982). This means that in the initial tenth of a millisecond (a relevant time interval for welding fume particle formation) accumulation causes particles to grow somewhere between 10^{-8} m/s and 10^{-4} m/s (for initial particle number concentrations of 10^{14} m^{-3} and 10^{18} m^{-3} respectively). Vapor condensation growth rates (from Equation 3.3) are about 10^{-7} m/s - meaning both condensation- and collision- based mechanisms will contribute to particle growth in the nucleation range.

After collision, particles will coalesce if liquid, or if solid, sinter or remain in particle chains as weakly bound agglomerates or fused aggregates resembling fractals. Single particles larger than the mean free path will have formed through collision and sintering. Because of their sharp planes, it may be assumed that the primary particles of GMAW fume solidified before agglomeration (see Figure 3.5; compare with the shielded metal arc welding (SMAW) fume). If so, one can effectively see the thermal history of the fume particles based on the size of the primary particles measured with electron microscopy.The cooling rate of smaller particles will be greater than that for larger particles (see Figure 3.6). This data could either be used to determine the thermal profile around the evaporation source of the fume (as attempted with another method by Mori, et al. 1991) or to measure the diffusivity of nanoparticles, which may be substantially different from that of the correlating bulk material.

Direct evidence of sintering can be seen from transmission electron microscopy. The initial stage of sintering is characterized by contact being made between two particles (in the two-particle model) and the formation of a neck (Figure 3.7). The neck can be formed in several different ways: by lattice diffusion of atoms from within the particles or by grain boundary diffusion (along the interface of the two particles). Both of these mechanisms densify the particle because mass is moved from within the particles to the neck region. Alternatively atoms can move to the neck by surface diffusion or by evaporation/condensation. Neither of these mechanisms leads to densification because no material is removed from within the particles. Unfortunately analysis of these photographs does not reveal which mechanism is dominant in this case. Figure 3.8 shows a pair of particles in the latter stage of sintering.

If primary particles coalesce, their diameter growth can be modeled with Equation 3.5 from Ulrich and Riehl (1982):

$$\frac{d\mathsf{d}}{d\mathsf{t}} \;=\; \frac{2\gamma}{\eta_p}\left[(1+\alpha)^{\frac{1}{3}} - 1\right] \qquad\qquad 3.5$$

where α is the number of neighbor primary particles that combine with an individual primary particle (for silica, this value is about 4) and η_p is the viscosity of the parti-

VG MICROSCOPES
HB603
MIT-CMSE

HT 250.00 kV
MODE STEM IMAGE
BRIGHT NORMAL
MAG 200k x
ROTATION   0.0°
PROBE SIZE #2
PROJ CL FREE
EXPOSURE 34.7S

USER VG VGM
28-Jul-1998 13:12
FILE VG1277N.IMG

100nm

VG MICROSCOPES
HB603
MIT-CMSE

HT 250.00 kV
MODE STEM IMAGE
BRIGHT NORMAL
MAG 50k x
ROTATION   6.0°
PROBE SIZE #2
PROJ CL FREE
EXPOSURE 34.7S

USER VG VGM
28-Jul-1998 11:33
FILE VG1265N.IMG

400nm
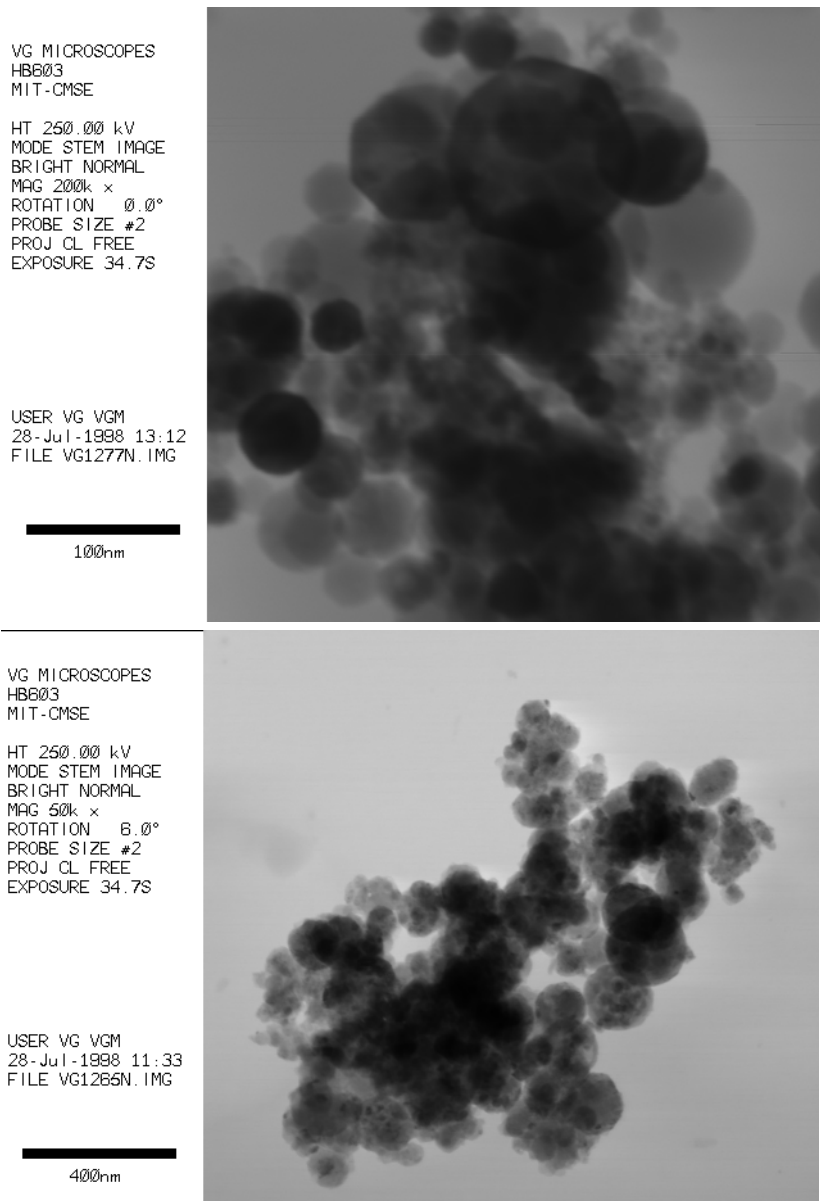
Figure 3.5 Transmission electron microscopy of fume from mild steel gas metal arc welding (top) and shielded metal arc welding (bottom).
Compare the sharp planes of the GMAW fume with the spheroid agglomeration of the SMAW fume. Density differences inside SMAW fume are also noticeable.

a.

b.

$$\frac{dT_a}{dt} > \frac{dT_b}{dt}$$
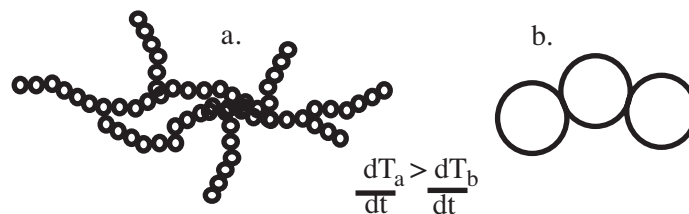
Figure 3.6 Dependence of primary particle size on cooling rate
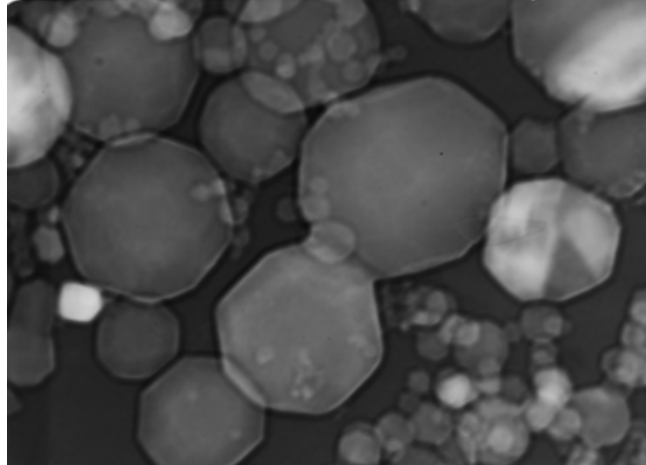
Figure 3.7 (Top) Mild steel GMAW fume (6.1 mg) of dispersed with 2 ml of acetylacetone + 0.004 g of iodine. Magnification = 270 000 X.
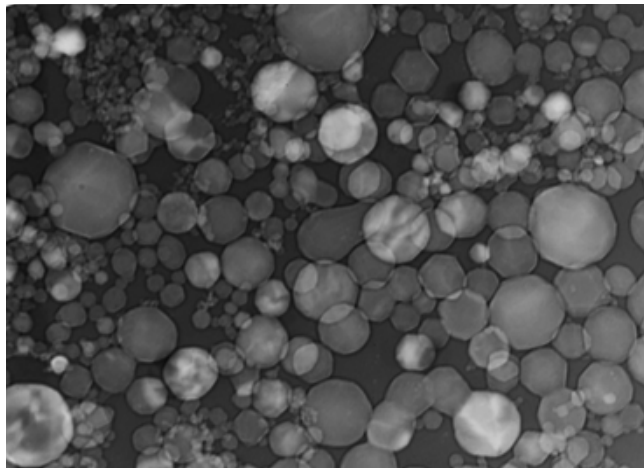
Figure 3.8 (Bottom) Mild steel GMAW fume (6 mg) dispersed with 2.5 ml ethanol + 10^{-3} mol of lauric acid. Magnification = 140 000 X.

cles. For example, materials like metals with high surface energies and low viscosities coalesce more quickly than oxides and halides. If primary particles do not reflect this, then they solidified before fusing, in which case, diffusivities and melting points of the various solids determine sinter growth. Halides with their lower melting point sinter more quickly than oxides, so their primary particles would be greater in size than oxide particles under the same conditions. This seems to be the case for welding fume when comparing fume created with or without welding fluxes, but more complete primary particle size distributions would need to be measured from transmission electron microscopy to confirm this finding.

3.3 Coarse Particle Range

Coarse particles are greater than 1 micrometer in diameter and are as large as the size that can remain airborne, usually about 20 micrometers, depending on the density of the particles and the ambient air speed. Coarse particles are created mechanically, either from the breakup of a larger liquid mass or from erosion of a solid. The

latter will not be treated here, because the emphasis is on high-temperature metallurgical processes, but some insight into the lower size limit of liquid droplets will be provided.

Whether droplets are formed by nature (e.g., waterfalls, impacts, etc.) or by technology (atomization by spraying, spinning, etc.) the size of the droplets emerging from a liquid will be determined by the size of the perturbations in the surface of the liquid as controlled by the surface tension of the liquid. The balance between inertial and surface forces shown in Equation 3.6 determines the size of perturbations that will grow into droplets.

$$W = \frac{d\rho_p v^2}{6\gamma} \qquad\qquad 3.6$$

γ is surface energy or tension, ρ_p is the density of the liquid, d is the size of the stable perturbation or droplet and v is the relative velocity of the liquid. W is the Weber number, which represents sufficient analysis for liquids of relatively low viscosities, like metals. For more viscous liquids, like metal oxide slags, one may also want to consider the Ohnesorge number, O, as shown in Equation 3.7:

$$O = \frac{\eta_p}{\sqrt{6\rho_p\gamma d}} \qquad\qquad 3.7$$

where η_p is the viscosity of the liquid droplets (Process Associates of America, 2003).

From Equation 3.6, it is easy to find the velocity where the surface forces equal the inertial forces in magnitude (i.e., W = 1) and thus creates the droplet of any given size.

Before exploring the question of the origin of the force that breaks up a larger droplet into smaller ones, the cooling rates of hot metal droplets should be considered. It may be possible for droplets to freeze before they can divide into smaller droplets. In Appendix A, the heat balance of spatter droplets is considered. The results are graphed in Figure 3.9 (Figure A.2 in Appendix A). If the relative velocity of a liquid was great enough to form droplets of a certain diameter, as suggested by Equation 3.6, and one assumed that the minimum distance to travel during a droplet breakup was the diameter of the droplet, then one could estimate the time required for a droplet to divide into smaller droplets; in other words, the droplet diameter is divided by the velocity given by Equation 3.6. When comparing Figure 3.9 to Table 3.2 it is clear that iron droplets will not freeze before they can break up into smaller droplets.

As with the ratio between surface energy and the heat of vaporization for liquid metals in Table 3.1, the ratio between surface energy and density at the melting point for common metals does not have a large range (see Table 3.3). Figure 3.10 shows the velocity required to form droplets from a liquid metal with an average surface energy and density. One can see that at around 1 micrometer, the required
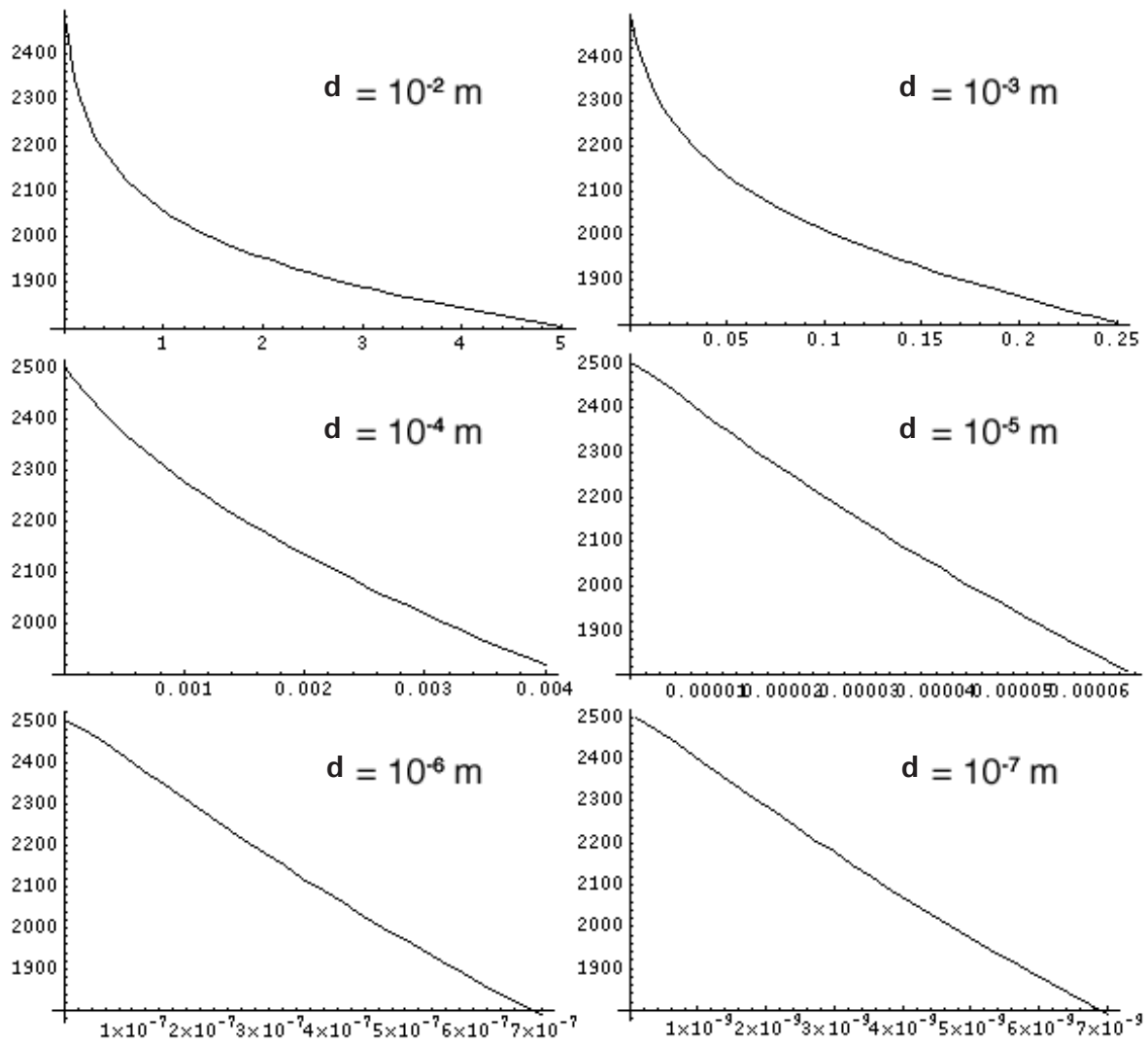
Figure 3.9 Calculated change in temperature (K) of iron welding spatter droplets of various diameters (d) with time (s)
(Same as Figure A.2 in Appendix A).

Table 3.2 Estimated time for a droplet to break up into smaller droplets

log Droplet Size (m)	log Velocity (m/s)	log Time (s)
-2	-1	-1
-3	0	-3
-4	1	-5
-5	2	-7
-6	3	-9
-7	4	-11

Table 3.3 Surface tension and density at melting point for various metals (Brandes, 1983)

	Density (kg/m^3)	Surface energy (J/m^2)	Ratio * 10000
Al	2385	0.91	3.8
Ba	3321	0.28	0.8
Ca	1365	0.36	2.6
Cr	6280	1.70	2.7
Cu	8000	1.29	1.6
Fe	7015	1.87	2.7
K	827	0.12	1.3
Mg	1590	0.56	3.5
Mn	5730	1.09	1.9
Mo	9340	2.25	2.4
Na	927	0.20	2.1
Ni	7905	1.78	2.2
Si	2510	0.87	3.4
Ti	4110	1.60	4.0
Zr	6511	1.48	2.3
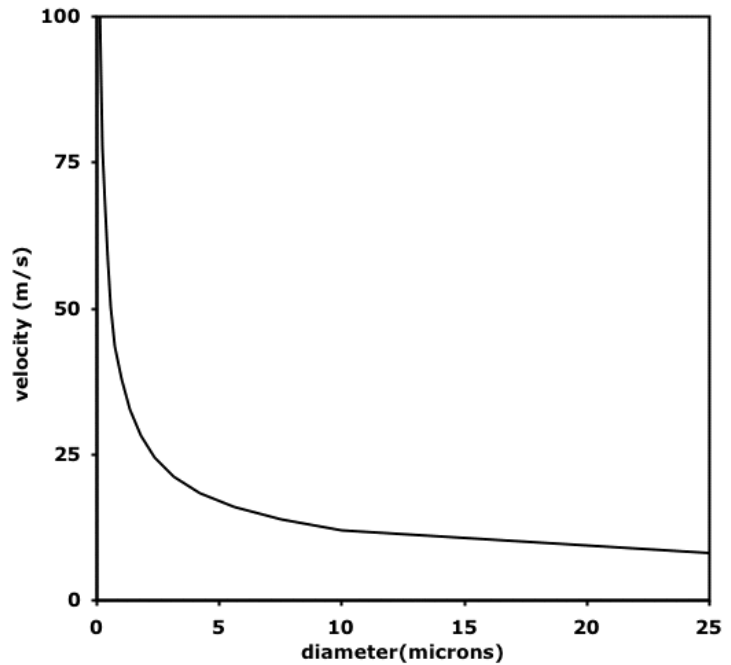
Figure 3.10 Velocity required to form droplets of a certain size from average liquid metal

velocity suddenly becomes greater, which explains why particles formed from liquid metals are not easily made smaller than 1 micrometer. Manufacturers report that gas atomization is not able to create particles smaller than tens of micrometers (Moll, 2000) Similar sizes have been reported from exploding microwires (Vijayan & Rohatgi, 1985) and in laser heating (Craciun & Craciun, 1998) (see Figure 3.11), where fine particle sizes were also found. With laser ablation, it was noted that the larger the difference between the melting and boiling points, the less likely that particles larger than 1 micrometer would form; for oxide ceramics, no coarse particles were ever found (Riehemann, 1998).

While studying vacuum arcs, researchers found particles created from cathode sputtering that were 30 to 100 micrometers in size. They also found pits, or artifacts of particle ejection, 0.1 to 100 micrometers in size, on many types of electrode surfaces. The electrodes studied included those from arcs in fuse wires, arcs caused by electric breakdown and parting contacts, arcs on copper alloy, gold, and palladium cathodes, arcs in vacuums or atmospheric ambients. These arcs had current densities of 10^4 to 10^8 A/cm^2. Therefore it was observed that particle ejection during
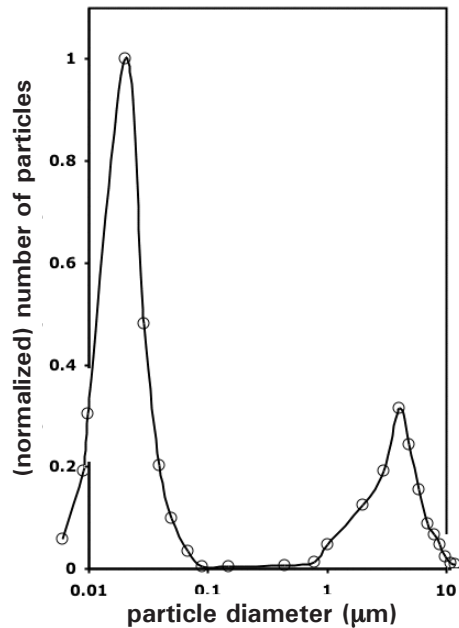
Figure 3.11 Particle distribution found in laser ablation (Riehemann, 1998)

arcing occurred regardless of the arcing conditions, although greater currents tended to create more particles. (Lafferty, 1980).

It is probable that in the cases of laser ablation, vacuum arcs, welding and other metallurgical processes involving high-energy-density heat sources, micrometer-sized particles are formed from the bursting of vapor bubbles. This has been reported to be the source of the large and only briefly airborne spatter droplets in gas metal arc welding[1] (Ma & Apps, 1983; Suga & Kobayashi, 1984).These vapor bubbles can form from dissolved gases in the molten metal, like nitrogen or carbon monoxide[2], or from evaporated metal. When vapor bubbles encounter the liquid-vapor interface (see Figure 3.12), they break down, creating small particles (a few micrometers in size for water); they later create larger particles when the column pulled from the disturbed liquid surface breaks up.

Richardson (1974) discussed this phenomenon in his book, from which Figure 3.12 is taken. He reported that the critical size for a stable vapor bubble is too large for evaporated metal to homogeneously nucleate according to classical nucleation the-

---

1. This is probably not the case for gas tungsten arc welding (GTAW) where surface temperatures have been calculated to be less than boiling (Block-Bolton and Eagar, 1984); this, along with the fact that the weld pool velocity is only about 1 m/s (Mendez, 1999) partially explains why GTAW does not create as much fume as other welding processes.

2. It has been found that welding electrodes that contain less carbon create less fume (Feree, 1995). Such steels contain lower amounts of dissolved carbon monoxide and therefore may bubble less.
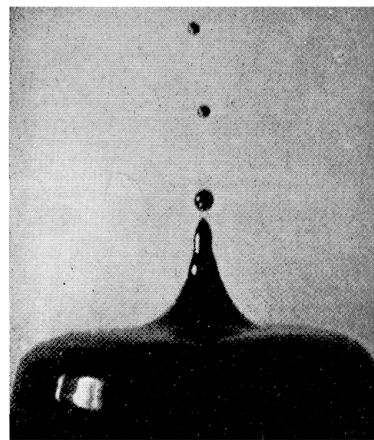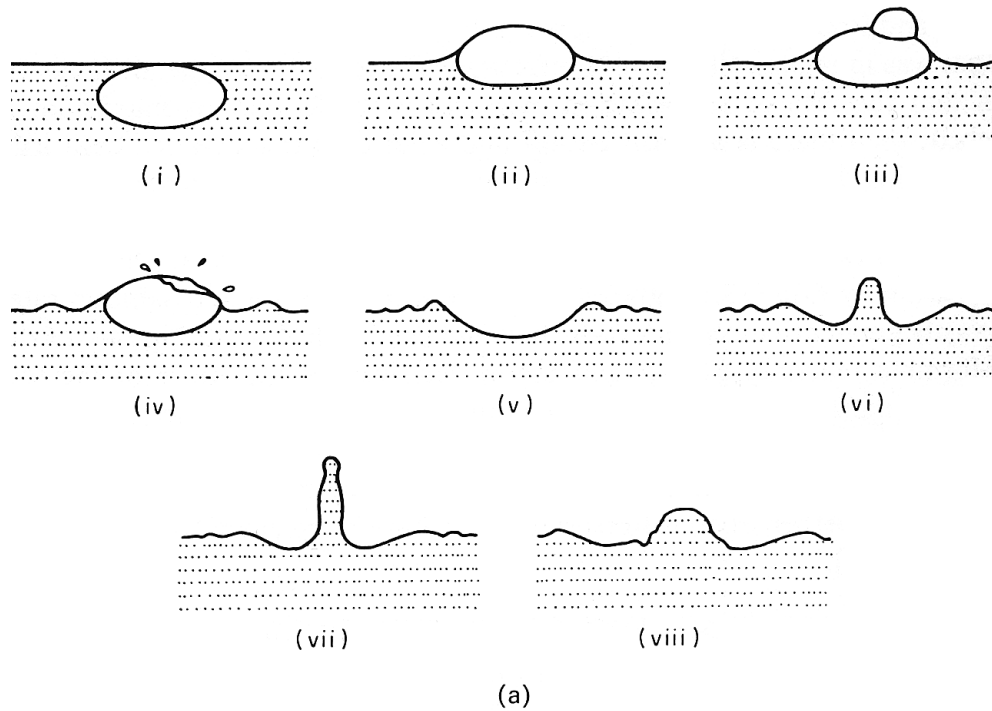
Figure 3.12 How spatter can form from liquids when gas bubbles escape (Richardson, 1974)
(a) series of events in the bursting of an air bubble about 0.5 cm across on the surface of water

(b) ejection following burst of 50 mm^3 bubble of N_2 from 1.0 cm mercury drop

(c) ejection caused by bubble of CO bursting from carbon iron drop about 0.8 cm across, levitated in flowing oxygen

Reprinted with permission from Elsevier.

ory; however he observed that bubbles do form and that there must be another phenomenon that causes this. This may be caused by heterogeneous nucleation at crevices in the vessel in which the liquid was held. Another possibility is that it is caused by dissolved gases like nitrogen. A more recent study with lasers does indicate that subsurface superheats can cause vapor bubbles to form that burst forth creating spatter (Craciun & Craciun, 1998).
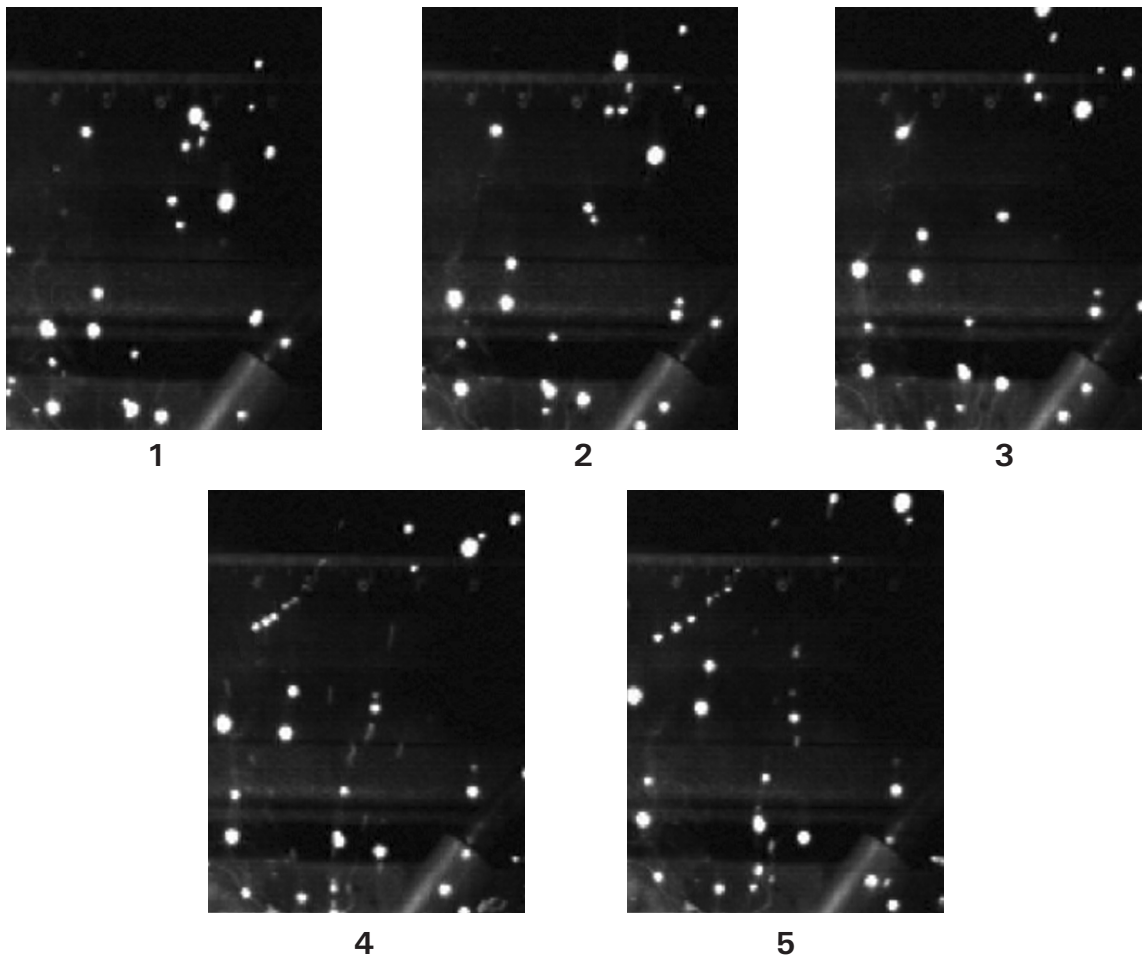
Figure 3.13 Sequential frames (interval = 6 ms) from high-speed videography of CO_2-shielded mild steel GMAW

In Figure 3.13, a series of video frames taken at 6 millisecond intervals of a GMAW welding arc, one can see a particle in the upper left first slightly glow brighter and then explode into many smaller particles. This is a fairly common event in metallurgy (Dreizin, 2000). It is suggested that this is caused by nitrogen dissolution, which first heats the particle and then breaks up the particle when the gas escapes from the cooling liquid metal.

How big must vapor bubbles be to create microdroplets? If all the energy formed in creating the bubble were transferred to formation of the ejected microdroplet, the relation in Equation 3.8 would apply:

$$P_{bubble}\Delta V_{bubble} = \frac{4\gamma}{d_{bubble}} \times \frac{\pi}{6}d_{bubble}^3 = \pi d_{droplet}^2\gamma \qquad 3.8$$

which can be reduced to saying that the diameter of the bubble would be about 1.2 times greater than the diameter of the ejected droplets. From nucleation theory (see Section 3.1), the superheating (instead of supercooling) required to nucleate bub-

bles of one micrometer can be determined with Equation 3.1. For iron, a temperature of almost 4000K would be necessary. For smaller bubbles, even greater temperatures would be required. Such superheats are possible only with high-energy-density heat sources like electric arcs with consumable electrodes (Ma & Apps, 1983; Mendez, et al., 2000), electron beams or lasers (Tanaka, et al., 1987). However there is naturally a practical limit to the extent of the superheat, because there is a balance between energy input and evaporative heat loss, which means that the maximum surface temperature of iron electrodes in an electric arc is about 3800K (Cobine & Berger, 1955). So again, it is very difficult, even without purpose, to create liquid metal droplets smaller than 1 micrometer.

Bursting vapor bubbles is not the only source of microdroplets. A 1986 paper by Krause and Preβ reported the composition of fume created from resistance welding, which involves no flux or slag. This is a cooler process than arc welding and significant vaporization does not occur; therefore the fume from resistance welding must consist of coarse particles formed from liquid metal. This is substantiated by the fact that the ratio of chromium and nickel to iron in the resistance welding fume was the same as that of the parent metal. So here airborne particles formed without significant vaporization and bubbling.

In welding, other processes can influence droplet creation. Right before a drop detaches from a consumable electrode, a neck forms. Because current is still flowing, this neck experiences severe joule heating, much like the exploding microwires (Vijayan & Rohatgi, 1985) mentioned earlier, where, it appears possible to form metal particles smaller than 1 micrometer, but only when a great enough current density can vaporize the wire instantaneously. Joule heating, Q_{joule}, is dependent on the current and the width of the current path, as shown in Equation 3.9,

$$Q_{joule} = \frac{4\pi\Omega I^2 t}{\sigma d_{neck}^2} \qquad 3.9$$

where I is current and σ is conductivity and d_{neck} is the width of the neck. Using typical values for iron and 1.5 milliseconds for time and 0.1 millimeters for the width of the neck (conservative estimates from Figure 3.14, a shadowgraph of a welding drop detaching from a 1.6mm wire electrode while welding at 240 amperes) ,, one can calculate that the heat input is 10^5 J/mole. The heat of vapor-
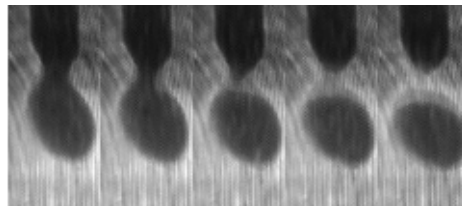
Figure 3.14 Series of frames spaced 0.5 milliseconds from high speed video of electrode laser shadow from gas metal arc welding with 1.6 mm electrode, 2%O_2-Ar, 240 amperes.

Images captured from video from Jones, 1996. Notice the lighter areas suggesting overheated areas around the neck.

ization for iron is almost 4 times that, so this does not quite match the situation described by the exploding wire researchers, where energy greater than heat of vaporization was required to create droplets smaller than 25 micrometers. Therefore it is doubtful that joule heating of the neck during drop detachment creates coarse particles, although more intense vaporization may occur that could create condensed fine particles.

However, it is possible that as large molten drops detach from the electrode, metal droplets will form, as seen in Figure 3.15, where droplets a few hundreds of micrometers can be seen. But unless there are forces other than inertial forces acting on the microdroplets, it is doubtful based on the relationship of Equation 3.6 that droplets will form that are small enough to remain airborne.
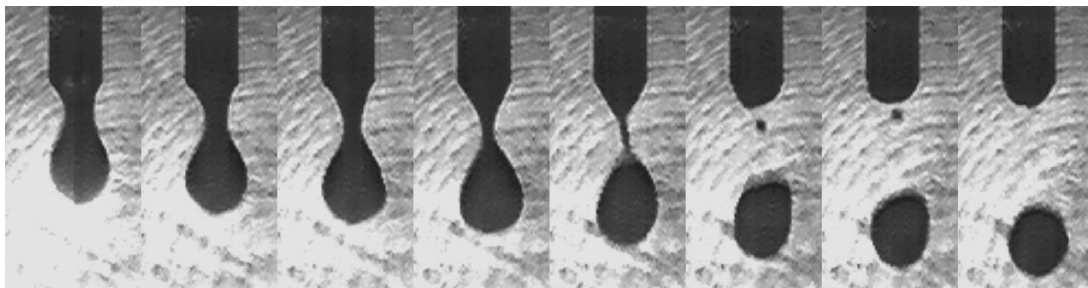
Figure 3.15 Series of frames spaced 0.5 milliseconds from high speed video of electrode laser shadow from gas metal arc welding with 1.6 mm electrode, 2%O_2-Ar.

Images captured with same equipment and method as those found in Jones, 1996.

Surface charging of the metal from the arc may affect the relationship expressed in Equation 3.6. Lord Rayleigh (1882) predicted that in high electrical fields, the charges on the surface of a droplet would counter surface tension, so that when the fissility, Ξ, is greater than 1, the particle would disintegrate into smaller more stable microparticles (Duft et al., 2003). Fissility is defined in Equation 3.10:

$$\Xi = \frac{q^2}{8\pi^2 \varepsilon_o \gamma d^3} \qquad 3.10$$

where q is the surface charge and ε_o is the permeability of vacuum. This effect has be used by so-called liquid metal ion sources (LIMS), which utilize the Rayleigh instability to direct a stream of submicron particles (Vladimirov, et al., 1995; Forbes, 2001). However the electric field typically used for LIMS is $\sim 10^{10}$ V/m; for welding, the highest voltage used is ~ 50V over a distance of about 1 cm. At the most conservative values chosen for the variables, the fissility of Equation 3.10 is always less than 1 for welding, and probably for most other high-temperature metallurgical processing.

3.4 Conclusion and Examples

This is how the observed particle sizes in the nuclei, accumulation and coarse ranges are based on physical properties common to most materials and to all metals. To finish the discussion about the particle size of airborne particles, graphs of the particle size distribution of fumes created from a variety of welding processes are presented here. These are examples of particle size ranges and can also be an introduction to the methods researchers use to measure particle sizes.

Figure 3.16 through Figure 3.20 show the mass distribution of welding fume with respect to particle size. These were determined with various types of impactors, which are chambers designed to collect particles according to their sizes by allowing progressively smaller particles to pass by successive plates in the chamber. Particles smaller than the mean free path of gas can not be separated this way, so these graphs do not indicate the nucleation range. However, the accumulation and coarse ranges can be seen. Of note are the size similarities among the fumes created by various processes used by various researchers. The only major difference is that shielded metal arc welding tends to create more coarse particles and larger agglomerates.

Figure 3.21 through Figure 3.23 show the results of two researchers who used a laser particle counter and electrical aerosol analyser to monitor the number concentrations of welding fume. These methods can detect smaller particles than impactors can separate, but are still somewhat limited. Figure 3.21 and Figure 3.22 are essentially the same, despite being created from data from different researchers who used different methods to measure the number distribution. Figure 3.22 contains data from 31 different sets of welding parameters, albeit for the same electrode and shielding gas. Again it should be noted that the particle size range is more dependent on general physics of air than on welding parameters. Part of the reason the data in Figure 3.22 are so similar is because the researcher mixed and diluted the air, effectively causing the particles to agglomerate as much as they were ever going to, before they were measured. Figure 3.23 shows the results she had before mixing. Strong indications can be seen of particles in nucleation ranges, that over time, agglomerated into the accumulation range. In all of these figures, the coarse range is not indicated because the equipment could not measure particles that large.

Figure 3.24 is similar to those just mentioned, in that a scanning mobility particle sizer was used to count number concentrations while the fume was airborne. Here again are the particles in the nucleation range, as they agglomerated into the accumulation range. Both time and distance from the welding arc allowed the particles to agglomerate more before being measured. Different shielding gases caused different amounts of vaporization to occur, so that with the gas where the fume formation rate is the highest, one can see a strong peak in the nucleation range. Finally, the fluxes from flux-cored arc welding (which are similar to those in SMAW) caused agglomerates to grow larger. This may be because fume from FCAW or SMAW has a lower density (3 to 4 g/cm^3) than does fume from GMAW (5 to 6 g/cm^3) (Hewett, 1995), but it is probably because the former welding processes have much higher fume formation rates. This indicates a higher concentration of particles, which causes a quicker accumulation process. Thus larger agglomerates form in the same

sampling time. Again the equipment was not able to detect coarse particles, but the same researcher used a different aerosol analyzer calibrated to detect particles in the coarse range. Figure 3.25 shows those results. Figure 3.26 combines some of the data from Figure 3.24 with the data shown in Figure 3.25, illustrating how welding fume is distributed in the 3 particle size ranges with which aerosol researchers are familiar.

Because there are 4 orders of magnitude of airborne particle size (from 1 nanometer to 10 micrometers), one must use different methods to analyze particles of different sizes. Primary particles formed in the nucleation range can be see individually with transmission electron microscopy (TEM). Figure 3.27 shows the primary particle size distribution found with a TEM. Figure 3.28 shows the distribution of agglomerates sizes from the accumulation range (measurements were taken with a scanning electron microscope). Figure 3.29 also used a scanning electron microscope (SEM) to measure coarse particles of welding fume, or "microspatter," a term coined by several welding fume researchers (Deam, et al., 1997; Quimby and Ulrich, 1999).These studies with microscopes confirm that welding fumes are typical aerosols.
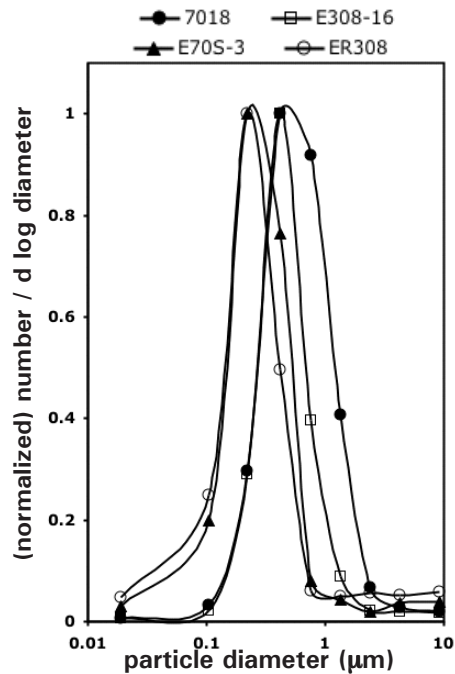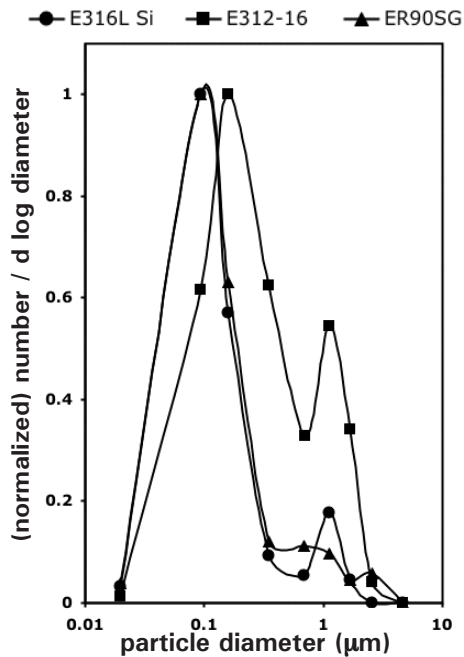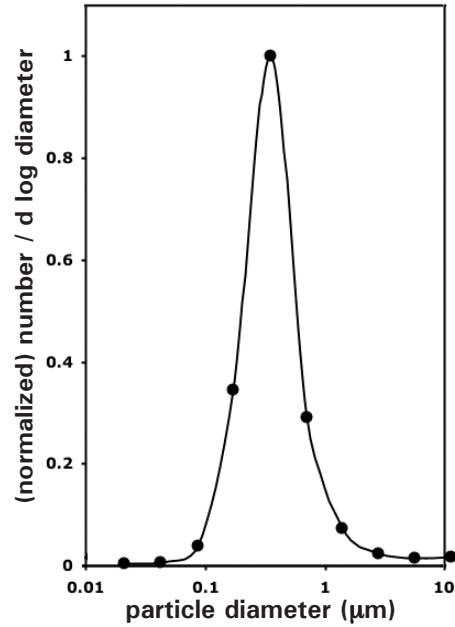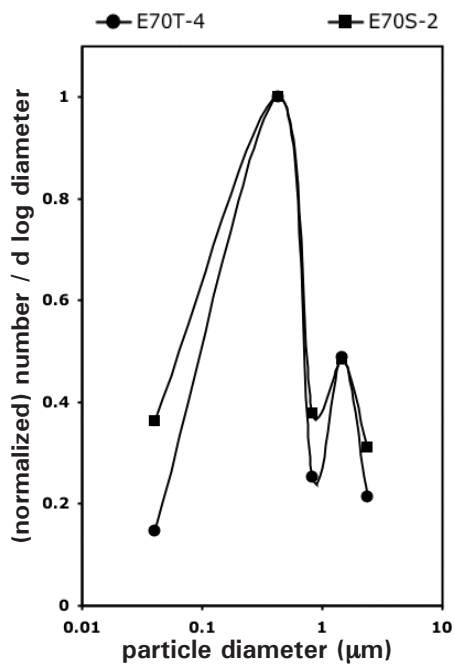
Figure 3.16 (Top Left) Weld fume mass distribution (inertial separation) (Heile & Hill, 1975)

Figure 3.17 E70S-2 wire: 300A 34V CO_2 shielded; E70T-4 wire: fluorspar core, self-shielded

Figure 3.18 (Top Right) SMAW fume mass distribution from 0.3 m above weld (low pressure cascade impactor; smallest cutoff = 150 nm) (Berner & Berner, 1982)

Figure 3.19 (Low Left) SMAW, GMAW fume mass distribution (cascade impactor; smallest cutoff = 80 nm) (Eichhorn & Oldenburg, 1986)

E312-16 = SMAW 2.5 mm dia, 28V 70A

ER316L Si & ER90SG = GMAW 1.2 mm wire, 27–30V 260–300A, 2%O_2-Ar shielding gas

Figure 3.20 (Low Right) Mild, stainless steel SMAW, GMAW fume mass distribution (micro-orifice uniform deposit [cascade] impactor; cutoff = 71 nm) (Hewett, 1995).
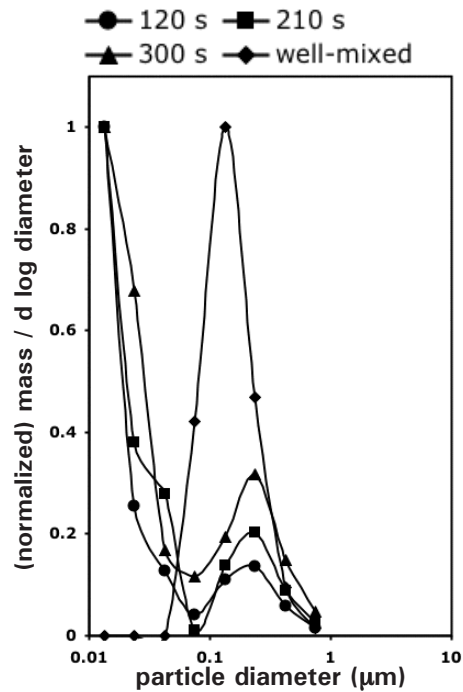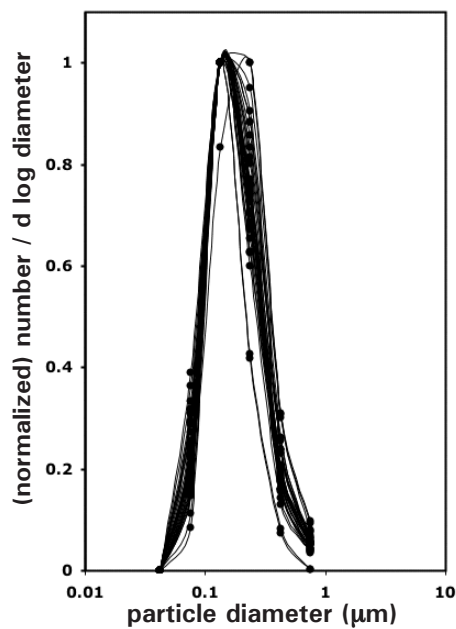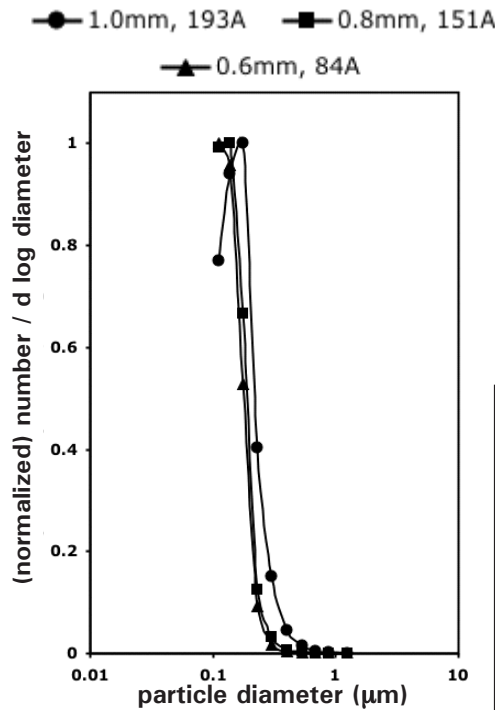
Figure 3.21 (Top Left) Size distribution of 20%CO_2-Ar shielded GMAW fume from ER70S-6 wire

of various diameters (laser particle counter, 0.1−7.5 micrometer range) (Jin, 1994)

Figure 3.22 (Bottom Left) Size distribution of well-mixed & cooled GMAW fume created with 31 different voltage and current settings (pulsed and straight) with E70S-3 wire and 8%CO_2-Ar

shield (electrical aerosol analyzer, 0.003 −1 micrometer range) (Ren, 1997)

Figure 3.23 (Bottom Right) Size distribution of welding fume when sampled at various times (seconds) after formation (electrical aerosol analyzer, 0.003 −1 micrometer range) (Ren, 1997)
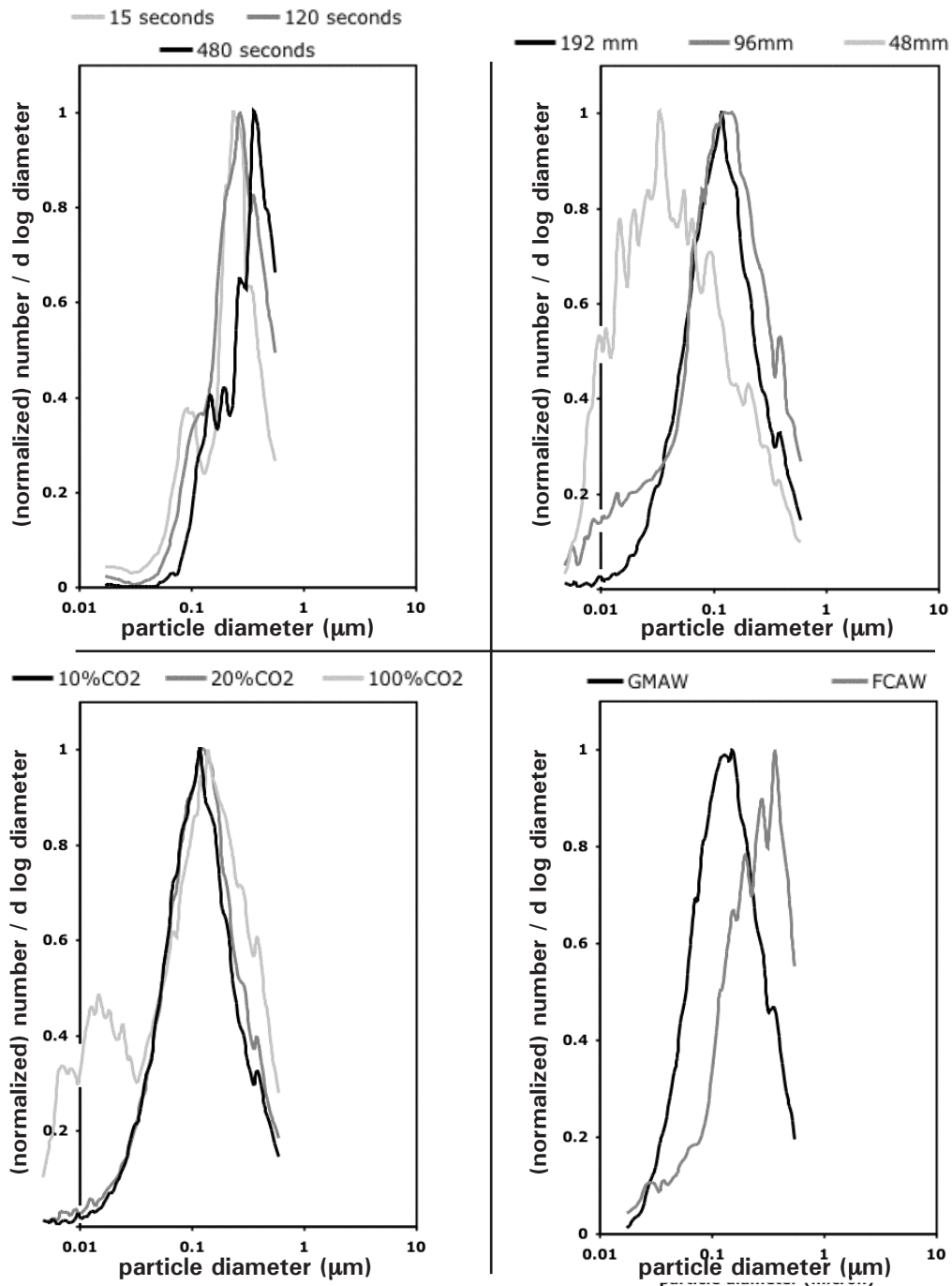
Figure 3.24 Effects on fume size distribution (clockwise from upper left) a. time after welding before sampling, b. distance from weld to sampler, c. GMAW vs. FCAW (self - shielded E71T-11) d. shield gas (Zimmer, 2001)

 Unless noted, sampled with scanning mobility particle sizer (SMPS) with range of 16.5 nm−562 nm, 192 mm above weld with 0.89 mm dia. ER70S-6 wire, 20.5 V, ∼200A, wfs = 161 mm/s, 10 mm CTWD
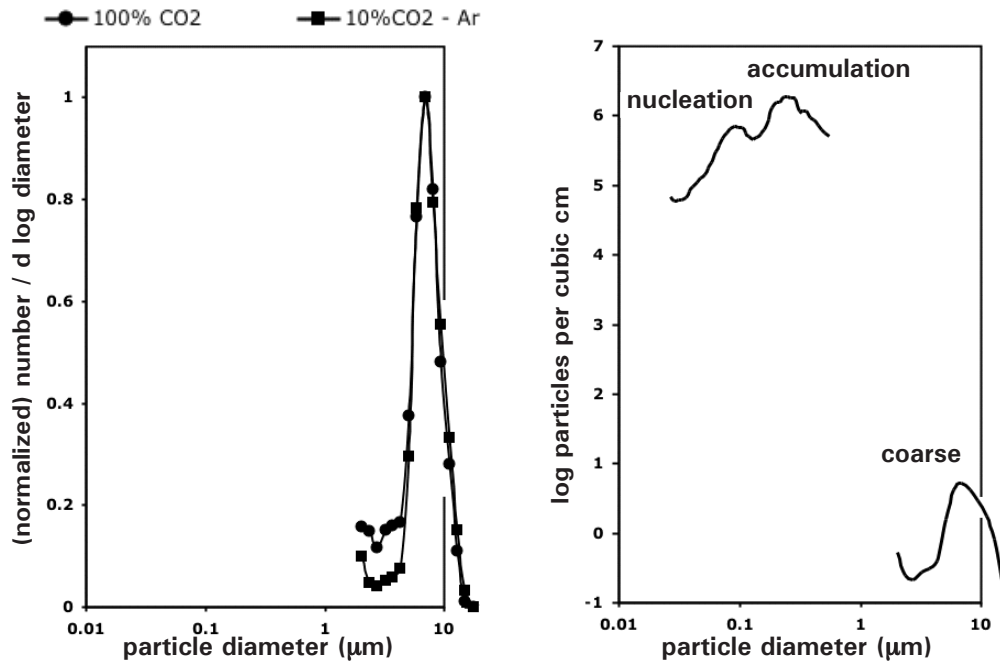
Figure 3.25 (Left) Size distribution of mild steel GMAW fume (Aerosizer particle size analyzer); total no. concentration for both shielding gases was ~25 cm^{-3} (Zimmer, 2002)
Figure 3.26 (Right) Combined particle size distribution (SMPS + Aerosizer) of mild steel GMAW fume (Zimmer, 2002)
By mass, coarse fraction was two-orders of magnitude smaller than accumulation range.
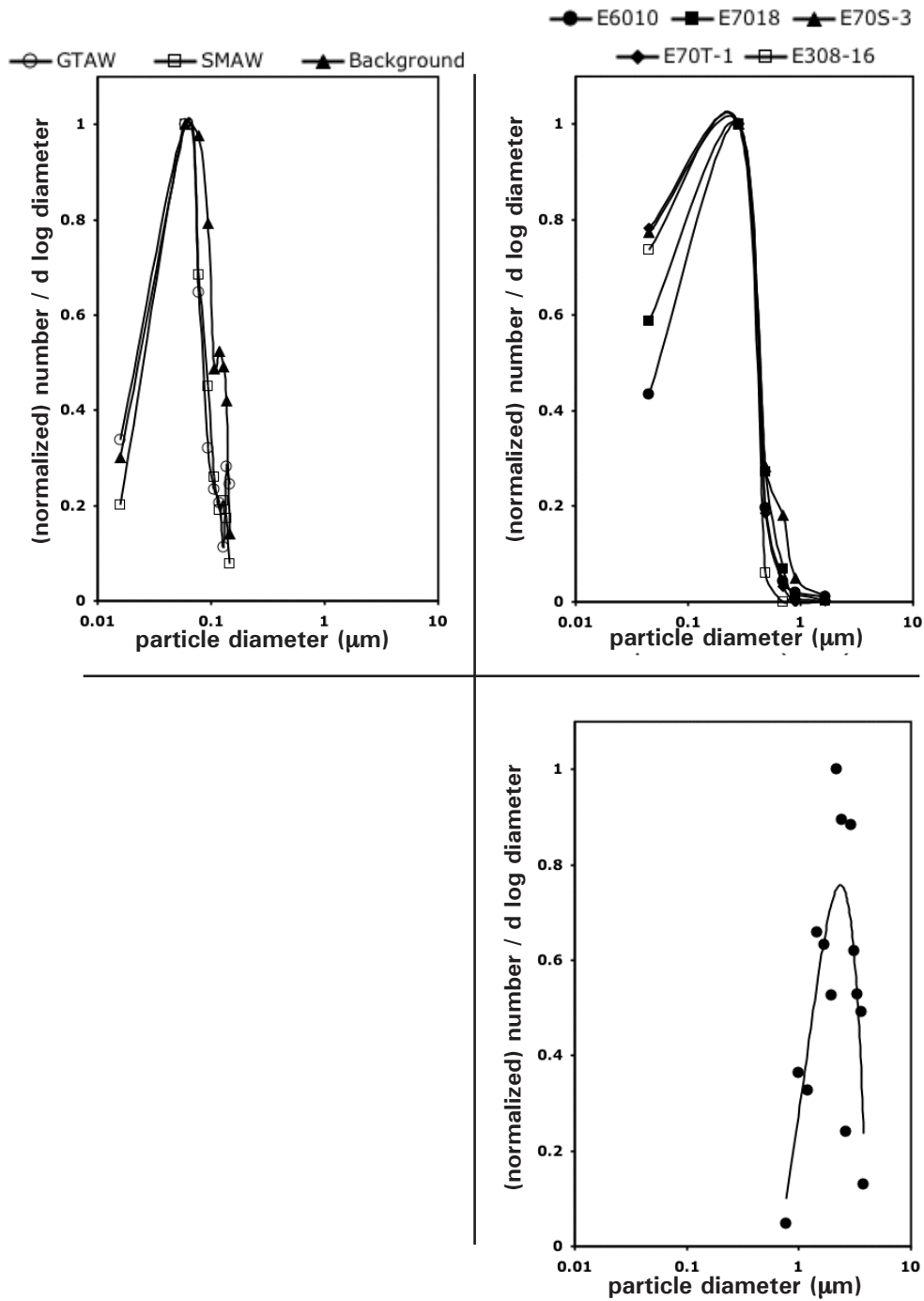
Figure 3.27 Upper (Left) Size distribution of primary particles in Inconel 6251 welding fume agglomerates (automated image analysis of transmission electron micrographs) (Farrants, et al., 1989)

Figure 3.28 (Upper Right) Size distribution of SMAW & GMAW fume (extrapolated diameters (0.1−2.8 micrometer) of > 1000 particles per fume, from scanning electron micrographs) (Fasiska, et al., 1983)

Figure 3.29 (Lower Right) Size distribution of steel welding fume collected on filters (scanning electron microscopy) (Gustafsson, et al., 1986)

References

Berner, V., & Berner, A. (1982). Mass size distributions and elemental frequency distributions of arc welding smokes. *Journal of Aerosol Science,* 13, 191–193.

Block–Bolton, A., & Eagar, T. W. (1984). Metal vaporization from weld pools. *Metallurgical Transactions B,* 15B, 461–469.

Brandes, E. A. (Ed.). (1983). *The Smithells Metals Reference Book* (6th ed.). London: Butterworth–Heinemann.

Buckle, E. R., Tsakiropoulos, P., & Pointon, K. C. (1986). Preparation and properties of metallic aerosol–particles. *International Metals Reviews,* 31(6), 258–288.

Craciun, V., & Craciun, D. (1998). Does the subsurface superheating effect really exist? *Proceedings of the Advances in Laser Ablation of Materials Symposium, 1998 San Francisco,* Singh, R. K., Lowndes, D. H., Chrisey, D. B., Fogarassy, E. & Narayan, J. (Eds.). Warrendale, PA: Materials Research Society.

Cobine, J. D., & Burger, E. E. (1955). Analysis of electrode phenomena in the high-current arc. *Journal of Applied Physics,* 26(7), 895–900.

Deam, R., Bosworth, M., Chen, Z., French, I., Haidar, J., Lowke, J., Norrish, J., Tyagi, V., & Workman, A. (1997). Investigation of fume formation mechanisms in GMAW*. Proceedings of the WTIA International Welding and Joining Research Conference, 10–12 Nov.1997 Victoria, Australia*, Silverwater, Australia: Welding Technology Institute of Australia.

Dreizin, E. L. (2000). Phase changes in metal combustion. *Progress In Energy and Combustion Science,* 26, 57–78.

Duft, D., Achtzehn, T., Müller, R., Huber, B. A., & Leisner, T. (2003). Rayleigh jets from levitated microdroplets. *Nature,* 421(January), 128.

Eichhorn, F., & Oldenburg, T. (1986). *Untersuchung der Scheissrauchentstehung beim Schweissen mit mittel- und hochlegierten Zusatzwerkstoffen*. Duesseldorf, BRD: DVS.

Farrants, G., Schuler, B., Karlsen, J., Reith, A., & Langard, S. (1989). Characterization of the morphological properties of welding fume particles by transmission electron–microscopy and digital image-analysis. *American Industrial Hygiene Association Journal,* 50(9), 473–479.

Fasiska, E. J., Wagenblast, H. W., & Nasta, M. (1983). *Characterization of Arc Welding Fume*. Miami, FL: American Welding Society.

Ferree, S. E. (1995). New generation of cored wires creates less fume and spatter. *Welding Journal*, 12, 45.

Forbes, R. G. (2000). Liquid-metal ion sources and electrosprays operating in cone-jet mode: Some theoretical comparisons and comments. *Journal of Aerosol Science,* 31(1), 97–120.

Friedlander, S. K. (1977). *Smoke, Dust and Haze: Fundamentals of Aerosol Behavior*. New York: John Wiley & Sons.

Gustafsson, T. E., Tossavainen, A., & Aitio, A. (1986). Scanning electron microscopic studies on flame cutting and welding fumes in a steel foundry*. Proceedings of the International Conference on Health Hazards And Biological Effects of Welding Fumes and Gases, Copenhagen, 18–21 February 1985* Danish Welding Institute, R. M. Stern, A. Berlin, A. Fletcher, K. Hemminki, J. Jarvisalo & J. Peto (Eds.). Amsterdam: Excerpta Medica.

Heile, R. F., & Hill, D. C. (1975). Particulate fume generation in arc welding processes. *Welding Journal,* 54(7), 201s–210s.

Hewett, P. (1995). The particle size distribution, density and specific surface are of welding fumes from SMAW and GMAW mild and stainless steel consumables. *American Industrial Hygiene Association Journal,* 56(2), 128–135.

Hinds, W. C. (1982). *Aerosol Technology: Properties, Behavior, and Measurement of Airborne Particles*. New York: John Wiley & Sons.

Hinds, W. C. (1993). Physical and chemical changes in the particulate phase. In Willeke, K. & Baron, P. A. (eds.), *Aerosol Measurement: Principles, Techniques, and Applications*. New York: Van Nostrand Reinhold.

Jin, Y. (1994). Fume generation from gas metal arc-welding processes. *Staub Reinhaltung Der Luft,* 54(2), 67–70.

Jones, L. A. (1996). *Dynamic Electrode Forces in Gas Metal Arc Welding*. Ph.D. Dissertation: Massachusetts Institute of Technology, Cambridge, MA.

Kodas, T. T., & Hampden-Smith, M. J. (1999). *Aerosol Processing of Materials.* New York: Wiley-VCH.

Lafferty, J. M. (Ed.). (1980). *Vacuum Arcs Theory And Application*. New York: John Wiley & Sons.

Ma, J., & Apps, R. L. (1983). New MIG process results from metal transfer mode control. *Welding and Metal Fabrication,* 51(4), 168–170.

Mendez, P., Jenkins, N. T., & Eagar, T. W. (2000). Effect of electrode droplet size on evaporation and fume generation in GMAW*. Proceedings of the Gas Metal Arc Welding for the 21st Century Conference, Dec. 6–8, 2000 Orlando, Florida*, Miami, Florida: American Welding Society.

Mendez, P.F. (1999) *Order of Magnitude Scaling of Complex Engineering Problems, and its Application to High Productivity Arc Welding.* Ph.D Dissertation: Massachusetts Institute of Technology, Cambridge, MA.

Moll, J. H. (2000). Utilization of gas-atomized titanium and titanium-aluminide powder. *JOM,* 52(5), 32–42.

Mori, T., Matsuda, A., Akashi, S. O., M., Takeoka, K., & Yoshinaka, M. (1991). The 3-dimensional distribution of chromium and nickel-alloy welding fumes. *Acta Medica Okayama,* 45(4), 233–240.

Poirier, D. R., & Geiger, G. H. (1994). *Transport Phenomena in Materials Processing*. Warrendale, PA: TMS.

Process Associates of America (2003).Ohnesorge Number [On-line]. Available: http://www.processassociates.com/process/dimen/dn_ohn.htm

Quimby, J. (1997). *Fume Formation Rates in Gas Metal Arc Welding.* M.S. Thesis: Chemical Engineering University of New Hampshire.

Quimby, J. B., & Ulrich, G. D. (1999). Fume formation rates in gas-shielded metal arc welding. *Welding Journal,* April, 142–149.

Rayleigh, Lord (1882). On the equilibrium of liquid conducting masses charged with electricity. *Philosophical Magazine,* 14, 184–186.

Ren, J. (1997). *Distribution of Particles in Welding Fume.* M.S. Thesis: Chemical Engineering University of New Hampshire.

Richardson, F. D. (1974). *Physical Chemistry of Melts in Metallurgy*. London: Academic Press.

Riehemann, W. (1998). Synthesis of nanoscaled powders by laser-evaporation of materials*.* Paper presented at the *Materials Research Society Symposium*, 501, 3–14.

Suga, T., & Kobayashi, M. (1984). Fume generation in CO_2 arc welding by flux-cored wire. *Yosetsu Gakkai Ronbunshu / Quarterly Journal of the Japan Welding Society*, 2(4), 68–75.

Tanaka, K., Ishizaki, K., Yumoto, S., Egashira, T., & Uda, M. (1987). Production of ultra-fine silicon powder by the arc plasma method. *Journal of Materials Science*, 22(6), 2192–2198.

Ulrich, G. D., & Riehl, J. W. (1982). Aggregation and growth of submicron oxide particles in flames. *Journal of Colloid and Interface Science*, 87(1), 257–265.

Vijayan, T., & Rohatgi, V. K. (1985). Characteristics of exploding-wire plasmas. *IEEE Transactions On Plasma Science,* 13(4), 197–201.

Vladimirov, V. V., Gorshkov, V. N., & Mozyrsky, D. V. (1995). The dynamical effects in liquid-metal ion sources. *Applied Surface Science,* 87/88, 112–116.

Whitby, K. T. (1978). The physical characteristics of sulfur aerosols. *Atmospheric Environment,* 12, 135–159.

Willeke, K. & Baron, P. A. (eds.) (1993). *Aerosol Measurement: Principles,*

Techniques, and Applications. New York: Van Nostrand Reinhold.

Zimmer, A. T. (2001). Characterization of the aerosols resulting from arc welding processes. *Journal of Aerosol Science,* 32, 933–1008.

Zimmer, A. T., Baron, P. A., & Biswas, P. (2002). The influence of operating parameters on number-weighted aerosol size distribution generated from a gas metal arc welding process. *Journal of Aerosol Science,* 33(3), 519–531.

Chapter 4

Airborne Particle Characterization

In order to determine the relationship between chemistry and the size of airborne particles, one must analyze the particles chemically. Because of the particles' sizes, chemical analysis is not easy. In this chapter, various chemical analysis techniques and their applications to particles are described, and welding fume is used as an example.

4.1 Particle Collection

Several researchers (see Chapter 2) have collected welding fume, primarily to measure its formation rate, but also to study its chemistry. In 1992, the American Welding Society published a standard for measuring the fume formation rate. The fume studied here was collected in a chamber designed by Professor Gael Ulrich and co-workers at the University of New Hampshire. They published the design in a thesis and a paper (both listed in Chapter 2) in which an excellent critique of fume collection methods can also be found. Here just the method of collection is described.

A weld was laid on a cylindrical pipe (see Figure 4.1) about 25 cm in diameter and 30 cm long. The pipe rotated inside a chamber which moved horizontally around the pipe. A GMAW torch was attached to the chamber through a hole so that a weld bead could be laid on the pipe forming a spiral as the pipe rotated and as the chamber moved.

A Hobart Arc-Master 500 power supply and a Hobart 2410 semiautomatic solid-state control wire feeder were used. The power supply was a primary inverter power source current-rated at 500 amps / 40 V at 100% duty cycle and suited for all types and modes of gas metal arc welding, including that done pulsed current. Shielding gas of any typical composition at various flow rates and any GMAW or FCAW wire of various diameters can be employed.

Negative pressure was applied to the chamber so that fume could be collected while the pipe was welded and shortly thereafter.. This either pulled the fume out of the chamber at a flow rate of ~2 L/min through filters (0.2 micrometer Corning [Nucleopore] PC filter, 37 mm dia.) stationed approximately 1 ft. above the arc or drew air at 28.3 L/min into a cascade impactor. The fume was then removed from the filters (see Figure 4.2) or from the impactor for analysis.

Table 4.1 lists the parameters that can be varied. Most were never changed for the research reported here. The parameters that changed are so indicated and will be described in the sections that follow.
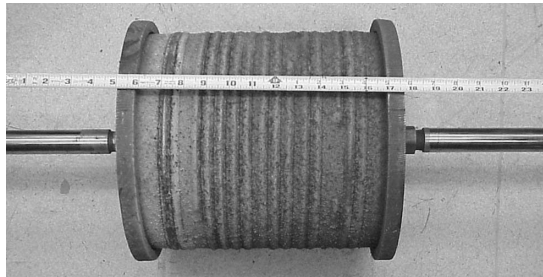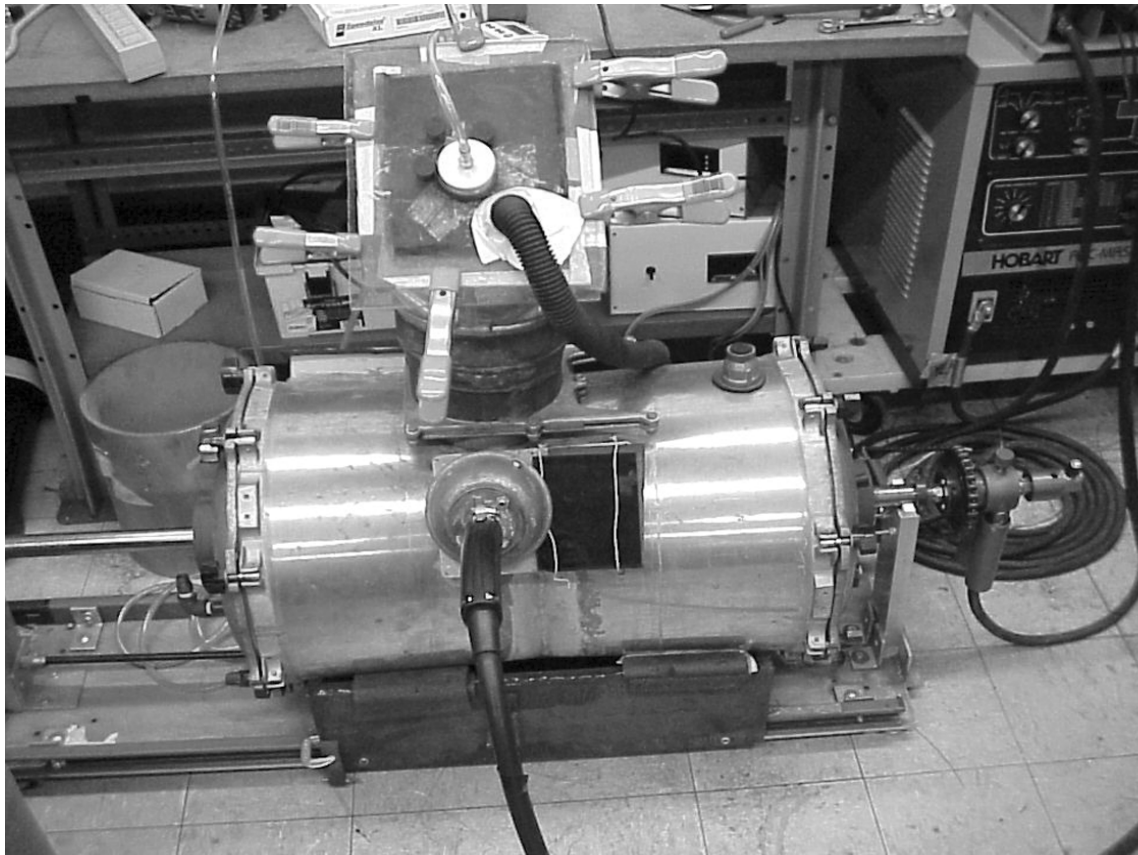
Figure 4.1 Welding fume collection chamber with welded pipe.
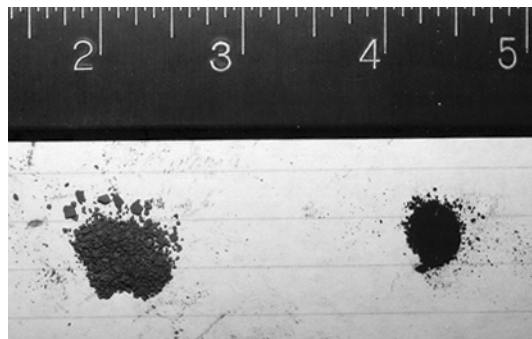
Figure 4.2 Photograph of mild steel welding fume, from SMAW (left) and GMAW (right). When airborne, welding fume is almost invisible; when collected it is brown-black.

Table 4.1 Parameters for Welding Fume Generation

Welding Parameter	Condition
Polarity	Positive electrode
Welding Travel Speed	~16 mm/s (14 in./min)
Contact Tip to Work Distance (CTWD)	~19 mm (0.75 in.)
Electrode Angle	~10 degree drag angle
Wire Diameter	0.045 in.
Shielding Gas Flow Rate	16.5 L/min, (unless self-shielded electrode used)
Shielding Gas Composition	Varied (a mixture of Ar, O2, CO_2 and/or He)
Work Piece Composition	A500 carbon steel or 304 stainless steel
Electrode Composition	GMAW or FCAW of varied steel composition
Wire Feed Speed (wfs)	Varied (determines current magnitude and transfer mode)
Voltage	Varied (determines metal transfer mode)
Current (Steady / Pulsed)	Steady current is set by voltage and wire feed speed. With pulsed current, pulse width & frequency are varied.

4.2 Particle Characterization

Knowledge of particle size is important because a given characterization technique only provides accurate data for a specific size range. Many previous studies leave this fact unstated when reporting the results of welding fume characterization and thus give misleading conclusions. This has been fairly common in welding fume literature, particularly with studies involving energy dispersive spectroscopy with scanning electron microscopes.

Because fume is a powder, it is easily prepared as a bulk material, e.g., for X-ray analysis; it only becomes difficult to prepare if one wishes to analyze individual discrete particles, although for transmission electron microscopy, their small sizes aid sample preparation enormously by in comparison with samples that must be thinned by ion sputtering and similar processes. (Appendix B describes the preparation of TEM samples from welding fume.) Therefore, there are many studies using X-ray diffraction and electron microscopes.

Table 4.2 is a review of various methods that can be used to characterize welding fume (and other particulate matter). The methods are categorized by the information they provide and the particle size range for which they are applicable.

Table 4.2 Characterization Methods for Particle Size and Chemistry

Characterization Method	Size Range (μm)	Detection Limit	Notes NA = not applicable
Particle Size Distribution			
Impactors (various types)	0.1–20	NA	Size distribution by mass chemically analyze size groups
Electric aerosol analyzer (EAA) and differential mobility particle sizer	0.01–1	NA	Size distribution by number
Aerodynamic particle sizer	0.1–25	NA	Size distribution by number
Scanning electron microscope (SEM); high resolution (HRSEM)	0.5–50 0.002–1	NA	Particle sizes can be measured from micrographs
Electron probe microanalysis (EPMA)	0.5–50	NA	Particle sizes can be measured from micrographs
Transmission electron microscope (TEM)	0.001–1	NA	Particle sizes can be measured from micrographs
Light microscopy	1–400	NA	
Elemental Composition			
X-ray fluorescence spectrometry (XRF)	bulk	100 ppm	Atomic numbers > 10 very fast
Neutron activation analysis (NAA)	bulk	0.01%	Atomic numbers > 10, requires nuclear reactor
Optical emission spectrometry and mass spectrometry	bulk	1-10 ppm	Atomic numbers > 10
Atomic absorption spectrometry (AAS)	bulk	10 ppm	
Energy dispersive spectrometry with SEM (SEM-EDS)	1–50	0.1%	Atomic numbers > 10
Wavelength-dispersive spectrometry with EPMA (EPMA-WDS)	1–50	0.1%	Atomic numbers > 4
Energy dispersive spectrometry with TEM (TEM-EDS)	0.01–0.5	0.1%	Atomic numbers > 5 scanning TEM can map element distribution at nm resolution
Proton induced X-ray emission spectrometry (PIXE)	>5	0.1%	Atomic numbers > 10
Laser microprobe mass spectrometry (LAMMS)	>1	10 ppm	All elements
Secondary ion mass spectrometry (SIMS)	>5	10 ppm	Light element capable
Auger electron spectrometry (AES)	>0.1	0.1%	Atomic numbers > 3 lower sample must be conductive
X-ray induced photo-electron spectrometry (XPS or ESCA)	>5	0.1%	Surface composition (3–5nm deep) contamination error common

Table 4.2 Characterization Methods for Particle Size and Chemistry

Characterization Method	Size Range (µm)	Detection Limit	Notes NA = not applicable
Chemical Speciation			
X-ray diffraction (XRD)	bulk	NA	Only of crystalline material particles must be > 0.05 micrometers or they will seem amorphous
X-ray induced photoelectron spectrometry (XPS or ESCA)	bulk	NA	Need appropriate standards Collect on non-interacting filter (e.g., PVC porous membrane filter)
Selected area electron diffraction with TEM (TEM-SAED)	~0.3	NA	Only of crystalline material

For further details, the following have reviewed the characterization of particles:

Kodas, T. T., & Hampden-Smith, M. J. (1999). *Aerosol Processing of Materials.* New York: Wiley-VCH.

Ortner, H. M., Hoffmann, P., Stademann, F.J., Weinbruch, S., & Wentzel, M. (1998). Chemical characterization of environmental and industrial particulate samples. *Analyst*, 123, 833–842.

Voitkevich, V. (1995). *Welding fumes: Formation, Properties and Biological Effects*. Cambridge, England: Abington Publishing.

Willeke, K. & Baron, P. A. (Eds.) (1993). *Aerosol Measurement: Principles, Techniques, and Applications*. New York: Van Nostrand Reinhold.

Examples of particle characterization by a specific technique include:

Calastrini, F., Del Carmine, P., Lucarelli, F., Mandò, P. A., Prati, P., & Zucchiatti, A. (1998). External-beam PIGE for fluorine determination in atmospheric aerosol. *Nuclear Instruments and Methods In Physics Research Section B*, 136-138, 975–980.

Dong, X. L., Zhang, Z. D., Zhao, X. G., Chuang, Y. C., Jin, S. R., & Sun, W. M. (1999). The preparation and characterization of ultrafine Fe-Ni particles. *Journal of Materials Research*, 14(2), 398–406.

Ersez, T., & Liesegang, J. (1991). Analysis of brown coal fly-ash using X-ray photo-electron-spectroscopy. *Applied Surface Science*, 51(1-2), 35–46.

Farmer, M. E., & Linton, R. W. (1984). Correlative surface analysis studies of environmental particles. *Environmental Science and Technology*, 18(5), 319–326.

Jambers, W., Debock, L., & Vangrieken, R. (1995). Recent advances in the analysis of individual environmental particles - a review. *Analyst*, 120(3), 681–692.

Jambers, W., Debock, L., & Vangrieken, R. (1996). Applications of micro-analysis to individual environmental particles. *Fresenius Journal of Analytical Chemistry*, 355(5-6), 521–527.

Keyser, T. R., Natusch, D. F. S., Evans, C. A., & Linton, R. W. (1978). Characterizing the surfaces of environmental particles. *Environmental Science and Technology*, 12, 768.

Konarski, P., Iwanejko, I., Mierzejewska, A., & Diduszko, R. (2001). Morphology of working environment microparticles. *Vacuum*, 63, 679–683.

Rickman, J. T., & Linton, R. W. (1993). Surface and depth profiling techniques using XPS applied to the study of nickel-containing environmental particles. *Applied Surface Science*, 68(3), 375–393.

Schmeling, M., Klockenkamper, R., & Klockow, D. (1997). Application of total-reflection X-ray fluorescence spectrometry to the analysis of airborne particulate matter. *Spectrochimica Acta Part B - Atomic Spectroscopy*, 52(7), 985–994.

Vissikov, G. P. (1992). Structural, phase and morphological features of plasma-chemically synthesized ultradispersed particles. *Journal of Materials Science*, 27, 5561–5568.

Yelsukov, E. P., Mikhailik, O. M., Konygin, G. N., Mikhailova, S. S., & Povstugar, V. I. (1999). Phase composition study of bulk and surface layers of stabilized iron powders. *Nanostructured Materials*, 12, 211–214.

In practice, there are two types of chemical characterization techniques: those that measure radiation proportional to the atomic number and those that measure from values proportional to the atomic mass. The former produce data easily transformed into molar / atomic fractions, whereas the latter create data reported as weight percentages. If one has reliable values for each element present the specimen is being analyzed, then one can convert from atomic fraction to weight percent and back. However, none of the analysis techniques is able to measure every element with the same accuracy, so invariably one receives an incomplete elemental analysis. When this happens, conversion between weight and atomic percentages is only qualita-

tive, because the entire mass is not characterized. Therefore, the elemental data from multiple techniques cannot be compared, except within the two major groupings presented here.

As it happens, the techniques that report mass instead of moles are also those with the more frequent inaccuracies in reporting data. For example, iron and aluminum cannot be determined with great accuracy with inductively coupled plasma mass spectrometry (ICPMS) when in high (greater than 5 wt%) concentrations. The bags used to contain the sample during neutron activated analysis (NAA) often contain aluminum, which distorts the analysis of that element.

These weaknesses are in addition to the inability of almost all techniques to accurately analyze any elements lighter than sodium. Even when a method can analyze elements down to, carbon, problems, like water condensation on the filament or surface contamination with carbon dioxide, can obscure important peaks like oxygen or fluorine. High-powered electron beams can also break down organics, causing a film of carbon to deposited on the sample. These very problems were encountered when the author performed transmission electron microscopy of welding fume. Because welding fume is composed of oxides (with some halides), lack of information on oxygen concentration makes it impossible to determine the entire molar/mass quantity of the fume.

Because of these limitations, the most convenient way to analyze welding fume is with the molar fraction of only the metals. Energy dispersive spectrometry and X-ray photon spectroscopy are good techniques for this, especially when one recalls the respective size limitations with respect to ultrafine particles.

A few remarks about energy-dispersive spectrometry should be made. When used with (scanning) transmission electron microscopy, the resolution of the microanalysis should be kept in mind. Because of electron interactions with the material, the possible resolution decreases with increasing atomic number. Thus, it may not be possible to measure the change in composition in a very small area. However, the thinner the sample analyzed, the less beam broadening will occur.

For a good reference on the methods involved in electron microscopy, see:

Hren, J. J., Goldsten, J. I., Joy, D. C. (Eds.) (1979) *Introduction to Analytical Electron Microscopy.* New York: Plenum Press.

The tables that follow (Table 4.4–Table 4.6) compare various chemical characterization techniques. The tables contain chemical data about several welding fumes collected and analyzed by the author from a E7018-A low hydrogen SMAW electrode and the electrodes listed in Table 4.3. The data are typical of what other researchers have found in welding fume (see Chapter 2 for references).

Table 4.3 Composition of GMAW and FCAW wire used to create welding fume (emission spectrometry and inert gas fusion)

wt%	ER70S-3 GMAW mild steel	E71T-GS FCAW mild steel	E308L GMAW stainless	E308FC FCAW stainless
Fe	98.04	91.69	67.01	61.93
Cr	0.046	0.190	20.83	18.80
Ni	0.038	0.028	9.766	9.010
Cu	0.160	0.002	<0.01	0.340
Co	0.000	0.001	0.000	0.100
Mn	1.162	0.731	1.773	2.058
Si	0.551	0.270	0.561	0.549
Al	0.000	3.143	0.000	0.410
Ti	0.000	0.001	0.000	2.407
Zr	0.000	0.000	0.000	0.579
Mo	0.005	0.002	0.046	0.270
K	0.000	0.025	0.000	0.110
Na	0.000	0.007	0.000	0.120
Ca	0.000	0.340	0.000	1.139
Mg	0.000	0.941	0.000	0.004
Ba	0.000	2.463	0.000	0.000
O	0.000	0.160	0.000	2.178
F	0.000	<0.001	0.000	<0.001
Cl	0.000	0.001	0.000	<0.001

Table 4.4 Analysis of bulk welding fume with techniques based on atomic numbers. Although not listed, oxygen is present in all fume and fluorine is present in SMAW fume.

Mole Fraction of Metals	SEM-EDS	STEM-EDS	XPS
2%O_2 Ar-shielded GMAW with 0.045" mild steel ER70S-3 wire at 30V, ~200amps			
Fe	0.877	0.887	0.767
Mn	0.098	0.104	0.233
Si	0.025	0.008	<0.01
SMAW with 0.094" mild steel E7018-A electrode at 70amps			
Fe	0.270	0.280	<0.01
Mn	0.099	0.103	0.052
Si	0.095	0.057	0.131
K	0.276	0.295	0.575
Ca	0.251	0.252	0.241
Na	0.011	0.013	<0.01

Table 4.5 Analysis of bulk welding fume with techniques based on atomic masses. NA = not analyzed. Oxygen and fluorine also not analyzed and not listed

wt%	ICPMS	XRF	NAA
2%O_2 Ar-shielded GMAW with 0.045″ mild steel ER70S-3 wire at 30V, ~200amps			
Fe	37.8	55.0	
Mn	8.8	12.8	
Si	NA	NA	
Cu	0.9	1.1	
Self-shielded FCAW with 0.045″ mild steel E71T-GS wire at 30V, ~170amps			
Fe	18.1	23.7	32.4
Mn	0.5	2.7	1.6
Ba	NA	NA	9.8
Mg	NA	NA	8.8
Al	56.3	NA	*
% undissolved in acid: 25			
*Aluminum present strongly but obscured by aluminum in sample bag			
Self-shielded FCAW with 0.045″ stainless steel E308FC wire at 30V, ~170amps			
Fe	10.3	21.4	
Cr	3.9	11.0	
Mn	2.6	11.0	
Ni	1	2.8	
Si	NA	NA	
Al	15.2	NA	
Ti	NA	NA	
Zr	NA	1.500	
K	NA	NA	
Na	NA	NA	
Ca	NA	NA	
% undissolved in acid: 63			
2%O_2 Ar-shielded GMAW with 0.045″ stainless steel E308L wire at 30V, ~200amps			
Fe	15.8–21.0		
Cr	12.5–13.1		
Mn	11.9–17.4		
Ni	1.0–2.5		
Si	not analyzed		
% undissolved in acid: > 50			
the range of values are collected from 4 different samples created at identical conditions			

**Table 4.6 X-ray diffraction of mild steel welding fume
GMAW (ER70S-3, 30V 300ipm) and SMAW (E7018-A 3/32", 70 amps)
See Figure 4.3and Figure 4.4 for X-ray diffraction spectra.**

	Chemical Phases Detected	Approx. Crystalline Amount of Sample (%)	Approx. Amorphous Amount of Sample (%)
GMAW	Fe_3O_4 (magnetite)	64	36
SMAW	(K, Na, Ca, Mn) F_2 (fluoride) $MnFe_2O_4$ (spinel)	71	29

Previous X-ray diffraction studies (see Section 2.10) have reported many phases in welding fume and have implicated that a single fume particle contained three or more phases. This is obviously not the case for ultrafine particles; a particle only a few nanometers in diameter could not have that many phases. It can be shown with transmission electron microscopy, that fume can be heterogeneous with the many phases contained individually in separate particles. However, larger particles (greater than 100 nm) which have coalesced or sintered from smaller particles may have several phases. This will be discussed later.
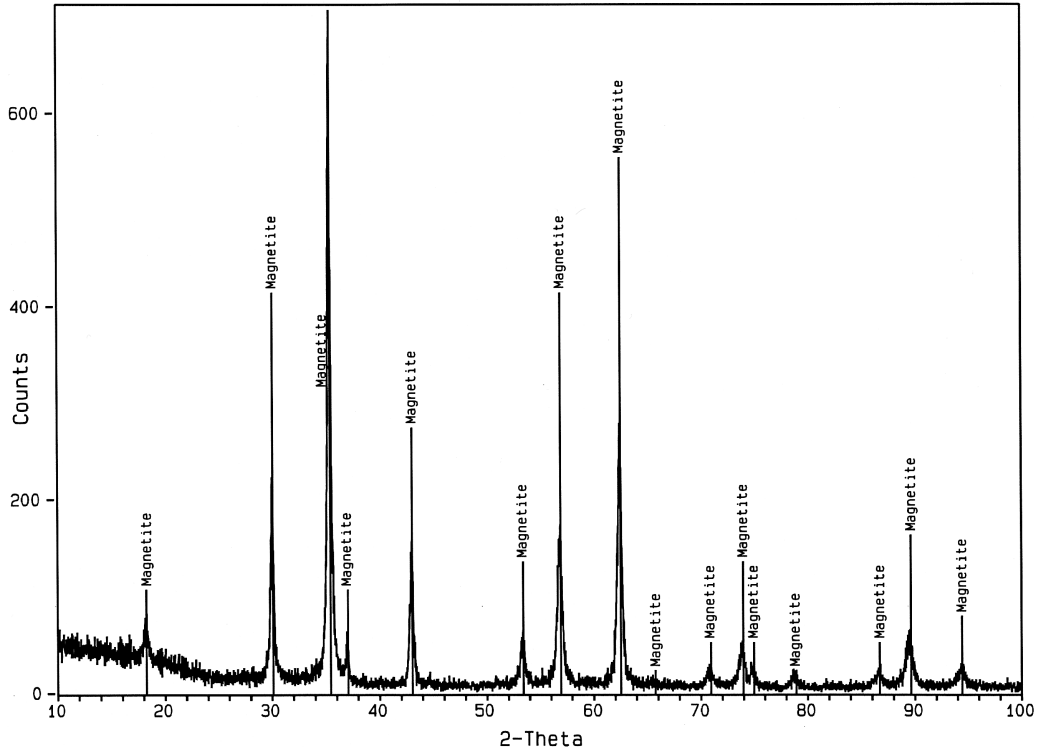
Figure 4.3 (Top) X-ray diffraction spectrum for mild steel GMAW fume
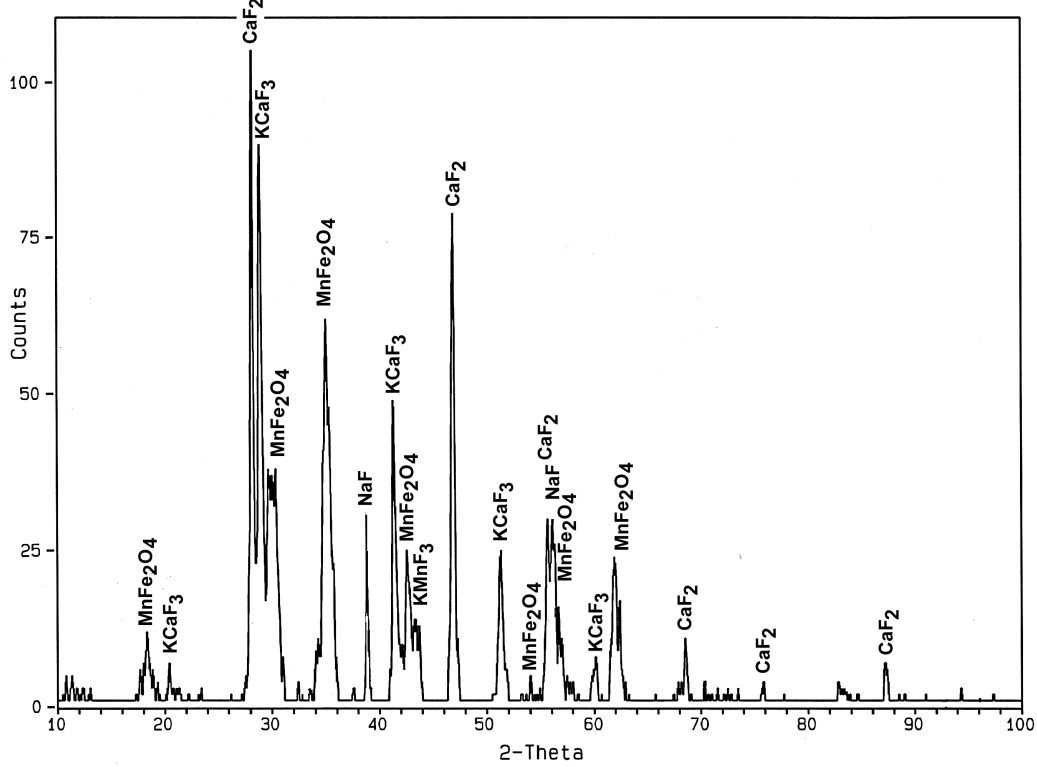
Figure 4.4 (Bottom) X-ray diffraction spectrum for mild steel SMAW fume

89

Chapter 5

Chemical Composition and Particle Size

To explain why their thermochemical calculations for vapor composition did not accurately predict fume composition, Gray, et al., (1980) proposed that welding fume was created both from a vapor and from fine molten droplets. They equated the measured bulk fume composition to the weighted average of the measured wire electrode composition, the theoretical metal vapor composition over the electrode, the measured base plate composition and the theoretical metal vapor composition over the base plate. From these they solved for the fractions of each of these four "sources" of fume for stainless steel. Although they did not study fume particle size, they were the first welding fume researchers to suggest that fume chemistry was related to the particle formation path and some of the few researchers who have tried to predict welding fume composition using thermodynamics.

Since then, seven studies on the relationship between size and composition have been reported (see Section 2.14 for references). Most have involved a chemical analysis of fume separated with impactors. Such studies can show the chemical difference between fine and coarse particles, but because the smallest cut-off size in any impactor is larger than approximately 100 nanometers, these studies cannot determine anything about primary particle chemistry can be determined. Energy dispersive spectrometry with transmission electron microscopy (TEM-EDS) is well suited for determining the composition of particles smaller than 1 micrometer, but only two groups of researchers have used this method. They reported qualitative results with little explanation (Fasiska et al., 1983; Grekula, et al., 1986; Kalliomaki, et al., 1987).

The size distribution of elements has been measured in other similar aerosols from sources like iron foundries (Dams & Zhang, 1987; Perrault, et al., 1992), incinerators (Linak, et al., 1994), and the general atmosphere (Davidson & Osborn, 1986; Hlavay, et al., 1992; Hlavay, et al., 1998). All report a general tendency for the highly volatile metals to be more strongly present in the accumulation or fine range than in the coarse range of particles.

Three groups of researchers have published excellent overviews about aerosols from combustion and waste incineration. Their works are good for studying general principles and theories about the relationship between particle chemistry and size. See Linak, et al., 1993; Lin & Biswas, 1994; Lighty, et al., 2000.

In this chapter, the relationship between particle size and particle composition is explored. This exploration is divided into a section about particles in the coarse range, which is followed by a section on fine particles. Each of these sections contains experimental data, the first from fume captured with a cascade impactor and the latter from transmission electron microscopy. The results are discussed and are shown to follow thermochemical behavior familiar to those involved in metallurgical processing.

References

Dams, R., & Zhang, Y. (1987). Elemental composition of dust in an iron foundry as determined by instrumental neutron activation analysis. *Journal of Radioactive and Nuclear Chemistry,* 110(2), 305–320.

Davidson, C. I., & Osborn, J. F. (1986). The sizes of airborne trace metal containing particles. In Nriagu, J. O. & Davidson, C. I. (Eds.), *Toxic Metals in the Atmosphere* (Vol. 17): Wiley Series: Advances in Environmental Science and Technology.

Fasiska, E. J., Wagenblast, H. W., & Nasta, M. (1983). *Characterization of Arc Welding Fume*. Miami, FL: American Welding Society.

Gray, C. N., Hewitt, P. J., & Hicks, R. (1980). The prediction of fume compositions in stainless steel metal inert gas welding*. Proceedings of Weld Pool Chemistry and Metallurgy International Conference April 1980*, Bailey, N. (Ed.). Cambridge, England: The Welding Institute, Abington Hall.

Grekula, A., Peura, R., & Sivonen, S. (1986). Quantitative energy dispersive x-ray microanalysis of welding fumes. *Proceedings of the International Conference on Health Hazards and Biological Effects of Welding Fumes and Gases February 1985*, R. M. Stern, A. Berlin, A. Fletcher, K. Hemminki, J. Jarvisalo & J. Peto (Eds.). Amsterdam: Excerpta Medica.

Hlavay, J., Polyak, K., Molnar, A., & Meszaros, E. (1998). Determination of the distribution of elements as a function of particle size in aerosol samples by sequential leaching. *Analyst,* 123, 859–863.

Hlavay, J., Polyak, K., & Wesemann, G. (1992). Particle-size distribution of mineral phases and metals in dusts collected at different workplaces. *Fresenius Journal of Analytical Chemistry,* 344(7–8), 319–321.

Kalliomaki, P. L., Grekula, J. A., Hagberg, & Sivonen, S. (1987). Analytical electron microscopy of welding fumes. *Journal of Aerosol Science*, 18(6), 781–784.

Lighty, J., Veranth, J., & Sarofim, A. (2000). Combustion aerosols: Factors governing their size and composition and implications to human health. *Journal of the Air & Waste Management Association,* 50(9), 1565–1618.

Lin, W.-Y., & Biswas, P. (1994). Metallic particle formation and growth dynamics during incineration. *Combustion Science and Technology,* 101, 29–43.

Linak, W. P., Srivastava, R. K., & Wendt, J. O. L. (1994). Metal aerosol formation in a laboratory swirl flame incinerator. *Combustion Science and Technology,* 101(1–6), 7–27.

Linak, W. P., & Wendt, J. O. L. (1993). Toxic metal emissions from incineration - mechanisms and control. *Progress In Energy And Combustion Science,* 19(2), 145–185.

Perrault, G., Dion, C., Ostiguy, C., Michaud, D., & Baril, M. (1992). Selective sampling and chemical speciation of airborne dust in ferrous foundries. *American Industrial Hygiene Association Journal,* 53(7), 463–470.

5.1 Coarse Particles

Coarse particles, because they are an order of magnitude larger in diameter and therefore three orders of magnitude greater in mass than fine particles, can dominate the bulk chemistry of airborne particles. Thus, even if they are few in number, it is important to determine the amount of coarse particles created in a fume formation process.

For welding fume, there seems to be a relationship between fume formation rates and spatter[1] formation rates. Some researchers attribute this relationship to spatter combustion (Gray, et al., 1982; Hewitt & Hirst, 1991), a theory examined in Appendix A. Others believe that spatter contains "sputter" or "microspatter" – droplets not visible to the human eye that contribute to airborne fume (Deam, et al., 1997; Quimby & Ulrich, 1999). In their 2002 study, Zimmer, et al., measured the concentration of particles in that size range (see Figure 3.26) and concluded that spatter does not significantly contribute to fume, although both spatter and fume formation rates increase and decrease in the same way with changing welding parameters.

In Section 3.3, it was discussed that bursting vapor bubbles can create coarse droplets/particles. Gray, et al. suggested this in 1980, but this was not mentioned again in successive papers. Because higher fume formation rates are linked with greater vaporization rates due to increased surface temperatures (Mendez, et al., 2000), it can be concluded that the reason for the correlation between fume and spatter rates is not because one causes the other, but rather that both are controlled by the same variables (e.g., surface temperature and electrical current).

In any case, it appears that coarse particles exist in welding fume, and even if they do not dominate the fume mass or chemistry, their elemental composition is likely the same as the input material, i.e., the welding electrode. This theory was tested in the following manner: fume was collected with a cascade impactor and particle size groups were analyzed with energy dispersive spectrometry in a scanning electron microscope. The following subsections discuss the findings.

5.1.1 Metal Distribution Determined with Cascade Impactor

Fume was created by arc welding in the fume chamber described previously (Section 4.1). Four different methods were employed: gas metal arc welding (GMAW)

---

1. Bits of metal greater than 10 micrometers that fly out from the weld zone and do not remain airborne.

with three different sets of parameters and correspondingly different metal transfer modes (globular, spray, and pulsed), and one type of self-shielded flux cored arc welding (FCAW). See Table 5.1 for details.

Table 5.1 Description of welding processes studied.

Welding Process	Shield Gas	Electrode AWS Designation	Current (amp)	Voltage (volt)	Wire Speed (ipm)	Pulse Width (ms)
globular GMAW	2%O_2,Ar	ER308L 0.045"	~130	30	180	
spray GMAW	2%O_2,Ar	ER308L 0.045"	~185	30	300	
pulsed GMAW	2%O_2,Ar	ER308L 0.045"	peak: ~325 ave: ~100	average: ~30 background:19	180	2.8
FCAW	none	ER308FC-0 0.045"	~170	30	530	

A cascade impactor (Thermo Andersen Nonviable Eight Stage Cascade Impactor Series 20-800 Mark II. See Figure 5.1) was connected to the chimney of the fume chamber. The vacuum supplied with the impactor drew 28.3 L/min of air from the chamber into the impactor where airborne particles were collected at various stages onto impaction plates. The plates from each stage were weighed before and after fume collection with a Mettler AE 163 microbalance with ± 50 microgram precision. Collection times that ranged from 10 seconds for FCAW to 4 minutes for pulsed GMAW were sufficient to obtain sufficient material to weigh, but care was also taken to collect for times no longer than necessary. Overloading on the impaction plates can cause some impacted particles to become re-entrained in the airflow and to re-impact at the incorrect stage (Thermo Andersen, 2002).

The air flow through an impactor is controlled by a jet plate at each stage so that particles impact on the corresponding collection plate according to their inertia. The largest particles impact on the first plate and are removed from the air stream, then slightly smaller on the next plate, and so on. An oil or grease on the stages can be used to prevent particle bounce, if that is a concern, but this was not done, because welding fume is known to adhere well to clean metal surfaces. At the final stage a filter collects all particles smaller than 0.4 micrometer. Not all of the eight stages of the impactor were used in this study; according to the manufacturer, this does not change the aerodynamics of the remaining stages.

Because the density and particle shape affect the aerodynamic diameter (the equivalent diameter of spherical particles with 1 g/cm^3 density) of the particles, it is important to measure the particle size that impacts at each stage for each type of particulate material that is measured. Fume particles were transferred to adhesive SEM stubs by pressing the stubs against impaction plates after collection. Scanning electron micrographs of the stubs were analyzed on a Macintosh Powerbook G4 computer using the public domain NIH Image program (developed at the U.S. National Institutes of Health and available on the Internet at http://rsb.info.nih.gov/
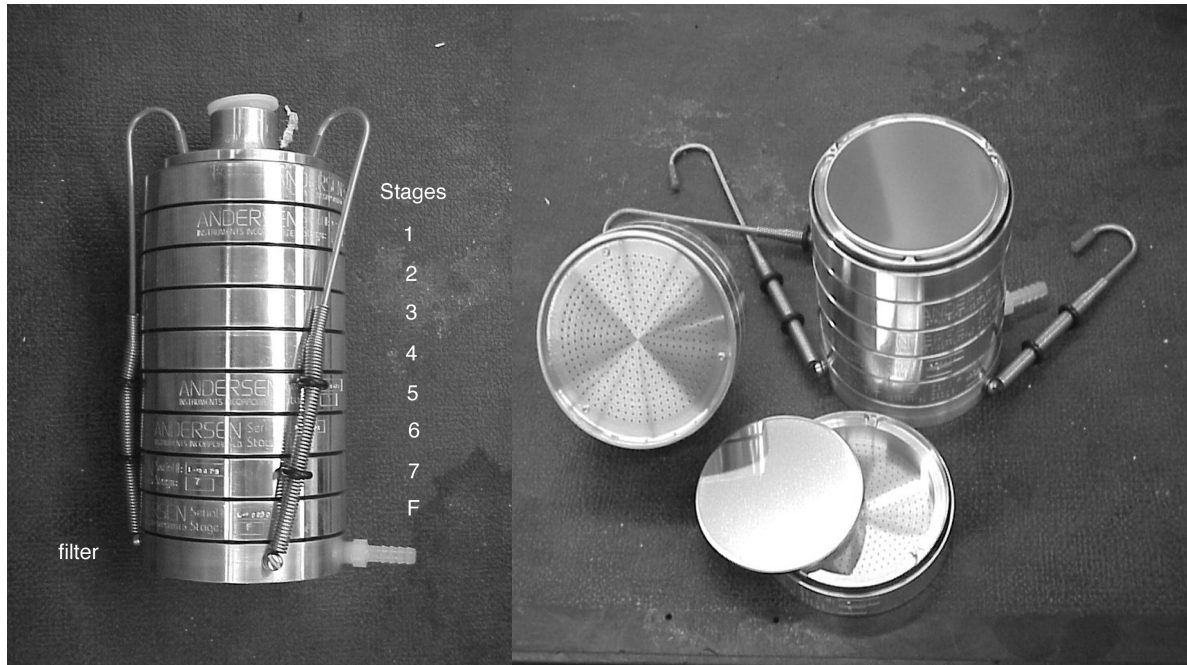
Figure 5.1 Andersen Cascade Impactor. Only stages 1, 5, 6 and F were used, along with the bottom filter.

nih-image/) to determine the particle size distribution collected on each plate. See Figure 5.2 through Figure 5.4. During collection, many particles impacted in piles that made measurement of a single particle difficult. Care was taken to create micrographs of regions where particle pileup did not occur. In addition, smaller welding fume particles often aggregate in the air before collection to form larger particle chains that behave and impact like larger spherical particles. These are obvious in the micrographs because they appear like fine hair or foam (especially in Figure 5.4). This was compared to particles collected from commercially prepared iron powder, which did not have the aggregation problem from smaller particles (see Figure 5.5) and which served as a control for the measured particle size distributions for the welding fume. During micrograph creation, regions covered with large masses of foam-like particles were avoided in order to aid particle size measurement. The effective particle diameter of an aggregate was calculated from the area of its two-dimensional image. However, the majority of the analyzed particles were individual spheres (or circles in the two dimensional micrographs), so this approximation was not a substantial part of the measurement. Table 5.2 lists the count median diameter (CMD) of the particles that impacted on each stage with the respective geometric standard deviation (σ_g).

As stated previously, the mass of each impaction plate was measured before and after collection. Fume collection and measurement was performed successfully four times for each fume type and then averaged. The resulting data are reported in Table 5.3 and Figure 5.6.

For the GMAW fumes, the data vary greatly from the lognormal ideal, because the fume is distributed in three ranges with three different modes. This is true also of
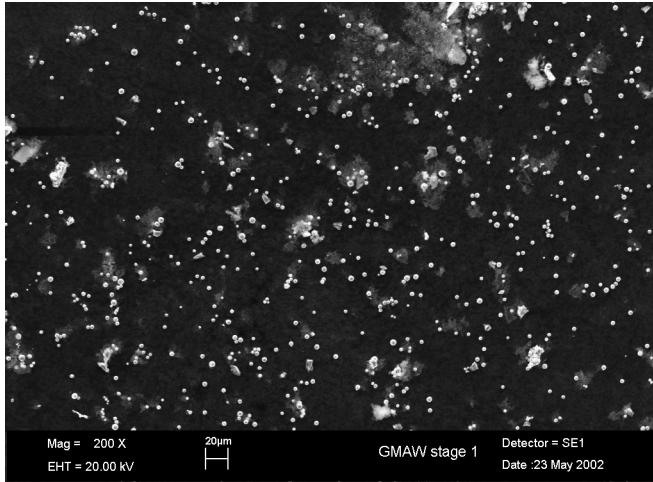
Stage1: $d_{aerodynamic} > 5.8 \ \mu m$
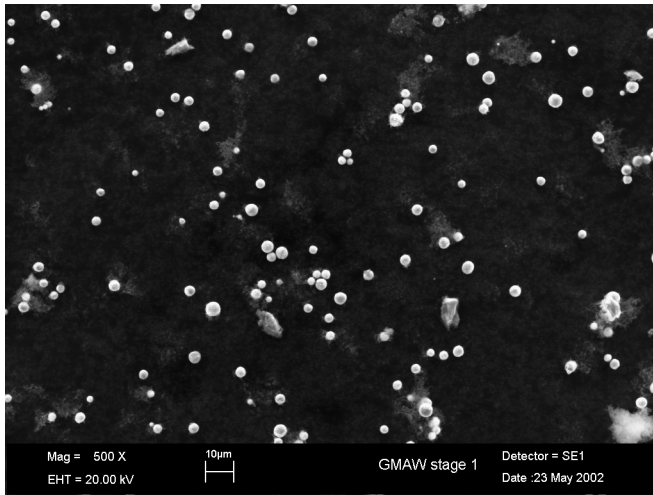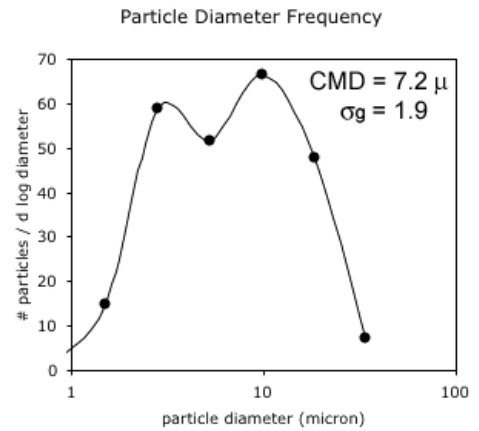
Stage 5: $d_{aerodynamic}$ 1.1 - 5.8 μm
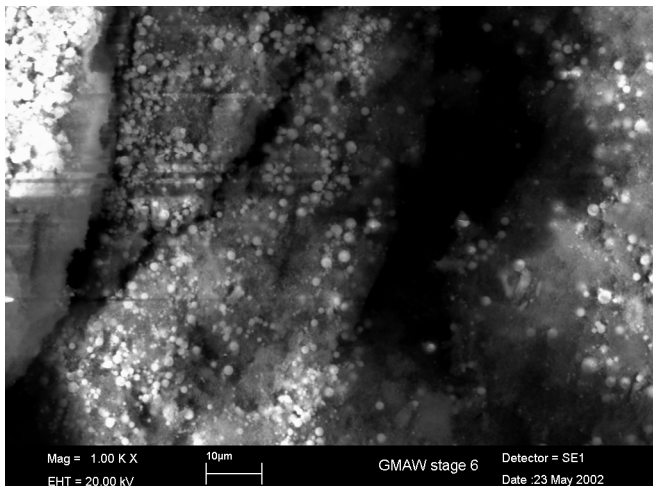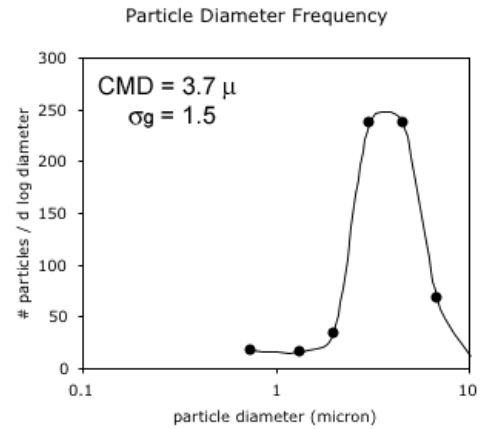
Stage 6: $d_{aerodynamic}$ 0.7 - 1.1 μm
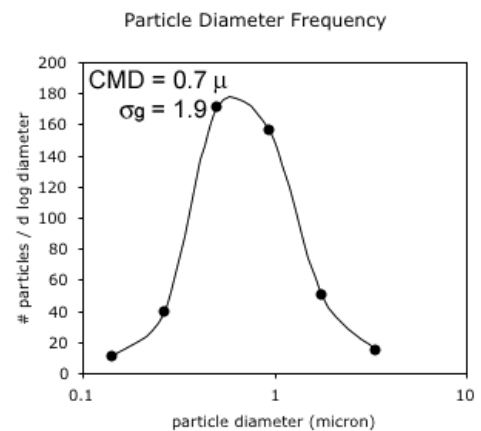
Figure 5.2 Scanning electron microscopy of stainless steel GMAW welding fume particles separated by a Thermo Andersen cascade impactor, using 4 stages and a filter. Particles transferred from stages numbered 1, 5 and 6, are shown here from top to bottom at 200x, 500x, and 1000x respectively.

Stage1: $d_{aerodynamic} > 5.8$ μm
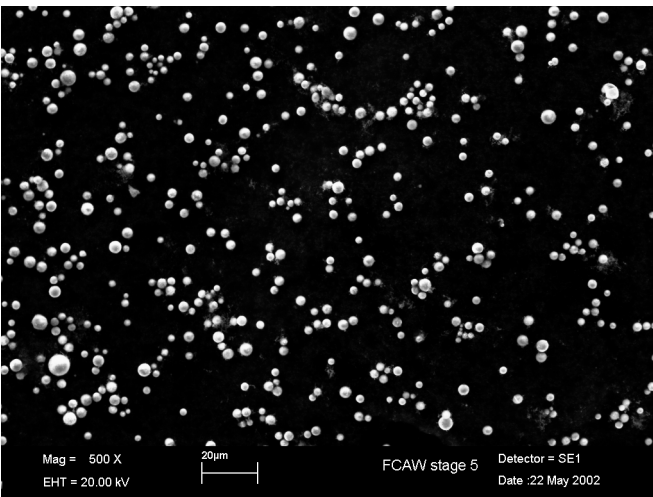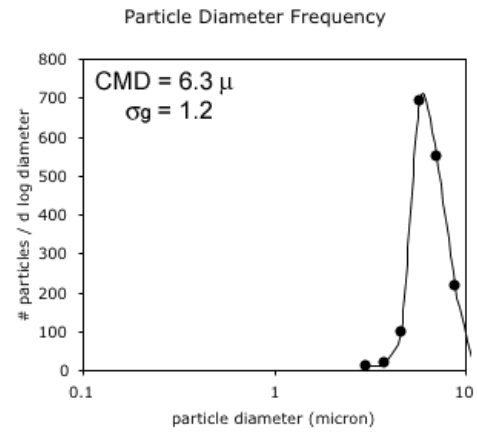
Stage 5: $d_{aerodynamic}$ 1.1 - 5.8 μm
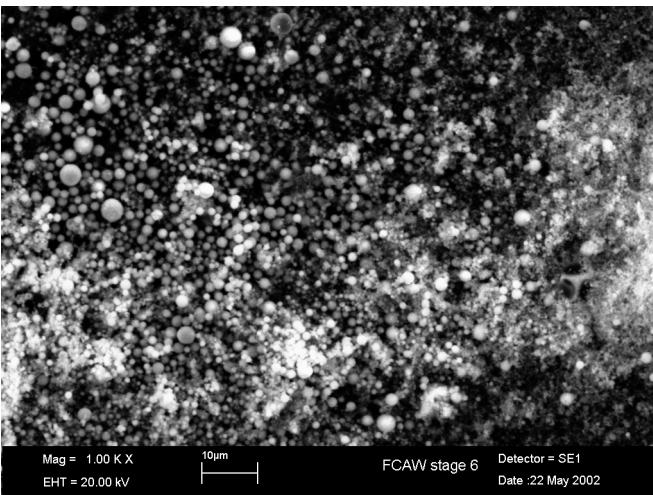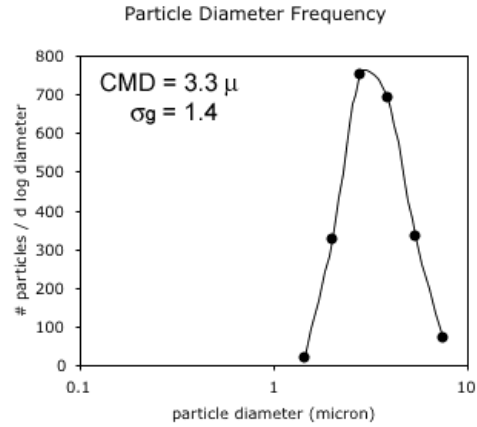
Stage 6: $d_{aerodynamic}$ 0.7 - 1.1 μm
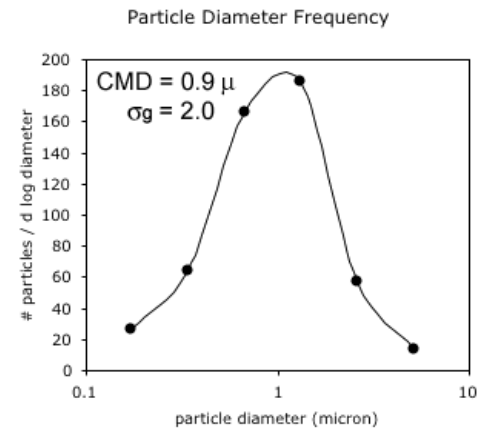
Figure 5.3 Scanning electron microscopy of stainless steel FCAW welding fume particles separated by a Thermo Andersen cascade impactor, using 4 stages and a filter. Particles transferred from stages numbered 1, 5 and 6, are shown here from top to bottom at 500x, 500x, and 1000x respectively.

GMAW
Stage F - 2000x
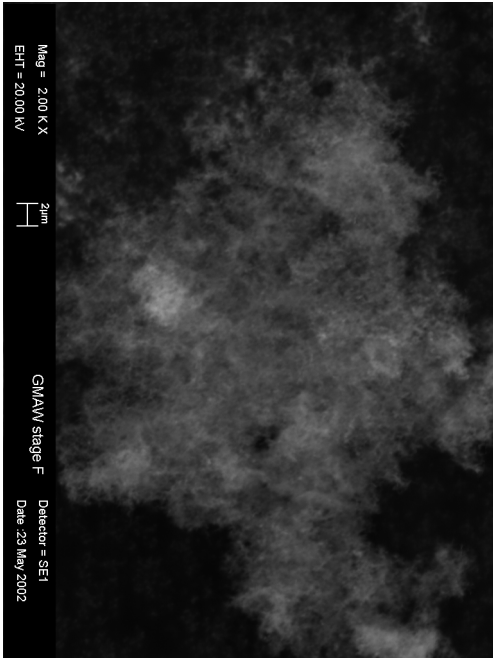
FCAW
Stage F - 1000x
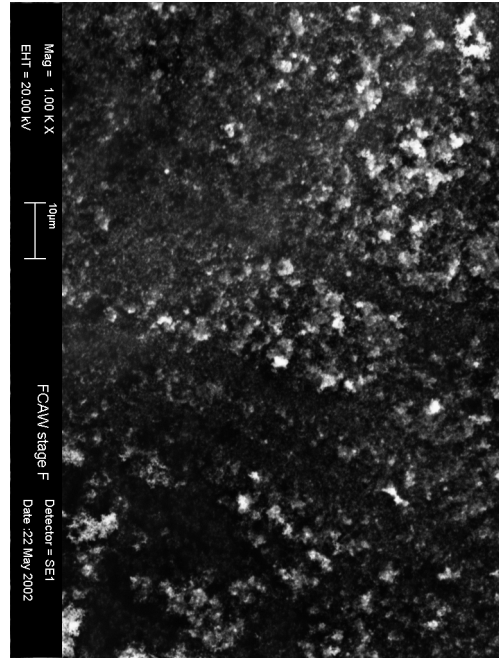
GMAW
filter - 1000x
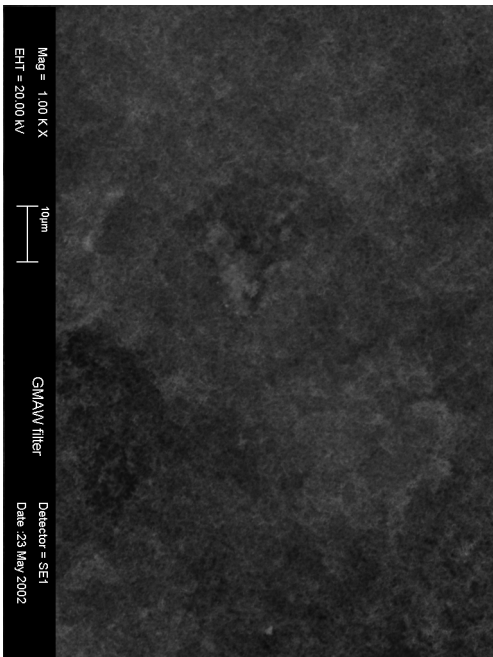
FCAW
filter - 1000x
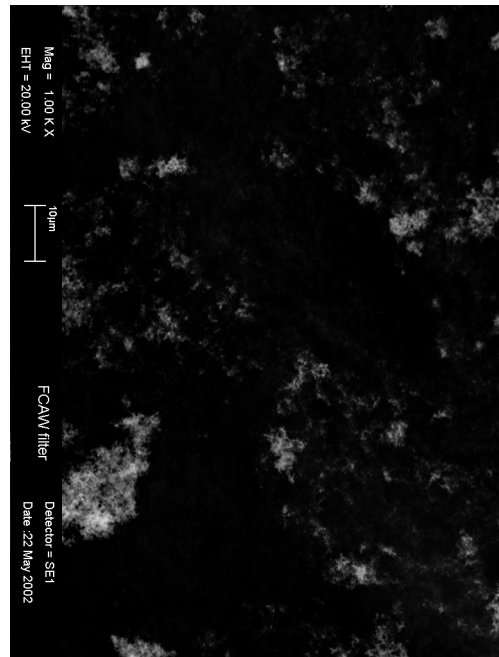
Figure 5.4 Scanning electron microscopy of stainless steel welding fume particles separated by a Thermo Andersen cascade impactor, using 4 stages and a filter. Particles transferred from stage F and from filter shown here.

Stage1: $d_{aerodynamic} > 5.8$ μm
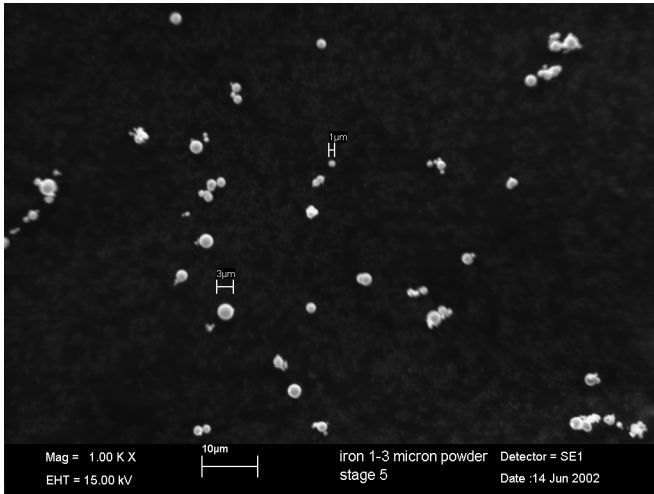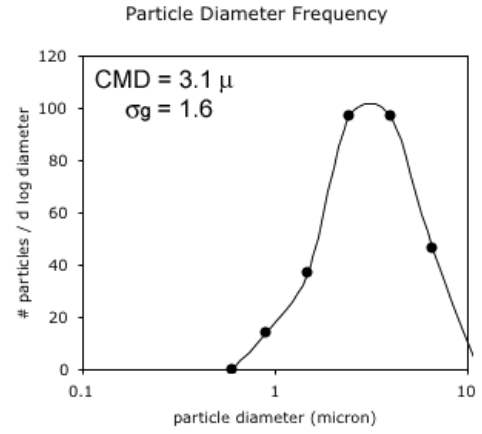
Stage 5: $d_{aerodynamic}$ 1.1 - 5.8 μm

Stage 6: $d_{aerodynamic}$ 0.7 - 1.1 μm

Figure 5.5 Scanning electron microscopy of iron particles separated by a Thermo Andersen cascade impactor, using 4 stages and a filter. Particles transferred from stages numbered 1, 5 and 6, are shown here from top to bottom at 500x, 1000x and 2000x respectively.

Table 5.2 Particle distribution by count median diameter (CMD) and geometric standard deviation (σ_g) collected by each impaction plate with 28.3 L/min flow rate

Impactor Stage	filter		F		6		5		1	
Aerodynamic Dia. (μm)	<0.4		0.4 to 0.7		0.7 to 1.1		1.1 to 5.8		>5.8	
Material	CMD	σ_g	CMD	σ_g	CMD	σ_g	CMD	σ_g	CMD	σ_g
Fe Powder 1-3 μm	NA	NA	NA	NA	0.8	1.7	2.3	1.5	3.1	1.6
spray GMAW fume	<0.5*	NA	<1*	NA	0.7	1.9	3.7	1.5	7.2	1.9
FCAW fume	<0.5*	NA	<1*	NA	0.9	2.0	3.3	1.4	6.3	1.2

* Using a standard SEM, it is difficult to resolve particles smaller than half a micron, especially when not separated and easily distinguishable. Because particles pile up during impaction, this is difficult to avoid. When many such particles are gathered together, they appear as foam or hair. Only the maximum particle size found is reported for stage F and the filter.

Table 5.3 Particle distribution, by percentage (%) of total fume mass collected

Stage	filter	F	6	5	1
GMAW Median Diameter (CMD)	0.2*	0.4*	0.7	3.7	7.2
globular mass %	75.1 ± 1.6	15.2 ± 0.5	8.3 ±1.1	0.6 ± 0.0	0.8 ± 0.1
spray mass %	86.3 ± 0.1	8.3 ± 0.2	4.7 ± 0.1	0.3 ± 0.0	0.4 ± 0.2
pulsed mass %	85.9 ± 0.7	6.2 ± 0.5	5.2 ±1.0	0.6 ± 0.1	2.0 ± 0.2

Stage	filter	F	6	5	1
FCAW Median Diameter (CMD	0.2*	0.4*	0.9	3.3	6.3
FCAW mass %	46.8 ±1.2	23.7 ±0.6	20.5 ±1.3	3.0 ±0.1	6.0 ±0.2

Approximating that maximum particle diameter $\approx$ CMDσ_g^2 with $\sigma_g \approx 1.5$
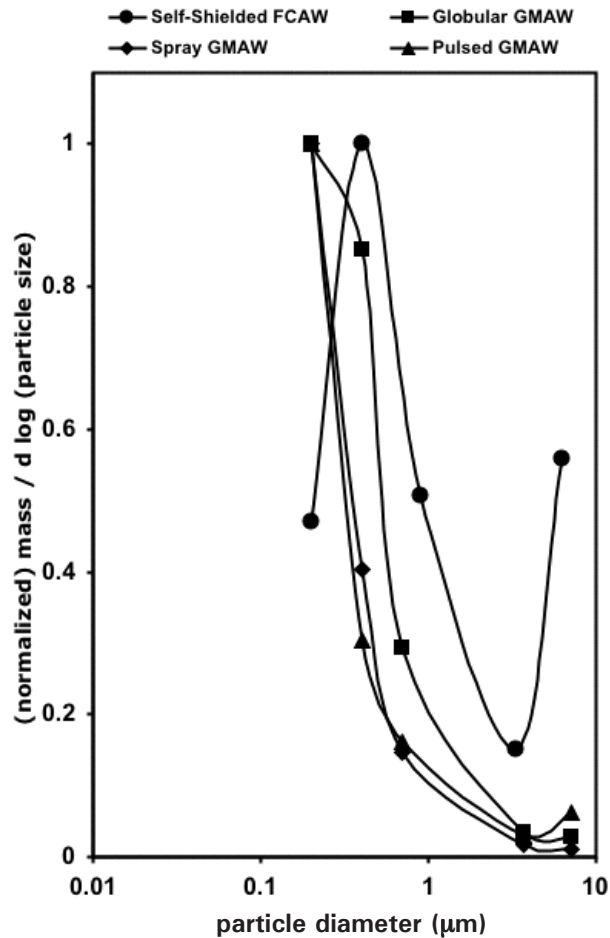
Figure 5.6 Frequency distribution of welding fume mass found with multistage impactor with respect to count median diameter of fume found on each stage. Mass fraction is normalized by dividing by the particle range of each stage, from CMD / σ_g to CMD*σ_g

the FCAW fume, but the accumulation range seems to dominate, so one can approximately measure the mass median diameter (MMD) of that range to be 0.2 micrometer. In the GMAW fumes, the nucleation range may dominate, as evidenced by the large portion of fume smaller than 0.4 micrometer. Globular GMAW fume may have moved more from the nucleation range to the accumulation range than spray or pulsed fumes did, because the particle concentration is greater, as evidenced by the greater fume formation rate of globular GMAW. FCAW fume has a much greater particle concentration (or fume formation rate) than GMAW, which is also why FCAW has such a strong accumulation range.

The fume formation rate of globular GMAW was about 2.7 times greater than that of spray GMAW, which was in turn 1.4 times greater than pulsed GMAW. FCAW formed fume at rates 10 times that of spray GMAW.
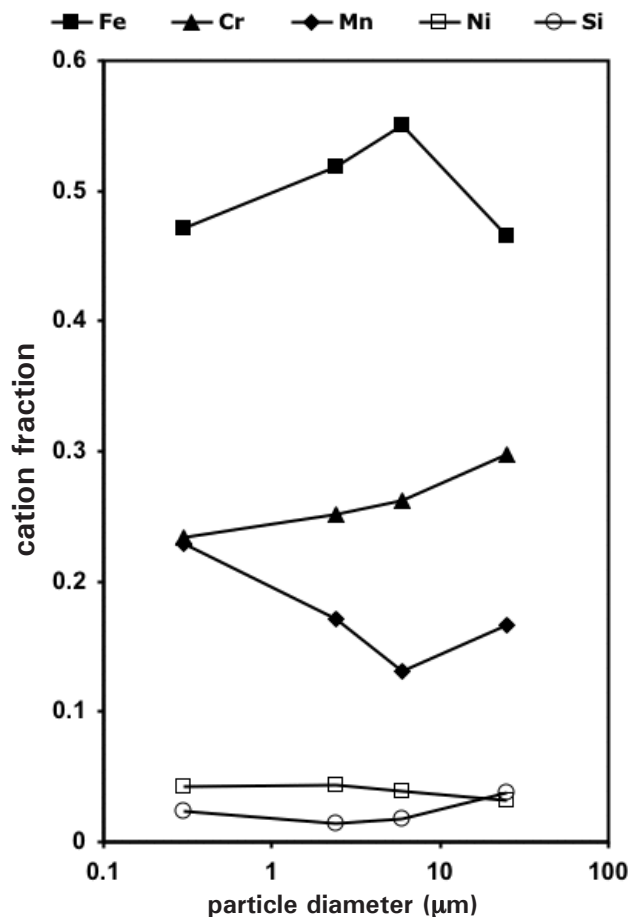
Figure 5.7 Metals content of stainless steel GMAW (spray conditions) fume collected in a multistage cascade impactor, as determined by energy dispersive spectrometry in a scanning electron microscope.

Table 5.4 Metals content of stainless steel GMAW (spray conditions) fume collected in a multistage cascade impactor, as determined by energy dispersive spectrometry in a scanning electron microscope.

CMD	0.2	0.7	3.7	7.2	weighted average (Table 5.3)	Electrode Composition (ICPMS)
MMD	0.3	2.4	6.0	24.8		
Fe	0.472	0.519	0.551	0.466	0.476	0.659
Cr	0.234	0.251	0.262	0.298	0.236	0.220
Ni	0.042	0.044	0.039	0.032	0.042	0.091
Mn	0.229	0.171	0.131	0.167	0.223	0.018
Si	0.024	0.015	0.018	0.038	0.023	0.011

Energy dispersive spectrometry of the particles transferred to the SEM stubs revealed the change in the composition of the particles with respect to size[1], as shown from Figure 5.7 to Figure 5.9 and in Table 5.4 and Table 5.5. Particle sizes in

the graphs refer to the Mass Median Diameter (MMD), as calculated with the Hatch-Choate relationship (Willeke & Baron, 1993) from the Count Median Diameter (CMD) measured from the micrograph of SEM stub to which the fume was transferred from each impactor stage. That relationship can be found in Equation 5.1:

$$MMD \ = \ CMD \exp(3(\ln\sigma_g)^2) \hspace{3cm} 5.1$$

The results are similar to those found by other researchers who have separated welding fume with cascade impactors to analyze it chemically. See Figure 5.10 through Figure 5.13. The differences between Figure 5.11 and Figure 5.12 show that different conclusions can be drawn from analyzing only a certain range of particle sizes; therefore, it is paramount to consider the entire range.

Table 5.5 Metals content of stainless steel FCAW fume collected in a multistage cascade impactor, as determined by energy dispersive spectrometry in a scanning electron microscope.

CMD	0.2	0.4	0.9	3.3	6.3	weighted average (Table 5.3)	Elec trode Comp.	source
MMD	0.3	0.7	3.8	4.6	7.0			
Fe	0.113	0.132	0.143	0.240	0.239	0.135	0.614	wire
Cr	0.081	0.092	0.100	0.110	0.133	0.091	0.200	wire
Ni	0.013	0.014	0.014	0.036	0.030	0.015	0.085	wire
Mn	0.101	0.101	0.117	0.068	0.075	0.101	0.021	both
Si	0.095	0.093	0.098	0.068	0.058	0.092	0.011	both
Al	0.150	0.107	0.065	0.074	0.084	0.116	0.008	core
Ti	0.080	0.085	0.104	0.131	0.157	0.092	0.032	core
Zr	0.013	0.008	0.010	0.019	0.031	0.012	0.004	core
K	0.120	0.118	0.138	0.059	0.041	0.117	0.002	core
Na	0.167	0.173	0.128	0.117	0.072	0.153	0.003	core
Ca	0.061	0.073	0.083	0.071	0.075	0.069	0.016	core
Mg	0.006	0.004	0.000	0.007	0.005	0.004	0.000	core
F / F+O	0.19	0.36	0.42	0.00	0.00	0.26	<0.01	

1. Fume was also collected from each stage onto mixed-cellulose ester (MCE) membrane filters which were digested and analyzed by inductively coupled plasma mass spectrometry at Traveler's Insurance Laboratory, Hartford, Connecticut. Only 30 to 50% of the fume was digested and analyzed; thus the resulting data were not useful. The laboratory scientists were unable to explain why incomplete digestion occurred.
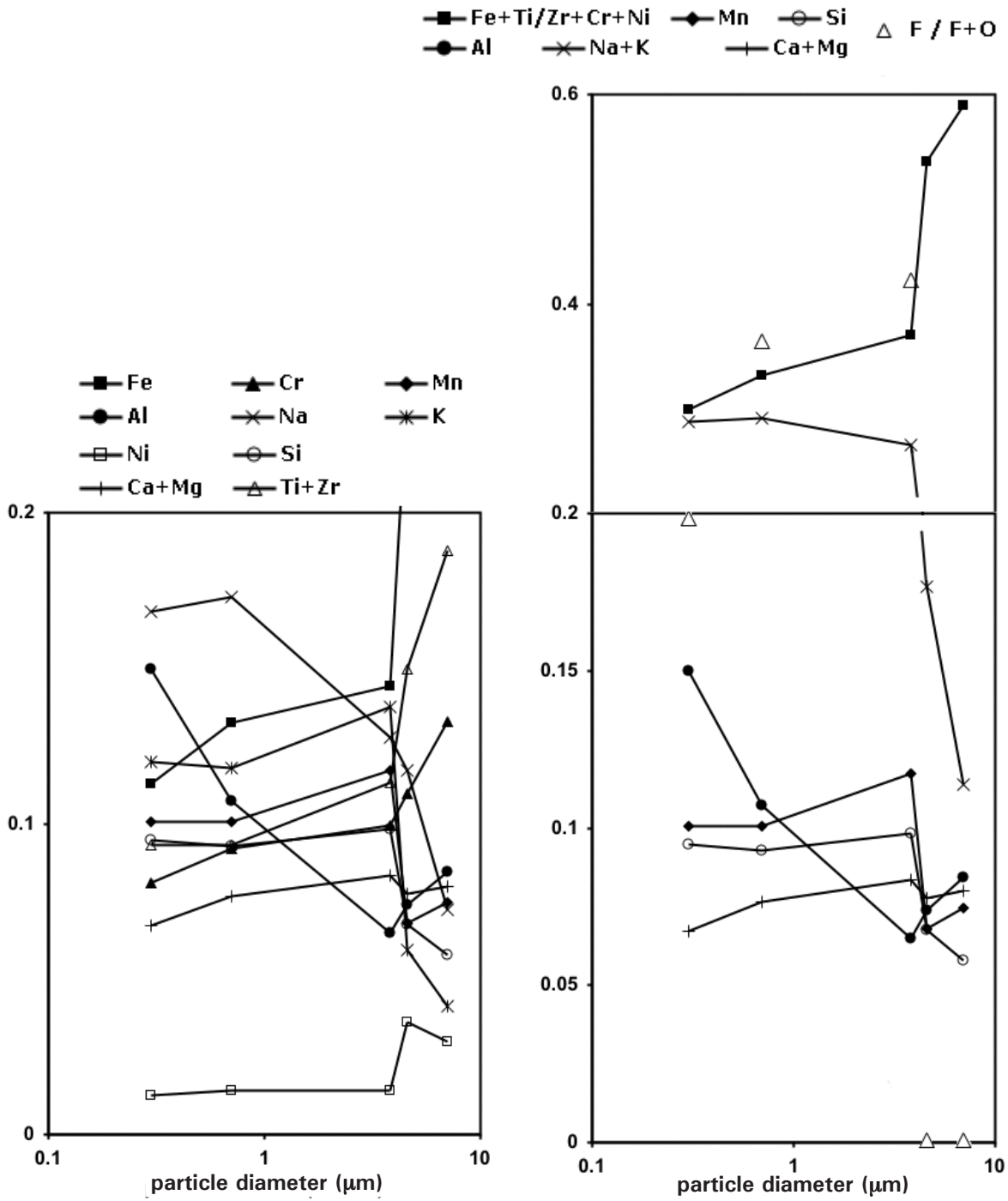
Figure 5.8 (Left) Mole fraction of metals in stainless steel FCAW fume collected in a multistage cascade impactor, as determined by energy dispersive spectrometry in a scanning electron microscope.

Figure 5.9 (Right) Metals in stainless steel FCAW welding fume, matched by chemical similarity and comparative volatility, by molar fraction
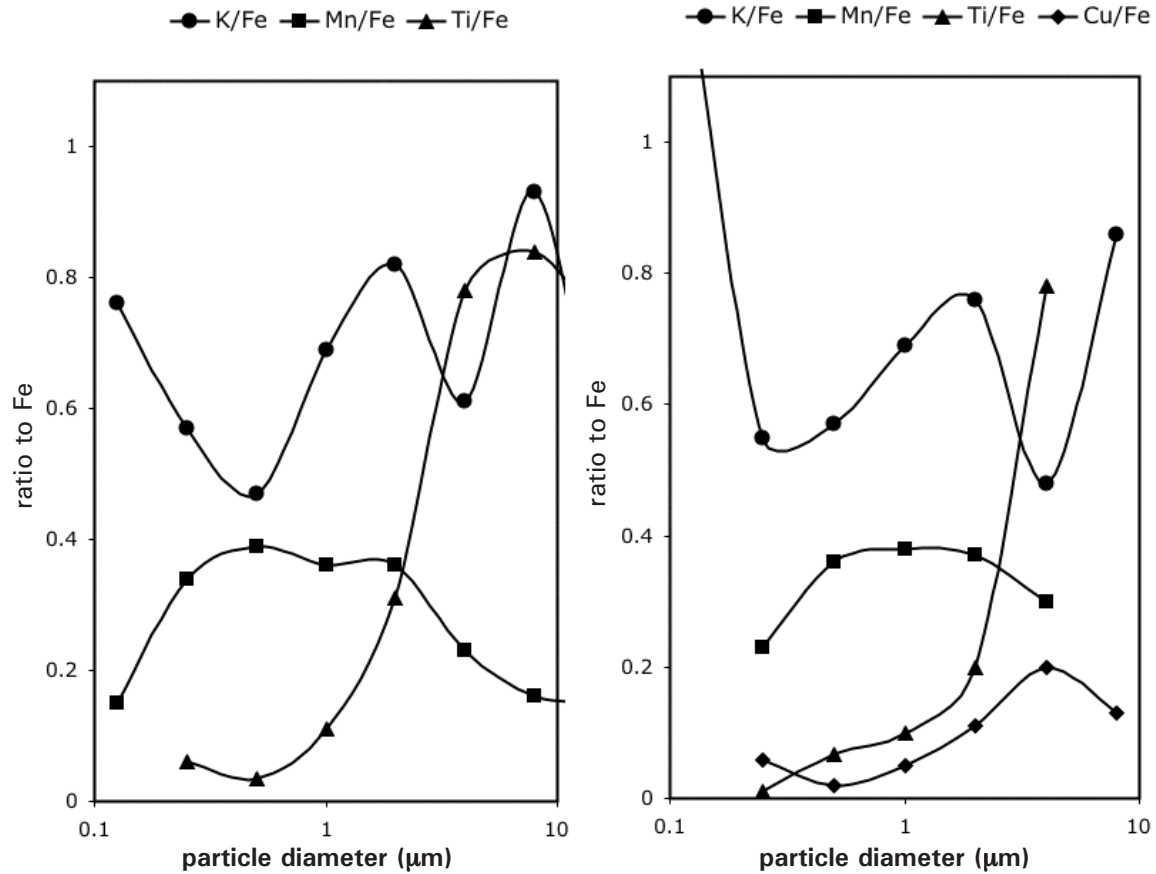
Figure 5.10 Elemental composition of SMAW fume with respect to aerodynamic diameter determined with low pressure cascade impactor (smallest cutoff at 150 nm) and energy dispersive spectrometry (Berner & Berner, 1982)
Berner and Berner believed that the welding fume was multimodal with an accumulation range of particles richer in iron and manganese from condensation and a coarse fraction enriched in welding flux atomized from liquid.

In addition, three samples each of stainless steel (spray) GMAW fume were collected onto polyvinyl chloride (PVC) membrane filters from stages 1 and F and from the impactor filter. These were weighed before and after fume collection. The filters were then analyzed with OSHA Method 215 at Traveler's Insurance Laboratory for hexavalent chromium content (CrVI). The averages of the resulting data are in Table 5.6.

The fume that was collected on the filter had the same concentration of hexavalent chromium that was found in the bulk fume, but the coarse fraction collected on stage 1 had hexavalent chromium concentrations below the detection limit. This suggests that CrVI is present mainly in fine particles that condense from vapor, not in coarse particles that form from liquid. This agrees with the findings by Kura (1998), presented in Figure 5.14. This analysis is only valid for welding fume created from non-slag forming electrodes, as the alkali metals found in fluxes can help form hexavalent chromium compounds not found in GMAW fume (Kimura, et al., 1979).
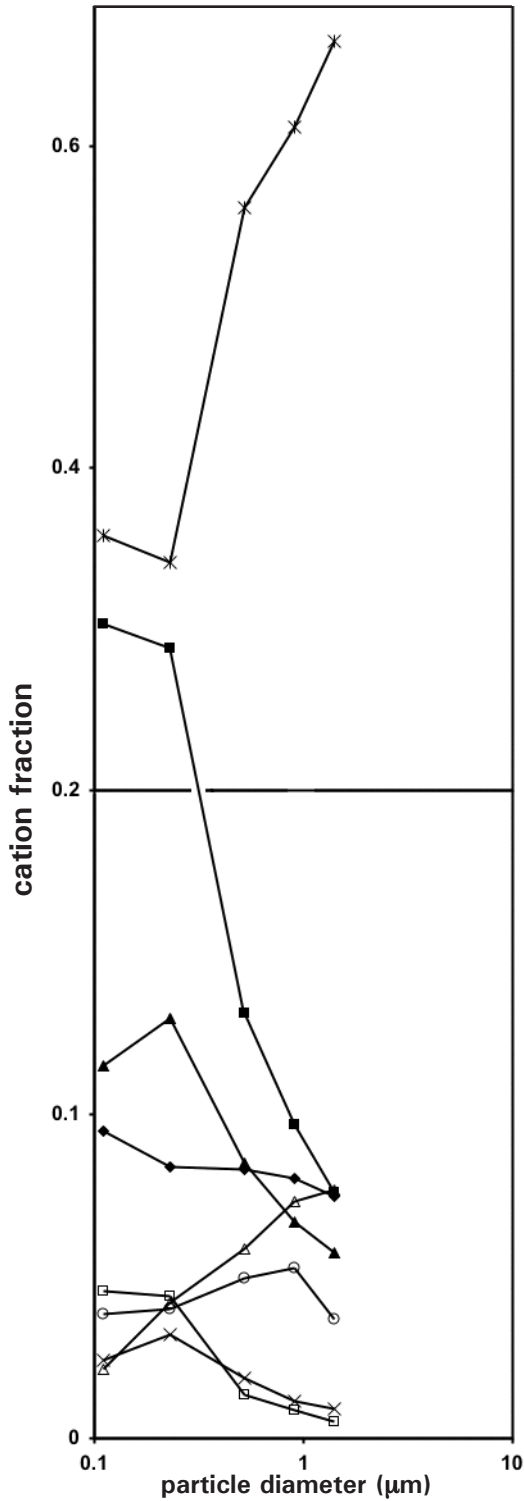
105
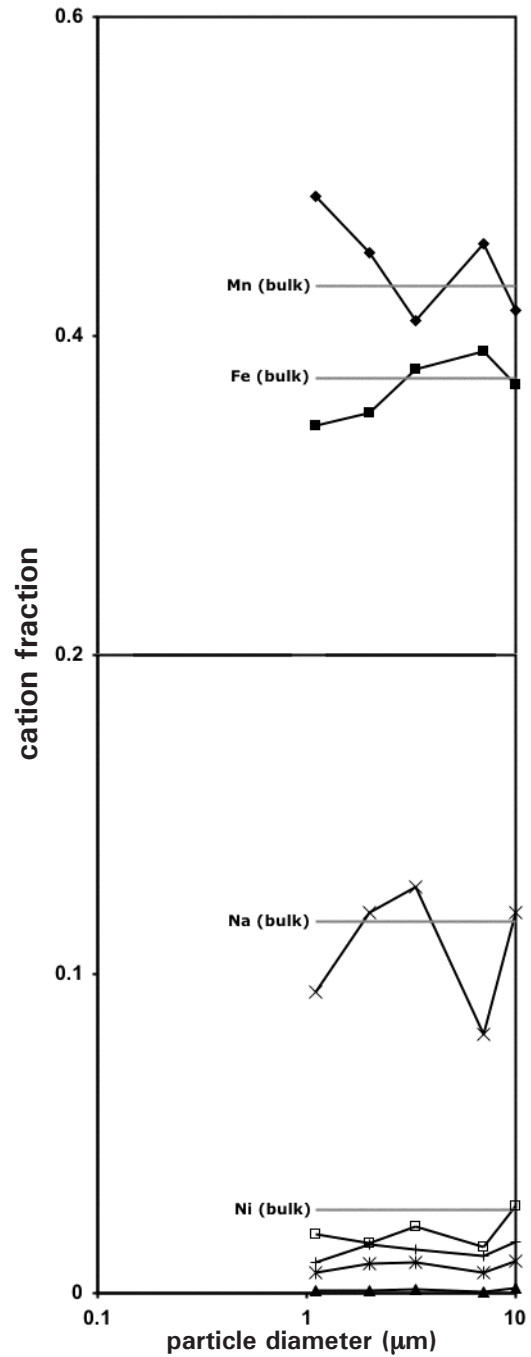
Figure 5.11 (Left) Metal content (SEM-EDS) of stainless steel stainless steel SMAW fume separated with cascade impactor by aerodynamic diameter (Narayana, et al., 1995)

Figure 5.12 (Right) Metals content (AAS) of high manganese hardfacing SMAW fume separated with cascade impactor by aerodynamic diameter (Tandon, et al., 1984)
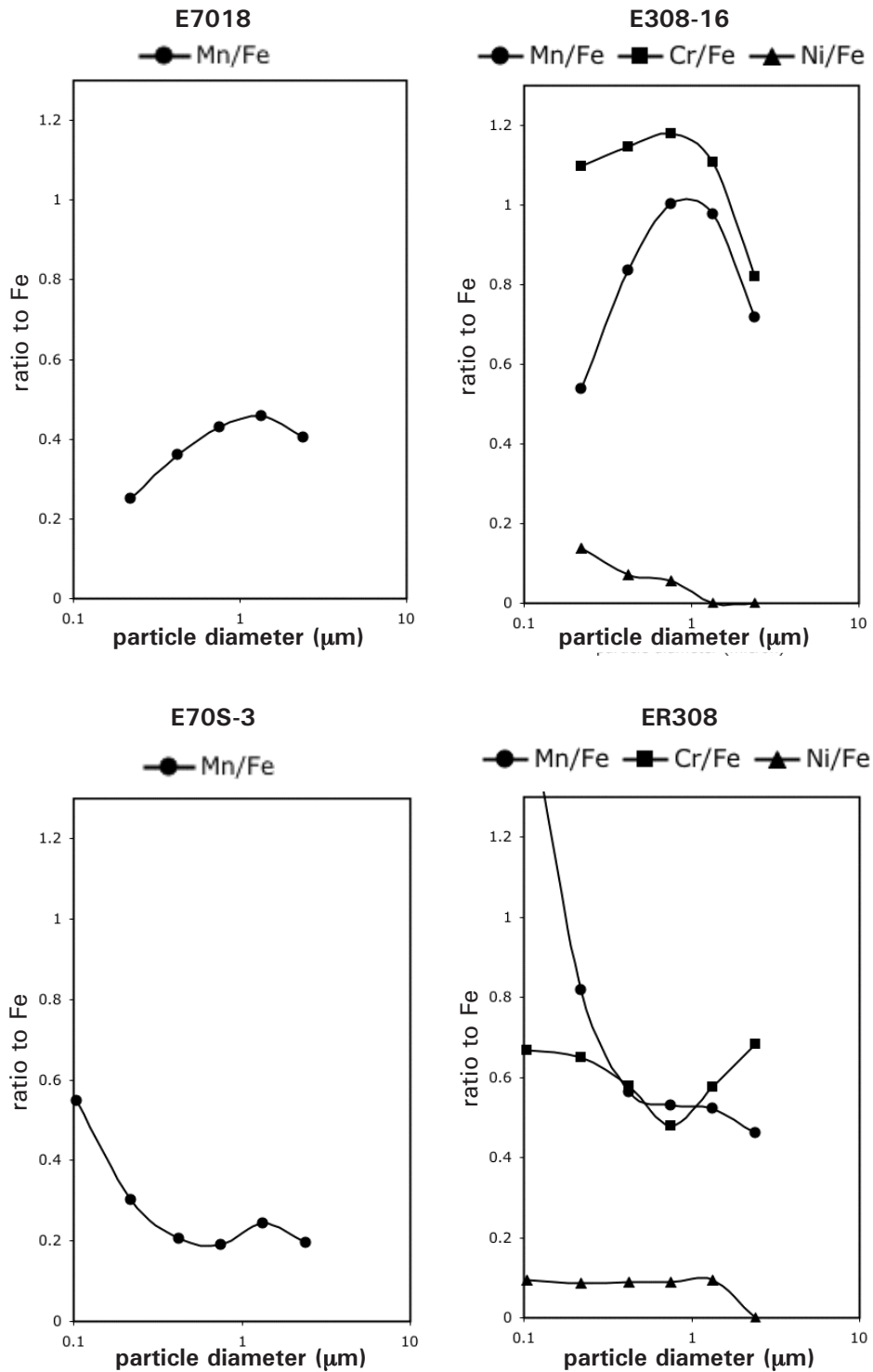
Figure 5.13 Metals fraction of SMAW and GMAW fume with respect to aerodynamic diameter, determined with micro-orifice uniform deposit [cascade] impactor (MOUDI) and mass spectrometry (Hewett, 1995)
Hewett did not believe the elemental variation with particle size was significant

Table 5.6 CrVI distribution in stainless steel GMAW fume

Stage	Bulk	filter	F	1
Particle Size	all	< 0.5	< 1	> 6
CrVI	0.2	0.2	0.1	<0.1
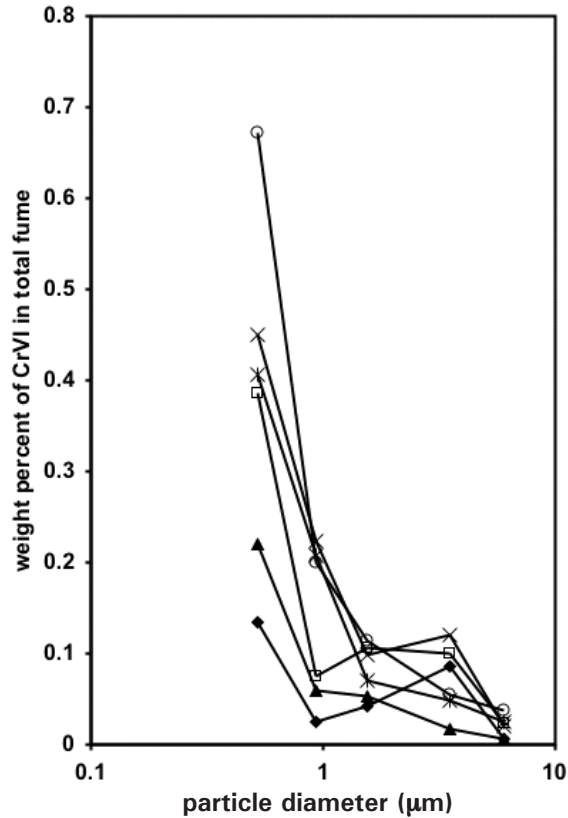
Figure 5.14 Distribution of CrVI in stainless steel (ER347) GMAW fume, six samples (Kura, 1998)

Since no coarse particles were found on stage F or on the filter (see Figure 5.4), one can easily say that, by mass, the FCAW fume contains no more than 30% coarse particles (or microspatter), spray GMAW fume has less than 6%, globular GMAW contains less than 10%, and pulsed GMAW fume has less than 8% microspatter. Because some non-microspatter agglomerates were also collected in upper stages, the mass of microspatter is less than these values. However, agglomerates are much less dense than microspatter, so they may not significantly affect these measurements.

5.1.2 Discussion

Given the findings, it was clear that, for GMAW, regardless of the welding parameters that cause different metal transfer modes, less than 10% of the mass of welding fume was microspatter (coarse particles). This means that the higher fume formation rates found during globular GMAW compared with spray GMAW are not

caused by an increased fraction of larger particles, but by an increased number of all sizes of particles. This finding suggests that there is more evaporation of the electrode in globular GMAW than in spray GMAW. In addition, the tests revealed that the particle size of pulsed current GMAW is not significantly different than that of straight current GMAW, despite speculation that it was (Irving, 1992). However, microspatter from FCAW is substantial. This may be because powder from the core of the wire is ejected or because the slag-forming flux is more easily atomized than liquid metal.

As Gray et al., (1980) first suggested, welding fume is formed from vapor and liquid sources. Vapor condensed particles (as indicated by the strong concentration of volatile metals; See Table 3.1) dominate the composition of particles smaller than about 1 micrometer. (This is also supported by the concentration of fluorides, which are more volatile than oxides, in smaller particles, illustrated in Figure 5.9.) Coarse particle formation from liquid metal droplets explains the increase in iron (decrease in manganese) with increasing particle size for GMAW fume in Figure 5.7.

However, the largest particles do not have the same composition as the source electrode (see Table 5.4 and Table 5.5). It is possible that vapor condensed on large particles and/or smaller particles agglomerated with the coarse particles (see Figure 5.2 and Figure 5.3) that impacted on the upper stages, thus shifting the composition toward that of the vapor. However, this should be a minor influence, because the coarse particles are much larger than any incidental fine particles that may stick to them.

Another source of coarse particles could be the slag formed from the flux during FCAW or the small amount of manganese silicate slag that forms during GMAW (see Figure 5.7). The fraction of iron, being less volatile than manganese, increases with particle size, while the fraction of manganese decreases. This relationship indicates a mixture of particles that condensed from vapor and particles that formed from liquid metal droplets. The ratio of these two particle types changes with particle size group, with condensed particles dominating the smallest size group and vice versa. However, with the largest particles, there is a decrease in iron, an increase in manganese and an increase in silicon. Because GMAW slag is composed of manganese silicate, it is likely that this sudden change is due to the domination of that size group by particles formed from slag.

This may also affect the composition of FCAW fume. At first glance, Figure 5.8 and Figure 5.9 show that large particles have a significantly lower concentration of volatile elements than small particles do. It seems clear that the smallest particles condensed from vapor. However, in Table 5.5 the concentration of flux elements in the largest particles of the fume is much greater than what is found in the electrode. The slag-forming oxides and fluorides of the flux must have formed relatively more coarse particles than the liquid metal from the wire sheath did. This contention is supported by the mass distribution measurements, which showed that FCAW, which forms more slag, created more microspatter than GMAW.

Researchers (Hewitt & Hirst, 1991) have observed that material from the flux core of the electrode is more strongly present in bulk fume than metal from the wire sheath. Voitkevich (1995) and Jenkins, et al. (1981) also reported finding large welding fume particles composed only of slag.

Coarse particles formed from liquid metal may be a bit smaller than those formed from liquid oxides because liquid metal oxides have a greater viscosity than liquid metals do. Liquid metals usually are denser and have greater surface energies than liquid oxides, indicating that they would form larger particles if just the Weber number of Equation 3.6 were considered. However, viscous forces should also be considered when one studies liquid metal oxides. The relationship between viscous, inertial and surface forces is shown by the Ohnesorge number in Equation 3.7. Because droplet size scales with the square of the viscosity, it is clear that when comparing the liquid droplet formation of dissimilar materials, viscosity is more important than density and surface tension.

This may also be related to the relative volatility of the considered elements and compounds; the more vapor bubbles that form and burst, the more microspatter of that particular material forms. However, this mechanism does not adequately account for why the ratio of titanium to iron in the largest size group of the FCAW fume is greater than the same ratio in the electrode. Titanium is less volatile than iron; the same comparison can be made for their oxides.

This discussion is complicated by the observation of Kobayashi, et al., (1983) that the arc in SMAW attaches to the molten metal droplet of electrodes with lime-type coatings, whereas it attaches to molten slag in non-lime (ilmenite) electrodes. This would indicate that the content of slag forming elements in fine particles might also vary according to the type of electrode coating and not just because of thermo-chemical activity. However, this phenomenon was not studied here.

Although fume does form from vapor and liquid, one must determine which liquid precursor is being broken up into droplets before predicting coarse particle composition.

There is an important conflict between data to consider. Figure 5.11 shows slag elements (Na and K) drastically increasing with particle size. This is markedly different from the behavior shown in Figure 5.8 and Figure 5.9. The best way to describe the discrepancy is to consider compound volatility in addition to elemental volatility. Fluorides, which preferentially form alkali metal compounds if those metals are present, are much more volatile than oxides. Figure 5.11 reports the composition of fume created from an electrode that probably did not contain any fluoride, so sodium and potassium would be present more strongly in the larger particles. In the fume analyzed for Figure 5.8 was formed, sodium and potassium reacted to form volatile fluorides that condensed and dominated the composition of the smaller particle ranges, leaving the less volatile oxide slag formers (e.g., titania) to dominate in the coarse particle range. The Kobayashi, et al., 1983 paper supports this finding, reporting that the alkali content of fume increases when a fluoride is added to the SMAW

electrode coating. This occurs because vapor-condensed particles dominate fume mass and alkali fluorides are relatively volatile, whereas alkali oxides are not.

It is easy to see that a discussion of coarse particles quickly turns into a conversation about what coarse particles are not. In other words, one defines coarse particles as the material that did not vaporize and recondense as fine particles and which more or less has the same composition as the parent material, whether of electrode wire or its flux. Such a derivative discussion is not helpful here, where the chemistry of fine particles is of greater relevance.

A final note: the composition of each particle size group does not accurately represent total fume composition. To obtain that information, a weighted average of the compositions of each size group should be made, using the measured masses to weight the average. If this is done, it is clear that the bulk composition of the fume is chiefly determined by the small particles. This discounts the theory proposed to explain why the bulk fume composition changes with metal transfer mode (Gray, et al., 1982). This theory suggested that globular GMAW, in comparison to spray GMAW, created more microspatter, which decreased the overall concentration of the more volatile elements in welding fume. If microspatter does not greatly affect composition, this theory does not apply. Instead the composition of the vapor mainly determines bulk fume composition.

References

Berner, V., & Berner, A. (1982). Mass size distributions and elemental frequency distributions of arc welding smokes. *Journal of Aerosol Science,* 13, 191–193.

Deam, R., Bosworth, M., Chen, Z., French, I., Haidar, J., Lowke, J., Norrish, J., Tyagi, V., & Workman, A. (1997). Investigation of fume formation mechanisms in GMAW*. Proceedings of the Technological Developments and Advances for Australian Industry, International Welding and Joining Research Conference 1997*, Silverwater, Australia: Welding Technology Institute of Australia.

Gray, C. N., Hewitt, P. J., & Dare, P. R. M. (1982). New approach would help control welding fumes at source (MIG and MMA) part two: MIG fumes. *Welding and Metal Fabrication,* October*, 393–397.

Gray, C. N., Hewitt, P. J., & Hicks, R. (1980). The prediction of fume compositions in stainless steel metal inert gas welding*. Proceedings of the Weld Pool Chemistry and Metallurgy International Conference*, Bailey, N. (Ed.). Cambridge, England: The Welding Institute, Abington Hall.

Hewett, P. (1995). The particle size distribution, density and specific surface area of welding fumes from SMAW and GMAW mild and stainless steel consumables. *American Industrial Hygiene Association Journal,* 56(2), 128–135.

Hewitt, P. J., & Hirst, A. A. (1991). Development and validation of a model to predict the metallic composition of flux-cored arc-welding fumes. *Annals of Occupational Hygiene,* 35(2), 223–232.

Jenkins, N., Moreton, J., Oakley, P. J., & Stevens, S. M. (1981). *Welding Fume – Sources, Characteristics, Control* (Vol. 1–2). Cambridge, England: The Welding Institute, Abington Hall.

Kimura, M., Kobayashi, M., Godai, T., & Minato, S. (1979). Investigations on chromium in stainless steel welding fumes. *Welding Journal*, July, 195s–204s.

Kobayashi, M., Maki, S., Hashimoto, Y., & Suga, T. (1983). Investigations on chemical composition of welding fumes. *Welding Journal,* 62(7), 190s–196s.

Krause, H.-J., & Press, H. (1986). Measurement of the welding fume quantities and analysis of the fume composition during resistance welding*. Proceedings of the International Conference on Health Hazards and Biological Effects of Welding Fumes and Gases*, R. M. Stern, A. Berlin, A. Fletcher, K. Hemminki, J. Jarvisalo & J. Peto (Eds.). Amsterdam: Excerpta Medica.

Kura, B. (1998). *Evaluation of Cr(VI) Exposure Levels in the Shipbuilding Industry, GCRMTC Project No. 32, ONR Cooperative Agreement No. N00014-94-2-0011,* Gulf Coast Region Maritime Technology Center, University of New Orleans.

Mendez, P., Jenkins, N. T., & Eagar, T. W. (2000). Effect of electrode droplet size on evaporation and fume generation in GMAW. *Proceedings of the Gas Metal Arc Welding for the 21st Century*, Miami, Florida: American Welding Society.

Narayana, D. S. S., Sundararajan, A. R., Manjula, B., Kumari, S. C. V., & Subramanian, V. (1995). Chemical characteristics of stainless steel welding fumes. *Journal of Aerosol Science,* 26, S531–S532.

Quimby, J. B., & Ulrich, G. D. (1999). Fume formation rates in gas-shielded metal arc welding. *Welding Journal,* April, 142–149.

Tandon, R. K., Crisp, P. T., Ellis, J., & Baker, R. S. (1984). Generation rate, particle size and chemical measurements of fume from some hardfacing and HSLA steel electrodes, AWRA document no. P9-68-84. *Australian Welding Research,* 13(12), 45–49.

Thermo Andersen (2002). *Operator Manual: 1 ACFM Non-viable Sample Series 20-800*. Thermo Andersen, Symrna, GA.

Voitkevich, V. (1995). *Welding Fumes: Formation, Properties and Biological* effects. Cambridge, England: Abington Publishing.

Willeke, K. & Baron, P. A. (Eds.) (1993). A*erosol Measurement: Principles, Techniques, and Applications.* New York: Van Nostrand Reinhold.

Zimmer, A. T., Baron, P. A., & Biswas, P. (2002). The influence of operating parameters on number-weighted aerosol size distribution generated from a gas metal arc welding process. *Journal of Aerosol Science*, 33(3), 519–531.

5.2 Fine Particles

As suggested, the composition of fine particles is more important than that of coarse particles. Chapter 3 shows that fine particles condense from vapor, meaning that the composition of fine particles is determined by the composition of the vapor and by the relative volatilities of elements and compounds in that vapor. Equation 3.1 shows how particle size is determined by the supercooling of the vapor, which also controls the composition of the condensing particles and is discussed more in detail later. The composition of agglomerates and coalesced particles in the accumulation range is the sum of the composition of the primary particles and reflects the bulk composition of the vapor.

Two topics will be addressed in the discussion of fine particles: first, the relationship between the chemical composition of primary particles with size, and second, vapor composition. In addition, the compositional variation with particle radius is discussed.

5.2.1 Relationship between Composition and Primary Particle Size

To study the composition of primary particles in welding fume, a scanning transmission electron microscope equipped with energy dispersive spectrometry was employed.

Other researchers (Fasiska, et al., 1983) have used transmission electron microscopy to study approximately 5 to 10 particles per fume type. They studied only particles larger than 100 nanometers. Because their goal was to study electron diffraction, quantitative compositional data were not collected. They noted that in some particles, multiple crystals were present. In the fumes created from electrodes with fluxes, the particles were found to be mixtures of K / Ca fluorides and Fe / Mn oxides. The mild steel GMAW fume particles had spinel structures with 6–12% Mn and 3–7% Si.

A group of Finnish researchers (Grekula, et al., 1986; Kalliomaki, et al., 1987) collected samples of fume created from mild and stainless steel in SMAW and GMAW on TEM grids and analyzed them with energy dispersive spectrometry in a scanning transmission electron microscope. Particle size was only qualitatively described, so no definitive conclusions could be made. However, the authors observed that the largest particles (about 1 micrometer) were of close composition to the electrode. They also observed that the concentration of manganese was lowest in the smallest particles, while the reverse was true with the concentration of nickel.

No literature was found that reports a quantitative relationship between primary particle size and chemistry for welding fume or other oxide nanoparticles.

The machine used in this study had the capability to create elemental composition maps. The relative brightness of each mapped pixel corresponded to the relative intensity of the X-ray signal from the chosen element at each respective point of microanalysis. Cation maps can be seen for mild steel fume created with GMAW (Figure 5.15), SMAW (Figure 5.16), and FCAW (Figure 5.17 and Figure 5.18). Oxygen maps for the FCAW agglomerates are found in Figure 5.19 (Fluorine was also detected but not mapped).

It can be seen that, with the possible exception of the fume from GTAW or from some GMAW, welding fume is not homogeneous. This elemental segregation can be most readily observed with an examination of the composite elemental maps. In addition, the oxygen maps for the FCAW fume do not include all of the fume particles, indicating that not all of the fume is an oxide. It is likely that the rest of the fume is fluoride, but this was not tested, because of the microscope's inability to analyze for fluorine at the time. The inhomogeneity of the fume observed in these figures probably formed during the agglomeration of primary particles of various compositions.

Why do particles that condensed from the same well-mixed gas, have different compositions? To answer this question, the composition of individual particles was measured quantitatively.

Welding fume was created using the parameters listed in Table 5.7. To study how particle composition varies with size, the fume was collected directly onto standard TEM grids immersed in the welding fume plume, allowing particles to collect on the grid by thermophoresis.

TEM Image　　**Fe**　　**Mn**

O

TEM Image　　**Fe**　　**Mn**

O
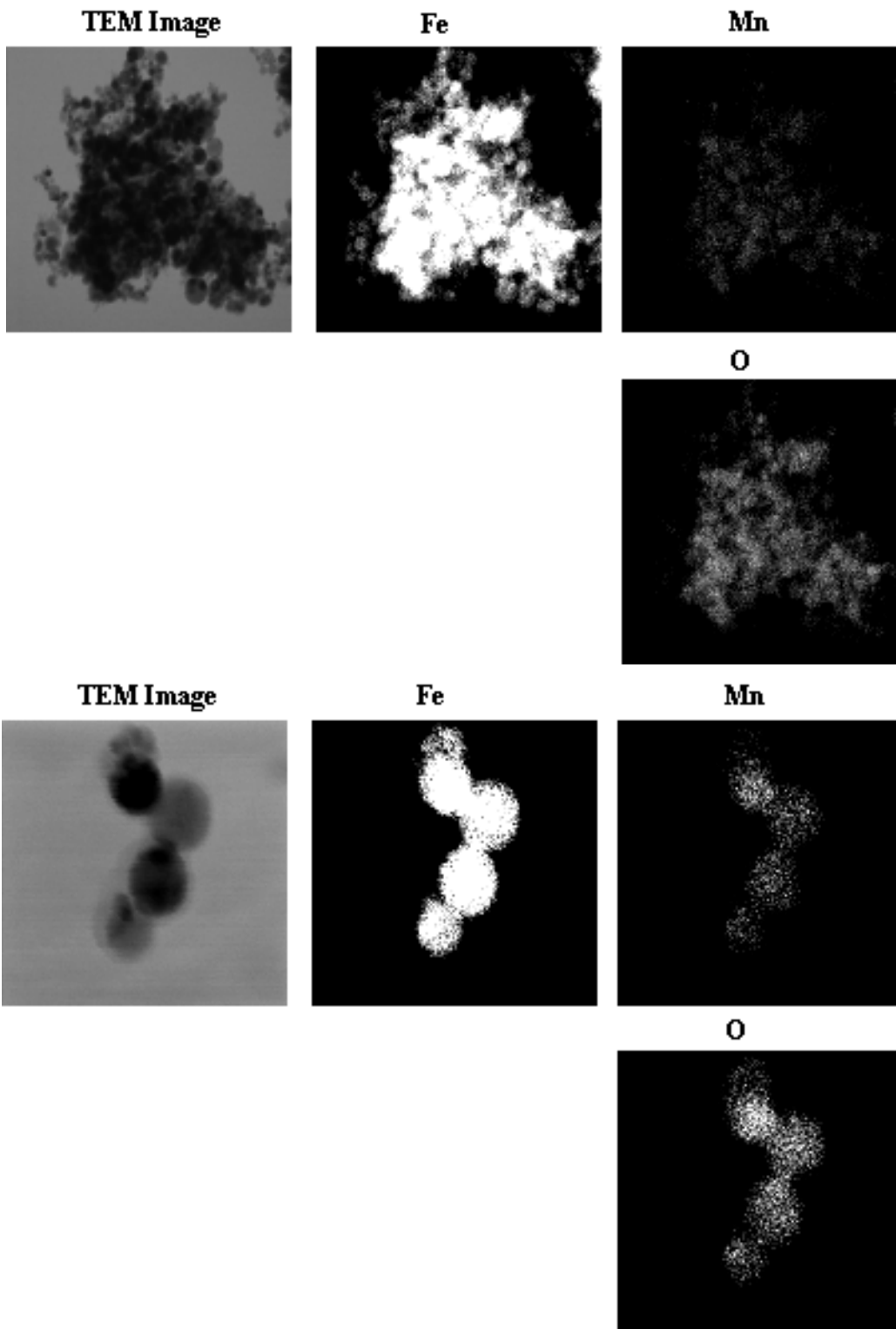
Figure 5.15 Transmission electron micrograph and elemental maps from energy dispersive spectrometry of mild steel gas metal arc welding fume.
Silicon and carbon were not included because of normal contamination.
ER70S-3 0.045″ wire at 30V DCEP, 300ipm with 50 cfh of 2%O_2-Ar shielding gas.

Fe

Mn

Si

K

Ca

Na
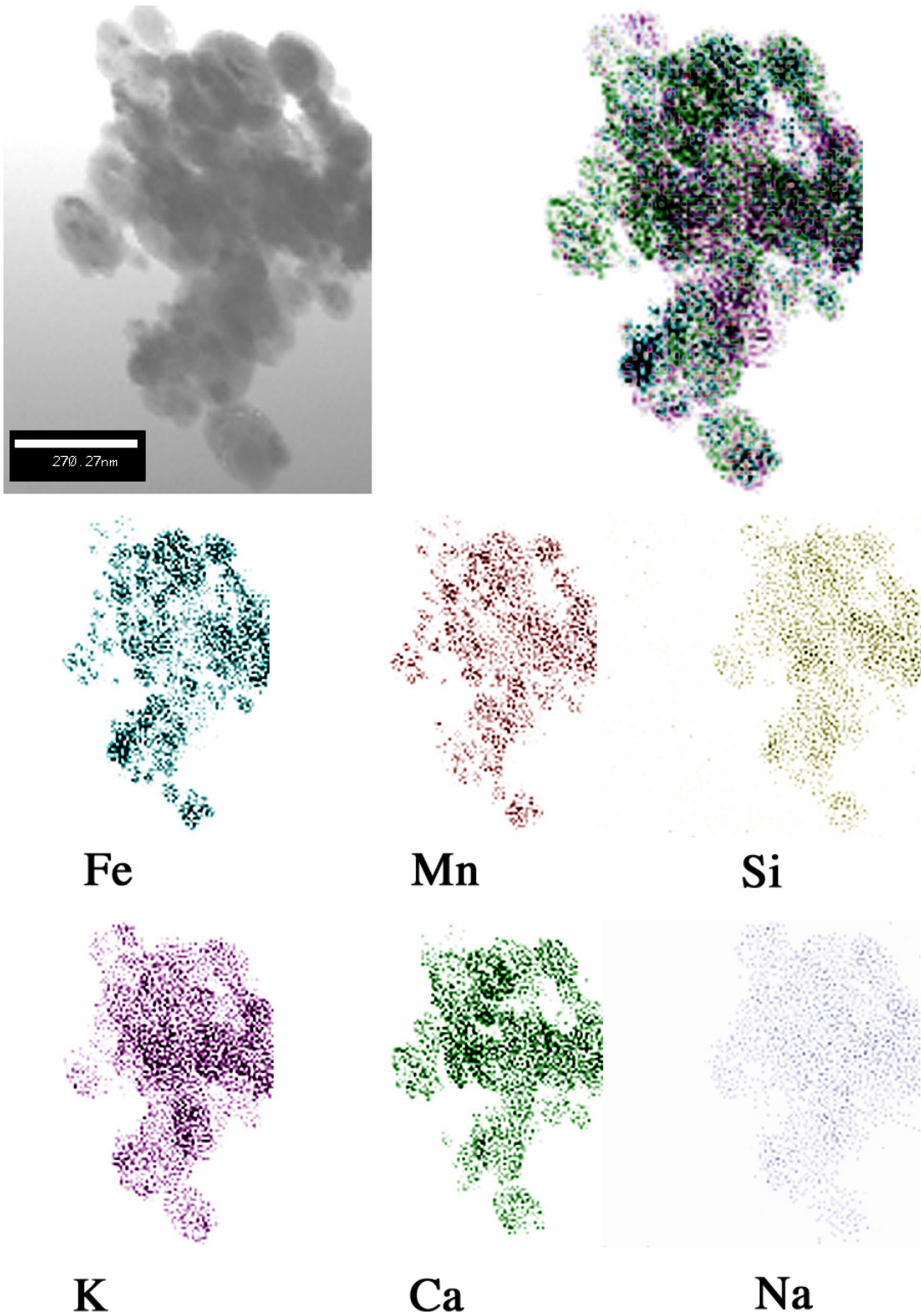
Figure 5.16 Transmission electron micrograph and cation maps from energy dispersive spectrometry of mild steel shielded metal arc welding fume. Composite map in upper right. Carbon was not included because of normal contamination.

Welding parameters: 3/32" diam.E7018-A electrode, 70amps.
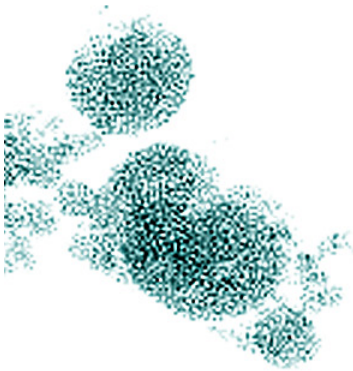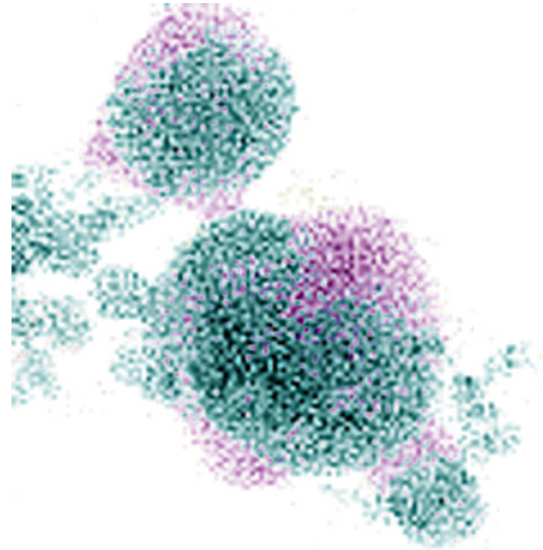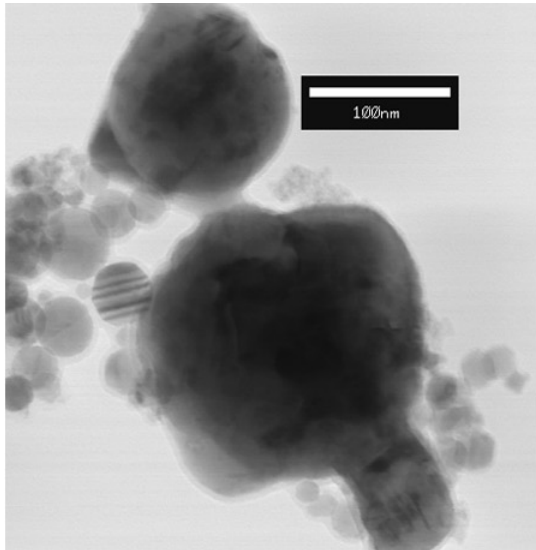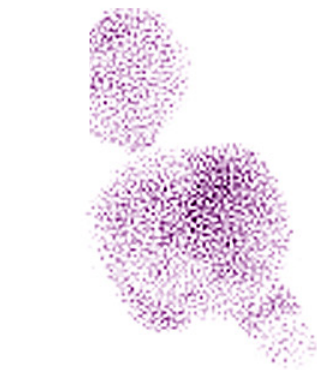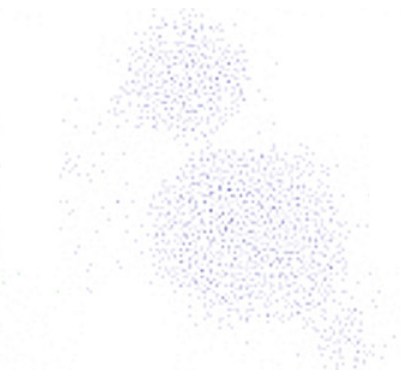
Figure 5.17 Transmission electron micrograph and cation maps from energy dispersive spectrometry of mild steel FCAW fume. Composite map in upper right.
Silicon and carbon were not included because of normal contamination.
Self-shielded E71T-GS, 0.045″ dia. 30 V, ~170 amperes.

117
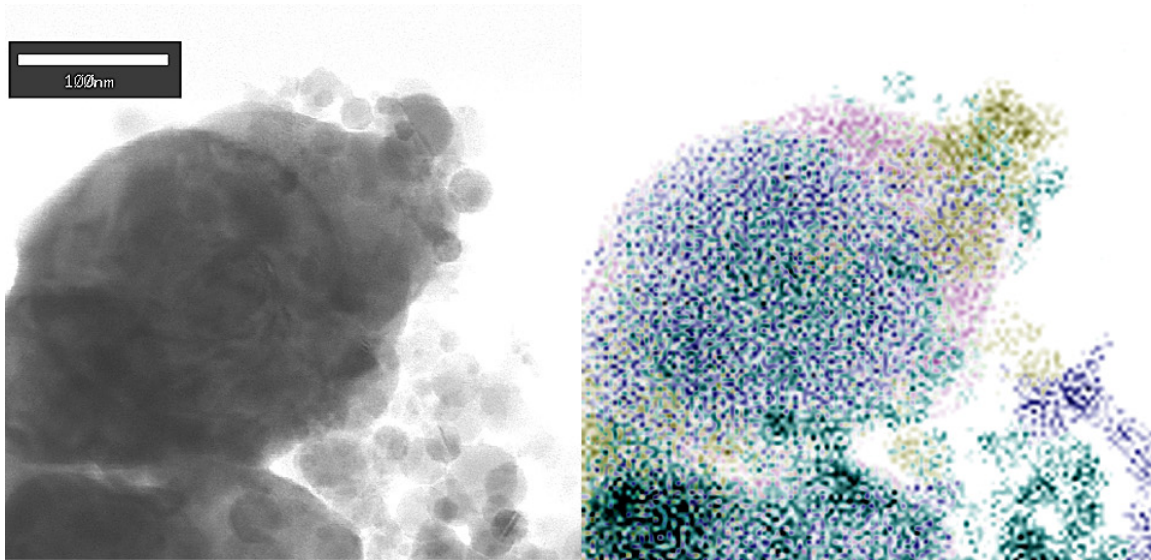
Figure 5.18 Transmission electron micrograph and cation maps from energy dispersive spectrometry of mild steel FCAW fume. Composite map in upper right.
Silicon and carbon were not included because of normal contamination.
Self-shielded E71T-GS, 0.045" dia. 30 V, ~170 amperes.
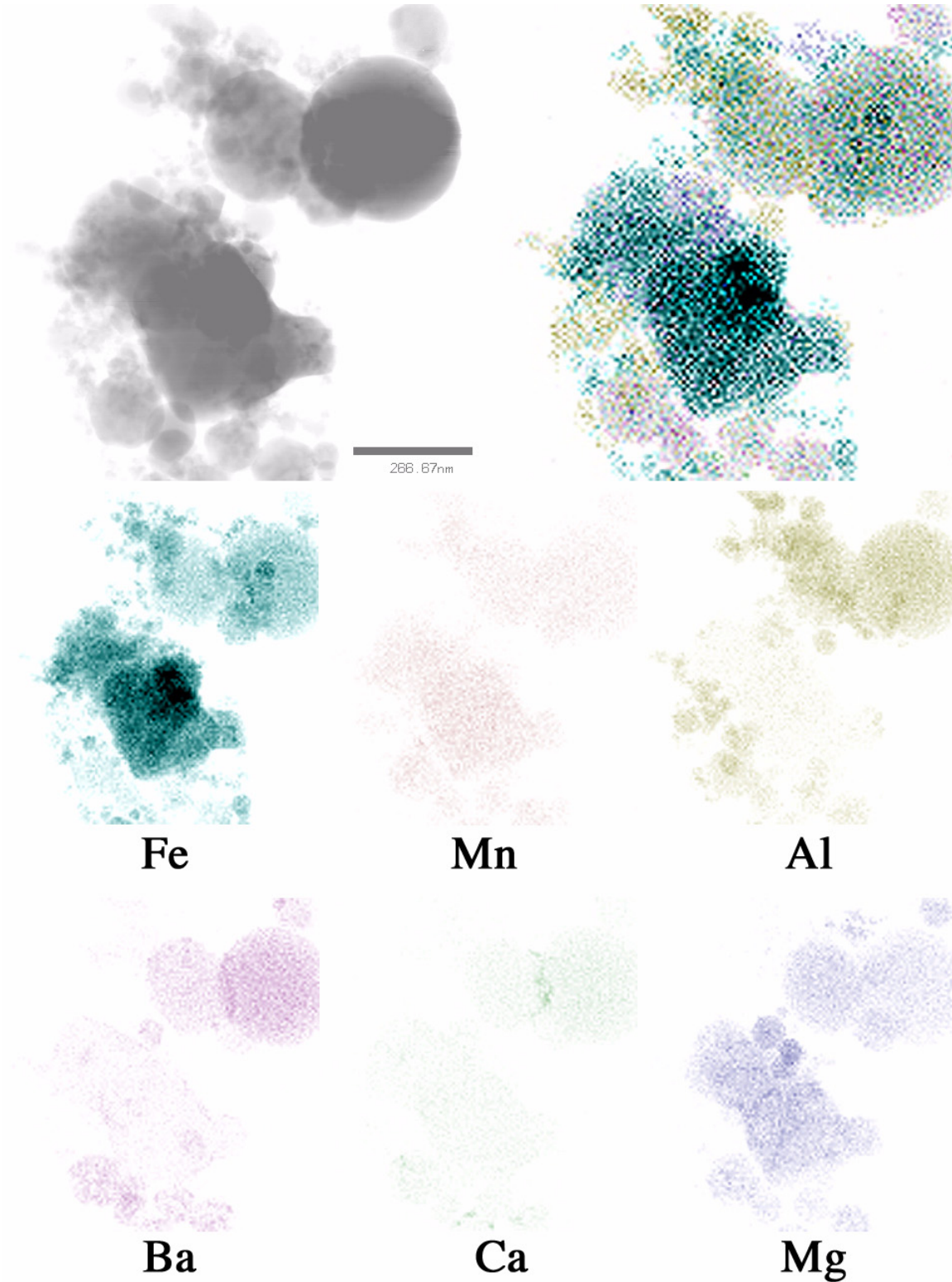
Figure 5.19 Transmission electron micrograph and cation maps from energy dispersive spectrometry of mild steel FCAW fume. Composite map in upper right.

Silicon and carbon were not included because of normal contamination.

Self-shielded E71T-GS, 0.045" dia. 30 V, ~170 amperes.
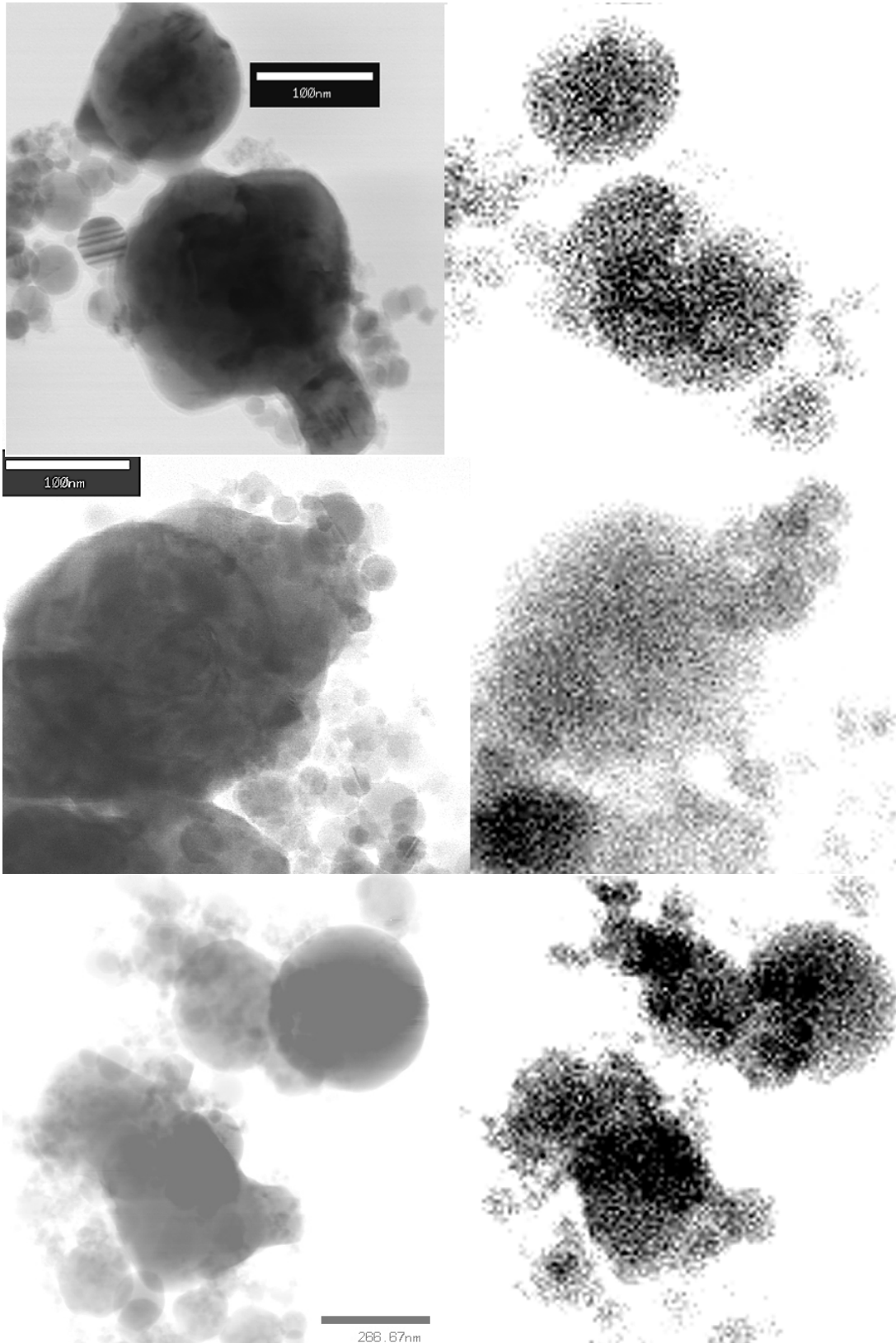
Figure 5.20 Transmission electron micrograph and oxygen concentration map from energy dispersive spectrometry of mild steel FCAW fume composed of oxides and fluorides. Same agglomerates as in Figure 5.17, Figure 5.18, and Figure 5.19.

Table 5.7 Description of welding processes studied with scanning transmission electron microscopy - energy dispersive spectrometry.

Welding Process	Shield Gas	Electrode AWS Designation	Current (amp)	Voltage (volt)	Wire Speed (ipm)
mild steel GMAW	2%O2,Ar	ER70S-6 0.045″	∼175	30	∼300
stainless steel GMAW	2%O2,Ar	E308L 0.045″	∼175	30	∼300
mild steel FCAW	none	E71T-GS 0.045″	∼160	30	∼300
stainless steel FCAW	none	ER308FC-0 0.045″	∼160	30	∼300
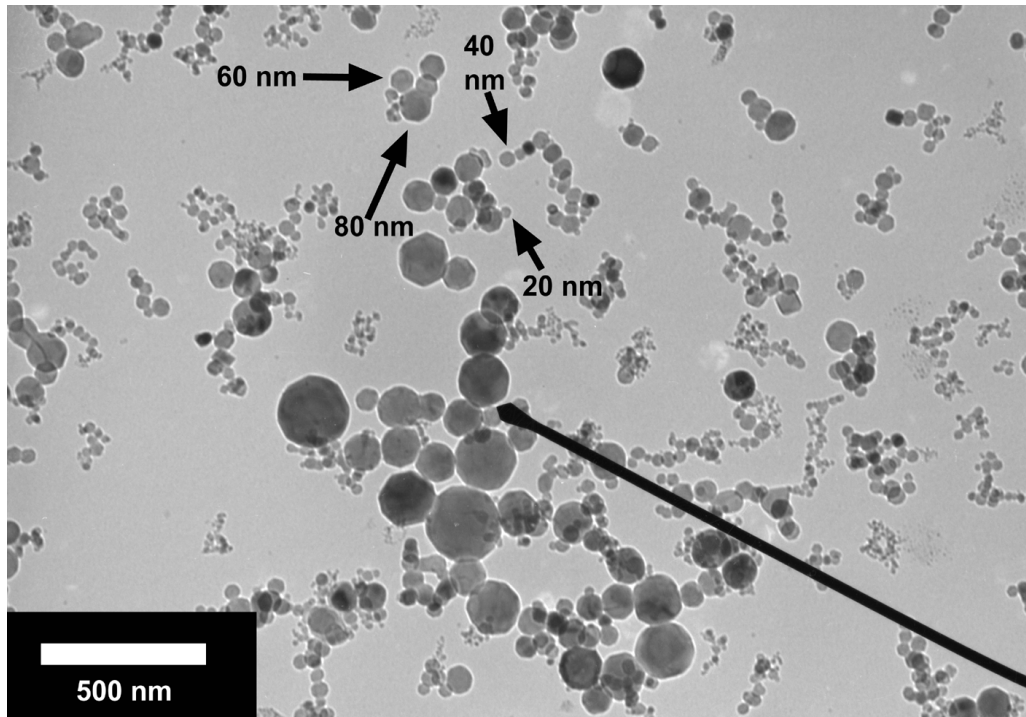
Figure 5.21 Transmission electron micrograph (50 000x) of mild steel gas metal arc welding fume Reprinted from Jenkins & Eagar (2003) with permission of The Minerals, Metals, and Materials Society (TMS).

With a transmission electron microscope (see Figure 5.21), 30 primary particles (as opposed to aggregates or agglomerates) per size group (20, 40, 60, 80 nanometers) were analyzed with energy dispersive spectrometry. Because the electrons travel through the entire sample and therefore through multiple particles if stacked on one another, care was taken to analyze only one particle at a time.The mean composition for each particle size can be found in the following graphs (Figure 5.22 to Figure 5.25) and associated tables (Table 5.8 to Table 5.12).

Table 5.8 Atomic fraction of metals content in mild steel gas metal arc welding fume per size group (30 particles each), determined with energy dispersive spectrometry / transmission electron microscopy. Manganese mole fraction of the electrode was 0.012.

	20 nm	Standard Deviation	40 nm	Standard Deviation	60 nm	Standard Deviation	80 nm	Standard Deviation	Bulk Fume
Fe	0.881	0.050	0.901	0.050	0.933	0.037	0.888	0.147	0.89
Mn	0.119	0.050	0.099	0.050	0.067	0.037	0.112	0.147	0.11
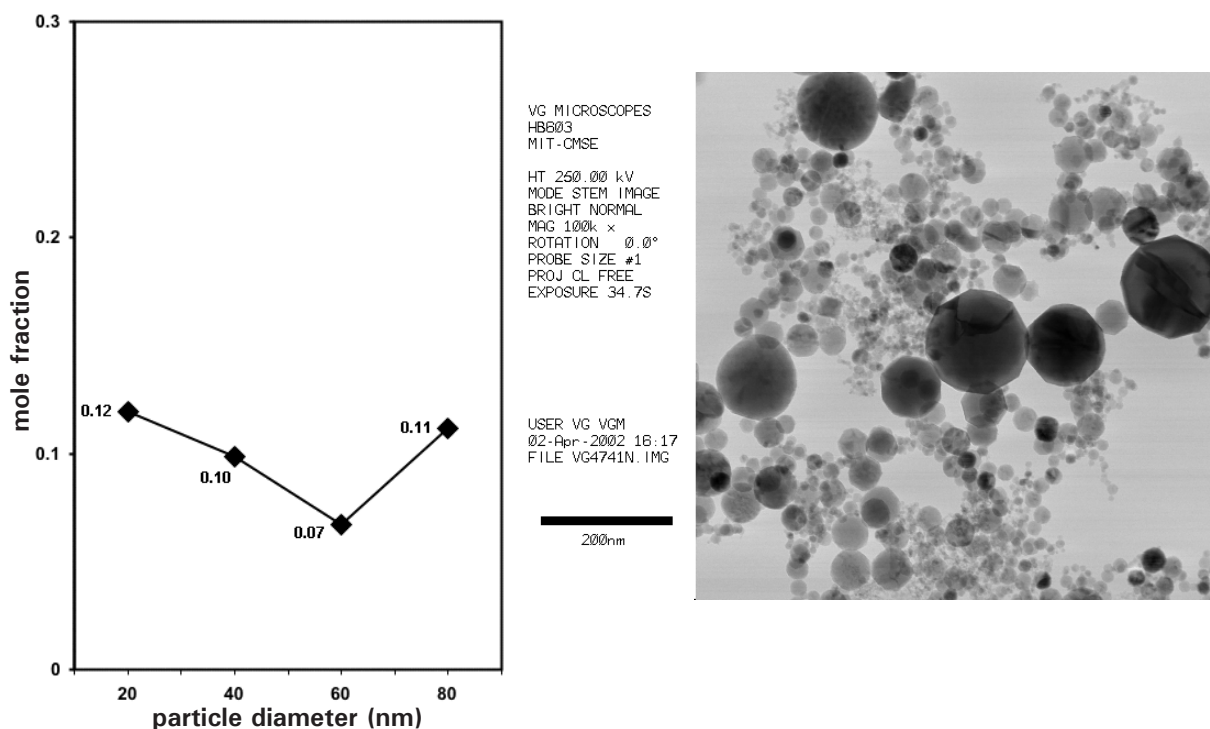
Figure 5.22 Mole fraction of manganese with respect to iron in mild steel gas metal arc welding fume as a function of particle size, determined with energy dispersive spectrometry / transmission electron microscopy (representative micrograph included).
Graph reprinted from Jenkins & Eagar (2003) with permission of TMS.

Table 5.9 Atomic fraction of metals content in stainless steel gas metal arc welding fume per size group (30 particles each), determined with energy dispersive spectrometry / transmission electron microscopy. Bulk fume by SEM-EDS; Electrode by ICPMS.

	20 nm	Stan. Dev.	40 nm	Stan. Dev.	60 nm	Stan. Dev.	80 nm	Stan. Dev.	Bulk Fume	Elec-trode
Fe	0.442	0.114	0.498	0.033	0.512	0.055	0.480	0.163	0.472	0.659
Cr	0.257	0.136	0.212	0.046	0.228	0.067	0.233	0.091	0.234	0.220
Ni	0.049	0.034	0.025	0.013	0.025	0.015	0.027	0.020	0.042	0.018
Mn	0.232	0.076	0.249	0.056	0.217	0.069	0.234	0.203	0.229	0.091
Si	0.020	0.012	0.016	0.006	0.018	0.025	0.026	0.030	0.024	0.011
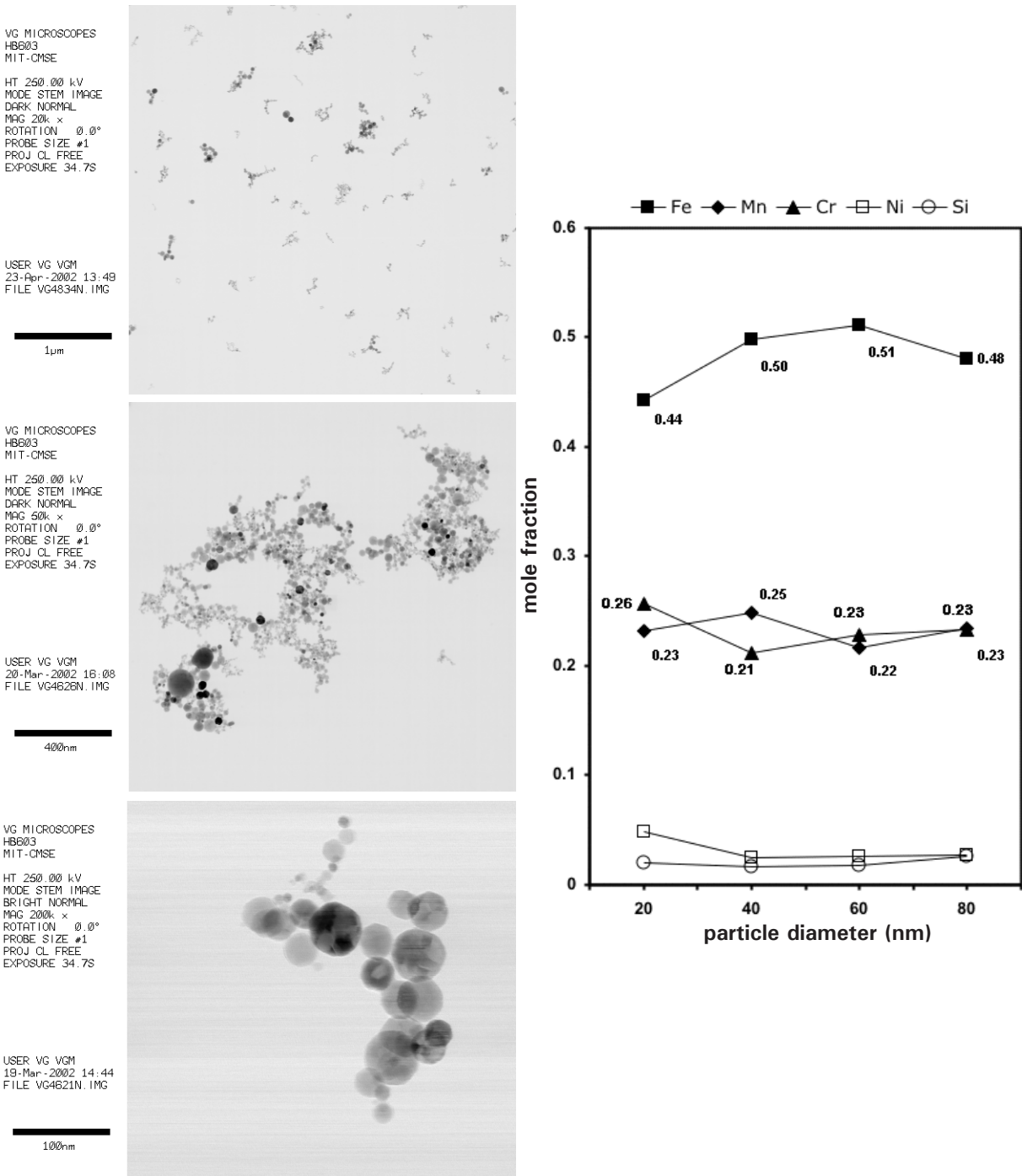
Figure 5.23 Atomic fraction of metals content in stainless steel gas metal arc welding fume as a function of particle size, as determined with energy dispersive spectrometry / transmission electron microscopy (representative micrographs included).
Graph reprinted from Jenkins & Eagar (2003) with the permission of The Minerals, Metals, and Materials Society (TMS).
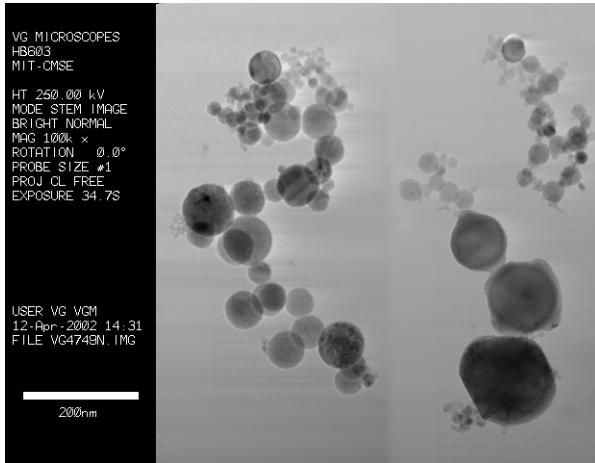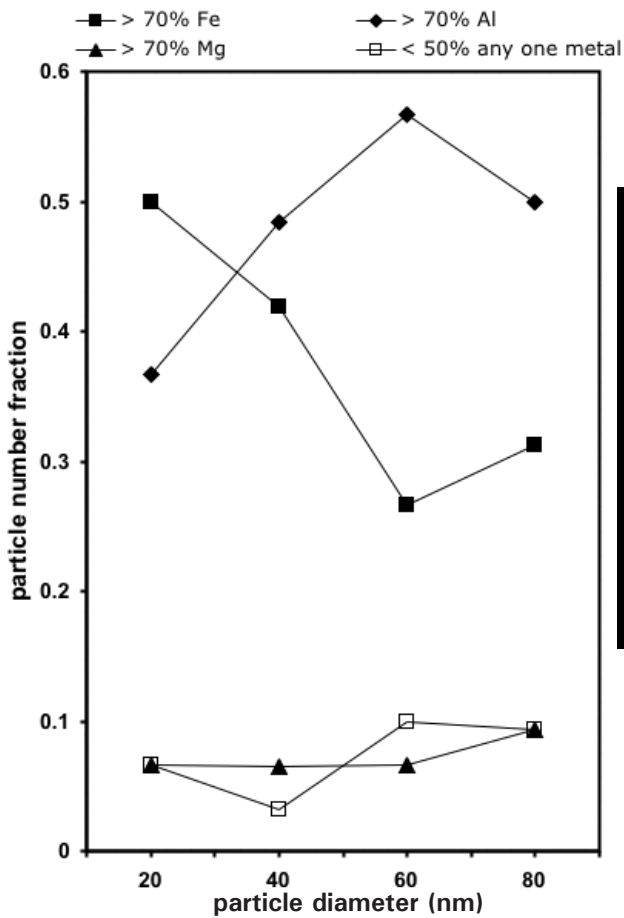
Figure 5.24 Metals content in mild steel flux cored arc welding fume as a function of particle size, as determined with energy dispersive spectrometry / transmission electron microscopy (representative micrographs included).

Table 5.10 (Left) Metals content in mild steel flux cored arc welding fume as a function of particle size (energy dispersive spectrometry / transmission electron microscopy)
Table 5.11 (Right) Mild steel flux-cored electrode (E71T-GS) composition; metals only

Particle Size Group (nm)	20	40	60	80
# particles > 70% Fe	15	13	8	10
# particles > 70% Al	11	15	17	16
# particles > 70% Mg	2	2	2	3
# particles <50% any 1 metal	2	1	3	3

mole fraction	Electrode Comp.	
Fe	0.887	wire
Cr	0.002	wire
Mn	0.007	both
Si	0.005	both
Al	0.063	flux
Ca	0.005	flux
Ba	0.010	flux
Mg	0.021	flux

124
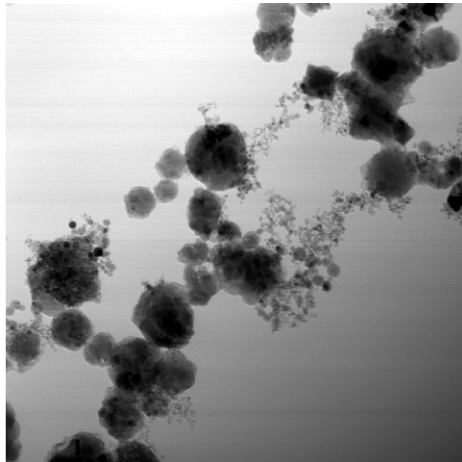
Figure 5.25 Atomic fraction of metals content in stainless steel flux cored arc welding fume as a function of particle size, as determined with energy dispersive spectrometry / transmission electron microscopy (representative micrographs included).

Table 5.12 Atomic fraction of metals content in stainless steel flux cored arc welding fume per size group (30 particles each), as determined with energy dispersive spectrometry / transmission electron microscopy. Bulk fume composition by SEM-EDS; Electrode composition by ICPMS.

	20 nm	Standard Deviation	40 nm	Standard Deviation	60 nm	Standard Deviation	80 nm	Standard Deviation	Bulk Fume	Electrode
Fe	0.527	0.194	0.491	0.226	0.299	0.258	0.227	0.203	0.113	0.614
Cr	0.187	0.090	0.202	0.098	0.185	0.134	0.119	0.114	0.081	0.200
Ni	0.093	0.088	0.046	0.029	0.021	0.024	0.013	0.015	0.013	0.085
Mn	0.088	0.092	0.109	0.083	0.151	0.158	0.142	0.110	0.101	0.021
Si	0.041	0.037	0.041	0.035	0.061	0.058	0.161	0.237	0.095	0.011
Al	0.004	0.006	0.016	0.055	0.056	0.127	0.077	0.152	0.150	0.008
Ti	0.022	0.069	0.014	0.042	0.073	0.106	0.063	0.086	0.080	0.032
Zr	0.003	0.010	0.002	0.004	0.008	0.012	0.005	0.008	0.013	0.004
Mo	0.002	0.002	0.002	0.005	0.007	0.026	0.002	0.004	–	0.001
K	0.019	0.088	0.044	0.144	0.085	0.143	0.115	0.189	0.120	0.002
Na	0.000	0.000	0.002	0.008	0.002	0.009	0.012	0.033	0.167	0.003
Ca	0.012	0.045	0.030	0.081	0.045	0.095	0.058	0.158	–	0.016
Ba	0.002	0.005	0.001	0.003	0.006	0.010	0.005	0.008	0.061	0.000
Mg	0.000	0.001	0.001	0.001	0.001	0.001	0.002	0.005	0.006	0.000

Although variation from the mean is often large, which is reflective of the variable nature of the welding arc and the random collisions of small particles, there is a trend in how mean composition varies with particle size.

When particles collide, agglomerate, and then coalesce with other particles, variation of the overall composition with particle size is lost. (As already noted, internal variation can still exist within an aggregate. This will be explored in detail later.) This can be seen in the 80 nanometer size groups for all of the fume except that from stainless steel FCAW. The composition is approximately equivalent to the mean composition of the other particle size groups, particularly if weighted by particle mass. Although the particles smaller than 80 nm differ with size from one another, if combined they would have the same composition as the initial vapor. This is evidenced by the composition of the particles 80 nm in size, which is essentially the same composition of the welding fume as measured by bulk analysis. It can be concluded that these particles were not formed from single nuclei, but from the collision and coalescence of several nuclei. The compositional variation is also greater in this size group because collision is random and is not determined by thermodynamic driving forces.

It makes sense that the 80 nm particle size group is dominated by particles that formed through the collision of smaller particles. As described in Chapter 3, the mean free path of argon is approximately 70 nm, so growth by vapor condensation is limited for particles similar in size.

The nature of particle growth could be confirmed by examining the crystal structure of the individual particles; particles formed from multiple nuclei would likely be poly-crystalline, whereas single nuclei would be single crystals. A paper by Ehrman, et al., (1999) reported polycrystalline behavior in coalesced particles. Such an exami-nation, however, did not take place in this study.

What caused the variation in composition in the smaller particles that did not form through particle collision (in this example, 20 nm – 60 nm)?

In gas metal arc welding, the molten metal at the tip of the electrode emits vapor, which is mixed with the inert shielding gas traveling at approximately 100 m/s through a 10–20 mm hot zone, from plasma arc temperatures substantially above 3000K (the approximate boiling point of iron) to room temperature (Mendez, et al., 2002).

This means vapor and particles are in the hot region for about 10^{-4} seconds with a temperature gradient of about 10^7 K/s. Particles nucleate, grow, and are blown out of the hot vapor rich areas where they cease growing. The size of the particle is determined by a combination of the critical diameter for nucleation and the conden-sation growth rate. Therefore, the size of the particle indicates the temperature at which the particle was formed. The temperature in turn indicates the elemental composition of the condensed particle.

Barring differences about what causes the instabilities that drive the phase change, vapor condensation in a binary mixture is very similar to liquid solidification. Gases behave ideally at high temperatures, so a simple isomorphic binary phase diagram can be used to describe the condensation process. See Figure 5.26, a simple ideal binary of iron and manganese at 0.3 atmospheres pressure. (Whether this is the binary of the metals or of the metal oxides is inconsequential for the current analy-sis, because both are ideal. The oxidation state of the vapor will be discussed later.) Two notes should be made about the vapor pressure.

First, it should be explained why a pressure of 0.3 atmosphere was chosen. Eagar (2000) stated that the metal vapor pressure in an arc, depending on where in the arc, is 0.05 to 0.3 atmospheres, in order to maintain a conductivity great enough to maintain the arc current. Researchers (He, et al., 1997) measured pressures of 0.2 to 0.3 atmosphere in the region about 10 mm from the center during thermal plasma melting of an iron-manganese alloy. Grong & Christensen (1983) calculated the metal vapor pressure to be 0.1 atmosphere from electrode mass loss measure-ments. A quick mass balance can also be calculated. A typical shielding gas flow rate is 25 L/min and a normal wire feed speed is 1.25 mm/s. A fume formation rate of 10 mg fume per gram of wire is common, which is equivalent to saying that 1%
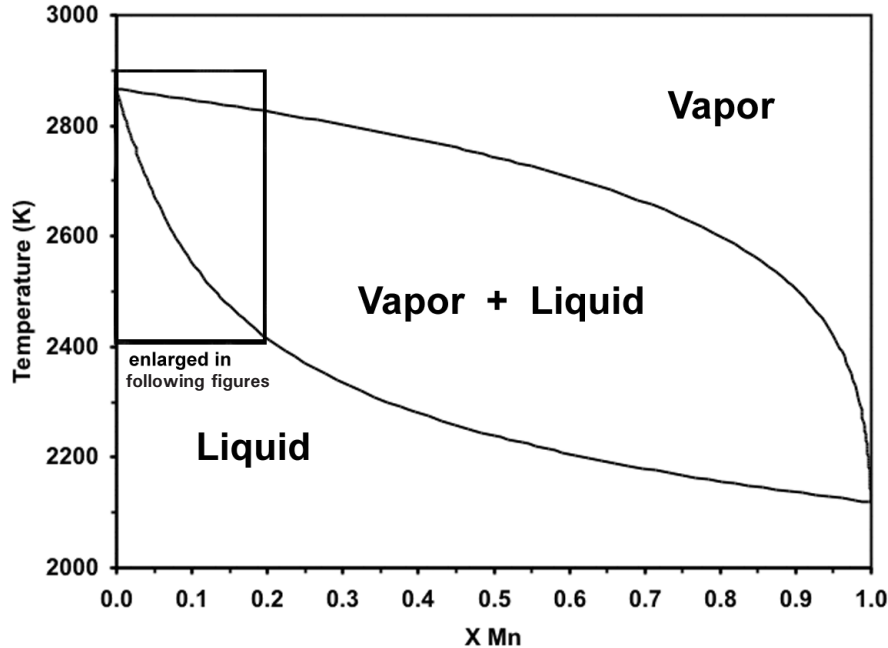
Figure 5.26 Iron-manganese phase diagram at 0.3 atmosphere pressure (Sundman, 1991). Reprinted from Jenkins & Eagar (2003) with permission of The Minerals, Metals, and Materials Society (TMS).

of the wire evaporates. The resulting ratio of vapor to argon would be equivalent to 0.04 atmosphere[1].

There is probably more vapor in the arc that does not create fume. Haidar (1999) calculated that 10% of the electrode evaporates and Bosworth and Farmer (1999) measured about 3%, so the corresponding vapor pressures would be 0.1 to 0.4 atmospheres. (The vapor that does not form welding fume condenses in the weld-pool. A weldpool was created with GMAW on a base of pure Sn using an iron electrode with a single pulse brief enough to prevent liquid metal transfer. SEM-EDS showed that the previously pure Sn had 5% Fe in it after the single pulse of welding current.) 0.3 atmosphere is a reasonable assumption, but the use of any value in the range mentioned would not greatly change the treatment here.

Second, it should be mentioned that the vapor pressure over small particles is increased with respect to the vapor pressure over a flat surface of the same material, as described by the Kelvin equation. When combined with the Clapeyron equation, one can derive the change in boiling point as follows:

---

1. An interesting observation is that shielding gases generally have approximately an equivalent amount of oxygen in them. Corderoy, et al. (1980) believed that metal vapor in the arc acted as an oxygen-getter because their calculations indicated that only a quarter of the oxygen, that should reach the welding droplet, did so. Perhaps an oxidation reaction is the reason why some vapor is converted to fume and the rest recondenses in the weld pool.

128

$$T_{b,\,particle} = T_{b,\,\infty}\left(1 - \frac{4\Omega\gamma}{L_v d}\right) \qquad\qquad 5.2$$

where d is the diameter of the particle, L_v is the heat of evaporation, γ is the surface energy, and Ω is the molar volume. When evaluated with typical values for the properties of iron and manganese, the boiling point is lowered only by about 15K for a particle with the radius of 10 nanometers. This is small enough to ignore for this analysis. The only complication in this calculation is that the surface energy and perhaps the heat of evaporation may also be dependent on particle size. Although studies about boiling point depression with curvature are rare, researchers do report that the depression of the melting point of metals due to curvature is only significant when the particle radius is less than 10 nanometers (Bachels, et al., 2000; Alymov and Shorshorov, 1999; Storozhev, 2001).

Although the compared phase changes are first order and analogous, the distribution and compositional variation of second phase particle size in the vapor system described here are different from that commonly found in a solidifying liquid for the following reasons:

• The cooling rate is much faster than typical cooling rates in liquids. The cooling rate of the vapor in a welding arc is about 10^7 K per second. (For comparison, the cooling rate of amorphous metal casting is $\sim 10^5$ K per second.) Even at nucleation rates greater than the "measurable" rate of 1 nucleus per cubic centimeter per second and at the maximum particle growth rate predicted by the Langmuir equation, it would take several seconds for all of the vapor to completely condense. However, in just a microsecond, the vapor is cooled about 10K, which substantially changes the criteria for stable nuclei. This is part of the reason that the size distribution of primary particles in welding fume is as broad as it is.

• Welding fume particles are quickly blown by the plasma jet out of the hot zone around the welding arc. Since the particles are removed from the system, subsequent heterogeneous nucleation, that is to say, growth, is limited. Therefore, as the mixture is brought to a lower temperature, more particles homogeneously form, but of a smaller radius than that of the ones removed. As the temperature lowers, many particles of various sizes (and compositions) are created.

• If the particles were to remain in the vicinity of other particles, competitive growth could also occur; the larger particles would grow at the expense of the smaller particles by solute diffusion through the cooling mixture. In rapid vapor condensation, the small particles are not consumed by larger particles unless they collide with them.

• In a solidifying liquid, the presence of minor alloying components can affect the solubility of other alloying elements. Gaseous metals behave as individual non-interactive atoms; therefore, the solubility of a selected species in the vapor will not be affected by the overall composition of the vapor mixture. However, this might not be the case when the vapor mixture contains reactive elements such as oxygen because some metals form gaseous oxide species. In this case, azeotropic behavior in the resultant phase diagram might occur.

Particle size can be modelled in two ways; one in which particle formation is dominated by nucleation (Figure 5.27), the other by growth (Figure 5.28).

In the nucleation dominated model, Equation 3.2:

$$d^* = \frac{-4\gamma\Omega T_b}{L(T_b - T)} \qquad\qquad 3.2$$

can be used with the phase diagram to determine the relationship between particle size and elemental composition. This model has been explained by Jenkins and Eagar (2003). The iron-manganese vapor solution is supercooled until nucleation commences. The first nuclei are iron-rich particles. Additional particles nucleate at lower temperatures and at higher manganese levels.

The problem with this model is that the compositions shown in Figure 5.22 are much too rich in manganese to correspond to the nucleus sizes predicted at the supercoolings measured from Figure 5.27. Alternatively, it can be considered that particle formation can be dominated by growth, as characterized by Equation 3.3:

$$\frac{d\text{d}}{d\text{t}} \propto \frac{\Omega(P_A - P_{A, \infty})}{\sqrt{2\pi M_A RT}} \qquad\qquad 3.3$$

Here the temperature at which the particle initially nucleates would be important, as would be the changing temperature at which the particle grows. As the vapor cools and condenses, the condensate composition follows the bubble point line, the analog to the solidus in a liquid-solid phase diagram. If diffusion in the solid is fast enough, when the temperature is lowered beneath the two phase region, the condensate will equilibrate to be the same composition as the vapor, which should not greatly change composition. This is assuming that it is an open system, replenished by the evaporation of the welding electrode. If diffusion in the solid is slow compared with growth, then particles will not equilibrate, and iron-rich cores with manganese-rich shells will develop.

However, the interdiffusion coefficients (D) for iron alloys at about 1500K are around 10^{-8} cm^2/s. (A little more accurate value would be 10^{-4} cm^2/s, which is typical for liquid iron alloys at 2000K. Very small particles with high surface-to-volume ratios would not have properties much different from those of liquids.) With a diffusion distance (x) equal to a particle radius of 10 nanometers, one finds that the diffusion time is $\sim 10^{-4}$ seconds (see Equation 5.3), similar to the residence time in the hot zone around the welding arc. Based on this rough analysis, it is possible that equilibrium growth does not occur; manganese rich shells may form. This is not to say that such shells endure over time. Homogenization of the particle may occur post-condensation. This will be discussed later.

$$x \approx \sqrt{Dt} \qquad\qquad 5.3$$

When typical values are used in Equation 3.3 (which becomes an equality if it is assumed that all vapor molecules stick when they collide with the particle and if the

130
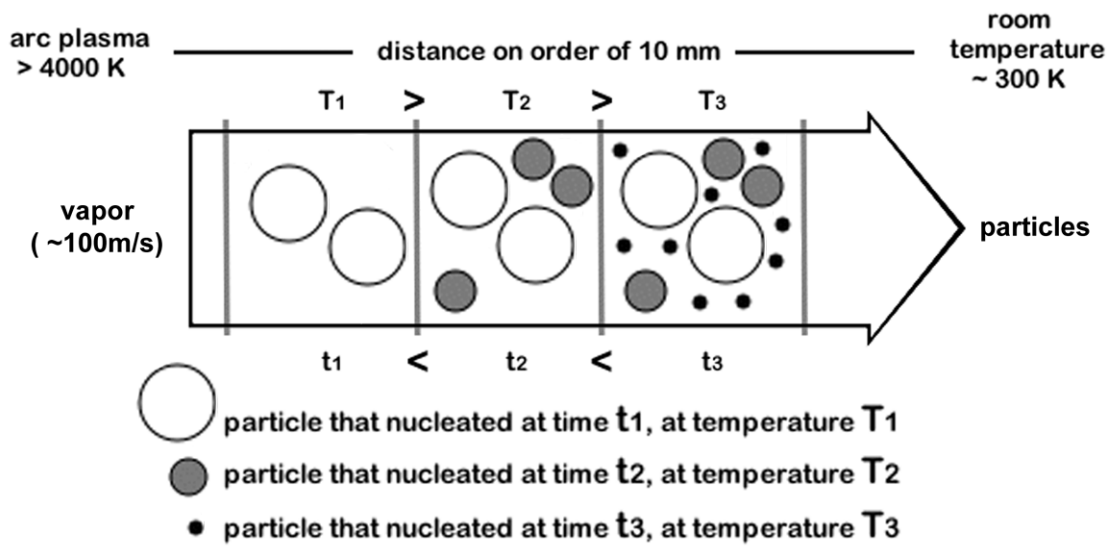
Nucleation in Iron - Manganese Vapor
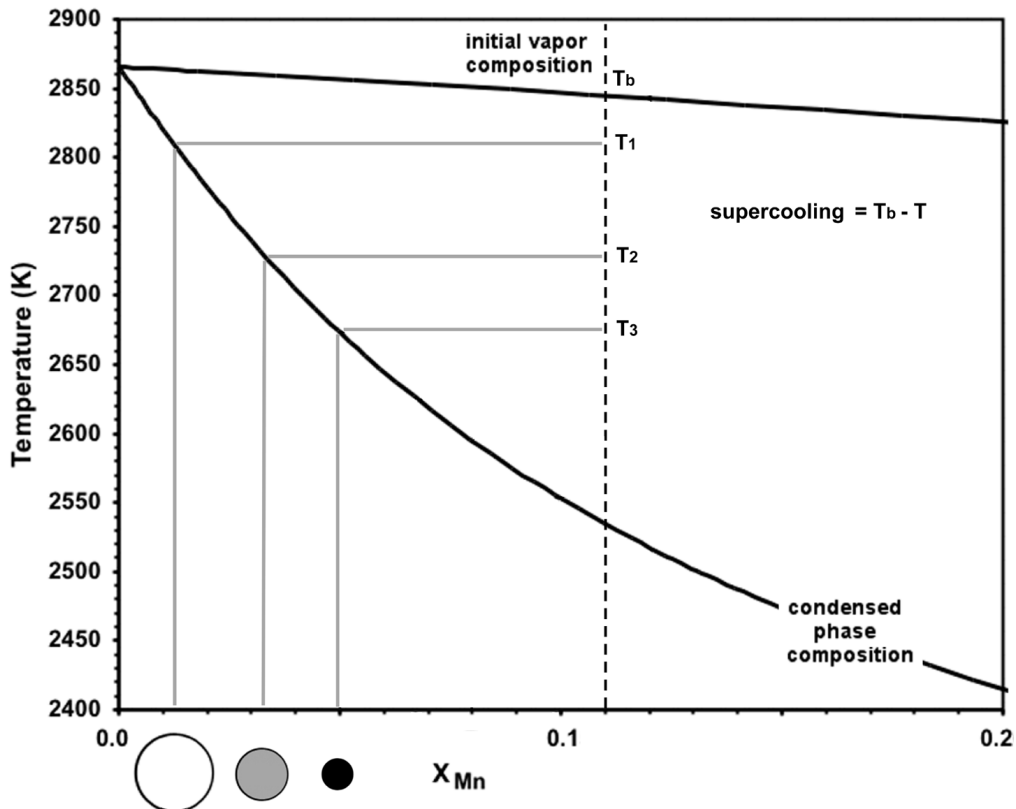
Figure 5.27 Nucleation dominated formation model for welding fume particles. Phase diagram of iron-manganese system calculated at 0.3 atmosphere pressure.
Reprinted from Jenkins & Eagar (2003) with permission of The Minerals, Metals, and Materials Society (TMS).
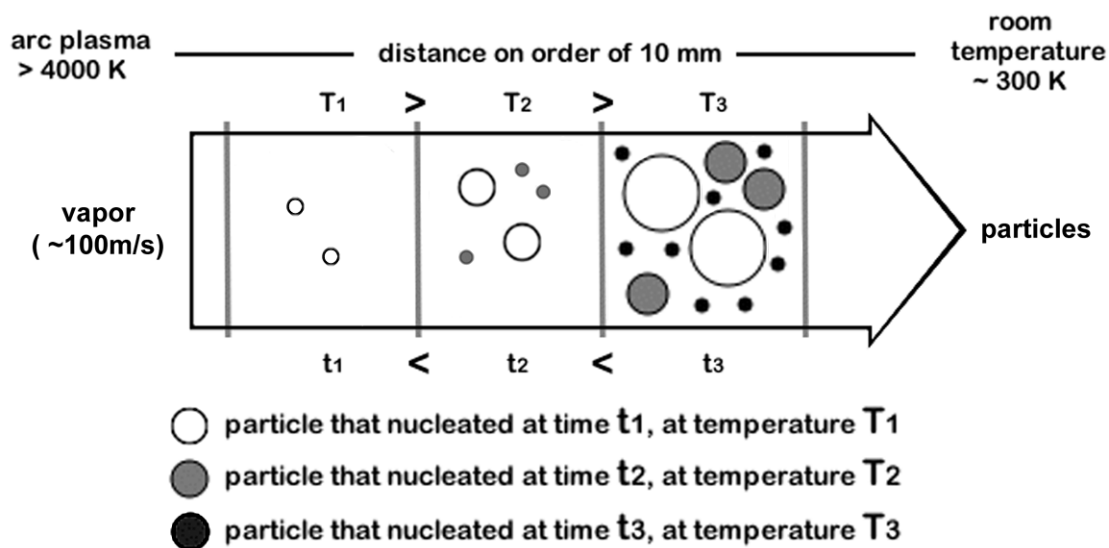
Growth in Iron - Manganese Vapor
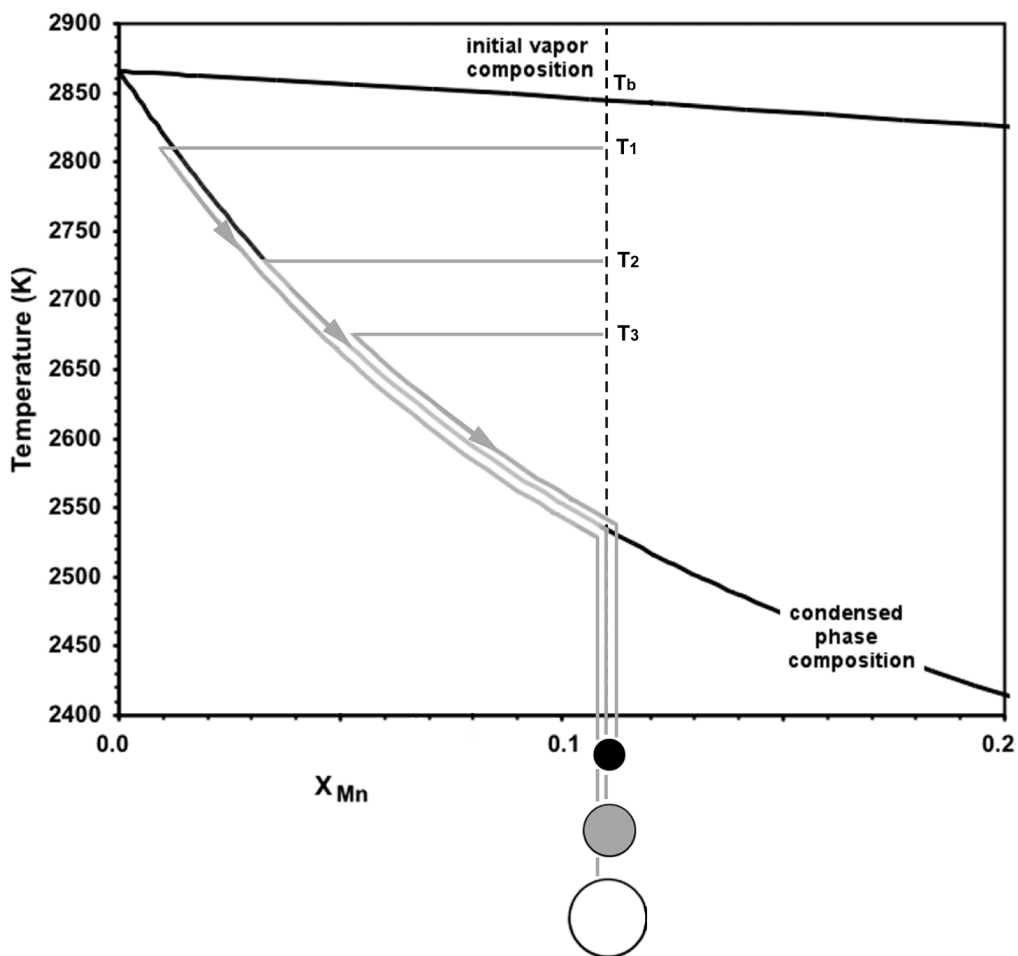
Figure 5.28 Growth dominated formation model for welding fume particles. Phase diagram of iron-manganese system calculated at 0.3 atmosphere pressure.

particle is smaller than the mean free path of the carrier gas), it can be shown that growth occurs quickly, but is limited by the amount of time the particles are in the hot zone. The maximum possible growth rate for an iron-manganese vapor is about 100 micrometers/second; in 10^{-4} seconds that would be about 10 nanometers. The high growth rate indicates that it may be possible that the vapor may become locally enriched, as if it were a quasi-closed system. This also shows that growth does not account for the entire particle size.

As with many things, the actual condensation behavior is likely to be a mixture of both theories. The composition of the particles may be able to illustrate the extent of this mixture. If Figure 5.22 is examined, one can see how the manganese content of the GMAW fume particles decreases with particle size until reaching 80 nanometers which seems to be an aggregate of smaller sizes and of equivalent composition to the vapor. Assuming that the concentration gradient of the material that condenses during growth is linear, which is reasonable at low manganese concentrations and large supercoolings, one can calculate the width of the growth section necessary to average out the lower concentration of a nucleus, whose size and composition is determined by the intersection of the bubble point line and Equation 3.2. See Figure 5.29 and Equation 5.4.
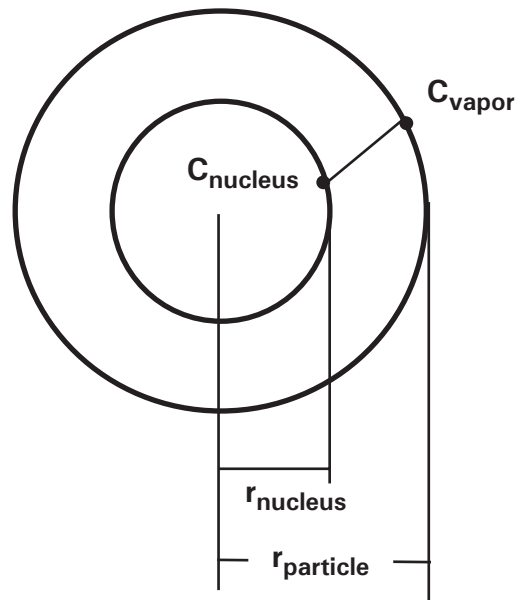
Figure 5.29 Composition of condensation particle before homogenization.

$$C_{particle} = \left(1 - \left(\frac{r_{nucleus}}{r_{particle}}\right)^3\right)\left(\frac{C_{vapor} + C_{nucleus}}{2}\right) + \left(\frac{r_{nucleus}}{r_{particle}}\right)^3 C_{nucleus} \qquad 5.4$$

If the molar fraction of manganese in the vapor, and therefore of the surface of a particle, is 0.11, a particle with a diameter of 60 nm with a manganese fraction of 0.07 would have been created from a nucleus of about 2 nm in diameter with a composition of 0.04. This poses a problem, because this suggests that the particle

grew by ~50 nm in the time where the maximum growth only allows for 10 nm. Similar problems are found with calculations with the other particle sizes.

A solution can be found if vapor enrichment is considered. Although the bulk concentration of the vapor would remain 0.11, it is possible that local depletion of iron into the particles enriches the vapor around the particle. In this case, the surface manganese concentration of the particle could be approximated as 1.0. This also addresses the concern that the smallest particles have a concentration of manganese greater than the bulk vapor, which should not be possible if the vapor were not enriched. The concentration gradient would not be linear and would thus be similar to what is described by the Scheil equation for liquid solidification in closed systems. Having the gradient increase with the fifth power suffices for the following example.

With these assumptions and approximations, one can calculate the following table from the data presented in Figure 5.22: These values serve to illustrate how fume

Table 5.13 Approximate values for particles of similar composition to those found in Figure 5.22 assuming vapor enrichment

particle diameter (nm)	particle composition (molar fraction of Mn)	nucleus diameter (nm)	nucleus composition (molar fraction of Mn)
20	0.12	15	0.005
40	0.10	30	0.002
60	0.07	50	0.001

particles can form as solute-poor nuclei surrounded by solute-rich shells, but it should be remembered that these calculations are dependent on the assumptions about the enriched vapor composition and the concentration profile from the nucleus to the particle surface.

As stated earlier, if thermodynamically unstable, this core-shell feature would homogenize very quickly, leaving homogenous particles of an averaged composition.

From this analysis, one can extrapolate that the smaller the particle, the greater the concentration in volatile element, even if the resulting composition is greater than the bulk vapor composition.

The particles formed from stainless steel GMAW exhibit similar behavior. There is a visible increase of iron with particle size up to 60 nanometers. It is difficult to see a steady decrease in the concentration of manganese and chromium, partially because of the usage of molar fractions in Figure 5.23. When the fraction of one element increases, the others must decrease. This could be better explained with a three-dimensional phase diagram, but it would be complicated to illustrate. Because of this, the trend in the change of compositions is more difficult to see in mixtures of

three or more major components. It is easier to see the general trend in composition if the data of Figure 5.23 are grouped by elemental boiling point, as in Figure 5.30.
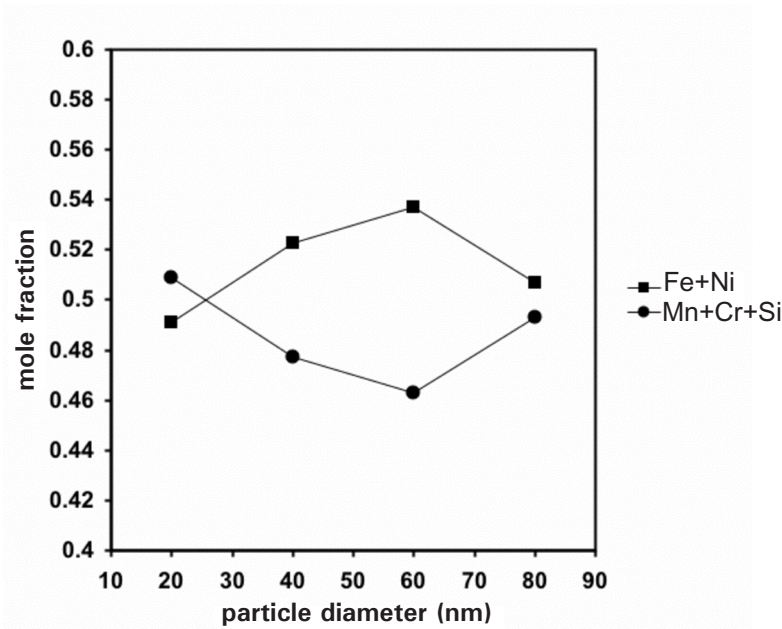
Figure 5.30 Mole fraction of metals content, grouped by boiling point, in stainless steel gas metal arc welding fume as a function of particle size, as determined with energy dispersive spectrometry / transmission electron microscopy.
Reprinted from Jenkins & Eagar (2003) with permission of The Minerals, Metals, and Materials Society (TMS).

The change in composition with particle size is rather different with the stainless steel FCAW fume. The concentration of volatile elements increases, rather than decreases, with particle size. This fume is different from the GMAW fume for two reasons. First, there is a higher concentration of metal vapor in the arc, allowing more growth to occur. Second, the electrode contains fluorine, which forms gaseous compounds at low temperatures. These compounds can continue to condense on existing particles, causing particles to grow larger at lower temperatures to eventually match the composition of the vapor, as described in Figure 5.28. The fluorides may not homogeneously nucleate, but may use pre-existing iron-rich particles as heterogeneous sites for nucleation. This is the likely cause for the increase in volatile elements with size.

The mild steel flux-cored welding fume contains particles that are more difficult to characterize. There seem to be three types of particles: iron-rich, aluminum-rich, and magnesium-rich, with each group containing more than 70% of the respective element. If these particles were to solidify from a liquid, they would perhaps form from an eutectic reaction in which the liquid solidifies into two different phases of different compositions. However, it is hard to imagine a metal binary system in which there is a miscibility gap in the liquid with a critical temperature above the boiling point, a main characteristic of an eutectic vapor-liquid phase diagram. Iron and aluminum also form intermetallics, thus indicating strong chemical affinity, that signals

complete miscibility in the liquid (Arroyave, 2003). It is not clear why these metals, with similar boiling points, would segregate so strongly.

This behavior is perhaps caused by the presence of oxygen in the system. As stated before, even in argon-shielded gas metal arc welding, some oxygen is present in the shielding gas, both by design and because of mixing from the external atmospheric air. In flux-cored arc welding, even more oxygen is present, either because it is shielded with an external flow of CO_2 or because it is self-shielded, often with compounds that break down to form CO_2. Carbon dioxide dissociates to form oxygen. In addition, fluxes are often oxides, which provide even more oxygen. Eagar (2003) estimates that the shielding in FCAW may exceed 0.1 atmosphere of oxygen.

A ternary vapor-liquid phase diagram for iron, aluminum and oxygen may reveal how the metals segregate upon condensation. Aluminum has stronger affinity for oxygen as a liquid and solid; aluminum oxide and iron metal are immiscible. However, iron oxide is somewhat stable as a vapor whereas aluminum oxide will dissociate before boiling, so the iron may oxidize as a gas, leaving aluminum metal behind. In addition, both Fe-O and Al-O have miscibility gaps in the metal-rich liquid regions of their respective binary phase diagrams. This may indicate azeotropic behavior in the vapor-liquid equilibrium.

More evidence that the metal vapors oxidize before condensation could be found with the flux-cored arc welding fume. Some researchers report that they were able to coat metal nanoparticles with a halide coating to prevent oxidation after condensation (Axelbaum, et al. 1997). FCAW fume could be examined to see if the non-halide center of individual particles was oxidized or not. If oxidized, this would indicate pre-condensation oxidation. The data in Chapter 4 from the X-ray diffraction of SMAW (which essentially has the same chemistry as FCAW) fume shows that this fume is composed of a fluoride and an oxide. This is the same fume shown in the elemental map found in Figure 5.16, which indicates that this fume may have an oxide core with a fluoride shell. If so, then that would suggest that the core condensed as an oxide directly from the vapor.

References

Alymov, M. I., & Shorshorov, M. K. (1999). Surface tension of ultrafine particles. *NanoStructured Materials*, 12, 365–368.

Arroyave, R. (2003). Personal communication, Massachusetts Institute of Technology.

Axelbaum, R. L., Dufaux, D. P., Frey, C. A., & Sastry, S. M. L. (1997). A flame process for synthesis of unagglomerated, low-oxygen nanoparticles: Application to Ti and TiB_2. *Metallurgical and Materials Transactions B,* 28B, 1199.

Bachels, T., Guntherodt, H. J., & Schafer, R. (2000). Melting of isolated tin nanoparticles. *Physical Review Letters,* 85(6), 1250–1253.

Bosworth, M., & Farmer, A. (1999). Metal vapour transfer in GMAW [MIG/MAG welding] and its contribution to fume formation. *Australasian Welding Journal,* 44(Third Quarter), 42–47.

Corderoy, D. J. H., Wills, B., & Wallwork, G. R. (1980). Gas/weld metal reactions in MIG arc plasma*. Proceedings of the International Conference on Health Hazards and Biological Effects of Welding Fumes and Gases*, Copenhagen, R. M. Stern, A. Berlin, A. Fletcher, K. Hemminki, J. Jarvisalo & J. Peto (Eds.). Amsterdam: Excerpta Medica

Eagar, T. W. (2000). Personal communication, Massachusetts Institute of Technology.

Eagar, T. W. (2003). Personal communication, Massachusetts Institute of Technology.

Ehrman, S. H., Friedlander, S. K., & Zachariah, M. R. (1999). Phase segregation in binary SiO_2/TiO_2 and SiO_2/Fe_2O_3 nanoparticle aerosols formed in a premixed flame. *Journal of Materials Research*, 14(12), 4551–4561.

Fasiska, E. J., Wagenblast, H. W., & Nasta, M. (1983). *Characterization of Arc Welding Fume*. Miami, FL: American Welding Society.

Grekula, A., Peura, R., & Sivonen, S. (1986). Quantitative energy dispersive x-ray microanalysis of welding fumes. *Proceedings of the International Conference on Health Hazards and Biological Effects of Welding Fumes and Gases*, R. M. Stern, A. Berlin, A. Fletcher, K. Hemminki, J. Jarvisalo & J. Peto (Eds.). Amsterdam: Excerpta Medica.

Grong, O., & Christensen, N. (1983). Factors controlling MIG weld metal chemistry. *Scandinavian Journal of Metallurgy,* 4, 155–165.

Haidar, J. (1999). An analysis of heat transfer and fume production in gas metal arc welding. III. *Journal of Applied Physics,* 85(7), 3448–3459.

He, G. W., Ishii, K., Sakai, Y., & Kashiwaya, Y. (1997). Spatial distribution of metallic vapor in ar thermal plasma on melting of Fe and Fe-Mn alloy. *Tetsu To Hagane - Journal of the Iron and Steel Institute of Japan,* 83(12), 838–843.

Jenkins, N. T., & Eagar, T. W. (2003). Submicron particle chemistry: Vapor condensation analogous to liquid solidification. *JOM,* June, 44–47.

Jenkins, N.T. and Eagar, T.W. Stability of hexavalent chromium in mixed metal oxide particles. In preparation.

Kalliomaki, P. L., Grekula, J. A., Hagberg, & Sivonen, S. (1987). Analytical electron microscopy of welding fumes. *Journal of Aerosol Science,* 18(6), 781–784.

Mendez, P. F., Ramirez, M. A., Trapaga, G., & Eagar, T. W. (2002). Scaling laws in the welding arc. In *Mathematical Modelling Of Weld Phenomena* (Vol. 6). London: Institute of Materials.

Storozhev, V. B. (2001). The liquid-phase sintering and coalescence of small solid particles. *Aerosol Science and Technology,* 34(2), 179–185.

Sundman, B. (1991). A program for performing thermodynamic calculations. In *User Aspects of Phase Diagrams*, Hayes, F.H. (Ed.) London: Institute of Metals.

5.2.2 Internal Heterogeneity

Transmission electron micrographs seem to indicate that not all welding fume particles are homogenous internally (for examples, see Pilyankevich and Naumenko, 1984 or Voitkevich, 1995). Various researchers have tried to analyze the surface of welding fume (see Chapter 2) and other metal oxide particles, such as foundry dust, using X-ray photon spectroscopy (XPS) (Minni, et al., 1984; Tandon, et al., 1985; Voitkevich, 1988; Perrault, et al., 1992; Michaud, et al., 1993), secondary ion mass spectrometry (SIMS) (Van Craen, et al., 1982; Van Craen, et al., 1983), or Auger electron spectroscopy (AES) (Grekula, et al,. 1986; Minni, et al., 1990). Except for SIMS, (which apparently has not been applied to welding fume) these techniques do not have a resolution fine enough (see Chapter 4) to analyze just one particle, suggesting that these studies report compositional data that are suspect (For a discussion about the problems of XPS analysis of fine particles, see Tandon, et al., 1985). However, the general consensus is that the lighter elements enrich the surfaces of particles.

Analyzing the composition throughout an individual particle with transmission electron microscopy is a reliable way to observe internal heterogeneity. Ehrman, et al. (1999) reported important findings on aggregated and coalesced particles. TEM images revealed multiple discrete phases that had segregated within mixed oxide (Si-Ti and Si-Fe) particles only tens of nanometers in diameter. As discussed earlier, particles collide and coalesce, but whether they homogenize is naturally dependent on the miscibility of the material of the original particles and the time scale for homogenization. This is not only true for larger particles formed from the collision of smaller ones, but also for those smaller particles that condensed directly from the gas. These may have compositional gradients formed because of the difference in vapor pressures of the respective elements and compounds.

Because of the nanoscale of these particles, it is doubtful that they would remain in a metastable state, such as that of a compositional gradient in a single phase or that created from the fusion of dissimilar particles. This is also an important issue when examining hexavalent chromium (a possible carcinogen) in particles, because hexavalent chromium is not stable at room temperatures and atmospheric oxygen pressures. Yet researchers measure its existence in welding fume. Either there is a

way it is stable (Jenkins & Eagar, in preparation) or the unstable phases have been quenched into the particle (see McAllister & Bosworth, 1999). If the latter, it may not be reasonable that such small particles would remain in the metastable state for a significant amount of time.

From the data used by Hong & Yoo (2002) for Fe_3O_4, one can see that the bulk diffusion coefficient (D) extrapolated to room temperature is approximately 10^{-17} cm^2/s. The diffusion length is $\sim 2*(Dt)^{1/2}$. If it is set equal to the size scale of a particle (i.e., 10 nanometers) then the time (t) for an unstable phase to degrade would be equal to about 7 hours (see Equation 5.3). This does not consider quick diffusion paths such as those along grain boundaries or along the surface, nor does it consider that the effective melting temperature is probably lower for a nanoparticle than for its bulk material, which increases the diffusivity. Material properties can drastically change at a very small scale. Ohring (1992) says that although the characteristic diffusion time of Cu in bulk Ni at room temperature is more than 200 000 years, a 100 nm thin film of Cu-Ni will homogenize within an hour if held at room temperature. It is hard to imagine that nanoparticles do not homogenize quickly.

However, there is evidence that distinctly non-uniform nanoparticles exist. Many researchers and manufacturers boast of "stabilizing" metal particles with an ultrathin surface film of oxide (for examples, see Lowe, 2002; Kodas and Hampden-Smith, 1999; Hofmeister and Ködderitzsch, 1999). Therefore, although diffusion does not limit homogenization caused by concentration gradients, the change from a metastable metallic state is limited by slow oxidation rates at room temperature.

It has been suggested (Jayaganthan, 2002; Vallee, 2001) that surface segregation may occur more strongly in nanoparticles than in bulk; manganese may be enriched on the surface of an iron oxide nanoparticle for this reason. It would be interesting to explore the differences in surface energy between different transition metal spinels. Although miscible in one another, spinel compounds with lower surface energies may enrich the surfaces of ultrafine particles. The surface energy of a material is somewhat proportional to the heat of vaporization, because both are a measure of how easily internal bonds are broken. This may be the reason that researchers have reported that nanoparticle surfaces become enriched in more volatile elements during condensation. However, such enrichment would homogenize quickly, unless the compounds also happened to be immiscible. These surface forces also may cause larger particles that coalesced or sintered from smaller dissimilar particles to form spherically symmetrical phase regions or compositional gradients from an aggregate formed from random collisions.

The final and most probable possibility for internal heterogeneity would be two distinct stable immiscible phases, such as a halide and an oxide, or sometimes two oxides. Because the halides are more volatile and have smaller values for surface tension, a halide surface formed on a particle during the condensation on the surface of a oxide nanoparticle would remain stable.

During the STEM-EDS study of the variation of elemental composition with particle size, six large (>100 nm) particles were examined to determine whether internal

heterogeneity could be detected and quantified. The spot of the electron beam was focused on several points in a straight line along the diameter of a particle.
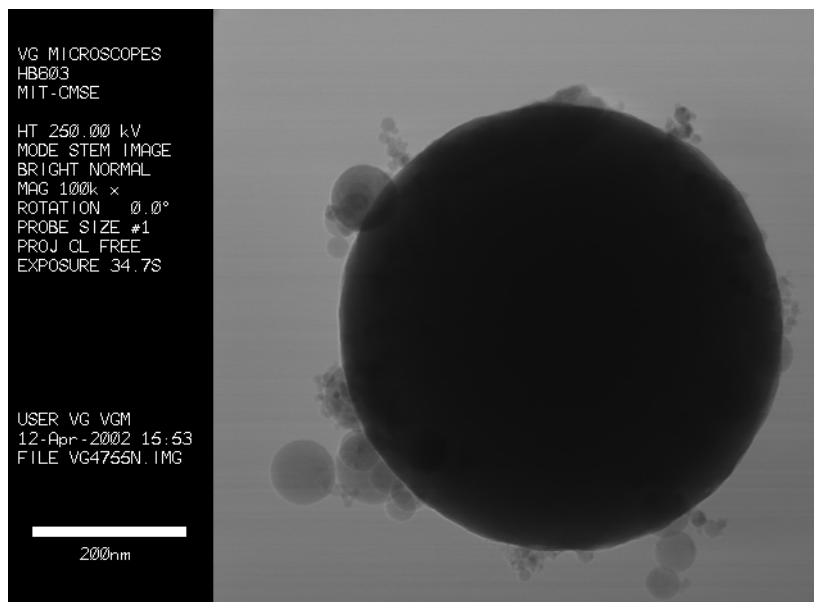
Figure 5.31 Large mild steel flux cored arc welding fume particle.
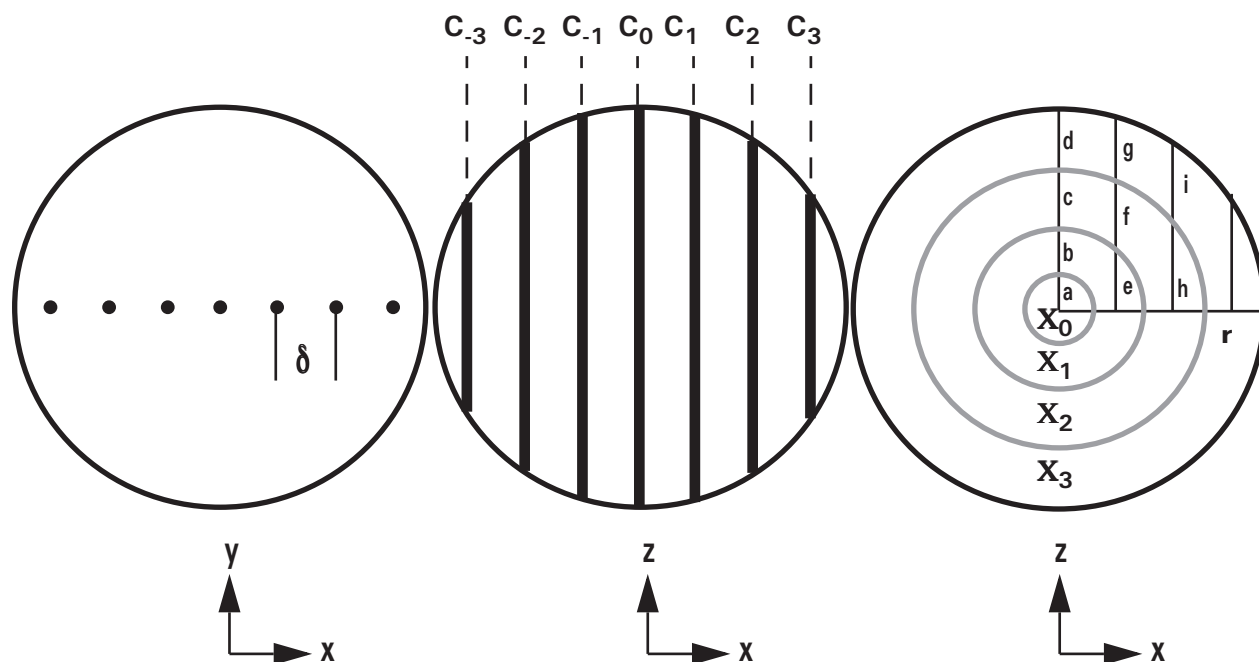
Figure 5.32 Transformation of data from spot elemental analysis of particle with transmission electron microscopy. Electron beam interaction with particle is approximated such that only the cylindrical cross-section at each spot is considered.

Because the electrons transmit through the entire particle, the average elemental concentration of the entire cross-section was measured at each spot, as illustrated in Figure 5.32, assuming that the electron beam (which is approximately 5 nm in diameter) does not broaden significantly as it passes through the particle.

Beam broadening is caused when electrons are scattered by elastic collisions with the material through which they transmit. Realistically, each spot's cross-section would resemble a cone, but a cylinder is an acceptable approximation in thin specimens. The thicker the TEM specimen, the greater the broadening. In a copper particle 10 nm in diameter, the beam broadens to be about 7 nm when it exits the particle; in a 300 nm copper particle, it spreads to about 100 nm. Beam broadening increases with increasing atomic number, so the lighter the element, the smaller the spread of the beam. Copper was the heaviest element found in significant quantities in the fume studied; however, because the fume consisted of oxides and fluorides, it was assumed that beam broadening for fume particles was much less than that of metallic copper. For example, the maximum width of the beam transmitted through a 100 nm thick film of MgO has been calculated to be 8.4 nm. Because the fume particles are 150 to 1000 nm in size and because the distance (δ) between spot measurements (resolution) was never less than 20 nm, it can be assumed that beam broadening did not significantly affect this analysis (Vander Sande & Hall, 1979; Hall, et al., 1981).

In any case, the measurements from each spot are not entirely indicative of the compositional variation throughout the particle; the composition measured at the middle would contain information about the whole particle, whereas the composition measured near the edge would be that of the surface. The data gathered were used to calculate an approximation of the radial variation in composition. This was done by graphically dividing the particle into spherical layers as thick as the regular distance (δ) between measurements. The composition (C_{+3}) measured nearest to the edge was assumed equivalent to the composition (X_{+3}) of the outermost layer. The next measured value(s) were set equal to an average of the compositions of the outermost layer and the next interior layer(s), weighted by the fraction in the respective layer of the line of measured composition. See Equations 5.5 to 5.8.

$$C_0 = \frac{1}{a + b + c + d}(a\chi_0 + b\chi_1 + c\chi_2 + d\chi_3) \qquad 5.5$$

$$C_1 = \frac{1}{e + f + g}(e\chi_1 + f\chi_2 + g\chi_3) \qquad 5.6$$

$$C_2 = \frac{1}{h + i}(h\chi_2 + i\chi_3) \qquad 5.7$$

$$C_3 = \chi_3 \qquad 5.8$$

a … i can be determined from the radius, r, and the measurement interval, δ.

Other more accurate methods, such as Abel inversion, exist to convert measurements of 2-D projections into 3-D coordinates. Since there were only a few data points, the approach used here was deemed sufficient.

Based on these calculations, approximate values for the composition (X) of each layer were determined. These can be found from Figure 5.33 to Figure 5.36 and
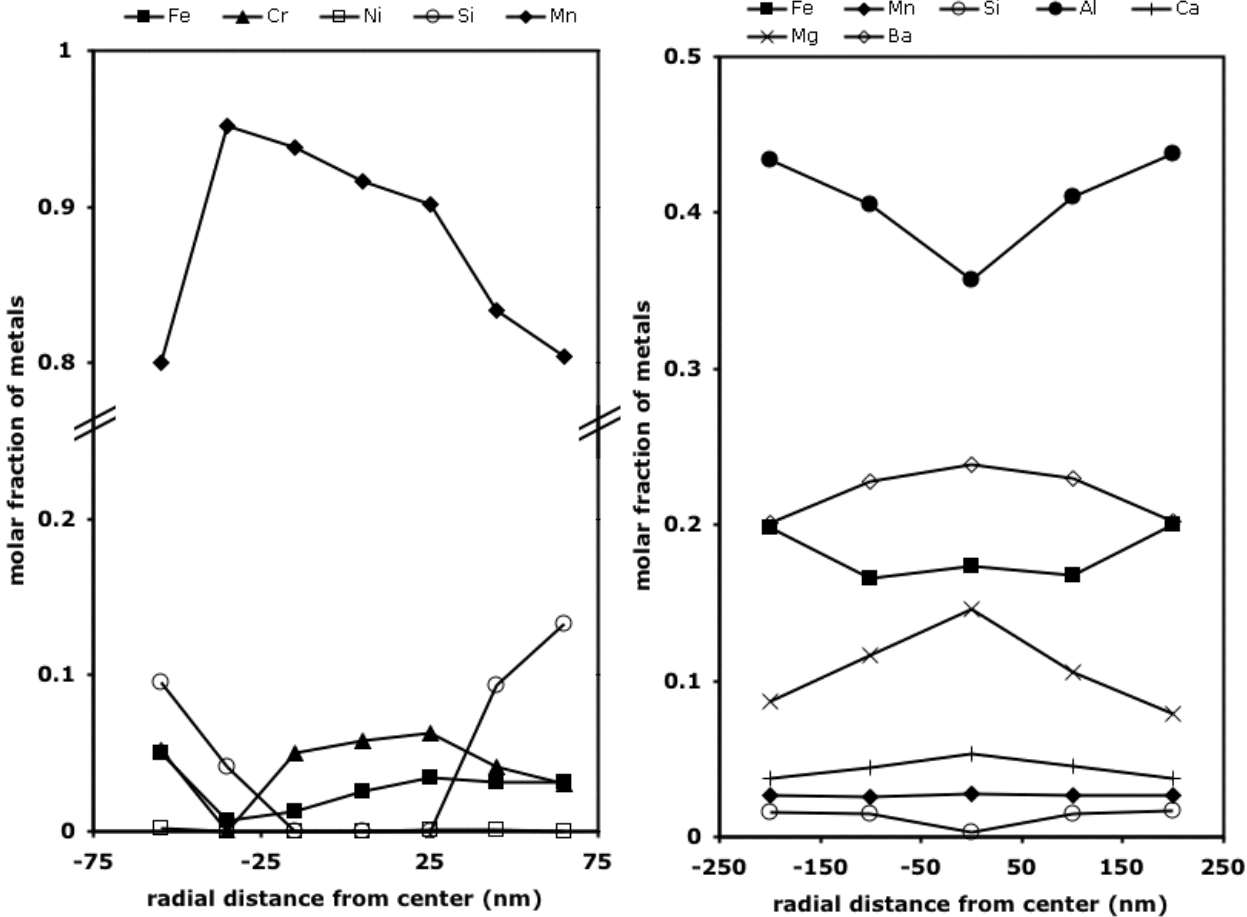
Figure 5.33 (Left) Composition profile of 175 nm stainless steel gas metal arc welding fume particle (scanning transmission electron microscopy / energy dispersive spectrometry)
Figure 5.34 (Right) Composition profile of 500 nm mild steel flux-cored arc welding fume particle (scanning transmission electron microscopy / energy dispersive spectrometry)

from Table 5.14 to Table 5.19. It is promising that symmetrical data was found from measurements of opposites sides of the particles, indicating the reliability of the data transformation.

Two of the mild steel FCAW fume particles (120 nm and 140 nm in diameter) did not appear to have any significant variation of composition across the particle. One was almost pure iron oxide, the other aluminum oxide. These two particles are typical of the phase separation between particles shown in the mild steel FCAW system earlier.
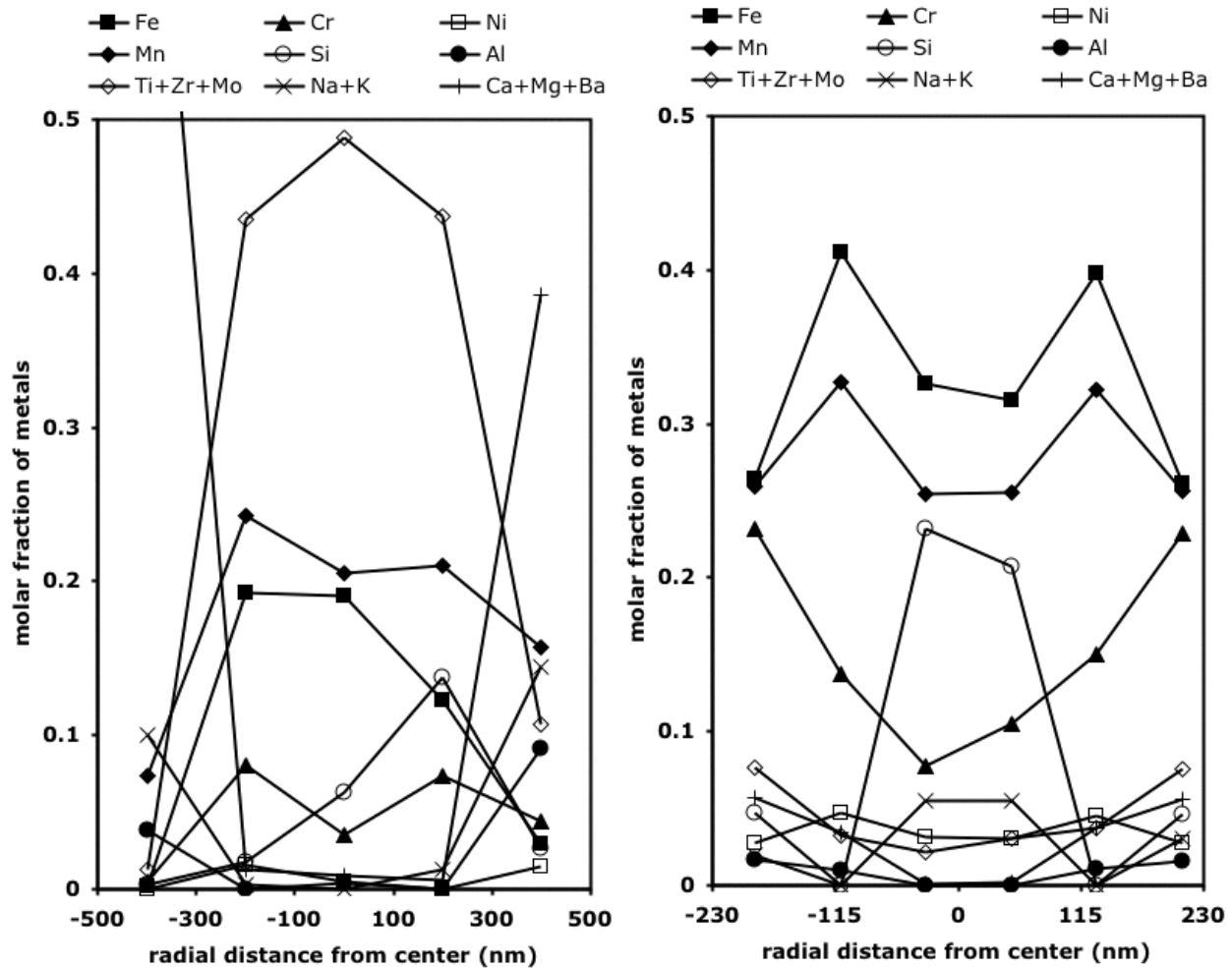
Figure 5.35 (Left) Composition profile of 1000 nm stainless steel flux-cored arc welding fume particle (scanning transmission electron microscopy / energy dispersive spectrometry)
Figure 5.36 (Right) Composition profile of 460 nm stainless steel flux-cored arc welding fume particle (scanning transmission electron microscopy / energy dispersive spectrometry)

However, another mild steel FCAW particle (Figure 5.34) composed mostly of aluminum seems to have a core enriched in alkaline earth metals. The surface of the stainless steel GMAW fume particle (Figure 5.33) appears to have more silicon. One stainless steel FCAW fume particle (Figure 5.35) most likely has a halide surface layer, whereas another FCAW fume particle (Figure 5.36) apparently has more chromium on the surface than in the center where it is silicon-rich.

This agrees with the findings of Minni, et al., (1984) who also found a silicate layer on GMAW fume particles. SMAW fume particles had fluoride surfaces with spinel cores. They also found that chromium enriched the surface as a hexavalent compound (K_2CrO_4) in stainless steel SMAW fume. Voitkevich (1988) observed that the core of a welding fume particle contained Fe and Mn oxides, (with some calcium fluoride if present), and that the surface consisted of layers of alkali metal (with some manganese) silicates and fluorides. This phase segregation will be assisted by the

core-shell growth mechanism described earlier. For example, silicon monoxide is more volatile than iron (or iron oxide), so it would be present strongly in the outer shell of a mild steel GMAW fume particle. A particle with a silica-rich surface would fail to homogenize because of immiscibility of silica and iron oxide.

It should be noted that, because they are larger than 100 nm, these particles were likely formed through the collision of smaller particles. This explains why Figure 5.35 shows a peak in silicon that is asymmetric; that region may have been a separate silicon-rich particle at one time. This phenomenon may have caused some of the compositional variation throughout the particles, and would be maintained by the immiscibility of some phases.

From this analysis, it can be seen that nanoparticles are not necessarily uniform internally. This is important for inhalation toxicology, because the biological reaction to particles may depend on the surface chemistry of the inhaled particles. It is difficult to create a simple theory for general behavior, (e.g., the radial function of composition is dependent on elemental volatility or surface energy), because the compositional gradients seem more complex than what a simple theory would explain. Instead, one would have to analyze the complex phase equilibrium of mixtures of 4 or more elements in order to predict the composition of welding fume particles. Luckily, similar analyses already exist for metallurgical slag systems, but such will not be discussed here. The most important point of this section is that chemical variation throughout a nanoparticle is caused by solid state phase separation.

For internal particle composition, it is therefore more important to determine which elements are present in the system, than it is to determine the order in which the elements condense. The following section on vapor composition addresses this issue.

Table 5.14 Composition measurements (scanning transmission electron microscopy / energy dispersive spectrometry) along a diameter of a 150 nanometer stainless steel gas metal arc welding fume particle

distance from center (nm)	-55	-35	-15	5	25	45	65	entire particle
Fe	0.050	0.032	0.035	0.031	0.033	0.032	0.032	0.036
Cr	0.053	0.029	0.046	0.042	0.044	0.036	0.031	0.041
Ni	0.002	0.000	0.001	0.000	0.001	0.001	0.000	0.001
Mn	0.800	0.867	0.891	0.851	0.848	0.820	0.805	0.852
Si	0.095	0.072	0.028	0.076	0.075	0.112	0.133	0.070
transformed data that better reflects dependence on radius as opposed to cross-section								
Fe	0.050	0.007	0.012	0.026	0.034	0.032	0.032	0.036
Cr	0.053	0.000	0.050	0.058	0.063	0.041	0.031	0.041
Ni	0.002	0.000	0.000	0.000	0.001	0.001	0.000	0.001
Mn	0.800	0.952	0.938	0.916	0.902	0.833	0.805	0.852
Si	0.095	0.041	0.000	0.000	0.000	0.093	0.133	0.070

Table 5.15 Composition measurements (scanning transmission electron microscopy / energy dispersive spectrometry) along a diameter of a 120 nanometer mild steel flux cored arc welding fume particle

distance from center (nm)	-40	-20	0	20	40
Fe	0.921	0.933	0.930	0.982	0.860
Mn	0.017	0.013	0.020	0.016	0.014
Si	0.055	0.050	0.042	0.000	0.088
Al	0.000	0.003	0.004	0.000	0.034
Ca	0.001	0.000	0.001	0.001	0.000
Ba	0.001	0.000	0.000	0.000	0.000
Mg	0.006	0.001	0.003	0.001	0.004
transformed data that better reflects dependence on radius as opposed to cross-section					
Fe	0.921	0.926	0.918	0.928	0.860
Mn	0.017	0.015	0.016	0.015	0.014
Si	0.055	0.053	0.059	0.050	0.088
Al	0.000	0.001	0.002	0.003	0.034
Ca	0.001	0.000	0.000	0.000	0.000
Ba	0.001	0.000	0.000	0.000	0.000
Mg	0.006	0.004	0.004	0.003	0.004

Table 5.16 Composition measurements (scanning transmission electron microscopy / energy dispersive spectrometry) along a diameter of a 140 nanometer mild steel flux cored arc welding fume particle.

distance from center (nm)	-50	-30	-10	10	30	50
Fe	0.000	0.000	0.001	0.000	0.001	0.001
Mn	0.000	0.000	0.000	0.000	0.000	0.000
Si	0.015	0.018	0.023	0.019	0.016	0.018
Al	0.981	0.978	0.975	0.978	0.979	0.979
Ca	0.002	0.001	0.000	0.001	0.001	0.001
Ba	0.001	0.001	0.002	0.001	0.001	0.001
Mg	0.001	0.000	0.000	0.000	0.002	0.000
transformed data that better reflects dependence on radius as opposed to cross-section						
Fe	0.000	0.001	0.002	0.000	0.001	0.001
Mn	0.000	0.001	0.000	0.001	0.001	0.000
Si	0.015	0.024	0.042	0.025	0.014	0.018
Al	0.981	0.974	0.954	0.972	0.979	0.979
Ca	0.002	0.000	0.000	0.002	0.002	0.001
Ba	0.001	0.001	0.002	0.001	0.001	0.001
Mg	0.001	0.000	0.000	0.000	0.004	0.000

Table 5.17 Composition measurements (scanning transmission electron microscopy / energy dispersive spectrometry) along a diameter of a 500 nanometer mild steel flux cored arc welding fume particle

distance from center (nm)	-200	-100	0	100	200	entire particle
Fe	0.198	0.182	0.187	0.194	0.164	0.189
Mn	0.027	0.026	0.027	0.027	0.024	0.024
Si	0.016	0.016	0.013	0.013	0.016	0.013
Al	0.434	0.420	0.415	0.411	0.474	0.446
Ca	0.037	0.041	0.042	0.043	0.039	0.039
Ba	0.201	0.214	0.215	0.221	0.205	0.180
Mg	0.087	0.101	0.101	0.091	0.079	0.109
transformed data that better reflects dependence on radius as opposed to cross-section						
Fe	0.198	0.165	0.173	0.167	0.200	0.189
Mn	0.026	0.026	0.028	0.026	0.027	0.024
Si	0.016	0.015	0.003	0.015	0.016	0.013
Al	0.434	0.405	0.357	0.410	0.438	0.446
Ca	0.037	0.044	0.053	0.045	0.037	0.039
Ba	0.201	0.227	0.239	0.230	0.203	0.180
Mg	0.087	0.117	0.146	0.106	0.079	0.109

Table 5.18 Composition measurements (STEM-EDS) along a diameter of a 1000 nm stainless steel FCAW fume particle

distance from center (nm)	-400	-200	0	200	400	entire particle
Fe	0.002	0.159	0.148	0.089	0.029	0.134
Cr	0.005	0.069	0.055	0.067	0.044	0.059
Ni	0.000	0.013	0.008	0.002	0.015	0.009
Mn	0.074	0.237	0.236	0.208	0.157	0.216
Si	0.003	0.016	0.061	0.097	0.027	0.055
Al	0.039	0.012	0.024	0.022	0.092	0.025
Ti	0.009	0.342	0.373	0.301	0.092	0.344
Zr	0.003	0.021	0.024	0.017	0.013	0.024
Mo	0.000	0.001	0.000	0.001	0.002	0.001
K	0.063	0.035	0.023	0.060	0.111	0.053
Na	0.038	0.015	0.005	0.022	0.033	0.024
Ca	0.762	0.070	0.032	0.106	0.375	0.049
Ba	0.001	0.011	0.010	0.008	0.009	0.008
Mg	0.002	0.000	0.000	0.000	0.001	0.000
transformed data that better reflects dependence on radius as opposed to cross-section						
Fe	0.002	0.193	0.190	0.123	0.029	0.134
Cr	0.005	0.081	0.035	0.073	0.044	0.059
Ni	0.000	0.016	0.005	0.000	0.015	0.009
Mn	0.074	0.242	0.205	0.210	0.157	0.216
Si	0.003	0.017	0.063	0.138	0.027	0.055
Al	0.039	0.000	0.004	0.000	0.092	0.025
Ti	0.009	0.411	0.461	0.420	0.092	0.344
Zr	0.003	0.023	0.027	0.017	0.013	0.024
Mo	0.000	0.000	0.000	0.000	0.002	0.001
K	0.063	0.003	0.000	0.005	0.111	0.053
Na	0.038	0.000	0.000	0.008	0.033	0.024
Ca	0.762	0.000	0.000	0.000	0.375	0.049
Ba	0.001	0.013	0.009	0.005	0.009	0.008
Mg	0.002	0.000	0.000	0.000	0.001	0.000

Table 5.19 Composition measurements (STEM-EDS) along a diameter of a 460 nm stainless steel FCAW fume particle

distance from center (nm)	-190	-110	-30	50	130	210	entire particle
Fe	0.265	0.343	0.322	0.294	0.317	0.244	0.280
Cr	0.232	0.185	0.175	0.190	0.201	0.228	0.181
Ni	0.028	0.038	0.034	0.031	0.035	0.026	0.030
Mn	0.260	0.297	0.281	0.282	0.295	0.266	0.258
Si	0.047	0.019	0.096	0.054	0.047	0.105	0.049
Al	0.016	0.013	0.008	0.010	0.023	0.010	0.016
Ti	0.070	0.051	0.050	0.043	0.046	0.057	0.048
Zr	0.006	0.002	0.002	0.002	0.001	0.004	0.002
Mo	0.001	0.001	0.001	0.000	0.000	0.001	0.000
K	0.013	0.004	0.020	0.026	0.024	0.029	0.044
Na	0.006	0.003	0.007	0.013	0.007	0.018	0.028
Ca	0.052	0.043	0.002	0.053	0.002	0.009	0.061
Ba	0.003	0.002	0.002	0.002	0.002	0.003	0.002
Mg	0.002	0.001	0.000	0.000	0.001	0.000	0.000
transformed data that better reflects dependence on radius as opposed to cross-section							
Fe	0.265	0.412	0.326	0.315	0.397	0.262	0.280
Cr	0.232	0.137	0.078	0.105	0.150	0.229	0.181
Ni	0.028	0.047	0.031	0.030	0.045	0.027	0.030
Mn	0.260	0.328	0.255	0.256	0.322	0.257	0.258
Si	0.047	0.000	0.231	0.207	0.000	0.046	0.049
Al	0.016	0.010	0.000	0.000	0.011	0.016	0.016
Ti	0.070	0.032	0.022	0.031	0.037	0.069	0.048
Zr	0.006	0.000	0.000	0.000	0.000	0.006	0.002
Mo	0.001	0.000	0.000	0.000	0.000	0.001	0.000
K	0.013	0.000	0.043	0.040	0.000	0.013	0.044
Na	0.006	0.000	0.012	0.015	0.000	0.018	0.028
Ca	0.052	0.032	0.000	0.000	0.035	0.052	0.061
Ba	0.003	0.002	0.001	0.002	0.002	0.003	0.002
Mg	0.002	0.000	0.000	0.000	0.000	0.002	0.000

References

Ehrman, S. H., Friedlander, S. K., & Zachariah, M. R. (1999). Phase segregation in binary SiO_2/TiO_2 and SiO_2/Fe_2O_3 nanoparticle aerosols formed in a premixed flame. *Journal of Materials Research,* 14(12), 4551–4561.

Grekula, A., Ristolainen, E., Tanninen, V. P., Hyvarinen, H. K., & Kalliomaki, P. L. (1986). Surface and bulk chemical analysis on metal aerosols generated by manual metal arc welding of stainless steel. *Journal of Aerosol Science,* 17, 1–9.

Hall, E. L., Imeson, D., & Vander Sande, J. B. (1981). On producing high-spatial-resolution composition profiles via scanning transmission electron microscopy. Philosophical Magazine, 43(6), 1569–1585.

Hofmeister, H., & Ködderitzsch, P. (1999). Nanosized silicon particles by inert gas arc evaporation. *NanoStructured Materials,* 12, 203–206.

Hong, J.- O., & Yoo, H.- I. (2002). Cross effect between ion and electron flows in Fe_3O_4. *Journal of Materials Research,* 17(5), 1213–1219.

Jayaganthan, R., & Chow, G. M. (2002). Thermodynamics of surface compositional segregation in Ni/Co nanoparticles. *Materials Science and Engineering,* B95, 116–123.

Jenkins, N. T., & Eagar, T.W. The stability of hexavalent chromium in submicron particles. In preparation.

Kodas, T. T., & Hampden-Smith, M. J. (1999). *Aerosol Processing of Materials*. New York: Wiley-VCH.

Lowe, T. (2002). The revolution in nanometals. *Advanced Materials & Processes*, 63–66.

McAllister, T., & Bosworth, M. (1999). Thermal mechanisms for the production of Cr(VI) [hexavalent chromium] in welding fume [in arc welding of stainless steels]. *Australasian Welding Journal,* 44(First Quarter), 42–46.

Michaud, D., Baril, M., & Perrault, G. (1993). Characterization of airborne dust from cast-iron foundries by physicochemical methods and multivariate statistical-analyses. *Journal of the Air & Waste Management Association,* 43(5), 729–735.

Minni, E., Gustafsson, T. E., Koponen, M., & Kalliomaki, P.-L. (1984). A study of the chemical structure of particles in the welding fumes of mild and stainless steel. *Journal of Aerosol Science,* 15(1), 57–68.

Minni, E., Hofmann, S., & Sivonen, S. J. (1990). An AES study of particles in the welding fumes of mild and stainless steel. *Surface and Interface Analysis,* 16(1–12), 563–564.

Ohring, M. (1992). *The Materials Science of Thin Films*. San Diego: Academic Press.

Perrault, G., Dion, C., Ostiguy, C., Michaud, D., & Baril, M. (1992). Selective sampling and chemical speciation of airborne dust in ferrous foundries. *American Industrial Hygiene Association Journal,* 53(7), 463–470.

Pilyankevich, A. N., & Im, N. (1984). Electron microscopic examination of the solid phase of the fumes formed in electric arc welding. *Welding Production,* 31(3), 46–47.

Tandon, R. K., Payling, R., Chenhall, B. E., Crisp, P. T., Ellis, J., & Baker, R. S. (1985). Application of x-ray photoelectron spectroscopy to the analysis of stainless-steel welding aerosols. *Applications of Surface Science,* 20(4), 527–537.

Vallee, R., Wautelet, M., Dauchot, J. P., & Hecq, M. (2001). Size and segregation effects on the phase diagrams of nanoparticles of binary systems. *Nanotechnology,* 12(1), 68–74.

Van Craen, M., Denoyer, E. A., Natusch, D. F. S., & Adams, F. (1983). Surface enrichment of trace metals in electric steel furnace dust. *Environmental Science and Technology,* 17, 435.

Van Craen, M., Natusch, D. F. S., & Adams, F. (1982). Quantitative surface analysis of steel furnace dust particles by secondary ion mass spectrometry. *Analytical Chemistry,* 54(11), 1786–1792.

Vander Sande, J. B., & Hall, E. L. (1979). Applications of dedicated scanning transmission electron microscopy to nonmetallic materials. *Journal of the American Ceramic Society*, 62, 246–254.

Voitkevich, V. (1995). *Welding Fumes: Formation, Properties and Biological Effects*. Cambridge, England: Abington Publishing.

Voitkevich, V. G. (1988). Etude, par spectroscopie photoelectronique a rayons X, de l'heterogeneite de la composition des particules de fumees de soudage [Investigation of heterogeneity of welding fume particle composition by the method of X-ray photoelectron spectroscopy]. *Welding in the World, Le Soudage Dans Le Monde,* 26, 108–111.

5.2.3 Vaporization

Many researchers have measured welding fume chemistry by many methods (see Chapter 2), but only a few have tried to predict the chemistry of the original vapor from thermodynamic equilibrium calculations. Doing so has been problematic, primarily because of the incomplete assumptions about temperature, which determines a thermodynamic equilibrium. It is clear that the temperature of the evaporating material will control the composition of the vapor (Khan & DebRoy, 1984).

Measuring the temperature of material while welding is extremely difficult. The transitory nature and extreme heat makes it hard to use thermocouples and calorimetric methods are difficult to set up *in situ*. Pyrometric techniques are nearly impossible because the intense radiation from the arc overwhelms detection of the infrared emissions of heated surfaces. Therefore many welding researchers rely on calculations of the weld metal temperatures.

The weld pool temperature is relatively simple to calculate. This has been performed several times, notably by Block-Bolten & Eagar (1984) who found that a natural upper limit to the pool temperature exists because of evaporative heat losses. For consumable electrodes in GMAW, the temperature of the welding droplet is more complicated to determine, because of an input of higher energy density, because of a more transitory nature (droplet detachment), and because measurements with which to compare the calculations are hard to obtain. Generally, values reported for the bulk temperature of the electrode are similar to those given by Levchenko (1996): 2400 K for the cathode, 2600 K for the anode and 2860–2970K for the droplet.

It should be noted that for GMAW, total vaporization is dominated by evaporation from the electrode rather than from the weld pool. Heile & Hill (1975) and Sreekanthan (1997) both compared the composition of fume collected while GMA welding with an electrode of a different composition than that of the base plate and both found that the fume composition was dominated by the electrode. A similar study of hexavalent chromium was performed. GMAW fume was collected while welding under spray conditions with E308L stainless steel welding wire on mild steel pipe and on stainless steel pipe at 31V, 175A with a $2\%O_2$-Ar shielding gas. ER70S-6 mild steel wire, which does not contain chromium, was used to weld at 33 V, 215A on a 304 stainless steel plate, also with spray transfer and with the same shielding gas. Fume was collected at 2.25 L/min for 30 seconds. The concentration of hexavalent chromium in fume created from the mild steel electrode was < 0.001 wt%. For the stainless steel electrode, it was 0.1 wt%, regardless of which base plate was used. Because mild steel does not contain chromium, the source of the hexavalent chromium in the fume must have been the electrode. From all of these findings, it is clear that GMAW fume composition is dominated by vaporization from the electrode, not from the weld pool. The reason for this is because the weld pool is much cooler than the electrode.

Fume researchers have simply assumed a single value for the GMAW droplet temperature to use in their thermodynamic calculations. Gray, et al., (1980) and Podgaetskii et al., (1989) reported thermodynamic equilibrium without explicitly stating

the temperature they used. Hewitt & Hirst (1991) considered fluxes in their calculations and Buki & Feldman (1980) included oxides, but they too did not report the temperature. McAllister & Bosworth (1999) assumed droplet temperatures were 1800–2200 K and were the first to include the effect of various shielding gases. Eagar, et al. (1998) calculated gaseous equilibria for hexavalent chromium using varied shielding gases, at 2673 K.

None of these researchers considered the change in temperature with time or how it changes with welding parameters. They also equated the surface temperature, which determines the composition of the evolved vapor and the fume formation rate, to the average temperature across the entire electrode droplet. This has led some to make incorrect assumptions. For example, it has been found that GMAW fume created during globular transfer has less volatile metals than fume created during spray transfer. This led Gray, et al., (1980) to propose the existence of fume that did not form from vapor, as discussed previously in section about coarse particles. They claimed that globular fume had a greater portion of coarse "unfractionated" particles and because of this, had a composition closer to the original electrode composition. They did not consider that the surface temperature of the welding droplet during globular transfer was substantially different from that of a droplet during spray transfer (Ma & Apps, 1982).

Haidar (1998; 1998; 1999), using a Cray supercomputer, performed a complete fundamental calculation of electrode droplet temperature and how it changes with time and welding parameters. The use of a supercomputer is not necessary if the droplet size is measured and a semi-empirical model created, like those in papers by Mendez, et al., (2000) and Bosworth & Deam (2000). A summary of such models can be found in Figure 5.37.

Smaller droplets, such as those formed during spray or pulsed transfer, have cooler surface temperatures than do larger droplets, like those from globular transfer, because there is a smaller barrier to heat transfer from the arc spot to the liquid-solid interface of the electrode. (However, smaller droplets may have greater average temperatures.) Therefore vapor of a composition enriched in the more volatile elements is evolved and further, less vapor forms. This can be observed in the change in fume composition with welding parameters, such as shielding gas oxidation potential (Figure 5.38 to Figure 5.41; Table 5.20) or current (Figure 5.42). Both of these welding parameters change the size of the welding droplet and therefore its vaporization rate. Conditions that create fume containing the greatest fractions of volatile metals (e.g., manganese) are the same that create the smallest electrode droplet. Such conditions also minimize total fume formation. Thus, efforts to decrease fume formation rates may also increase the fraction of manganese in the fume. Manganese emission rates may therefore not change significantly.
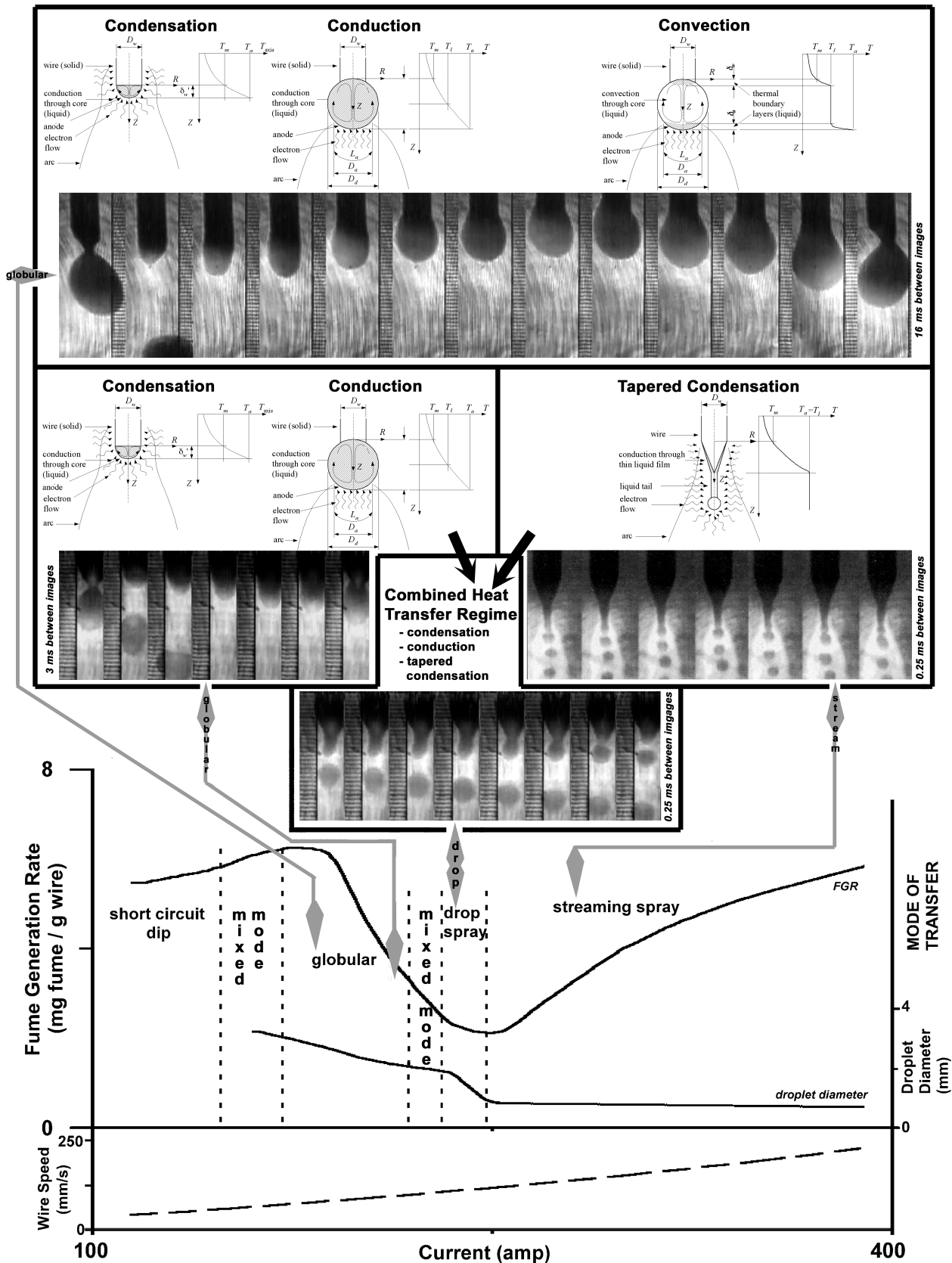
Figure 5.37 Heat transfer through GMAW electrodes is controlled by electrode droplet size. Shadowgraphs of are 2%O_2-Ar shielded GMAW mild steel electrode. See Mendez, et al., 2000 and Jones et al., 1998.
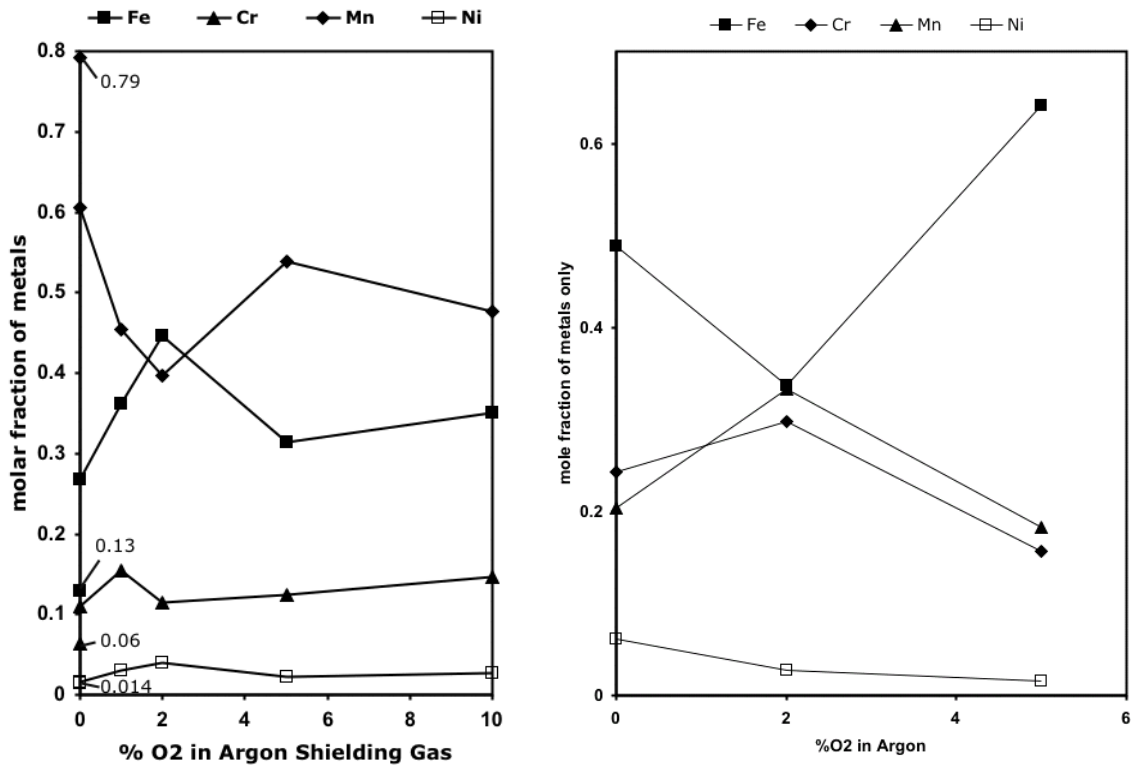
Figure 5.38 (Left) Effect of oxidation potential of shielding gas on bulk composition (ICPMS) of fume formed from single-pulse gas metal arc welding without droplet detachment (100 amps for 500 ms)

At 0% O$_2$, the composition of GTAW welding fume is also plotted with values. (Note: Silicon is likely present, but not included, so data of smaller magnitude, like that of nickel, may have significant error)

Figure 5.39 (Right) Fume composition versus oxidation potential of shielding gas in argon-shielded GMAW with 1.2 mm E308 stainless electrode (Sreekanthan, 1997).

Table 5.20 Effect of oxidation potential of shielding gas on bulk composition of fume formed from single-pulse gas metal arc welding (100 amps for 500 ms) of E308L wire without droplet detachment, reported as molar fraction of metals only as determined by ICPMS.

Note: Silicon is likely present, but not included, so data of smaller magnitude, like that of nickel, may have significant error

Atomic Fraction	0% O$_2$	1% O$_2$	2% O$_2$	5% O$_2$	10% O$_2$	Electrode
Fe	0.268	0.362	0.446	0.314	0.351	0.659
Cr	0.110	0.155	0.116	0.124	0.146	0.220
Mn	0.605	0.453	0.398	0.540	0.476	0.018
Ni	0.017	0.030	0.040	0.022	0.027	0.091

156
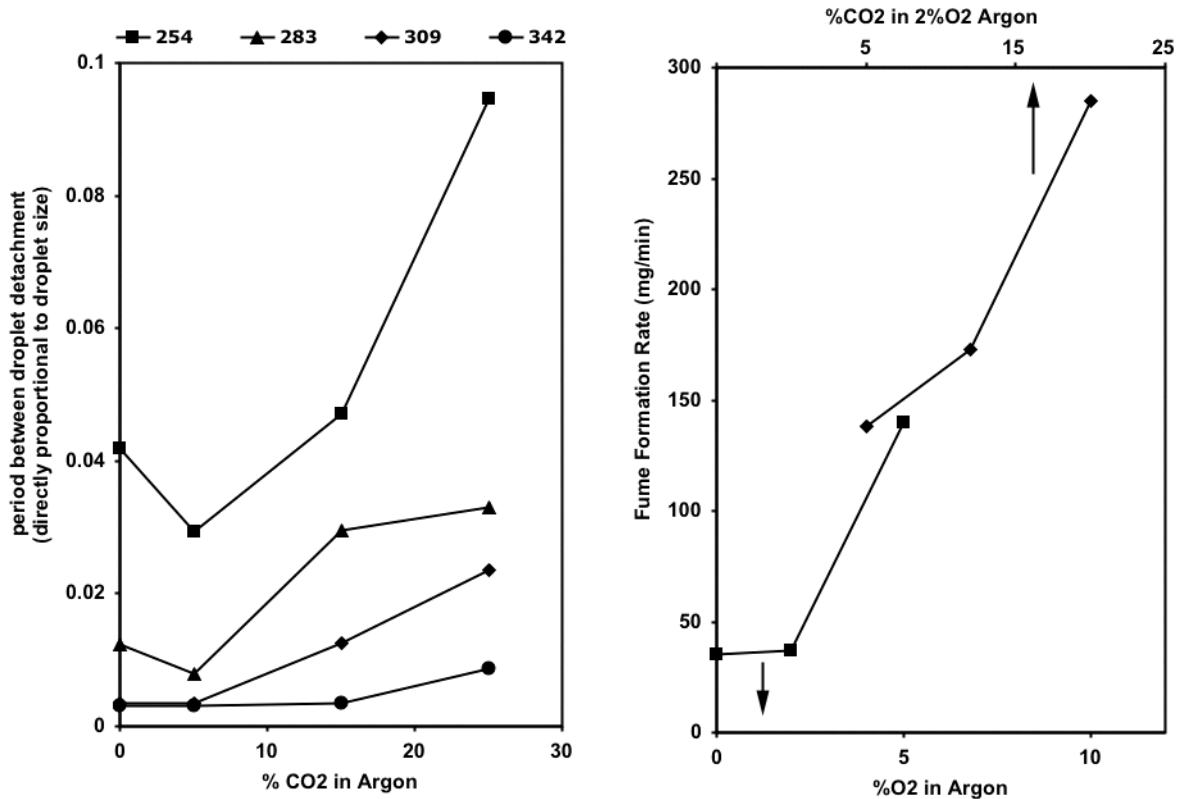
Figure 5.40 (Left) Electrode droplet period (which is directly proportional to droplet size) versus shielding gas composition in GMAW with1.6 mm mild steel electrode for various currents. Data from Rhee (1992).

Figure 5.41 (Right) Fume formation rate dependence on shielding gas in GMAW with1.2 mm mild steel electrodes using a current of 250 amperes. Data from Heile and Hill (1975) and Hilton and Plumridge (1991).

Based on an energy balance of a GMAW electrode, the surface temperature of the electrode droplet may exceed the boiling point (Mendez, et al., 2000). Haidar (1998) also calculated the surface temperature of a mild steel 1.2 mm GMAW electrode at 183A and compared it with the value measured pyrometrically by Villeminot (1967) at 160A. Both found that the surface temperature at the tip of the electrode droplet was 3115K. This is very close to, if not above, the boiling point of pure iron (e.g., 3025K according to Haidar, 3273K by Strem Chemicals, (1999), 3121K according to Sundman (1991)); it is definitely above the vapor-liquid transition for a typical iron alloy used in welding.

Like other phase changes, boiling generally occurs through heterogeneous nucleation. Bubbles form in crevices of the container that holds the liquid. Because heat is added at the solid-liquid interface and lost at the gas-liquid interface, superheating depends on crevice size where vapor bubbles heterogeneously nucleate (Hewitt, et al., 1982).

When energy is added by radiation, like in welding arcs or in laser or electron beams, the heat input is at the gas-liquid interface. The solid-liquid interface is
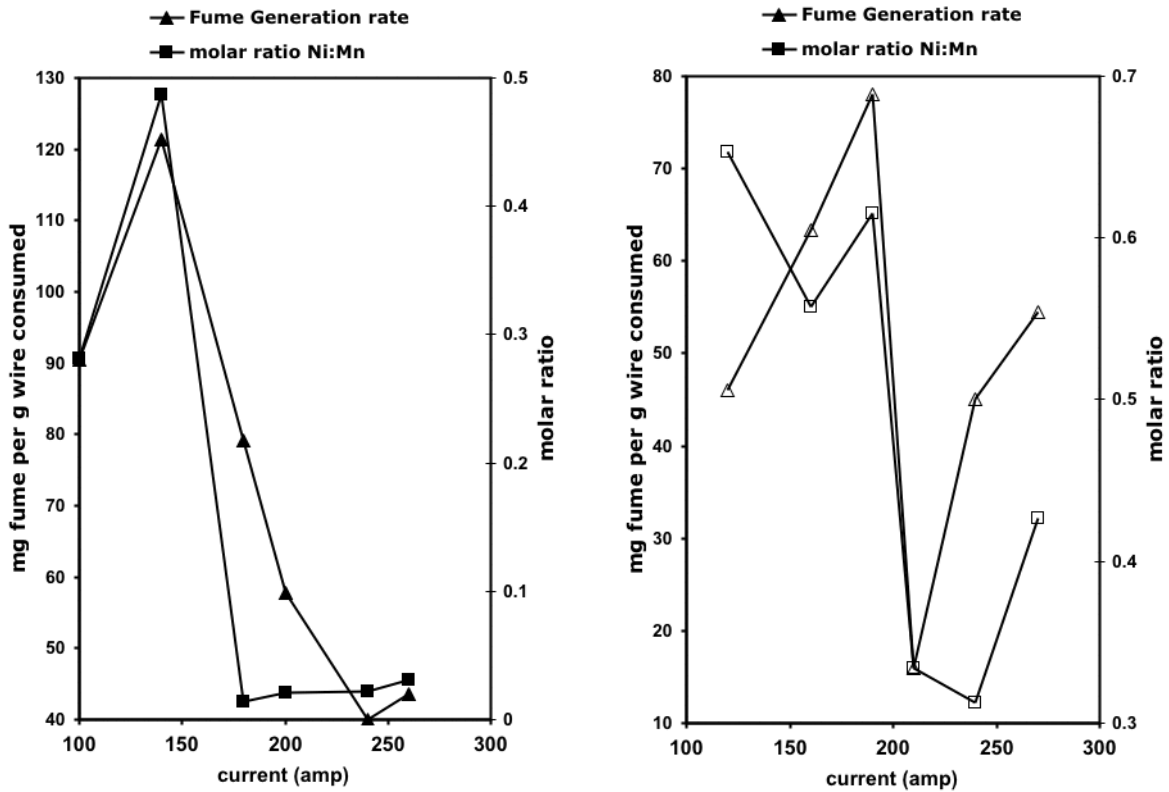
Figure 5.42 Fume generation rate and the nickel to manganese ratio both vary in the same way with current for argon shielded GMAW with two 1.2 mm electrodes: AWS ER307 Si (left) and ER308L Si (right). This indicates that the controlling variable is the same: electrode droplet surface temperature. Data adapted from Eichhorn and Oldenburg, 1986.

where heat is lost and is therefore the coolest part of liquid, meaning that bubbles will not nucleate there. The vapor phase must form bubbles homogeneously because there are not defects, such as grain boundaries, in the liquid[1]. For bubbles to form, superheating must be present in order to overcome the activation energy required to create new surfaces. Another difficulty for forming bubbles when heat is provided through radiation is that only a slender boundary layer near the surface will be hot enough for bubbles to nucleate in it. Under globular conditions, a 1.2 mm GMAW electrode droplet will have a thermal boundary layer approximately the size of 1/3 of the droplet (Mendez, et al., 2000). If the convective core of the droplet is at the boiling point, the surface temperature of the droplet would have to be near 3300K for a bubble 100 micrometers in diameter to form, according to classic nucleation theory. The surface temperature would have to be much greater for smaller bubbles. For a good experimental study of (laser) surface heated superheats, see Craciun & Craciun (1998).

Richardson (1974) states that classical nucleation predicts homogeneous super-heats much greater than what is observed, but this is probably because the mea-

---

1. It is conceivable that solid precipitates floating in the liquid may act as nucleation centers, but this has not been reported.

surements were made in liquids heated through the solid-liquid interface where crevices caused heterogeneous nucleation.

When gas-liquid interfaces are heated, evaporative cooling normally prevents super-heating. However, with high-energy-density heat sources and where heat loss is physically limited (like in a thin welding electrode), it is possible to inject energy into the system faster than it can be removed by evaporation, as calculated by the Lang-muir equation with even the most conservative estimates. (Cobine & Berger, 1955) The Langmuir equation is a function of the surface temperature; if an energy bal-ance is to be maintained, the surface temperature must increase until the conditions for balance are met. If the surface temperature exceeds the boiling point, superheat-ing occurs.

The superheat, or amount by which the boiling point is exceeded, will determine the chemical composition of the vapor, similar to how the supercooling determines the composition of a condensate, as discussed previously. See Figure 5.43, the iron-
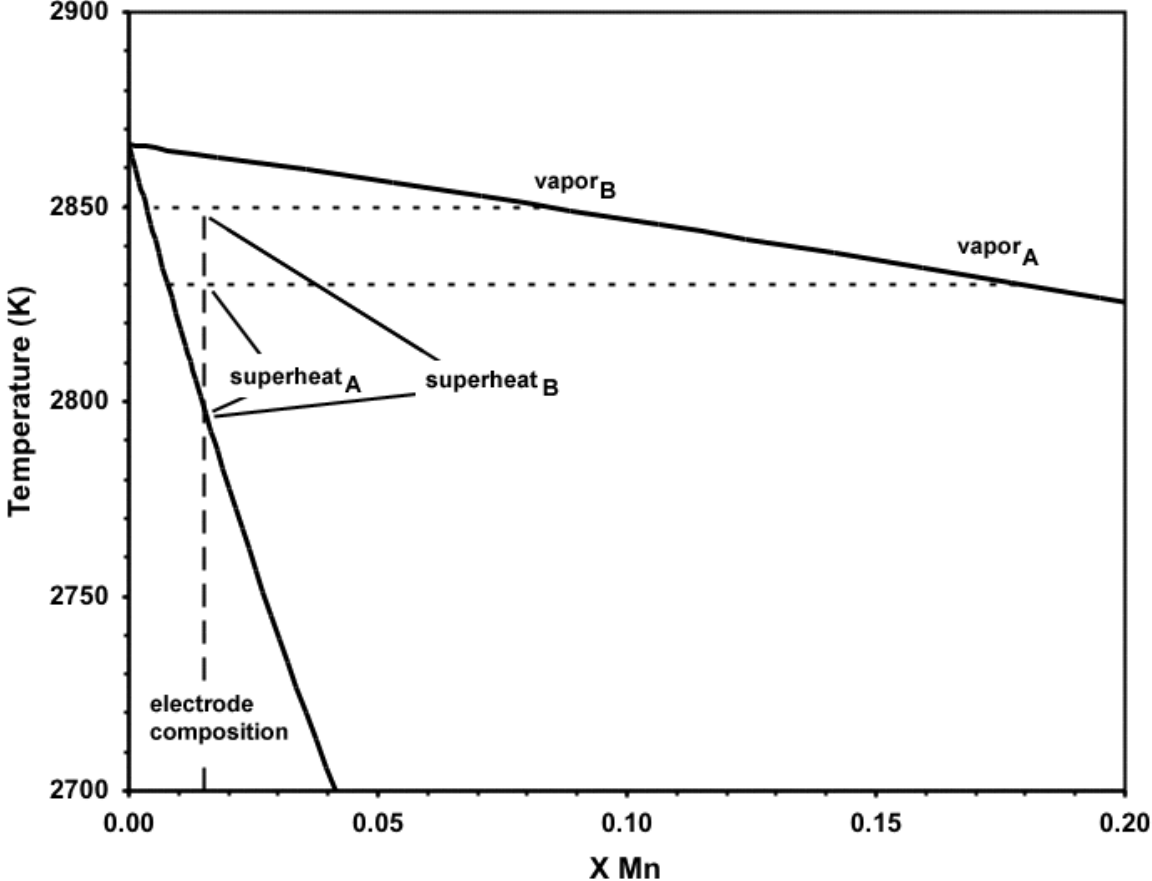
Figure 5.43 Iron-manganese vapor-liquid phase diagram at 0.3 atmosphere, adapted to show the effect of superheat on vapor composition

manganese phase diagram at 0.3 atmospheres, adapted to show the effect of superheat. One can see that even a small change in superheat will effect a large change in vapor composition, given the same initial composition of the liquid. In this

example, an increase of a mere 20K causes the vapor composition to decrease from 0.18 mole fraction of manganese to 0.08 when the liquid is initially at 0.015 mole fraction. Researchers have calculated that the vapor in a mild steel gas metal arc welding arc may be much as half manganese (Grong & Christensen, 1983).

As shown earlier, coarse particles do not make up a large enough fraction of GMAW welding fume to cause a significant change in fume chemistry. This fraction also does not change from spray transfer to globular transfer, meaning the change in composition, that other researchers (Gray, et al., 1982) have noted between the two modes is due to a change in the vapor composition, is caused by a change in surface temperature.

This is naturally a simple example of what can become complicated if one considers multicomponent alloys, the effect of halides on metal volatility (Tillman, 1994), the presence of surface active elements (Sahoo, et al., 1988) or the effect of a plasma on vaporization (Sahoo & DebRoy, 1988).

However, it illustrates how sensitive vapor composition is to temperature. As shown earlier, the bulk composition of welding fume is more or less the same as the composition of the originating vapor, especially from welding processes like GMAW that do not create significant amounts of coarse particles. Therefore, it is important to use appropriate values for the surface temperature of the liquid metal vapor source that one is trying to model.

References

Block-Bolton, A., & Eagar, T. W. (1984). Metal vaporization from weld pools. *Metallurgical Transactions B,* 15B, 461–469.

Bosworth, M. R., & Deam, R. T. (2000). Influence of GMAW droplet size on fume formation rate. *Journal of Physics D - Applied Physics,* 33(20), 2605–2610.

Buki, A. A., & Feldman, A. M. (1980). Prediction of composition of aerosol formed in welding in shielding gases. *Welding Production* 27(2), 8–12.

Cobine, J. D., & Burger, E. E. (1955). Analysis of electrode phenomena in the high-current arc. *Journal of Applied Physics,* 26(7), 895–900.

Craciun, V., & Craciun, D. (1998). Does the subsurface superheating effect really exist? *Proceedings of the Advances in Laser Ablation of Materials Symposium*, Singh, R. K., Lowndes, D. H., Chrisey, D. B., Fogarassy, E. & Narayan, J. (Eds.). Warrendale, PA: Materials Research Society.

Eagar, T. W., Sreekanthan, P., Jenkins, N. T., Murthy, G. G. K., Antonini, J. M., & Brain, J. D. (1998). Study of chromium in gas metal arc welding fume*. Proceedings of the Trends in Welding,* American Welding Society, Warrendale, PA: TMS.

Eichhorn, F., & Oldenburg, T. (1986). *Untersuchung der Scheissrauchentstehung beim Schweissen mit mittel- und hochlegierten Zusatzwerkstoffen*. Duesseldorf, BRD: DVS.

Gray, C. N., Hewitt, P. J., & Dare, P. R. M. (1982). New approach would help control welding fumes at source (MIG and MMA) part two: MIG fumes. *Welding and Metal Fabrication,* October, 393–397.

Gray, C. N., Hewitt, P. J., & Hicks, R. (1980). The prediction of fume compositions in stainless steel metal inert gas welding. *Proceedings of the Weld Pool Chemistry and Metallurgy International Conference*, Bailey, N. (Ed.). Cambridge, England: The Welding Institute, Abington Hall.

Grong, O., & Christensen, N. (1983). Factors controlling MIG weld metal chemistry. *Scandinavian Journal of Metallurgy*, 4, 155-165.

Haidar, J. (1998). A theoretical model for gas metal arc welding and gas tungsten arc welding. *Journal of Applied Physics,* 84(7), 3518–3529.

Haidar, J. (1998). Predictions of metal droplet formation in gas metal arc welding. II. *Journal of Applied Physics,* 84(7), 3530–3540.

Haidar, J. (1999). An analysis of heat transfer and fume production in gas metal arc welding. III. *Journal of Applied Physics,* 85(7), 3448–3459.

Heile, R. F., & Hill, D. C. (1975). Particulate fume generation in arc welding processes. *Welding Journal,* 54(7), 201s–210s.

Hewitt, G. F., Delhaye, J. M. & Zuber, N. (Eds.) (1982). *Multiphase Science and Technology* (Vol. 1). Washington: Hemisphere Publishing Corporation.

Hewitt, P. J., & Hirst, A. A. (1991). Development and validation of a model to predict the metallic composition of flux-cored arc-welding fumes. *Annals of Occupational Hygiene,* 35(2), 223–232.

Hilton, D. E., & Plumridge, P. N. (1991). Particulate fume generation during GMAW and GTAW. *Welding and Metal Fabrication,* December, 555–560.

Jones, L. A., Eagar, T. W., & Lang, J. H. (1998). Images of a steel electrode in Ar-2%O_2 shielding during constant current gas metal arc welding. *Welding Journal,* 77(4), 135s–141s.

Khan, P. A. A., & DebRoy, T. (1984). Alloying element vaporization and weld pool temperature during laser-welding of AISI 202 stainless-steel. *Metallurgical Transactions B - Process Metallurgy,* 15(4), 641–644.

Levchenko, O. (1996). Processes of welding fume formation (review). *Paton Welding Journal,* 8, no.4, April, 210–215.

Ma, J., & Apps, R. L. (1982). MIG transfer discovery of importance to industry. *Welding and Metal Fabrication,* September, 307–316.

McAllister, T., & Bosworth, M. (1999). Thermal mechanisms for the production of Cr(VI) [hexavalent chromium] in welding fume [in arc welding of stainless steels]. *Australasian Welding Journal,* 44(First Quarter), 42–46.

Mendez, P., Jenkins, N. T., & Eagar, T. W. (2000). Effect of electrode droplet size on evaporation and fume generation in GMAW. *Proceedings of the Gas Metal Arc Welding for the 21st Century*, Miami, Florida: American Welding Society.

Podgaetskii, V., Golovatyuk, A., & Levchenko, O. (1989). Mechanism of formation of welding aerosol and prediction of its composition in CO_2 welding. *Paton Welding Journal,* 1(8), 561–564.

Rhee, S., & Kannateyasibu, E. (1992). Observation of metal transfer during gas metal arc-welding. *Welding Journal,* 71(10), S381–S386.

Richardson, F. D. (1974). *Physical Chemistry of Melts in Metallurgy*. London: Academic Press.

Sahoo, P., Collur, M. M., & DebRoy, T. (1988). Effects of oxygen and sulfur on alloying element vaporization rates during laser-welding. *Metallurgical Transactions B - Process Metallurgy,* 19(6), 967–972.

Sahoo, P., & DebRoy, T. (1988). Effect of low-pressure argon plasma on metal vaporization rates. *Materials Letters,* 6(11–12), 406–408.

Sreekanthan, P. (1997). *Study of Chromium in Welding Fume*. M.S. Thesis: Materials Science and Engineering, Massachusetts Institute of Technology, Cambridge, Massachusetts.

Strem Chemicals, *Catalog No. 18*, Strem Chemicals, Newburyport, MA, 1999, 418.

Sundman, B.(1991) A program for performing thermodynamic calculations. In *User Aspects of Phase Diagrams*, Hayes, F.H. (Ed.) London: Institute of Metals.

Tillman, D. A. (1994). *Trace Metals in Combustion Systems*. San Diego: Academic Press.

Villeminot, P. (1967). Pyrometrie photographique appliquee au soudage. *Soudage et Techniques Connexes,* 21, 367.

Chapter 6

Conclusion

High-energy-density metallurgical processing (e.g., any process involving a heat source of more than 10 kW / cm^2, such as welding), can create significant amounts of submicron particles, the chemical composition of which can vary with size. Chemical heterogeneity with size is important for manufacturing and is critical in industrial hygiene because the respirability of airborne particles is dependent on particle size. The change in composition with particle size can be explained by principles of aerosol science and physical chemistry, as illustrated by a study of fume formed during welding.

Thus, the question to be answered in this thesis was:

What is the relationship between the size and composition of airborne particles formed from metallurgical processing?

This was answered by studying welding fume, an typical metallurgical aerosol. Welding fume is of particular concern because the American Conference of Governmental Industrial Hygienists (ACGIH) and the Occupational Safety and Health Administration (OSHA) have indicated that they will reduce exposure limits to chemicals found in welding fume. A Navy / Industry Task Group estimated that it would cost the U.S. Navy initially $3 to $22 million and afterwards $5 to $46 million annually to comply.

It was shown in Chapter 3 that welding fume is composed of typical airborne particles and can be therefore be described with general aerosol science. In Chapter 4, ways to correctly analyze the chemistry of particles were described and in Chapter 5, they were applied to welding fume. This knowledge was coupled with thermochemical data to understand the relationships between particle composition and particle size.

Knowledge of particle size is important because a given characterization technique only provides accurate data for a specific particle size range. Many previous studies leave this fact unstated when reporting the results of welding fume characterization and thus give misleading conclusions. This has been fairly common in welding fume literature, particularly with studies involving energy dispersive spectroscopy with scanning electron microscopes.

Also, previous X-ray diffraction studies of welding fume have reported many phases and have implied that a single nanoparticle contained multiple phases. This is not the case. It can be shown that if many phases are found in fume, they are contained individually in separate particles.

In practice, there are two types of chemical characterization techniques: those that measure radiation proportional to the atomic number and those that measure from values proportional to the atomic mass. The former produce data easily transformed into molar / atomic fractions, whereas the latter create data reported as weight percentages. Therefore, the elemental data from multiple techniques often cannot be compared, except within these two groups. The most convenient particle composition data to report is the molar fraction of only the cations. Energy dispersive spectroscopy from electron microscopy is a good technique for measuring this.

Particle formation is categorized into three major size ranges: the nucleation range, accumulation range, and coarse (particle) range. Those in the nucleation and accumulation ranges are often grouped together as "fine" particles.

The nucleation range includes particles created from the collision of atoms. The decisive parameter for particle size is the supercooling of the vapor. The upper limit to the nucleation range is the mean free path of the carrier gas; it is about 70 nanometers for air and for argon at standard conditions.

The accumulation range is made up of particles created from the collision, agglomeration and coalescence of smaller particles. Such particles are rarely larger than 2 micrometers. Agglomerates can coalesce or sinter to form spherical particles.

Coarse particles form from liquid droplets the sizes of which are controlled by surface, viscous and inertial forces. These forces physically limit the minimum size of coarse particles to ~1 micrometer. It is probable that in metallurgical processes involving high-energy-density heat sources, micrometer-sized particles are formed from the bursting of vapor bubbles. It was also found that spatter combustion does not contribute to fume formation.

Coarse particles, because they are an order of magnitude larger in diameter and therefore three orders of magnitude greater in mass than fine particles, can dominate the bulk chemistry of airborne particles. Their composition is likely the same as the input material, e.g., the welding electrode.

The composition of fine particles is determined by the composition of the vapor. The supercooling of the vapor controls the composition of the condensing particles and the particle size. The composition of agglomerates and coalesced particles in the accumulation range is the sum of the composition of the primary particles and reflects the bulk composition of the vapor.

A diagram of the materials properties that directly control the nature of airborne particles in a specific size range can be found in Figure 6.1. This was demonstrated by a study of welding fume, a typical metallurgical aerosol.

Fume was created by four types of arc welding (globular, spray, and pulsed GMAW, and FCAW) in a fume chamber. It was collected and separated into size groups with
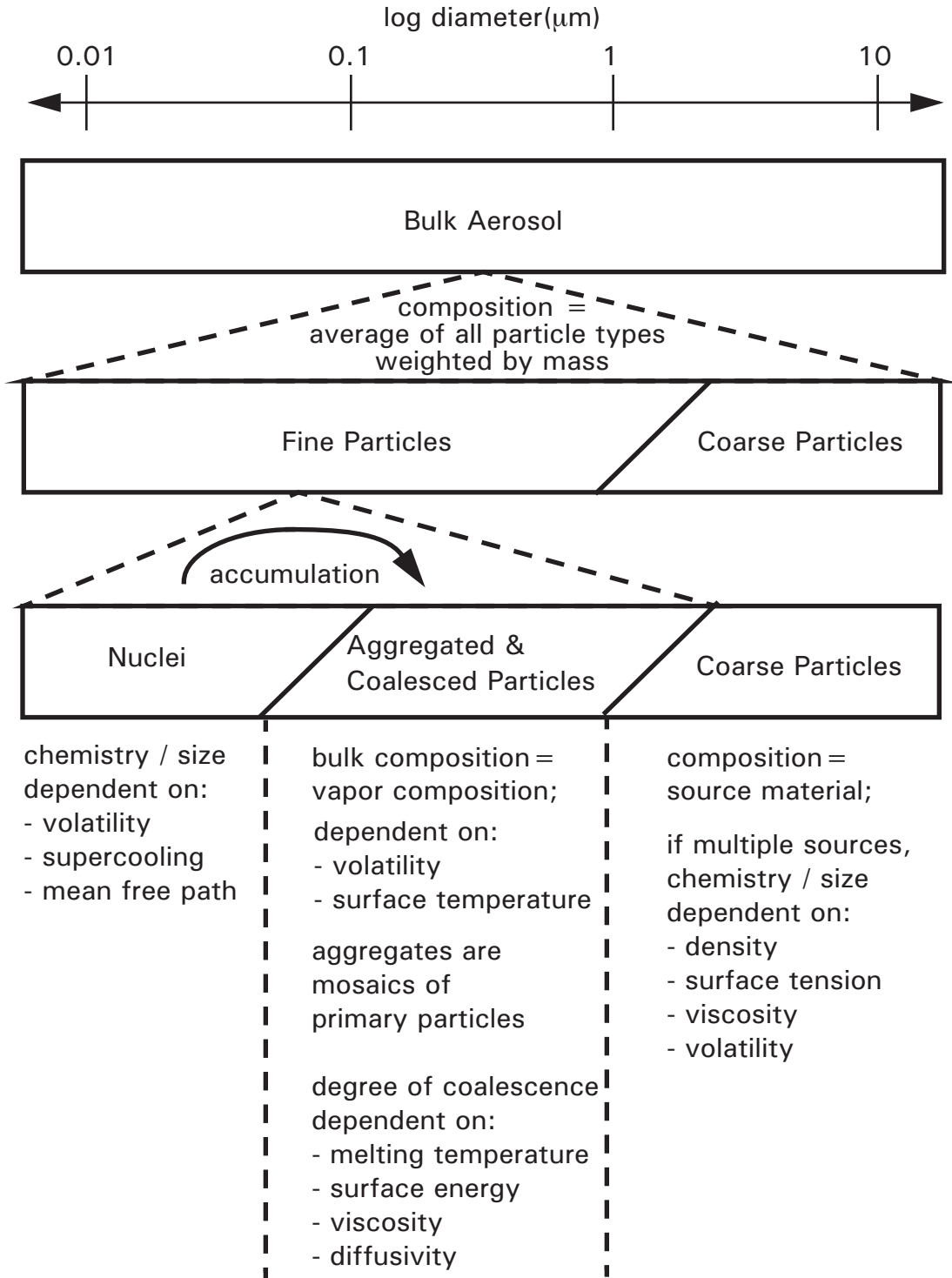
Figure 6.1 A diagram of the different types of forces and the materials properties that directly control the nature of airborne particles in a specific size range.

a cascade impactor. The mass distribution for each fume type was measured and the composition of each size group was determined with SEM-EDS.

It was found that the fume formation rate of globular GMAW was 2.7 times greater than that of spray GMAW which was in turn 1.4 times greater than pulsed GMAW. FCAW formed fume at rates 10 times that of spray GMAW. FCAW fume was found to accumulate more quickly than GMAW fume, because of a greater particle concentration from a higher rate of fume formation. The mass distributions of the GMAW fumes were similar to one another.

Findings suggest that for GMAW, hexavalent chromium is present mainly in fine particles that condense from vapor, not in coarse particles that form from liquid droplets.

Regardless of the welding parameters that caused different metal transfer modes in GMAW, less than 10% of the mass of welding fume was microspatter (coarse particles). This means that the higher fume formation rates found during globular GMAW as compared to spray GMAW are not caused by an increased fraction of larger particles, but rather by an increased number of all sizes of particles. This indicates that there is more evaporation of the electrode in globular GMAW than in spray GMAW. However, microspatter from FCAW contributes to almost a third of the fume.

The largest particles are not the same composition as the source electrode. Another source of coarse particles can be the slag formed from the flux during FCAW or the small amount of manganese silicate slag that forms during GMAW. Coarse particles formed from liquid metal can be a bit smaller than those formed from liquid oxides because liquid metal oxides have a greater viscosity.

Vapor condensed particles dominate the composition of size groups smaller than about one micrometer. Halides enrich smaller particles because of their volatility is greater than that of oxides. Coarse particle formation from liquid metal droplets explains the increase in iron and decrease in manganese with particle size for GMAW fume. Because of the mass distribution of welding fume, the bulk composition of welding fume is dominated by fine condensed particles.

The temperature of the evaporating material controls the composition of the vapor. GMAW fume composition is dominated by vaporization from the electrode, not from the weld pool, which has a lower temperature than the electrode. Hexavalent chromium content in GMAW fume is also controlled by the electrode composition, not by the base plate composition.

In GMAW, smaller electrode droplets (such as those formed during spray or pulsed transfer) have a cooler surface temperature than larger electrode droplets do (like those from globular transfer). Therefore vapor of a composition enriched in the more volatile elements is evolved from smaller electrode droplets. In addition, less vapor forms. Conditions that create fume containing the greatest fractions of volatile met-

als (i.e., manganese) are the same that create the smallest electrode droplet. Therefore, fume composition can be controlled by current and shielding gas composition.

The surface temperature of the electrode droplet may exceed the boiling point. Like other phase changes, boiling generally occurs through heterogeneous nucleation, but this can not occur when energy is added by radiation, like in welding arcs or in laser or electron beams. In these cases, the vapor phase must form bubbles homogeneously. This requires significant superheats; for iron, temperatures above 3300K would be required. High-energy-density sources can be adapted to more efficiently produce nanoparticles. For example, process similar to GMAW would make nanoparticles more efficiently than systems currently in use that resemble GTAW.

The superheat, or amount by which the boiling point is exceeded, will determine the elemental composition of the vapor, similar to how the supercooling determines the composition of a condensate. The bulk composition of welding fume is essentially the same as the composition of the originating vapor, especially from welding processes like GMAW that do not significantly create coarse particles. Therefore, it is important to use appropriate values for the surface temperature of the liquid metal vapor source which one is trying to model.

To study the composition of primary particles in welding fume, a scanning transmission electron microscope equipped with energy dispersive spectrometry was employed. It was found that the primary particles of welding fume are not homogeneous. Particles larger than the mean free path of argon at room temperature (70 nm) had the same composition as the vapor, indicating that they formed through the random collision of smaller particles. Particles 20 to 60 nm showed a trend in composition where the smaller particles were enriched in volatile metals. This was explained by non-equilibrium cooling along the bubble point line of a binary vapor-liquid phase diagram. This forms a volatile-element-rich shell around a less volatile core. This behavior is similar to that found in liquid solidification. Some metallurgical systems demonstrate immiscible behavior upon condensation, so that particles of distinctly different compositions form. If the system contains compounds of drastically different volatilities, large primary particles may be enriched in the more volatile compounds which heterogeneously nucleate on pre-existing particles.

Not all welding fume particles are homogenous internally. This may be from compositional gradients formed because of the difference in volatility of the elements and compounds in the vapor. Because of the nanoscale of these particles, they will not remain in a metastable state, such as that of a compositional gradient in a single phase or that created from the fusion of dissimilar particles, Nanoparticles homogenize quickly. However, non-uniform nanoparticles were found with STEM-EDS. Metal particles with surface films of oxide are metastable because of slow oxidation rates at room temperature. Surface segregation due to dissimilar surface energies of the respective materials in a particle may cause surface enrichment. Multiple distinct stable immiscible phases introduced by the collision and coalescence of dissimilar particles cause internal heterogeneity.

The change in composition with particle size, as found with SEM-EDS of the fume collected with the cascade impactor, and with STEM-EDS of primary particles, has been combined in Figure 6.2 and Figure 6.3.

As shown, the variation of composition with size in welding fume particles can be simply explained by using existing knowledge about aerosol science and thermodynamics. This explains the relationship between the size and composition of airborne particles formed during metallurgical processing.

This knowledge can be transferred to other fields. Greater control of nanoparticle production can be achieved by understanding the effects of the amount of super-cooling and cooling rate with regard to the chemical thermodynamics of the source vapor. This can be used to improve predictions about high temperature and / or nanoscale manufacturing. Manufacturing processes (e.g., VLS growth) that utilize nanopowders because precursors require size and chemical homogeneity. Better predictions can also be made about the size-based chemistry of airborne by-products during fabrication. These can be used to improve calculations of the toxic impact on the environment and workers. Specifically with regard to welders, this knowledge can be used when updating governmental guidelines about fume exposure.
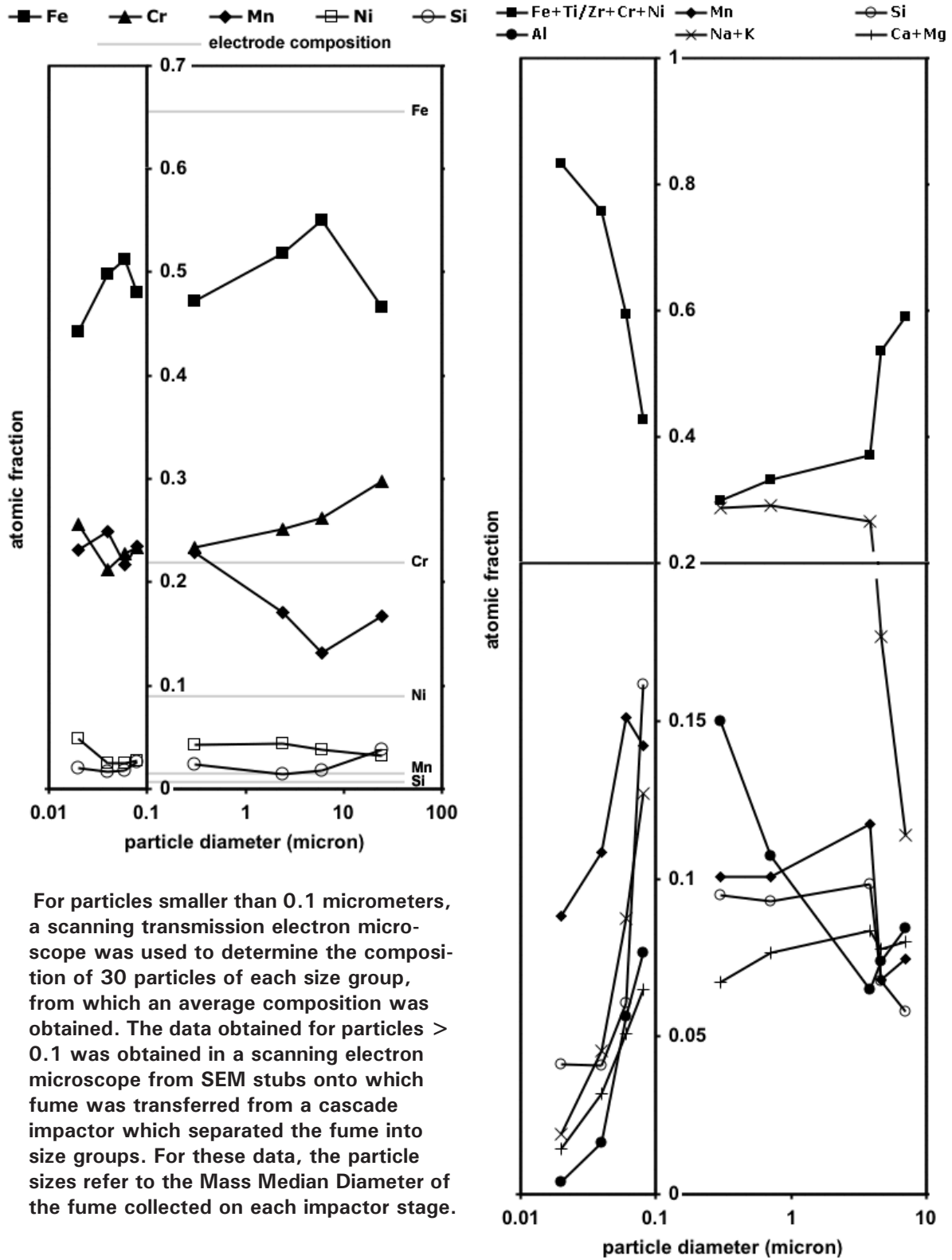
For particles smaller than 0.1 micrometers, a scanning transmission electron microscope was used to determine the composition of 30 particles of each size group, from which an average composition was obtained. The data obtained for particles > 0.1 was obtained in a scanning electron microscope from SEM stubs onto which fume was transferred from a cascade impactor which separated the fume into size groups. For these data, the particle sizes refer to the Mass Median Diameter of the fume collected on each impactor stage.

Figure 6.2 (Left) Metals content of stainless steel GMAW fume, as determined by energy dispersive spectrometry in electron microscopes.

Figure 6.3 (Right) Metal content (EDS) in stainless steel FCAW fume, as determined by energy dispersive spectrometry in electron microscopes.

Appendix A

Fume Formation from Spatter Combustion

Another theory for the link between correlated spatter and fume formation rates spatter has been suggested by fume researchers at the University of Bradford. They hypothesized that the greater fume formation rate observed during globular welding conditions is caused by vapor formed from combusting spatter droplets (Gray et al., 1980). This would explain why gas metal arc welding in globular mode creates both more fume and more spatter. This was concluded after examining spatter particles that were porous and obviously oxidized. In addition, they found that shielding a greater area around the arc (and presumably more of the hot spatter) reduced fuming.

With regard to the porosity, the dissolution of nitrogen that occurs when liquid iron is cooled was not considered. This is the main reason steel must be shielded from atmospheric gases during welding; if it is not, the resulting weld looks like Swiss cheese (Eagar, 2002). It is likely that the observed porosity of spatter particles is due to the escape of nitrogen gas.
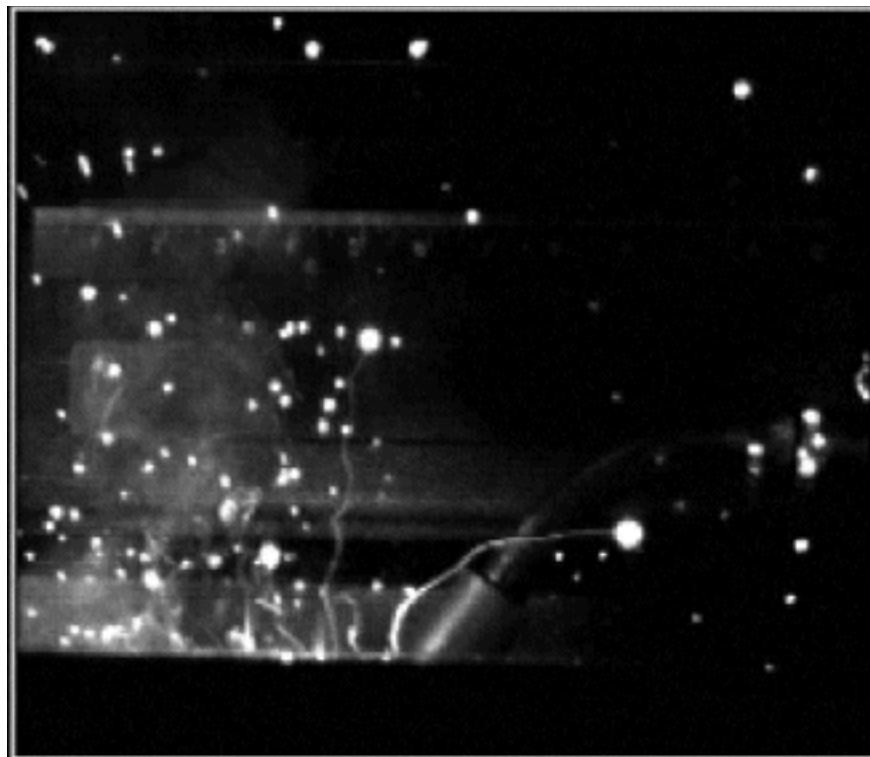

Figure A.1 Frame (duration = 1 ms) from high-speed videography of CO_2 - shielded mild steel GMAW

High speed videography does show that some spatter particles leave vapor trails (see Figure A.1). Porosity aside, the question whether spatter can vaporize enough to significantly contribute to the fume formation rate is addressed here.

The literature (Heile & Hill, 1975; Eichhorn & Oldenburg, 1986; Willingham & Hilton, 1986; Hilton & Plumridge, 1991; Castner, 1995; Castner, 1996; Deam, et al., 1997) reports fume formation rates for GMAW with 1.2 mm wire under various conditions from 0.05 g/min to about 0.35 g/min. Spatter rates for GMAW (using 1.2 mm wire with a variety of shielding gases at 200 amps, 30V) range from 0.5 g/min to 3.5 g/min (Liao and Chen, 1998) With these numbers, one can easily see that at least 10% of the spatter must evaporate for the increase in fume to be caused by the increase in spatter. Is that possible?

The temperature of a spatter droplet is controlled by heat losses by convection, radiation and evaporation and by heat evolved from combustion, as shown in Equation A.1:

$$\frac{VC_p}{\Omega A}\frac{dT}{dt} = Q_{convection} + Q_{radiation} + Q_{evaporation} + Q_{oxidation} \qquad A.1$$

where
V, volume of the droplet, is $\pi d^3/6$,
A, the area of the droplet, is πd^2,
d is the diameter of the spatter droplet,
Ω, the molar volume, is ~0.008 m^3/mole,
C_p, the heat capacity, is ~40 J/mole/K,
T is temperature and t is time.

It is conservatively assumed that the initial temperature of the droplet is 2500 K and that the temperature of the ambient air is 500 K.

The heat lost through convection can be determined as,

$$Q_{convection} = \frac{k_{air}}{d}\left[2 + 0.6\left(\frac{dv\rho_{air}}{\eta_{air}}\right)^{\frac{1}{2}}\left(\frac{C_{p,air}\eta_{air}}{M_{air}k_{air}}\right)^{\frac{1}{3}}\right](T-500) \qquad A.2$$

where the properties of the ambient air,
k_{air}, the thermal conductivity, is 0.03 W/m/K,
η_{air}, the viscosity, is 2×10^{-5} Ns/m^2, and
ρ_{air}, the density, is 1 kg/m^3.
The atomic mass of the air is M_{air}.

The velocity of the spatter droplet, v, was measured from high speed videography. The slower droplets moved at 0.2 m/s. However, by inspection, one can see that Equation A.2 is approximately equal to:

$$Q_{convection} = 2\frac{k_{air}}{d}(T - 500) \qquad \text{A.3}$$

for small diameters.

The radiative heat loss is found by:

$$Q_{radiation} = \varepsilon\sigma(T - 500)^4 \qquad \text{A.4}$$

where the Stefan-Boltzman number is 5.669×10^{-8} W/m^2/K^4 and the emissivity is assumed to be 0.7.

Evaporative heat loss can be modelled using the Langmuir equation, which, because it is for evaporation into a vacuum, may be an overestimate. In addition, vapor pressures for the more easily evaporated metals were used, instead of those for metal oxides, which may have been appropriate. These approximations may cause the modelled temperature of the droplet to decrease too rapidly, although this is unlikely with small droplet sizes where convective heat losses dominate. However, since this equation will also be used to determine the amount of vapor the spatter droplet forms, any inaccuracy in the droplet temperature will be offset by the overestimation of vaporization, resulting in a reasonable evaluation of possible fume formation.

$$Q_{evaporation} = \frac{P_{metal}}{\sqrt{2\pi M_A R k_B T}}L_{evaporation} \qquad \text{A.5}$$

The atomic mass of the steel is M_{steel}, and k_B is the Boltzman constant. P_{metal} is the vapor pressure of the steel and $L_{evaporation}$ is the heat of evaporation. Both are functions of temperature and composition. Approximating the steel as a 0.01 Mn-Fe alloy and using values from the NIST Chemistry Book (http://webbook.nist.gov/) for P_{metal} and $L_{evaporation}$, $Q_{evaporation}$ was approximated with a power law as:

$$Q_{evaporation} = 7x10^{-47}T^{15.734} \qquad \text{A.6}$$

in W/m^2.

The heat evolved through oxidation was calculated by multiplying the parabolic equation for iron oxidation given by Poirier and Geiger (1994) by the heat of oxidation, which is about 200 kJ/mole or about 4000 kJ/kg of reacted O_2. The protection of the shielding gas is neglected, which, as it turns out, makes little difference, because oxidation only contributes significantly to the heat balance at very short time intervals.

$$2 \times 10^{-4} \frac{(kgO_2)^2}{m^4 s} x t = \left[\frac{\Delta massO_2}{A} \right]^2 \qquad\qquad \text{A.7}$$

$$Q_{oxidation} = -5.66 x 10^4 \frac{W\sqrt{s}}{m^2} x \frac{1}{\sqrt{t}} \qquad\qquad \text{A.8}$$

The above equations were combined and solved numerically. The computed change in temperature for spatter droplets is plotted below in Figure A.2 for various droplet sizes, in the range from 2500 K (the maximum reported average temperature of electrode droplets (Haidar, 1999; Jelmorini, 1977) to 1800 K, the solidification temperature of iron.
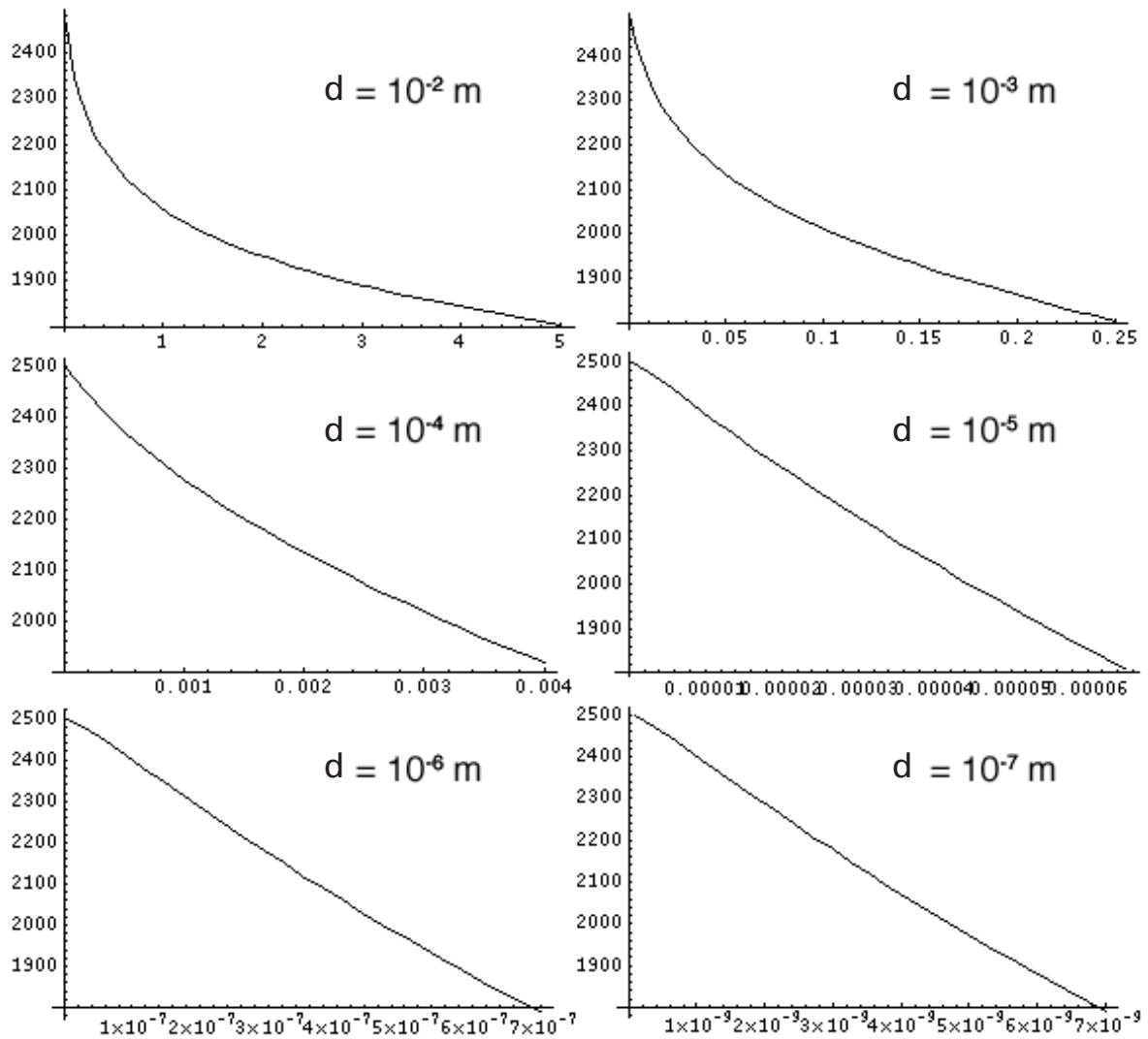

Figure A.2 Calculated change in temperature (K) of spatter droplets of various diameters (d) with time (s).

The resulting temperature profiles were re-entered into Equation A.6, multiplied by the spatter droplet surface area, divided by the heat of evaporation per mole of metal evaporated, but multiplied by the molar mass of Fe_2O_3, in order to compare to fume mass. This was then integrated over the temperature range. The resulting data is found in Table A.1.

Table A.1 Calculated fume mass created by an individual spatter particle

diameter	Mass (μg)	% spatter mass	Notes About Model
10 mm	418000	11	upper limit: particles > 10 mm do not have Bi << 1
1 mm	310	8.5	
0.1 mm	0.13	3.5	
10 μm	2.2×10^{-5}	0.6	
1 μm	2.1×10^{-9}	0.1	
0.1 μm	2.4×10^{-13}	0.0	lower limit: particles >0.1 μm act like gas molecules

One can see that only larger spatter droplets evaporate to any extent, which is substantiated by the videograph and the fume trails left by spatter droplets larger than 1 mm. If all spatter particles were 10 mm in diameter, it could be possible that the globular increase in fume formation rates is caused by spatter. Kheifets (1986), collected spatter particles formed from CO_2-shielded GMAW with 1.2 mm diameter at 27 V and 200 amps. 93% of the particles were smaller than 1.5 mm. That means that about 50% of the spatter mass is from particles smaller than 2 mm. Therefore it is not likely that evaporation from spatter contributes significantly to fume.

Since evaporation increases logarithmically with temperature, it makes sense that the cooling spatter droplet, never hotter than 2500 K, does not contribute to fume as much as the constantly heated welding electrode, the surface of which can be greater than 2500 K.

To simulate spatter combustion in order to measure the amount of fume it may create, a tungsten electrode arc melter (see Figure A.3),was used to melt a small amount of welding wire, equivalent to the mass of a large spatter particle. The air in the arc melter chamber was pure argon, but as soon as the arc was extinguished, pure oxygen was blown through the chamber and out through a PVC membrane filter, which collected any fume. This was repeated multiple times but no measurable amount of fume was detected.

It was concluded that spatter does not contribute to the metal vapor formed during welding. This is substantiated by researchers who report that when iron particles combust, they do so in the solid-phase, not in the gas phase (Sun, et al., 2000;

Figure A.3 Arc melter

Steinberg, et al., 1992). The correlation between spatter and welding fume formed from vapor is that the rates of formation of each are controlled by the same variable: electrode droplet temperature. Spatter forms when vapor bubbles nucleate and burst from the liquid metal of the molten electrode droplet. This is more likely with greater droplet surface superheats. A good discussion of the dependence of spatter on superheat can be found in the papers of Ma & Apps (1982; 1983). How this is controlled by welding parameters and it affects vaporization is explored elsewhere.

References

Castner, H. R. (1995). Gas metal arc welding fume generation using pulsed current. *Welding Journal*, 74(2), S59–S68.

Castner, H. R. (1996). Fume generation rates for stainless steel, nickel and aluminum alloys. *Welding Journal*, 75, 393s–401s.

Deam, R., Bosworth, M., Chen, Z., French, I., Haidar, J., Lowke, J., Norrish, J., Tyagi, V., & Workman, A. (1997). Investigation of fume formation mechanisms in GMAW. *Proceedings of the Technological Developments and Advances for Australian Industry International Welding and Joining Research Conference*, Silverwater, Australia: Welding Technology Institute of Australia.

Eagar, T. W. (2002). *Welding and Joining Processes Course,* Massachusetts Institute of Technology.

Eichhorn, R., & Oldenburg, T. H. (1986). Welding fumes emitted during welding of high-alloyed materials - evaluation of amount, chemical composition and morphology, including the influence of welding parameters*. Proceedings of the Conference of Health Hazards and Biological Effects of Welding Fumes and Gases*, R. M. Stern, et al. (Ed.). Amsterdam: Excerpta Medica.

Gray, C. N., Hewitt, P. J., & Hicks, R. (1980). The effect of oxygen on the rate of fume formation in metal inert gas welding arcs. *Proceedings of Weld Pool Chemistry and Metallurgy International Conference*, Cambridge, England: The Welding Institute, Abington Hall.

Haidar, J. (1999). An analysis of heat transfer and fume production in gas metal arc welding. III. *Journal of Applied Physics*, 85(7), 3448–3459.

Heile, R. F., & Hill, D. C. (1975). Particulate fume generation in arc welding processes. *Welding Journal*, 54(7), 201s–210s.

Hilton, D. E., & Plumridge, P. N. (1991). Particulate fume generation during GMAW and GTAW. *Welding and Metal Fabrication*, December, 555–560.

Jelmorini, G., Tichelaar, G. W., & Van Den Heuvel, G. J. P. M. (1977). *Droplet Temperature Measurements in Arc Welding* IIW Doc. 212–411–77.

Kheifets, A. (1986). Comparative evaluation of several methods of reducing metal spatter during CO_2 welding. *Automatic Welding USSR*, 39(3), 49–51.

Liao, M. T., & Chen, W. J. (1998). The effect of shielding gas compositions on the microstructure and mechanical properties of stainless steel weldments. *Materials Chemistry and Physics*, 55, 145–151.

Ma, J., & Apps, R. L. (1982). MIG transfer discovery of importance to industry. *Welding and Metal Fabrication*, September, 307–316.

Ma, J., & Apps, R. L. (1983). New MIG process results from metal transfer mode control. *Welding and Metal Fabrication*, 51(4), 168–170.

Poirier, D. R., & Geiger, G. H. (1994). *Transport Phenomena in Materials Processing*. Warrendale, PA: TMS.

Steinberg, T., Wilson, D., & Benz, F. (1992). The combustion phase of burning metals. *Combustion and Flame*, 91(2), 200–208.

Sun, J., Dobashi, R., & Hirano, T. (2000). Combustion behavior of iron particles suspended in air. *Combustion Science and Technology*, 150(1–6), 99–117.

Willingham, D. C., & Hilton, D. E. (1986). Some aspects of fume emissions from MIG welding stainless steel. *Welding and Metal Fabrication*, July, 226–229.

Appendix B

Surfactant Aided Dispersion of Nanoparticular Suspension of Welding Fume

Neil Jenkins, Simon Adelmann and Thomas Eagar

B.1 Abstract

Lauric acid was added to a suspension of welding fume particles in ethanol in order to create a dense and contact free suspension. Samples of varying concentrations of lauric acid were prepared and mixed ultrasonically. After mixing, the suspensions were clear and stable and therefore suitable for analysis in a TEM. The concentration of lauric acid was optimized in order to minimize particle overlap and agglomeration. This method of preparation was found to be cheap, quick, and easy. It can be used for the preparation of samples of welding fume for further analysis, such as chemical composition, particle size distribution, and respiratory damage on interaction with the human body.

B.2 Introduction

Welding fume is composed of complex particles, most of which consist of metal oxides and of materials from welding electrode fluxes. Primary particles of welding fume range in size from a few hundreths to a several tenths of a micrometer. They collect in aggregates and agglomerates ranging from 0.01 to 2 micrometers (Voitkevich, 1995). This occurs while airborne or during collection. Welding fume agglomerates clump in ways that impede the examination of individual primary particles. At the same time, successful microscopy requires a high number of particles per micrograph, so simple dilution is not the best answer. A possible method for the preparation of a dense, contact free suspension of welding fume that would aid particle analysis by electron microscopy was developed.

A dense contact-free suspension would ease the investigation of the chemical composition of individual particles and the determination of the particle size distribution of the fume. These studies would ultimately help explain the interactions of welding fume particles with the human respiratory system, which would eventually help protect both the health of welders and the welding industry.

Experimentation with the addition of a surfactant yielded promising results for the dispersion of iron/manganese oxide welding fume. Two systems were chosen for investigation: lauric acid (dodecanoic acid or $C_{12}H_{24}O_2$) (Moore, et al., 2001), in ethanol (Kimura & Bandow, 1983), and iodine in acetyl acetone (2,4-pentanedione) (Boccaccini, 2002). Initial TEM images showed the addition of iodine was not effective in separated agglomerates, while the addition of lauric acid yielded promising results. The addition of lauric acid as a surfactant was found to be an inexpensive

and easy way to achieve a contact free suspension. The solution can be prepared quickly and examined under a TEM almost immediately.

B.3 Experimental Methods

Welding fume was collected using gas metal arc welding of mild steel electrode wire in a chamber designed by Professor Gael Ulrich and co-workers at the University of New Hampshire (Quimby & Ulrich, 1999). Samples of this iron and manganese oxide welding fume were prepared for analysis by TEM by suspending it in ethanol. This was achieved by sonicating the mixture with an ultrasonic probe (Figure B.1),

Figure B.1 Ultrasonic probe.

which broke up some of the agglomerates. A drop of the suspension was pipetted unto a TEM sample grid (copper film strengthened with a carbon grid). The ethanol evaporated, leaving fume on the grid. The fume-ethanol ratio controlled particle number density on the grid film. The duration of sonication did not seem to have a sizeable effect on the amount of de-agglomeration, but this was not quantified. This method was based on the method developed by Cabot Corporation, Billerica, Massachusetts (Cambrey, 2000).

Different amounts of lauric acid were added as a surfactant, in order to obtain a dense, contact free suspension of nanoparticles. The concentration of surfactant added was varied from 1 mol/m^3 to 10^{-5} mol/m^3. The suspensions was prepared as follows:

0.09 g of welding fume was added to 30 ml of ethanol to form the fume suspension in the manner discussed previously. 0.01 moles (2.003 g) of lauric acid (dodecanoic acid or $C_{12}H_{24}O_2$), was dissolved in 0.01 L of ethanol and mixed with an ultrasonic

probe for 2 minutes to ensure full dissolution. 2 ml of the fume suspension (containing 0.006 g fume) was added to 1 ml of the surfactant solution (which contained 0.001 moles of lauric acid) and mixed with an ultrasonic probe for 2 minutes to ensure full mixing of the two solutions, and to allow the separation of metal oxide agglomerates. A droplet of the mixture was then dripped onto a TEM grid. The grid was left to dry over night before examination by TEM.

B.4 Results and Discussion

The TEM micrographs obtained show the qualitative difference in the sample prepared using a surfactant, and those without. The particles prepared without surfactant (the figures on the left: Figure B.2, Figure B.4, Figure B.6, and Figure B.8) can be seen to be in close contact with each other, often overlapping above and below, making individual particles indistinguishable from each other.
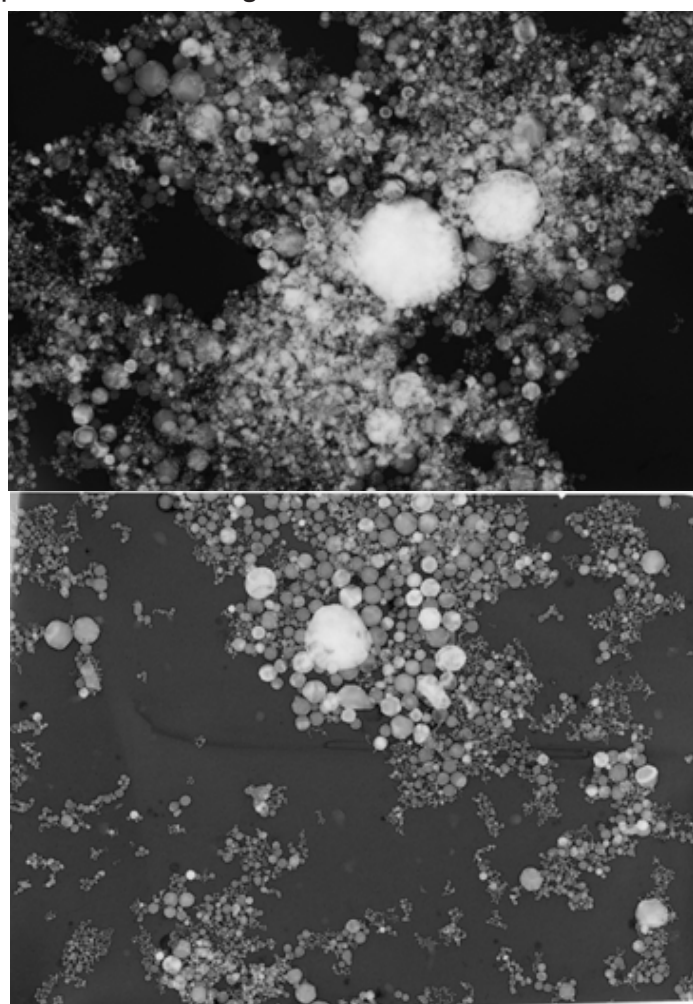

Figure B.2 (Top) Transmission electron micrograph 27 000x. 7.5 mg mild steel GMAW fume in 2.5 ml ethanol.
Figure B.3 (Bottom) Transmission electron micrograph 27 000x. 7.5 mg mild steel GMAW fume in 2.5 ml ethanol $+$ 10^{-3} mol lauric acid.
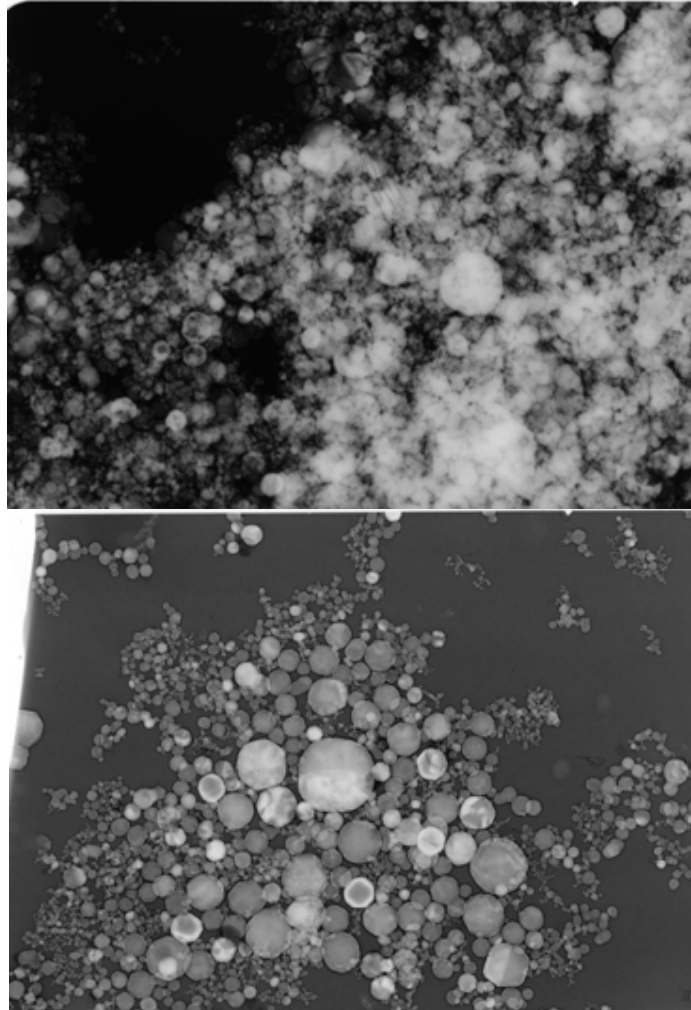
Figure B.4 (Top) Transmission electron micrograph 50 000x. 7.5 mg mild steel GMAW fume in 2.5 ml ethanol.

Figure B.5 (Bottom) Transmission electron micrograph 50 000x. 7.5 mg mild steel GMAW fume in 2.5 ml ethanol + 10^{-3} mol lauric acid.

This is in contrast to those created by adding varying amounts of lauric acid (the figures on the right: Figure B.3, Figure B.5, Figure B.7, and Figure B.9). These figures show that a dense contact free suspension could be achieved by the addition of lauric acid as a surfactant. The optimum amount of lauric acid was determined by systematic trial and error. It was found that optimum concentration of lauric acid is between 10^{-3} and 10^{-5} mol/m^3 for the amount of fume used in these cases. Large agglomerates of particles cannot be found in these suspensions. Furthermore, in regions where the particles are densely packed, the particles do not overlap and are easily distinguishable from one another.

The mechanism proposed for this dispersion is as follows. It is suggested that the surfactant attaches to the surface of the iron oxide particles. The carboxylate group, which is polar, and therefore lyophobic in ethanol, will be attracted to the oxide surface preferentially (Smith, 2002). However, the carbon backbone is non-
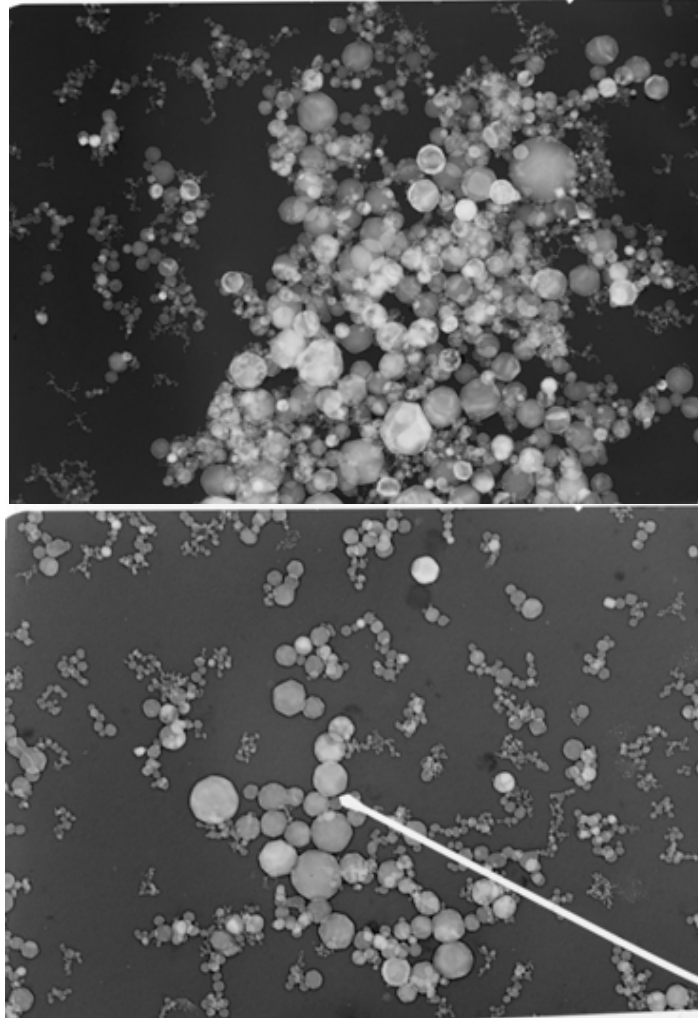
Figure B.6 (Top) Transmission electron micrograph 41 000x. 5 mg of mild steel GMAW fume in 2.5 ml ethanol.

Figure B.7 (Bottom) Transmission electron micrograph 50 000x. 7.5 mg of mild steel GMAW fume in 2.5 ml ethanol$+$ 10^{-5} mol lauric acid.

polar and therefore lyophilic in ethanol, meaning it will stand away from the surface in a brush-like fashion. The interactions of these brush-like molecules between approaching nanoparticles provides a regime of long distance repulsion by two mechanisms: steric repulsion and lyophilic repulsion; this disperses the nanoparticles (Ortiz, 2002).

B.5 Conclusions

A dense contact free suspension of welding fume nanoparticles was achieved in ethanol, by the addition of lauric acid as a surfactant. The concentration of lauric acid used was found to be a parameter in the effective dispersion of large agglomerates. Further work in this field would be complemented by the use of lauric acid as a surfactant. Such work might include a detailed statistical analysis of the primary particle size distribution of the fume and the investigation of the chemical composition of the larger particles. The first of these is very important in order to quantify
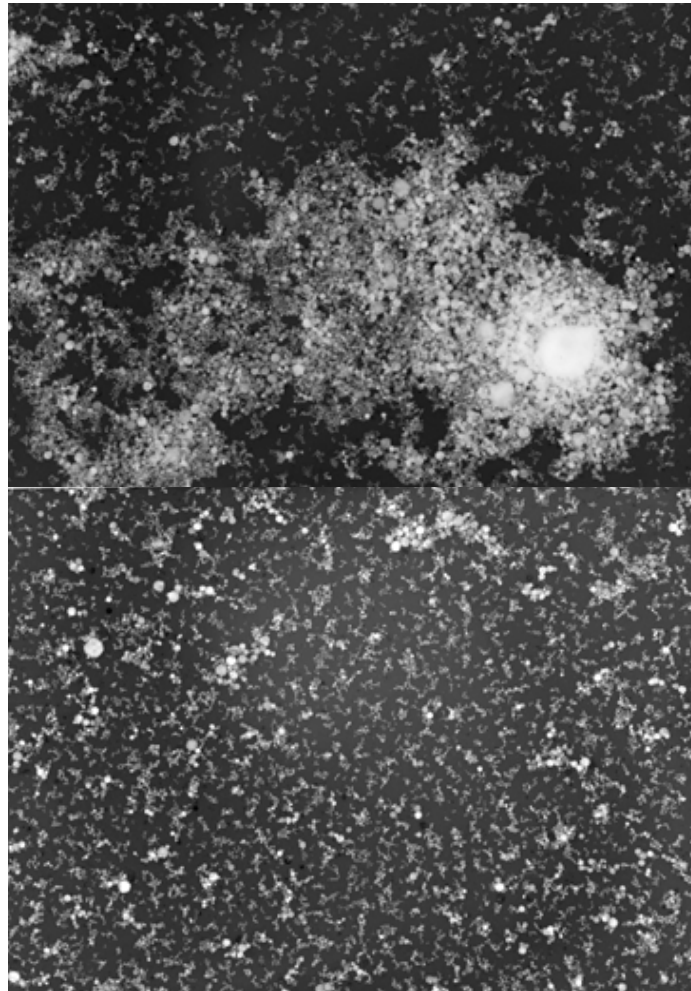
Figure B.8 (Top) Transmission electron micrograph 10 000x. 7.5 mg of mild steel GMAW fume in 2.5 ml ethanol.

Figure B.9 (Bottom) Transmission electron micrograph 10 000x. 6.0 mg mild steel GMAW fume in 2.0 ml ethanol $+$ 10^{-7} mol lauric acid.

the effects of lauric acid as a surfactant. One concern of using a hydrocarbon as a surfactant for analysis by TEM is that it may lead to 'cracking' of the hydrocarbon and the deposition of carbon which would obscure the image. Microtomy is suggested as a possible method of overcoming this.

References

Boccaccini, A. (2002). Personal communication, Imperial College, London.

Cambrey, J. (2000) Personal communication, Cabot Corporation, Billerica, Massachusetts.

Kimura, K. and Bandow, S. (1983). The study of metal colloids produced by means of gas evaporation technique. I. Preparation method and optical properties in ethanol, *Bulletin of the Chemical Society of Japan*, 56, 3578-3584.

Moore, R. Evans, S.D. Shen, T. and Hodson, C. (2001) Room-temperature single-electron tunneling in surfactant stabilized iron oxide nanoparticles, *Physica E* 9, 253–261.

Ortiz, C. (2002) *Nanomechanics of Biomaterials Course*, Massachusetts Institute of Technology.

Quimby, J. B., & Ulrich, G. D. (1999). Fume formation rates in gas-shielded metal arc welding. *Welding Journal,* April, 142–149.

Smith. R. (2002) *Ceramics Processing Course*, Massachusetts Institute of Technology.

Voitkevich, V. (1995). *Welding Fumes: Formation, Properties and Biological Effects*. Cambridge, England: Abington Publishing.

Biographical Note

Neil T. Jenkins was born and raised in southeastern Ohio. After two years of religious service in eastern Germany, he attended the Massachusetts Institute of Technology, graduating with a Bachelors of Science in Materials Science and Engineering, with a minor in German. He was awarded membership in Tau Beta Pi (the national engineering honor society) and in Phi Beta Kappa (the national humanities honor society). He also received a National Science Foundation Graduate Research Fellowship and National Defense Science and Engineering Graduate Fellowship, which funded his first few years as a doctoral student at Massachusetts Institute of Technology.